Mechanisms of Shear Stress Sensing in the Vasculature

Hannah Jane Gaunt

Submitted in accordance with the requirements for the degree of
Doctor of Philosophy

The University of Leeds

Faculty of Medicine and Health
Leeds Institute of Cardiovascular and Metabolic Medicine

August, 2018

Funded by the British Heart Foundation

The candidate confirms that the work submitted is her own and that appropriate credit has been given where reference has been made to the work of others.

Acknowledgements

First and foremost, with great thanks I would like to acknowledge the continued guidance and support of my supervisor, Professor David Beech. I am eternally grateful for all of the fantastic opportunities you have given me – how we have put up with each other for five years I do not know! I would also like to thank Marc Bailey and Jing Li for their supervision and constructive proof reading of my thesis.

I would like to thank all of the members of the Beech lab for their support. My PhD has been a continuous learning curve and I am grateful to you all for helping me along this journey. In particular I would like to thank Melanie, who has been a tremendous support throughout my PhD. I honestly don't know if I could have done this without you! Thank you for always giving your time to help me and for listening and answering all of my questions, however silly they may have been. I will always have your voice in my head reminding me, controls, controls, controls!! You have the patience of a saint and we are all very lucky to have you! I would also like to thank Alex Bruns, for being a continued support in the lab, after all where would I be without all of your western blotting expertise? Katie Simmons thank you for all of your chemistry knowledge and for being such a fab office neighbour. Thank you to Yasu Tanahashi for performing the patch experiments and Hema Viswambharan for carrying out the eNOS activity assay. I would also like to thank the members of the Schwarz lab at the University of Yale for making me feel so welcome during my visit and for all the help with the active G-protein pull down assay.

A massive thanks goes to Marj, for being such a great eNOS team member. I couldn't think of a better person to hand the project over to. I would also like to thank Fiona for performing RT-qPCR experiments for me – you will get the banoffee pie in return one day! Thank you both for teaching me all of the French words that I know. Even though most of them can't be mentioned here, I'm glad that I now know more words than Chateauneuf du pape and petit pois!

I have been very lucky to have made some fantastic friends during my PhD. Nik, K and Beth I don't know what I am going to do without you. I will miss Beth's sleepy face in the morning, Nikki's directness and Katie's inappropriate jokes. Thank you for always listening to me (even when I am annoying), always supporting me and

most of all, always galloping with me! I am so grateful for all of the memories that we have made and I can't wait to make so many more. Seriously guys, you have been the absolute best. Bob (Pete), Hol and Lara, thank you for always bringing me back to reality - we have had so many laughs! Pete thanks for being such a great student, Lara the whole liquid nitrogen Dewar does not need to go in the -80°C and Hol, did you ever find the pancreas? So many funny memories to look back on. A massive thanks to the McKeown group, especially Kat for all of your passion and enthusiasm. I have no doubt that you will be incredibly successful. I am still unsure what a cytokine is though…

The Enablers (Lynn & Niamh) – where do I start? Thank you for everything you have done for me. For grounding me and telling me to get over myself when I'm being high maintenance, for training me in wine drinking and for the endless advice and support that you have given me. Your passion for science is so refreshing and inspiring and all of your students are so lucky to be supervised by such great scientists. Oh how I am going to miss our office (see I am funny). Here's to many more years of friendship!

I would like to thank my Mum, Dad, Fi and Mol for all of the love and support you have given me throughout my studies. Thank you for always believing in me and for inspiring me to be driven and ambitious - you make your own luck right? Thanks also go to Soph whose strength inspires me every day, you have helped me through my PhD more than you know. A final thanks goes to Martin for being so patient and supportive (most of the time). Hopefully this makes all of the endless drives up to Leeds and all of the yummy dinners you have cooked me worth it! I hope that when you all read this you are proud and finally understand what Piezo1 is all about… or can at least pronounce it!

Thanks go to the British Heart Foundation who have funded my PhD studentship and to Martin Green for your generous gift to fund my international visits to Harvard and Yale University. I really hope that one day my work will make a difference.

Abstract

Background

Cardiovascular disease is usually associated with endothelial dysfunction. One characteristic of endothelial dysfunction is the lack of nitric oxide production and shear stress is an important contributing factor. Endothelial cells are exposed to the frictional force evoked by the flow of blood. Mechanotransduction of shear stress plays key roles in cardiovascular physiology and pathophysiology and is important in maintaining endothelial cell function. The mechanosensitive non-selective cation channel, Piezo1, is reported to be a direct sensor of shear stress in endothelial cells promoting their alignment, vascular development and as a sensor of whole body physical activity. Activation of Piezo1 by Yoda1 was sought to investigate the mechanism coupling Piezo1 to S1177 endothelial nitric oxide synthase (eNOS) phosphorylation.

Methods and Results

Data indicate that the chemical activator of Piezo1, Yoda1, is a useful research tool, not only mimicking mechanical stimulation of the channels but also facilitating study of Piezo1 channels without the need for mechanical stimulation. In human umbilical vein endothelial cells (HUVECs) eNOS was found to be rapidly phosphorylated predominantly at the key activating serine residue 1177/1179 by Yoda1 application independently of ATP and P2Y2 receptors. Instead, Fyn kinase and PKCδ are required for the integrity of this response without affecting Yoda1- or hypotonicity-evoked Ca^{2+} signals. Furthermore, the data suggest that Piezo1 somehow cross talks with CD31 and VE-Cadherin proteins of the mechanosensory triad to evoke eNOS phosphorylation. Over-expression studies using two independent methods for detecting protein-protein interaction provided evidence that Piezo1 is capable of interacting with CD31.

Conclusion

The data indicate the existence of direct coupling between Piezo1 and eNOS phosphorylation and that Fyn kinase and PKCδ are important mediators of this response. Furthermore, an important partnership between Piezo1 and CD31 and VE-Cadherin, key members of the mechanosensitive triad, was determined. Understanding Piezo1 partner proteins and signalling could be important for achieving better appreciation of how shear stress regulates cardiovascular structure and function.

Table of Contents

List of Tables

List of Figures

Abbreviations

AA	Arachidonic Acid
ACE	Angiotensin-Converting-enzyme
ADME	Absorption, Distribution, Metabolism, and Excretion
AMPK	5' Adenosine Monophosphate-Activated Protein Kinase
ASIC	Acid Sensitive Ion Channel
ATP	Adenosine Triphosphate
BAEC	Bovine Aortic Endothelial Cells
BH4	Tetrahydrobiopterin
BSA	Bovine Serum Albumin
CaM	Calmodulin
CaMKII	Ca^{2+}/Calmodulin-Dependent Protein Kinase II
Cav	Caveolin
CD31	Cluster of Differentiation 31
cDNA	Complimentary DNA
CFP	Cyan Fluorescent Protein
cGMP	Cyclic Guanosine Monophosphate
CNO	Clozapine-N-oxide
CRAC	Ca^{2+} Release Activated Ca^{2+}
DAPI	4',6-Diamidino-2-Phenylindole
DMEM	Dulbecco’s modified Eagle’s medium
DPBS	Dulbecco’s Phosphate Buffered Saline
DPM	Disintegrations Per Minute
EDHF	Endothelium-Derived Hyperpolarising Factor
EDRF	Endothelium-Derived Relaxing Factor
EGM	Endothelial Cell Basal Medium
EM	Electron Microscopy
eNOS	Endothelial Nitric Oxide Synthase

ER	Endoplasmic Reticulum
ERK	Extracellular Signal-Regulated Kinases
FAD	Flavin Adenine Dinucleotide
FBS	Fetal Bovine Serum
FCS	Fetal Calf Serum
FLIM	Fluorescence Lifetime Imaging Microscopy
FMN	Flavin Mononucleotide
FRET	Förster Resonance Energy Transfer
GFP	Green Fluorescent Protein
GPCRs	G-Protein Coupled Receptors
GsMTx4	Grammostola Spatulata Mechanotoxin 4
HEK	Human Embryonic Kidney
HIF	Hypoxia-Inducible Factor
hM4	Human-M4-Muscarinic
HRP	Horse Radish-Peroxidase
HUAEC	Human Umbilical Arterial Endothelial Cells
HUVEC	Human Umbilical Vein Endothelial Cells
ICAM-1	Intercellular Adhesion Molecule 1
IGF1	Insulin-Like Growth Factor 1
IKCa2+	Intermediate-Conductance Ca^{2+}-Activated K^{+} Channels
iNOS	Inducible Nitric Oxide Synthase
InsP3R	Inositol-1,4,5-trisphosphate Receptor
IP	Immunoprecipitation
IPTG	Isopropyl β-D-1-Thiogalactopyranoside
IPTG	Isopropyl β-D-1-Thiogalactopyranoside
K+	Potassium
KLF2	Krüppel-Like Factor 2
LDL	Low Density Lipoprotein
LEC	Liver Endothelial Cells

MCP-1	Monocyte Chemoattractant Protein-1
mT	mTurquoise2
NADPH	Nicotinamide Adenine Dinucleotide Phosphate
NCX	Na^{+}-Ca^{2+} Exchanger
NMR	Nuclear Magnetic Resonance
nNOS	Neuronal Nitric Oxide Synthase
NO	Nitric Oxide
NOS	Nitric Oxide Synthase
PCR	Polymerase Chain Reaction
PDGF	Platelet-Derived Growth Factor
PECAM-1	Platelet Endothelial Cell Adhesion Molecule
PFA	Paraformaldehyde
PGI2	Prostacyclin
PI3K	Phosphatidylinositol-4,5-Bisphosphate 3-Kinase
PKA	Protein Kinase A
PKC	Protein Kinase C
PLGF	Placenta Growth Factor
PMCA	Plasma Membrane Ca^{2+} ATPase
PP1	Protein Phosphatase 1
PVD	Peripheral Vascular Disease
PVDF	Polyvinylidene Fluoride
PYK2	Protein Tyrosine Kinase 2 ß
ROS	Reactive Oxygen Species
RT	Reverse Transcribe
RT-qPCR	Real Time- Quantitative Polymerase Chain Reaction
RyR	Ryanodine Receptor
SBS	Standard Bath Solution
SDS	Sodium Dodecyl Sulphate
SERCA	Sarcoplasmic Reticulum Ca^{2+} ATPase

SH3	Src Homology 3
siRNA	Short Interfering RNA
SKCa2+	Small-Conductance Ca^{2+}-Activated K^{+} Channels
SOCE	Store-Operated Ca^{2+} Entry
SOD	Superoxide Dismutase
STIM1	Stromal Interaction Molecule 1
TAE	Tris acetate EDTA
TM	Transmembrane
TRP	Transient Receptor Potential
TRPA	Transient Receptor Potential Ankyrin
TRPC	Transient Receptor Potential Canonical
TRPM	Transient Receptor Potential Melastatin
TRPML	Transient Receptor Potential Mucolipin
TRPP	Transient Receptor Potential Polycystin
TRPV	Transient Receptor Potential Vanilloid
VE-Cadherin	Vascular Endothelial Cell Cadherin
VECAM-1	Vascular Cell Adhesion Molecule 1
VEGF	Vascular Endothelial Growth Factor
VEGFR	Vascular Endothelial Growth Factor Receptor
YFP	Yellow Fluorescent Protein

Publications and Communications

First author

Gaunt, H.J. et al. A tight coupling pathway between Piezo1 channels and phosphorylated endothelial nitric oxide synthase. *Circulation Research*. **In Preparation.**

***Gaunt, H.J**., *Chuntharpursat, E. et al. Signalling complex of Piezo1 channels with CD31 mechano-sensor triad. *Nature Cell Biology*. **In Preparation.** (*) Equal contributors

Gaunt, H.J., Vasudev, N.S. & Beech, D.J. (2016). Transient Receptor Potential Canonical 4 and 5 proteins as targets in cancer therapeutics. ***European Biophysics Journal*** 45, 611-620. Review.

*Akbulut, Y., ***Gaunt, H.J**., Muraki, K., Ludlow, M.J., Amer, M.S., Bruns, A., Vasudev, N.S., Radtke, L., Willot, M., Hahn, S., Seitz, T., Ziegler, S., Christmann, M., *Beech, D.J., Waldmann, H. (2015). (-)-Englerin A is a potent and selective activator of TRPC4 and TRPC5 calcium channels. ***Angewandte Chemie Int Ed.*** 54, 3787-3791. (*) Equal contributors

Co-author

Miteva, KT*., Pedicini, L*., Wilson, LA., Jayasinghe, I., Brown, JMY., Marszalek, K., **Gaunt, HJ**., Deivasigamani, S., Sobradillo, D., Cutler, DF., Beech, DJ., and M^{c}Keown, L. A Ca2+ -regulated G protein (Rab46) couples physiological stimuli to functional Weibel Palade body trafficking. ***BioRxiv*****.** (Manuscript Submitted).

Morley, L., **Gaunt, H.J**., Hyman, A.J., Webster, P.J., Forbes, K., Walker, J.J., Simpson, N.A.B., Beech, D.J. (2018) Piezo1 is an important mechanosensing ion channel subunit in human placental endothelial cells. ***Human Molecular Reproduction*****. In Press.** Epub ahead of print.

Pedicini, L., Miteva, KT., Hawley, V., **Gaunt, H.J**., Appleby, H.L., Cubbon, R.M., Marszalek, K., Kearney, M.T., Beech, D.J and McKeown, L. Homotypic endothelial nanotubes induced by C-type lectin and thrombin. ***Scientific Reports.*** 2018 May 15;8(1).

Evans, E.L., Cuthbertson, K., Endesh, N., Rode, B., Blythe, N.M., Hyman, A.J., **Gaunt, H.J**., Ludlow, M.J., Foster, R. and Beech, D.J. (2017). A small-molecule inhibitor of Yoda1-activated Piezo1 channel activity. ***British Journal of Pharmacology.*** 2018 May;175(10)

*Rode, B., *Shi, J., *Endesh, N., Drinkhill, M.J., Webster, P.J., Lotteau, S.J., Bailey, M.A., Yuldasheva, N.Y., Ludlow, M.J., Cubbon, R.M., Li, J., Futers, S., Morley, L., **Gaunt, H.J**., Marszalek, K., Viswambharan, H., Cuthbertson, K., Baxter, P.D., Foster, R., Sukumar, P., Weightman, A., Calaghan, S.C., Wheatcroft, S.B., Kearney, M.T., *Beech, D.J. (2017). Piezo1 channels sense whole body physical

activity to reset cardiovascular homeostasis and enhance performance. ***Nature Communications*** 8(1):350.

Rubaiy, H.N., Ludlow, M.J., Henrot, M., **Gaunt, H.J**., Miteva, K., Cheung, S.Y., Tanahashi, Y., Hamzah, N., Musialowski, K.E., Blythe, N.M., Appleby, H.L., Bailey, M.A., McKeown, L., Taylor, R., Foster, R., Waldmann, H., Nussbaumer, P., Christmann, M., Bon, R.S., Muraki, K., Beech, D.J. (2017). Picomolar, selective and subtype specific small-molecule inhibition of TRPC1/4/5 channels. ***Journal of Biological Chemistry*** 292, 8158-8173.

Webster, P.J., Littlejohns, A.T., **Gaunt, H.J**., Prasad, K.R., Beech, D.J., Burke, D.A. (2017). AZD1775 induces toxicity through double-stranded DNA breaks independently of chemotherapeutic agents in p53-mutated colorectal cancer cells. ***Cell Cycle*** Mar 15:1-7.

Webster, P.J., Littlejohns, A.T., **Gaunt, H.J**., Young, R.S., Rode, B., Ritchie, J.E., Stead, L.F., Harrison, S., Droop, A., Martin, H.L., Tomlinson, D.C., Hyman, A.J., Appleby, H.L., Boxall, S., Bruns, A.F., Li, J., Prasad, K.R., Lodge, P.A., Burke, D.A., Beech, D.J. (2017). Upregulated WEE1 protects endothelial cells of colorectal cancer liver metastases. ***Oncotarget*** 8, 42288-42299.

Ludlow, M.J., **Gaunt, H.J**., Rubaiy, H.N., Musialowski, K.E., Blythe, N.M., Vasudev, N.S., Muraki, K., Beech, D.J. (2017). (-)-Englerin A-evoked cytotoxicity is mediated by Na+ Influx and counteracted by Na+/K+-ATPase. ***Journal of Biological Chemistry*** 292, 723-731.

Naylor, J., *Minard, A., ***Gaunt, H.J**., Amer, M.S., Wilson, L.A., Migliore, M., Cheung, S.Y., Rubaiy, H.N., Blythe, N.M., Musialowski, K.E., Ludlow, M.J., Evans, W.D., Green, B.L., Yang, H., You, Y., Li, J., Fishwick, C.W.G., Muraki, K., *Beech, D.J., Bon, R.S. (2016). Natural and synthetic flavonoid modulation of TRPC5 channels. ***British Journal of Pharmacology*** 173, 562-74. (*) Equal contributors.

Communications

(-)- Englerin A as a novel potent activator of TRPC4 and TRPC5 channels. **Hannah J. Gaunt**. Ion Channels as Disease Targets Session, 13th Annual Aurora Ion Channel Retreat, Vancouver. (2015)

Positive coupling of Piezo1 to eNOS phosphorylation. **Hannah J Gaunt**, Melanie J Ludlow, Kevin Cuthbertson, Richard Foster and David J Beech. IUPS 38th World Congress, Rhythms of Life, Rio de Janeiro (2017)

Chapter 1 Introduction

Endothelial cells are regarded as the ‘corner stones’ of the vascular system that are fundamental to almost all physiology. The continuous monolayer of endothelial cells that lines the inner surface of the entire vasculature creates a strategically located barrier between blood and tissues, surrounded by various cell types and extracellular matrices that influence their phenotype. Endothelial cells play important roles in physiological processes including: regulation of blood flow and blood pressure, and pathological processes such as atherosclerosis and hypertension (Khazaei et al., 2008; Herrmann and Lerman, 2001). Endothelial dysfunction, whether caused by physical injury or cellular damage, leads to compensatory responses that alter the normal homeostatic properties of the endothelium. Shear stress (the frictional force evoked by the flow of blood) and Ca^{2+} signalling are crucial for endothelial cell function as they drive a variety of signalling pathways (Tran et al., 2000; Chistiakov et al., 2017). Research examining how mechanosensory ion channels, namely the mechanosensitive ion channel Piezo1, drive endothelial cell signalling and physiology is important to help us further understand mechanisms behind endothelial dysfunction. This chapter will offer a short background discussing endothelial cells and how they regulate vascular physiology before considering endothelial dysfunction. Attention will then turn to mechanisms by which endothelial cells sense shear stress, focusing on Piezo1 channels, and to understand how Piezo1 mediated Ca^{2+} entry is important for endothelial function in physiology and disease. Better understanding of Piezo1 channels is important for achieving better appreciation of how shear stress regulates cardiovascular structure and function.

1.1 Endothelial cell biology; physiology and function

The endothelium is the largest organ in the body consisting of around 10^{13} cells and covering an area of 1-7 m^2 (Khazaei et al., 2008). Endothelial cells are strategically located between blood flowing through the vessel, and the surrounding vascular smooth muscle cells (Figure 1.1). This forms a semipermeable barrier regulating the transfer of molecules between the blood and adjacent tissues. In this regard they have been described as the ‘tissue-blood barrier’ (Irie and Tavassoli, 1991). These cells are therefore exposed to the frictional force, shear stress, as blood flows through the vascular system across the endothelium.

Endothelial cells control vascular homeostasis. Healthy endothelial cells function to place constraints on smooth muscle cell contraction, platelet aggregation, vascular smooth muscle growth, thrombosis and monocyte adhesion (Cooke, 2000). However, there are many factors that affect endothelial cell functions including chemical stimuli, such as various oxygen levels, paracrine signals and plasma constituents as well as mechanical forces such as shear stress. In response to changes in such stimuli endothelial cells secrete various factors to exert control over an array of synthetic mechanisms, all of which serve to maintain vascular tone and blood fluidity to provide homeostasis in the event of intimal injury (Cooke, 2000).

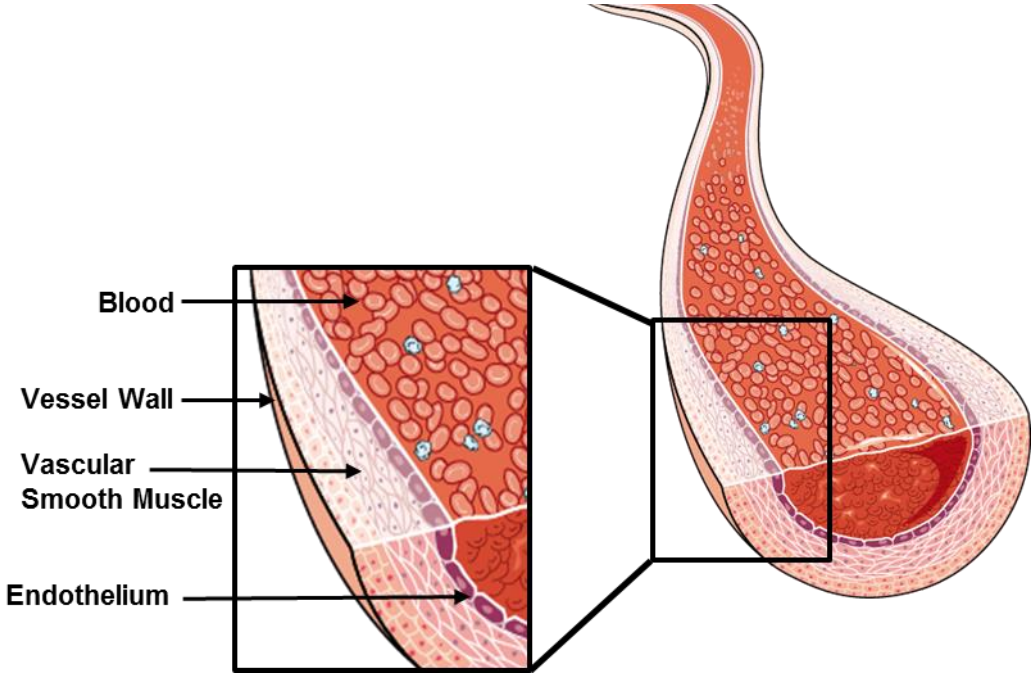

Figure 1.1 Schematic of an artery.

The vascular endothelium consists of a monolayer of endothelial cells that line the blood vessel. They are strategically located next to vascular smooth muscle cells and the flowing blood. *Schematic modified from servier medial art.*

1.1.1 Angiogenesis

In early embryogenesis the developing embryo is in an avascular state. However, as embryogenesis continues the complex vascular network begins to develop,

critical for the provision of oxygen and nutrients to allow growing organs to develop. This switching between avascular and vascular states, is orchestrated by both chemical signalling, and, the physiological force of shear stress. Initially, vasculogenesis occurs where a primitive vascular network is developed from haematopoietic progenitor cells. Endothelial cells migrate, differentiate and form tube-like structures which remodel into blood vessels (Carmeliet, 2005). Once developed, blood vessels usually remain quiescent. However, the growth of new vessels from those pre-existing at the embryonic stage may be required, for example during wound healing or neo intima formation. This is termed angiogenesis. Vascular development does require a fine balance, however, as proliferation is a feature of diseases including diabetic retinopathy, rheumatoid arthritis and cancer development (Carmeliet, 2005; Khazaei et al., 2008).

Endothelial cells are key players in angiogenesis. They have the remarkable capability to rapidly switch from their quiescent state to their proliferative and migratory state in which they are the main mediators of angiogenesis. Secretion of proteases leads to the disruption of the endothelial cell basement membrane and matrix interactions allowing them to proliferate, migrate and synthesise a new basement membrane. This forms a sprout that will eventually develop into a new vessel (Khazaei et al., 2008).

There are two principal stimuli that are thought to stimulate angiogenesis, ischemia and hypoxia, as well as some less studied factors including shear stress (Simons, 2005). Angiogenesis can be stimulated by the hypoxia-inducible factor (HIF)-1α system that is triggered by a reduction in tissue oxygenation. HIF-1α activates the transcription of many genes and growth factors, including vascular endothelial growth factor (VEGF), one of the most potent mediators of angiogenesis (Simons, 2005). Shear stress is a physiological parameter that can guide vascular architecture to stimulate angiogenesis. Endothelial cells sense changes in shear stress that trigger molecular events, enabling vascular remodelling and development. It is reported that there is a shear stress threshold of above 10 $dyn.cm^{-2}$ that when surpassed induces angiogenic sprouting regardless of whether the shear is applied luminally or transmurally (Galie et al., 2014). Endothelial cells are thought to integrate signals from shear stress and local VEGF to achieve vessel dilation and sprouting (Song and Munn, 2011). It is suggested that damaged occluded vessels that are exposed to little shear stress become hypoxic and

produce VEGF. These vessels dilate and become leaky allowing VEGF to leave and promote a positive VEGF gradient on nearby endothelial cells from other vessels. Positive VEGF gradients initiate vessel sprouting towards the diseased vessel.

1.1.1.1 Vascular Endothelium Growth Factor

The most prominent genes that are induced by HIF-1α and are directly involved in angiogenesis is the VEGF family. VEGF is a potent angiogenic factor and was first described as an endothelial specific mitogen that is an essential growth factor for vascular endothelial cells (Leung et al., 1989; Keck et al., 1989). To date, the VEGF family is comprised of 5 members, VEGF-A, -B, -C, -D, -E, placenta growth factor (PlGF) and snake venom VEGF (Takahashi and Shibuya, 2005). Human VEGF-A (known in the literature as VEGF) has at least 9 subtypes, $VEGF_{165}$ in particular is reported to play a central role in vascular development and angiogenic processes. VEGF-A is a dimeric glycoprotein that exhibits two major biological activities; one is mediating endothelial cell proliferation and the other is the capacity to increase vascular permeability (Keck et al., 1989). It exhibits these processes by interacting with three tyrosine kinase receptors, vascular endothelium growth factor receptor (VEGFR) 1, VEGFR-2 and VEGFR-3. Each receptor has seven extracellular domains, a single transmembrane region, and a consensus tyrosine kinase sequence interrupted by a kinase insert domain (Hoeben et al., 2004).

VEGF-A acts mainly via VEGFR-1 and VEGF-2. VEGF-1 is a 180 kDa high-affinity receptor for VEGF-A expressed on vascular endothelial cells, macrophages, monocytes and haematopoietic stem cells (Takahashi and Shibuya, 2005; Hattori et al., 2002; Sawano et al., 2001). VEGFR-1, which binds VEGF-A with a 10-fold higher affinity compared to VEGFR-2, is involved in promoting signalling pathways involved in angiogenesis under pathological conditions such as cancer, ischaemia and inflammation (Figure 1.2) (Takahashi and Shibuya, 2005). VEGFR-2 is a 200-230 kDa high-affinity receptor for VEGF-A. It is expressed in vascular and lymphatic endothelial cells as well as other cell types including megakaryocytes and haematopoietic stem cells (Katoh et al., 1995). It is the major mediator of VEGF-A induced mitogenesis and angiogenesis VEGF-A. It is also responsible for signals initiating endothelial cell permeability, growth and survival signalling (Figure 1.2) (Takahashi and Shibuya, 2005). The ligands for VEGFR-3 on the other hand are VEGF-C and VEGF-D and are essential for lymphangiogenesis. VEGF-C knockout

mice present with deficient lymph vessel sprouting that was rescued by VEGF-C and VEGF-D (Karkkainen et al., 2004). VEGF-A does not bind to VEGFR-3 in endothelial cells.

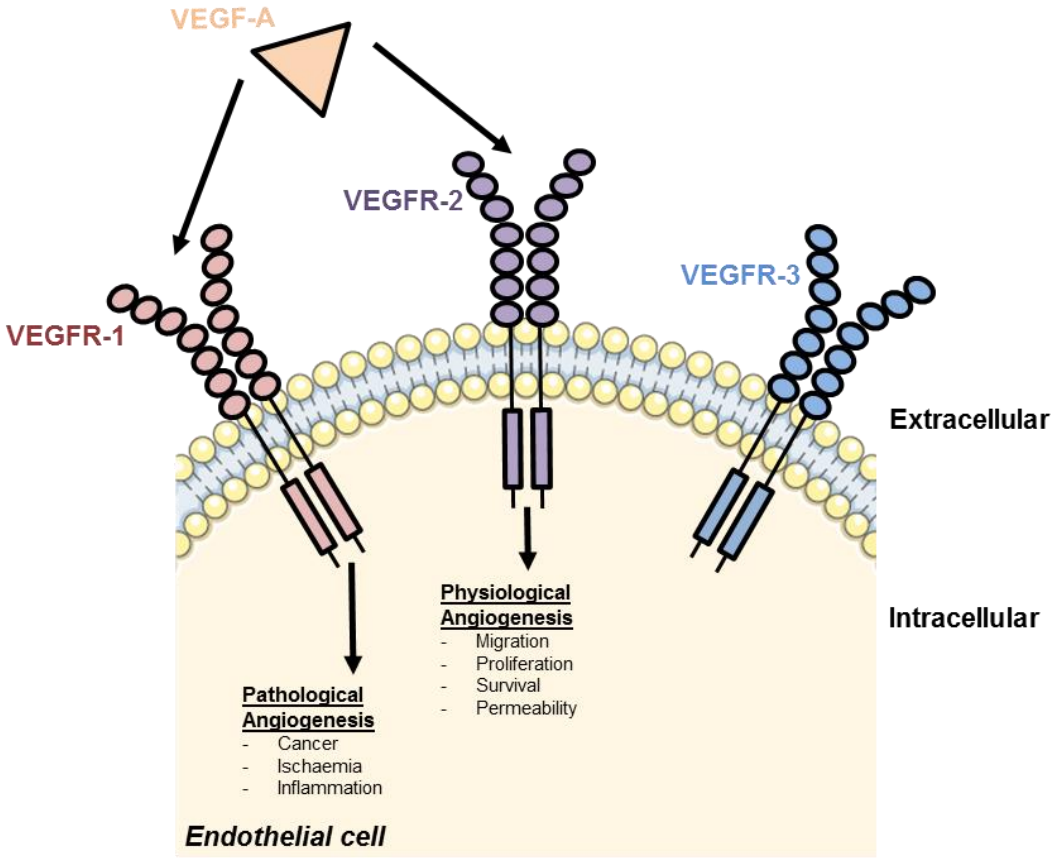

Figure 1.2 VEGF-A regulation of angiogenesis in endothelial cells.

Vascular endothelial growth factor (VEGF) binds to VEGF receptor-1 and 2 (VEGFR1 and VEGF2) to stimulate downstream signalling in endothelial cells. VEGF does not bind to VEGFR-3 in endothelial cells.

1.1.2 Regulation of blood vessel tone

Endothelial cells play a crucial role in controlling vessel tone and homeostasis in response to changes in hemodynamic force. They do this by controlling the production and release of nitric oxide (NO); the main vasodilator released by endothelial cells. Vascular homeostasis entails keeping a tightly controlled balance between a vasodilatory state, which is often associated with anti-oxidant, anti-

inflammatory and anti-thrombotic effects on one hand, and a vasoconstrictor state on the other, which is associated with pro-oxidant, pro-inflammatory and pro-thrombotic effects.

1.1.2.1 Endothelial nitric oxide synthase

In 1980, Furchgott and Zwadzki first described the existence of an endothelium-derived relaxing factor (EDRF) (Furchgott and Zawadzki, 1980). They demonstrated in rabbit aortic rings that the acetylcholine evoked relaxation was abolished when the intact endothelium was removed. In fact, in aortic rings with denuded endothelium acetylcholine was able to cause constriction. Several years later NO was established as the EDRF (Palmer et al., 1987). NO is generated by the conversion of L-arginine to L-citrulline by the NO synthase (NOS) family of enzymes (Figure 1.3) (Palmer et al., 1988). There are three members of the NOS family, ‘neuronal’ NOS (nNOS/NOS I), ‘inducible’ NOS (iNOS/NOS II) and ‘endothelial’ NOS (eNOS/NOS III) (Forstermann et al., 1994). eNOS is the predominant NOS isoform present in the vasculature and is responsible for the production of most of the NO in this tissue. In the vasculature NO causes dilation of vessels through guanylyl cyclase stimulation increasing cyclic guanosine monophosphate (cGMP) in smooth muscle cells to decrease Ca^{2+}, stimulating them to relax (Figure 1.3). NO also regulates proliferation and migration of endothelial cells, extracellular matrix degradation and angiogenesis (Cooke and Losordo, 2002).

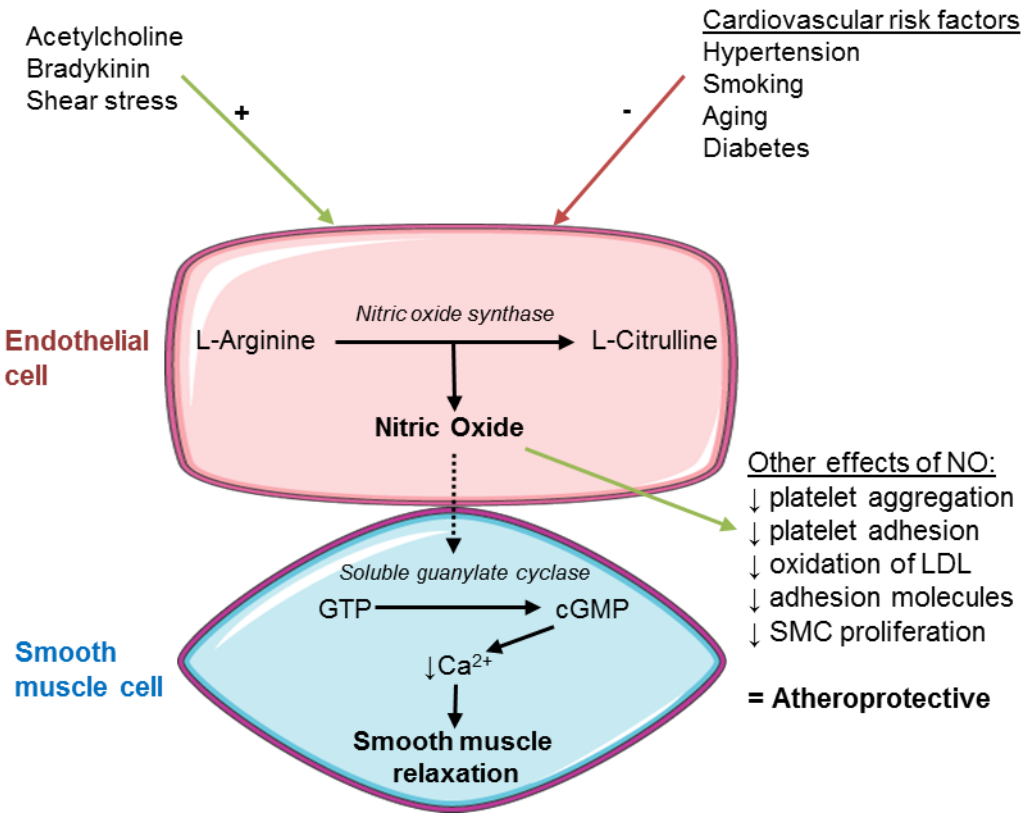

Figure 1.3 Nitric oxide regulation of the cardiovascular system.

Nitric oxide synthesis by the conversion of L-Arginine to L-Citrulline is catalysed by endothelial nitric oxide synthase. Nitric oxide diffuses into smooth muscle cells. Here soluble guanaylate cyclase catalyses the conversion of GTP to cGMP that causes contraction. This process can be potentiated or attenuated by various stimulants or cardiovascular risk factors.

eNOS is a 1,203 amino acid, 133 kDa protein that has a bi-domain structure functioning as a dimer. It is compiled of an N-terminal oxygenase domain containing binding sites for heme, L-arginine and tetrahydrobiopterin (BH4) and a COOH-terminal reductase domain with binding sites for nicotinamide adenine dinucleotide phosphate (NADPH), flavin mononucleotide (FMN), flavin adenine dinucleotide (FAD) and Ca^{2+}/Calmodulin (CaM) (Fleming, 2010). During the synthesis of NO, NADPH derived electrons are transferred to FAD, FMN and then to the heme located in the oxygenase domain of the opposing monomer. This allows the heme iron to bind oxygen and catalyse the stepwise synthesis of NO from L-arginine. Initially eNOS was classified as a Ca^{2+}/CaM-dependent enzyme with low but measureable activity at low resting levels of intracellular Ca^{2+} (Busse and Mulsch, 1990). Under basal conditions caveolin (Cav) maintains eNOS in an inactivated state. An increase in intracellular Ca^{2+} binds to CaM and disrupts the eNOS-Cav

interaction. Association of CaM with its binding site is generally suggested to activate NO synthesis by enabling the reductase domain to transfer electrons to the oxygenase domain (Fleming, 2010). Evidence now suggests that numerous physical and chemical stimuli affect eNOS activity. Fluid shear stress, generated by drag of blood creating a laminar frictional force against endothelial cells, is an example of a physical stimuli activating eNOS. Chemical stimuli include acetylcholine and bradykinin (Figure 1.3) (Fleming, 2010).

1.1.2.1.1 Phosphorylation sites evoking eNOS activation

eNOS can be phosphorylated at multiple sites and depending on the site this can activate or inhibit its activity. The sites that are important in this thesis will be discussed in more detail (Figure 1.4). S1177 is rapidly phosphorylated in human umbilical vein endothelial cells (HUVECs) by various stimuli including shear stress (Dimmeler et al., 1999), VEGF (Dimmeler et al., 2000) and Bradykinin (Fleming et al., 2001) leading to an increase in eNOS activation and NO production. The kinase involved in the phosphorylation of S1177 eNOS varies depending on the stimuli, for instance, shear stress evokes S1177 phosphorylation via AKT/PI3K, protein kinase A (PKA) and 5' adenosine monophosphate-activated protein kinase (AMPK) (Boo et al., 2002b; Hurt et al., 2002; Zhang et al., 2006) whereas VEGF acts via AKT/PI3K (Dimmeler et al., 2000)(Figure 1.4). The bradykinin-, Ca^{2+} ionophone-, phosphorylation of S1177 is mediated by the Ca^{2+} sensitive kinase CAM kinase II (CAMKII) (Schneider et al., 2003).

There are other serine phosphorylation sites on eNOS that evoke eNOS activation. S633 is phosphorylated by shear stress and VEGF (Boo et al., 2002a) via PKA, but this is much slower than S1177. Bradykinin-stimulated phosphorylation of S633 is independent of Ca^{2+} and is abolished by inhibiting PKA (Michell et al., 2002). On the other hand, bradykinin-stimulated phosphorylation of S615 is Ca^{2+} dependent and acts at this site via AKT by increasing Ca^{2+}-CaM sensitivity whereas VEGF acts to phosphorylate this site via PKA (Michell et al., 2002).

1.1.2.1.2 Phosphorylation sites evoking eNOS inhibition

As well as sites that activate eNOS activity there are phosphorylation sites that inhibit it. The T495 site is constitutively phosphorylated in all endothelial cells

examined to date. It acts as a negative regulatory site that suppresses eNOS activity (Fleming et al., 2001). One way in which phosphorylation of this site dampens eNOS activity is by preventing the binding of CaM. Bradykinin elicits CaMKII mediated phosphorylation of eNOS S1177 but CaMKII independent phosphorylation of T495. To allow agonists, i.e. bradykinin to activate eNOS the stimulation of a phosphatase, probably protein phosphatase 1 (PP1), is critical to dephosphorylate T495 and thus, facilitate CaM binding and NO production (Fleming et al., 2001). The constitutively active kinase which phosphorylates eNOS T495 is most likely protein kinase C (PKC), however there is some confusion regarding the specific isoform/isoforms involved (Michell et al., 2001; Davda et al., 1994). Y657 is another inhibitory phosphorylation site on eNOS and it was initially linked to shear stress mediated phosphorylation (Ayajiki et al., 1996) via protein tyrosine kinase 2 ß (PYK2) (Fisslthaler et al., 2008). A number of other stimuli have been reported to lead to PYK2 activation in endothelial cells including insulin (Fisslthaler et al., 2008) and Angiotensin II (Yin et al., 2003). Insulin is interesting. It is reported to evoke vasodilation *in-vivo* however, reports suggest that it fails to activate eNOS in freshly isolated arteries (Fleming et al., 2003; Randriamboavonjy, 2004) even though it stimulates rapid AKT mediated S1177 eNOS phosphorylation. It could be possible that activation of PYK2 mediated Y657 phosphorylation of eNOS antagonises the effects of S1177 phosphorylation (Fisslthaler et al., 2008).

As well as regulating vasomotor functions, NO also has cardio-protective functions. It has actually been described as a ‘major weapon’ of endothelial cells to fight vascular disease. NO is a potent inhibitor of leukocyte adhesion to the vessel wall which may protect against the onset of atherogenesis (Matthys and Bult, 1997). Furthermore, NO also protects against smooth muscle cell proliferation as well as platelet aggregation and adhesion, which protects smooth muscle from exposure to platelet-derived growth factors (PDGF) (Jeremy et al., 1999). Thus, NO can also protect against fibrous plaque formation in the later stages of atherogenesis. NO is a particularly important mediator of endothelium-dependent vasodilation, anti-inflammatory and antithrombotic effects of the endothelium and endothelium-dependent vasomotion (Landmesser et al., 2004). Other endothelium-derived vasodilators include prostacyclin (PGI_2), a cyclooxygenase-dependent metabolite of arachidonic acid (AA) (Dusting et al., 1978) and the putative endothelium-derived hyperpolarising factor (EDHF).

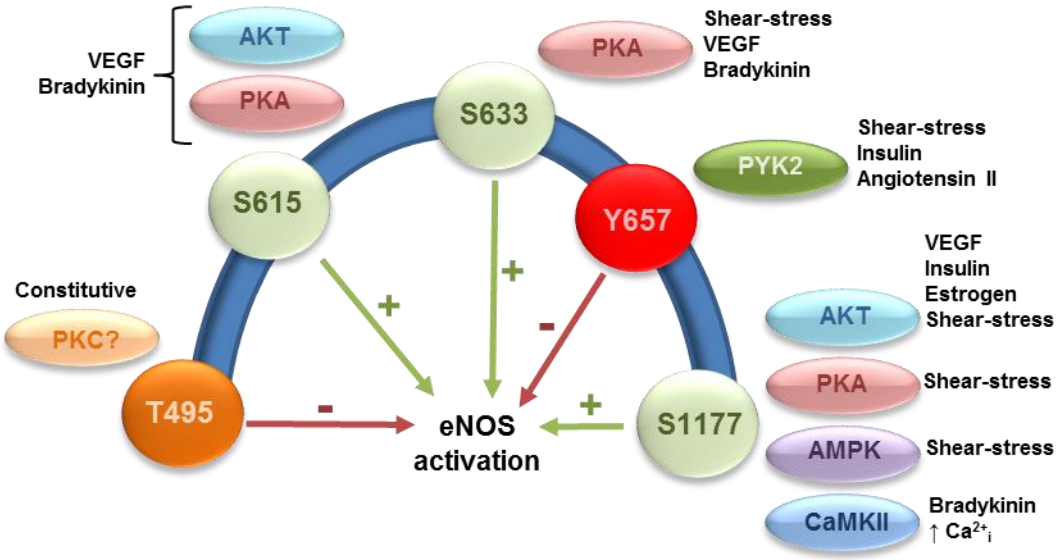

Figure 1.4 The regulation of eNOS by different phosphorylation sites.

Schematic of relevant confirmed eNOS phosphorylation sites and their effect on eNOS activity (green arrows indicate activation and red arrows indicate inhibition). Adapted from a review by (Fleming, 2010).

1.1.2.2 Endothelium-derived hyperpolarising factor

In 1988 Taylor and Weston first described the concept of NO independent relaxation (Taylor and Weston, 1988). They suggested that endothelial-dependent relaxation of vascular smooth muscle cells reflected the release of an additional factor to NO. Relaxation of the vascular tone of small resistance arteries appears to be predominately due to the action of a hyperpolarising factor that is distinct from NO (Garland et al., 1995), whereas NO plays more of a prominent role contributing to relaxation of large conducting arteries. The hyperpolarising factor that leads to NO independent relaxation is named EDHF.

Hyperpolarisation occurs in endothelial cells as a result of activation of the small and intermediate-conductance Ca^{2+}-activated K^+ channels (SK_{Ca}^{2+} and IK_{Ca}^{2+}), triggering positively charged K^+ efflux (Edwards et al., 1998). This in turn, leads to hyperpolarisation of vascular smooth muscles cells, evoking vessel relaxation. The mechanism underlying EDHF has not been definitively determined (Busse et al., 2002). However, a couple of hypotheses have been proposed. One idea is that gap junctions exist between endothelial cells and smooth muscle cells allowing the movement of small molecules. Therefore, the electrical signal may simply be

transferred freely between the cells. Another hypothesis is that a substance might be released from endothelial cells that acts on smooth muscle cells.

Even though the role of EDHF in cardiovascular disease remains to be further elucidated, the contribution of EDHF and its importance in small arteries suggests an opportunity to control systemic blood pressure. Better understanding of molecular regulators of blood pressure could lead to developing novel drug treatments for hypertension and other vascular disorders.

1.2 Endothelial dysfunction

Vascular pathology, such as cardiac disease and stroke, remains amongst the commonest cause of death worldwide. Most forms of vascular disease are due to functional changes in the vascular wall. Endothelial dysfunction can be caused by injury or cellular damage that leads to compensatory responses that alter the normal homeostatic properties of the endothelium. Endothelial dysfunction leads to an imbalance between factors that usually maintain vascular homeostasis including relaxing and contracting factors, pro and anti-coagulant mediators and growth-promoting and growth-inhibiting factors (Cooke, 2000). It is increasingly recognised that these compensatory responses can lead to various cardiovascular pathologies including atherosclerosis, angina, myocardial infarction, coronary artery disease and hypertension (Cooke, 2000; Khazaei et al., 2008). Therefore, the endothelium is often the site at which cardiovascular disease begins and consequently can act as a measure of cardiovascular health. Thus, investigation into targeting endothelial dysfunction and treatment of early endothelial dysfunction is important.

1.2.1 Atherosclerosis

Atherosclerosis is a systemic disease triggered by chronic inflammatory processes. It is characterised by the thickening of the intimal and medial layers of the arteries due to the deposition of atheromatous plaques along the vessel together with loss of elasticity (Lahoz and Mostaza, 2007). The main risk factors pre-disposing patients to atherosclerosis are hypertension, smoking, aging and diabetes, all of which contribute to endothelial dysfunction. Endothelial dysfunction leads to the switch of endothelial cells to their pro-inflammatory and pro-thrombotic phenotype leading to the increased expression of leukocyte adhesion molecules and

cytokines. These changes increase monocyte adhesion and penetration through the vascular wall.

1.2.1.1 Atherosclerosis progression and development

It is widely reported that impaired endogenous atheroprotective mechanisms occur at branch points in arteries. These areas are particularly vulnerable as the endothelial cells are subject to disturbed flow. Absence of a laminar frictional force may reduce the local production of NO, which in turn would render the vessels pro-inflammatory (Libby, 2002; Topper et al., 1996). Healthy endothelium, in areas of laminar flow, does not in general support binding of white blood cells. However, early after initiation of atherogenic risk factors, patches of endothelial cells begin to express cell surface markers that bind to leukocytes and cause enhanced endothelial cell permeability (Libby, 2002). Vascular cell adhesion molecule 1 (VECAM-1), in particular, binds to the type of leukocytes involved in atherogenesis. After being fed a high-cholesterol diet, VECAM-1 knockout mice show significantly reduced areas of atherosclerotic lesions compared to littermate controls (Cybulsky et al., 2001). Once adherent to the endothelium, pro-inflammatory cytokines provide a chemotactic stimulant that mediates the migration of adherent leukocytes into the intimal layer of the vessel. This transmigration is suggested to be due to certain chemoattractant molecules including, monocyte chemoattractant protein-1 (MCP-1) (Gu et al., 1998). Once this migration has occurred an immune response is triggered. Macrophages express scavenger receptors for modified lipoproteins permitting them to ingest lipid, including low density lipoprotein (LDL) and become foam cells. Lipoproteins, monocytes and macrophages are able to accumulate in the vessel wall due to an increase in vessel permeability, a key characteristic of endothelial dysfunction. Atherosclerotic lesion progression leads to the switch of medial smooth muscle cells to their migratory and proliferatory phenotype and an increase synthesis of extracellular matrix molecules such as collagen, elastin and proteoglycans as a protective mechanism to repair the endothelium (Libby et al., 2011). Macrophages and smooth muscle cells that have accumulated in the intimal layer of the vessel begin to die and their lipid contents can accumulate in the central region of the plaque, this is the necrotic core (Libby et al., 2011). Plaque development compromises the artery lumen as it narrows. Thinning of the fibrous cap of the plaque leads to loss of integrity of the cap which in turn, triggers clot development which results in blockade of the vessel lumen and subsequent blockage of blood flow (Libby et al., 2011; Khazaei et al., 2008). Obstruction of

vessels i.e. coronary arteries, supplying the heart with blood results in a heart attack and obstruction of vessels supplying the brain with blood results in a stroke.

1.2.2 Endothelial cells in hypertension

In healthy vessels, the endothelium maintains a balance between opposing dilation and constriction signals to maintain vascular tone. An imbalance in this homeostasis, leaning to towards excessive constriction and vascular wall thickening and stiffening leading to hypertension is a major feature of endothelial dysfunction. Endothelial damage occurs in many vascular beds during hypertension. However, it is unclear whether hypertension is the cause or result of this damage (Bleakley et al., 2015). It was first suggested that endothelial dysfunction is proportional to the course of chronic hypertension and thus, was suggested to be a consequence of hypertension (Moncada and Vane, 1979). Moreover, Panza et al demonstrated that clinically effective antihypertensive therapy does not improve endothelial dysfunction (Panza et al., 1993).

As already discussed, in healthy endothelium, NO synthesis is catalysed by eNOS and once generated it is able to diffuse into the vascular smooth muscle to cause vessel relaxation as well as inhibiting leukocyte adhesion and having anti-thrombotic and anti-proliferative effects. However, as a free radical, NO is subject to scavenging by both reactive oxygen species (ROS) and superoxide which further enhances NO scavenging thereby further reducing NO bioavailability (Bleakley et al., 2015). Even though superoxide is degraded by superoxide dismutase (SOD), superoxide scavenges NO three times faster than this, subsequently further reducing NO bioavailability (Flammer and Luscher, 2010; Bleakley et al., 2015). In hypertension, the chronic increase in systemic pressure in the microvasculature leads to premature aging and increased endothelial cell turnover. The endothelium then regenerates. However, this regenerated endothelium has an impaired ability to release relaxing factors consequently causing vasoconstriction (Bleakley et al., 2015). The microcirculation is the most vulnerable to insult from sustained pressure elevation, namely the cerebral, ocular and renal beds. Investigations currently underway are likely to produce novel therapeutic strategies which target endothelial dysfunction in the prevention or treatment of atherosclerosis and other vascular diseases (Cooke, 2000). Various Ca^{2+} sensitive ion channels have been linked to the progression of various cardiovascular diseases, including hypertension and thus could be attractive therapeutic targets.

1.3 Ca^{2+}: the key signalling cation in endothelial cells

Endothelial cells can regulate vascular homeostasis and perform a variety of physiological functions by way of complex intracellular signalling pathways. Many of these intracellular signalling pathways feature Ca^{2+}, a highly ubiquitous and versatile second messenger. Ca^{2+} has been described as a dynamic master intracellular regulator of mammalian cell biology (Berridge et al., 2003; Clapham, 2007). Finely tuned control of intracellular Ca^{2+} and its signalling is fundamental for both survival and death in biological organisms. Ion channels that are permeable to Ca^{2+} often have a positive effect on cell activity including; proliferation, migration and survival. However, more recently a role for Ca^{2+} as a cytotoxic trigger of either apoptotic or necrotic cell death has been discovered (Clapham, 2007; Orrenius et al., 2003; Berridge et al., 2000). Ca^{2+} triggers numerous cellular events including exocytosis during synaptic transcription and gene expression and transcription, which occur over a more prolonged time course (Figure 1.5) (Dolmetsch et al., 1998). All of these processes are essential for vascular development and physiological function (Beech, 2013). In vascular endothelial cells, Ca^{2+} channels are reported to play a pivotal role mediating cell migration, proliferation and angiogenesis as shown by tube formation (Li et al., 2011a; Li et al., 2011b; Li et al., 2014). Thus, careful regulation of intracellular Ca^{2+} levels is essential. Aberrant Ca^{2+} signalling is described as a key feature of a variety of diseases including cardiovascular disease (Clapham, 2007; Monteith et al., 2012).

1.3.1 Ca^{2+} handling and homeostasis

Ca^{2+} cannot be chemically altered and thus cells must import, chelate, store or extrude Ca^{2+} in order to maintain intracellular Ca^{2+} homeostasis. The resting intracellular Ca^{2+} concentration is strictly maintained at approximately 100 nM which is considerably lower than the extracellular concentration that is in the mM range (Clapham, 2007). Ion channels are one of the many proteins involved in the coordination of Ca^{2+} signalling, orchestrating Ca^{2+} handling whilst ensuring the maintenance of a 20,000-fold Ca^{2+} gradient across the plasma membrane, creating a strong inward driving force (Clapham, 2007; Berridge et al., 2003). A finely tuned regulation of Ca^{2+} is critical and a slight increase or decrease in intracellular Ca^{2+} can be cytotoxic to the cell. To overcome such an event Ca^{2+} levels need to be buffered to maintain normal intracellular Ca^{2+} levels.

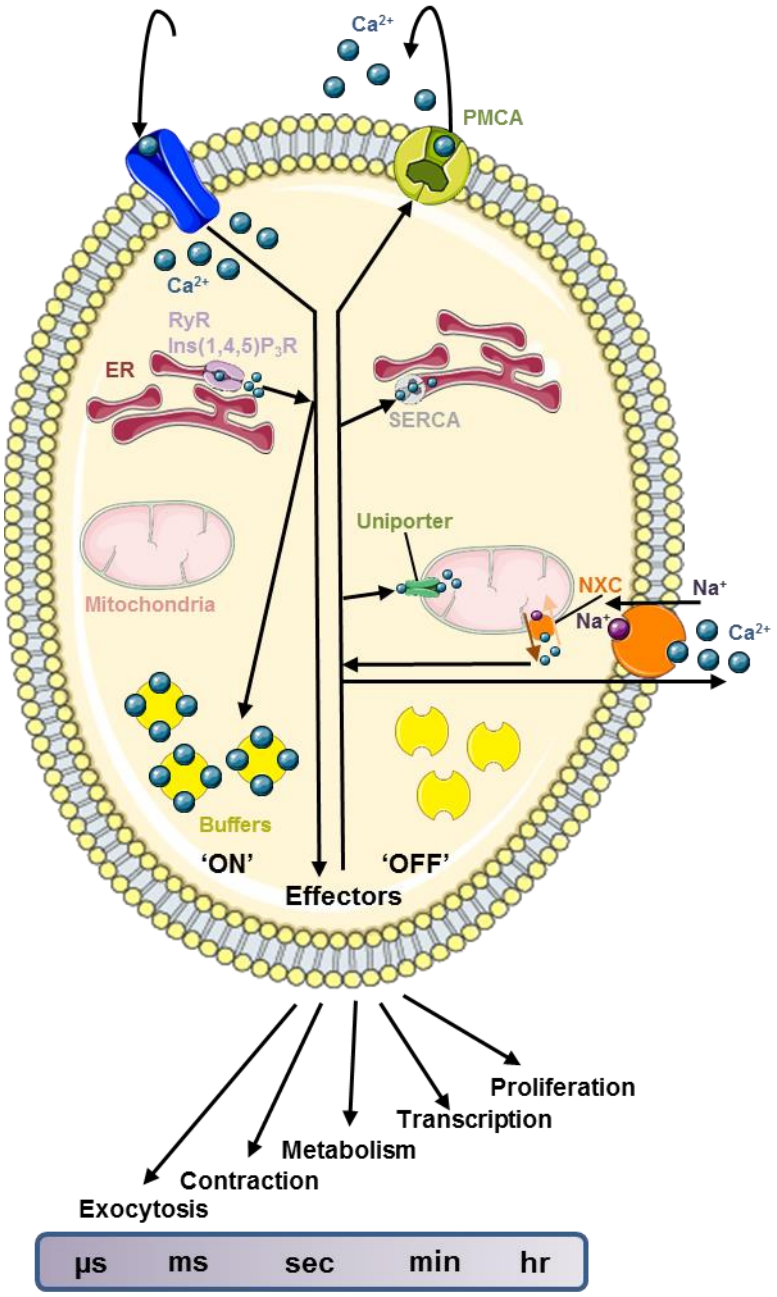

Figure 1.5 Overview of Ca^{2+} handling.

Stimuli induce Ca^{2+} entry from the extracellular side of the cell. The majority of Ca^{2+} is stored in the endoplasmic reticulum (ER) where it is released through inositol-1,4,5-trisphosphate receptor (Ins(1,4,5)P3R) and ryanodine receptor (RYR) related mechanisms and recycled via the sarcoplasmic reticulum Ca^{2+} ATPase (SERCA) extrusion pump. Ca^{2+} also sequesters in the mitochondria where it is pumped in via the uniporter**.** Most of the Ca^{2+} (indicated by the blue circles) is bound to buffers leaving the remainder to bind to effectors and activate a dynamic range of cellular processes that can be achieved over a range of time periods. Ca^{2+} leaves the cell through various exchangers (NCX) and pumps (PMCA) ensuring a 20,000 fold gradient is kept constant granting cell survival. Adapted from (Berridge et al., 2003).

1.3.1.1 Ca^{2+} buffers, pumps and exchangers

Ca^{2+} chelating proteins have evolved to bind Ca^{2+}, playing roles in buffering Ca^{2+} homeostasis and triggering cellular processes (Figure 1.5). CaM is a small, ubiquitous cytoplasmic Ca^{2+} buffer and sensor. Ca^{2+} binds to CaM which, in turn, propagates signals to proteins containing CaM binding sites that cannot bind Ca^{2+} directly (Clapham, 2007). Ca^{2+} is stored in intracellular organelles including the endoplasmic reticulum (ER) and mitochondria contributing to intracellular Ca^{2+} homeostasis (Figure 1.5). Mitochondria have been reported to be recruited to areas of high Ca^{2+}. Here, Ca^{2+} enters the mitochondria through mitochondrial Ca^{2+} specific uniporters to enhance local Ca^{2+} buffering (Yi et al., 2004; Kirichok et al., 2004). The main internal Ca^{2+} store lies within the ER and it has been reported that there is significant interplay between both the ER and mitochondria with regards to Ca^{2+} storage (Pizzo and Pozzan, 2007). Release of Ca^{2+} from the ER is controlled by the inositol-1,4,5-trisphosphate receptor (InsP3R) and the ryanodine receptor (RYR) (Berridge et al., 2003; Clapham, 1995) The reuptake and recycling of Ca^{2+} back into internal stores is regulated by the sarcoplasmic reticulum Ca^{2+} ATPase (SERCA) pump (Figure 1.5). Chronic activation of ER stress by abnormal lipid load inhibiting the SERCA pump has been reported to play an important role in the development of insulin resistance and diabetes in obesity (Hotamisligil, 2010; Fu et al., 2011). Additionally, mutations in InsP3R1 *in-vivo* uncovered a novel role of InsP3R1 in regulation of glucose homeostasis and development of diet-induced diabetes (Ye et al., 2011).

Ca^{2+} extrusion from the cell is often powered by ATP dependent mechanisms and allows the movement of Ca^{2+} against its concentration gradient. Plasma membrane Ca^{2+} ATPases (PMCA) can respond to modest increases in intracellular Ca^{2+} levels. Similarly, the Na^{+}- Ca^{2+} exchanger (NCX) facilitates Ca^{2+} extrusion from the cell in exchange for a Na^{+} ion and this has much greater transport rates (Figure 1.5) (Berridge et al., 2003). Endothelial cell dysfunction has been linked to altered NCX activity and Ca^{2+} handling in diabetic cardiomyopathy (Sheikh et al., 2012). Moreover, glucose has been reported to control the transcription, expression and activity of Ca^{2+} extrusion mechanisms by inducing an increase in NCX and decrease in PMCA (Herchuelz et al., 2007).

1.3.1.2 Ca^{2+} entry mechanisms

Voltage-gated Ca^{2+} channels are located on the plasma membrane of excitable cells where they transduce changes in voltages to transient increases in intracellular Ca^{2+} (Catterall, 2011). Upon depolarisation the voltage sensing mechanism of the channel responds, allowing Ca^{2+} entry. There are 10 members of the voltage-gated Ca^{2+} family with three subtypes (Cav1, 2 and 3). More specifically, the Cav1.2 (L-type) channel is involved in excitation-contraction coupling of cardiomyocytes (Catterall, 2011). This channel is the target for various Ca^{2+} antagonist drugs including nifedipine, nimodipine and verapamil used therapeutically to treat hypertension and arrhythmias. Voltage-gated Ca^{2+} channels have evolved our knowledge of Ca^{2+} channels over the years forming the basis of our understanding. A study in 1999 discovered that the inhibition of these voltage-gated Ca^{2+} channel only led to a partial suppression in contraction of the heart (Pierre and Davenport, 1999) and thus, it was hypothesised that other Ca^{2+} channels must be involved. Research into other Ca^{2+} channel modulators as therapeutics is now an attractive area of research.

Store-operated Ca^{2+} entry (SOCE) is a form of Ca^{2+} entry in which Ca^{2+} can enter the cells in response to depletion of the intracellular ER Ca^{2+} store. Depletion of these stores activates a highly selective inward Ca^{2+} current; entitled ICRAC (Ca^{2+} release activated Ca^{2+} current) (Hoth et al, 1992). Orai1 and stromal interaction molecule 1 (STIM1) are the biological components that form the CRAC channel. The discovery of Orai1 emerged through a study of severe combined immune deficiency, where a mutation in Orai1 causes a defect in Ca^{2+} entry of T cells (Feske et al., 2006; Prakriya et al., 2006). It has since been discovered that Orai1 is an essential pore subunit of the CRAC channel (Prakriya et al., 2006). STIM1 was discovered the previous year during a RNAi screen (Roos et al., 2005) where knock-down of STIM1 abolished CRAC channel activity. STIM1 encompasses an EF-hand, which has been considered to act as an ER Ca^{2+} sensor (Zhang et al., 2005). If STIM1 senses depletion of Ca^{2+} in the ER it signals to the Orai1 channel in the plasma membrane through a complex process of conformational change, redistribution and clustering with Orai1 proteins activating them to open and enable Ca^{2+} entry into the cell (Cahalan, 2009; Beech, 2012). A major physiological role of SOCE has been implicated in the VEGF induced endothelial function opening up novel opportunities for chemical modulation of angiogenesis (Li et al., 2011a). SOCE channels have also been linked to the development of cancer and metastasis (Prevarskaya et al., 2011; Prevarskaya et al., 2014).

Transient receptor potential (TRP) channels form an important family of promiscuous non-selective cationic channels ubiquitously expressed throughout the body. The initial discovery of the TRP protein dates back to photo-transduction studies in *Drosophila melanogaster*. A spontaneous mutant lead to the observation of a transient response to steady light, in contrast to the sustained response seen in wild-type flies with intact photoreceptors (Minke et al., 1975). 20 years later the mutated gene was cloned (TRPC1) and the TRP non-selective cationic channel was discovered (Wes et al., 1995). It has now been determined that there are 28 genes encoding TRP proteins (Damann et al., 2008). The mammalian TRP family of ion channels contains 6 subfamilies: TRPC (canonical), TRPM (melastatin), TRPV (vanilloid), TRPA (ankyrin), TRPP (polycystin) and TRPML (mucolipin). TRP channels are able to heteromultimerise, increasing their complexity further. Heteromultimerisation can increase the variety of TRP channel characteristics, which can be both advantageous and disadvantageous for their pharmacology. TRP channels are highly expressed in the sensory system where they are activated by various stimuli including menthol and other cold stimuli (<15°c) (TRPM8), capsacin (TRPV1) and cannabinoids i.e. Wasabi (TRPA1) (Jordt et al., 2004; Jordt et al., 2003; McKemy, 2005; Caterina et al., 1997; McKemy et al., 2002). TRPC channels however are reported to play a role in the progression of cardiovascular diseases and cancers where they activate migration and proliferation of various cell types promoting tumour growth and metastasis and neointimal hyperplasia after stent insertion (Chen et al., 2014; Edwards et al., 2010). Although initially hailed as the CRAC channel, the TRPC subfamily has been suggested to be involved in SOCE. Knockdown of TRPC1, TRPC6 and Orai1 but not TRPC3 suppresses SOCE (Brough et al., 2001; Jardin et al., 2008; Liu et al., 2000; Salido et al., 2009). Experiments utilising TRPC channel blockers suggest TRPC channels are only partially mediating the SOCE signal in vascular smooth muscle cells (Li et al., 2011b). Furthermore, it is reported that STIM1 mediates both Orai1 and TRPC1 mediated SOCE and that TRPC1 is associated with Orai1 and STIM1 in a TRPC-Orai1-STIM1 ternary complex (Collins et al., 2013). Although many research groups have provided evidence supporting a role for TRPC proteins in SOCE, this role is still not widely accepted (Salido et al., 2009). Whether any of the TRPC channels function as SOCCs remains controversial.

Piezo is a family of mechanosensory ion channels consisting of two members, Piezo1 and Piezo2. They have been discovered to be important for mechanically

evoked Ca^{2+} entry in various cell types. The FAM38A gene encoding Piezo1 was discovered to be responsible for the mechanically-activated current in the mouse neuroblastoma cell line, Neuro 2A, in response to prodding with a blunt glass pipette (Coste et al., 2010). Piezo1 has now been reported to be important in shear stress-evoked Ca^{2+} entry in multiple cell types including endothelial cells, red blood cells, cancer cells (gastric, breast and lung), pancreatic acinar cells, epithelial cells of the kidney, lung and bladder (Li et al., 2014; Miyamoto et al., 2014; Cahalan et al., 2015; Romac et al., 2018; Yang et al., 2014; McHugh et al., 2010; McHugh et al., 2012). Piezo1 is discussed in more detail later in this chapter.

1.4 Shear stress sensing in the vasculature

Mechanotransduction defines the conversion of mechanical force into cellular signals and it is essential for physiological function. The ability for cells to sense and adapt to their environment is critical for their survival and they have developed specialised sensors for this. Mechanical forces influence every area of physiology, from the development of the embryo e.g. development of the immature vascular plexus to development of adult physiology, including the senses of touch and hearing. Moreover, pathological mechanical forces resulting in subsequent mechanosignalling induces tumour metastasis and atherosclerosis (Conway and Schwartz, 2013; Wei and Yang, 2016). In the cardiovascular system, the mechanical force evoked by the frictional force on endothelial cells created from the flow of blood is a critical determinant of vascular homeostasis and pathological processes. Human physiological shear stress ranges from 1 – 70 $dyn.cm^{-2}$ depending on the blood vessel. Arteries experience higher shear stress compared to veins and larger vessels, e.g. the aorta, have lower shear than smaller vessels (Tzima et al., 2005). As hemodynamic forces control the development, structure and function of blood vessels it is not surprising that these forces have been implicated in the pathogenesis of vascular disorders. Vascular smooth muscle cells present in the vessel wall are sensitive to cyclic stretching and this is reported to stimulate synthesis of collagen (Leung et al., 1976; Rodriguez-Feo et al., 2005). However, an abundant synthesis of collagen can lead to the development of fibrosis and an increased vessel stiffness. Moreover, an increase in cardiac load evokes cardiac remodelling resulting in cardiac hypertrophy (Dorn, 2007). Inflammatory flow patterns, including disturbed flow and low flow conditions contribute to atherosclerotic plaque formation (Hahn and Schwartz, 2009).

In-vivo blood flow exhibits different patterns depending on vessel geometry. Laminar flow is characterised by uniform flow which occurs in straight areas of the vasculature, such as the descending aorta. In these areas endothelial cells are not proliferative, they align in the direction of flow and form large stress fibres (Figure 1.6) (Givens and Tzima, 2016). Areas of laminar flow are also highly anti-inflammatory expressing gene regulators such as krüppel-like Factor 2 (KLF2) and produce NO and VEGF. Thus, are relatively resistant to atherogenesis (Figure 1.6) (Parmar et al., 2006). On the other hand, areas of disturbed and oscillatory flow, i.e. bifurcation points in vessels are much more atheroprone. Endothelial cells exposed to this flow pattern are cobblestone like in appearance, are much more proliferative and express inflammatory adhesion molecules, e.g. VECAM-1 (Malek et al., 1999). Shear stress acting on endothelial cells is sensed by mechanosensors and this is subsequently converted into biochemical signals which triggers changes in transcription and alters endothelial cell function.

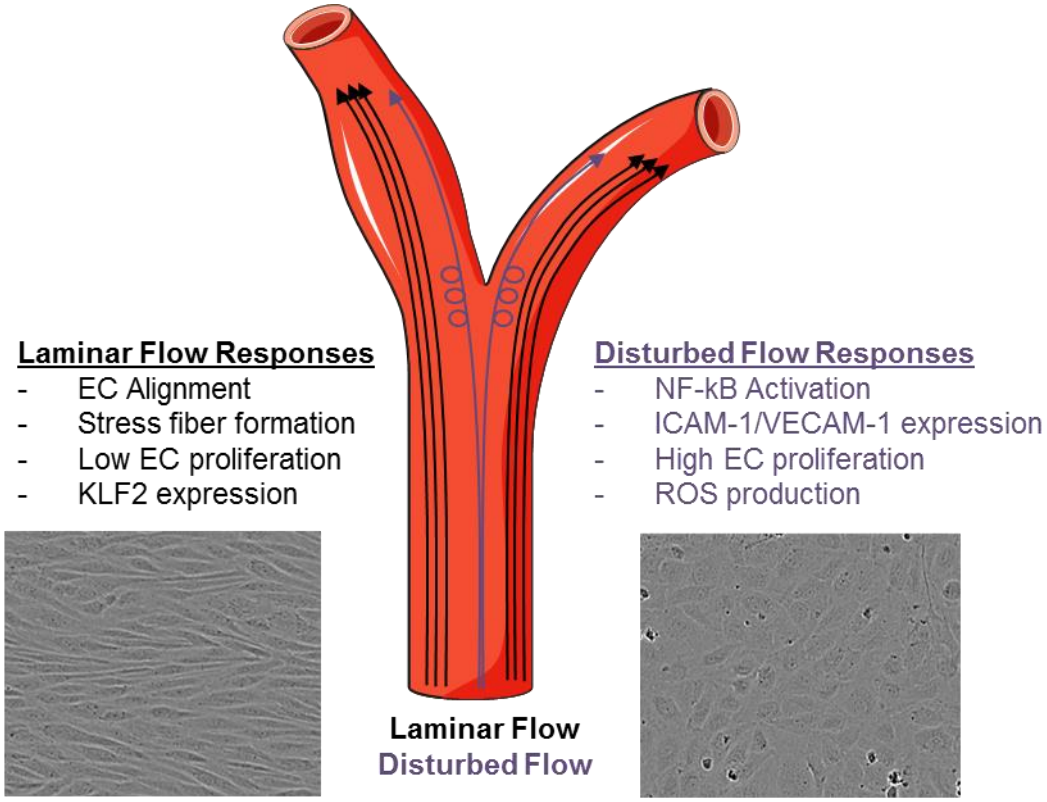

Figure 1.6 The main types of blood flow in the vasculature.

Laminar flow that occurs in straight regions of vessels evokes endothelial cell (EC) alignment, stress fiber formation, low EC proliferation and expression of anti-inflammatory genes. Areas of disturbed flow, at bifurcations of arteries are much more atheroprone. ECs are much more proliferative and express inflammatory genes including VECAM-1.

1.4.1 Mechanosensors of endothelial cells

The mechanisms by which endothelial cells sense and respond to shear stress remain enigmatic. Acute onset of shear stress triggers a variety of events including the modulation of various membrane proteins, extracellular matrix proteins and adhesion molecules. The proposed mechanisms by which endothelial cells sense shear stress are summarised in Figure 1.7 and some of the mechanisms pertinent to this thesis will be discussed in more detail below.

1.4.1.1 CD31 / VE-Cadherin / VEGFR2 expressing triad complex

Endothelial cell functions are dependent on adhesion proteins. Platelet endothelial cell adhesion molecule (PECAM-1), also known as cluster of differentiation 31 (CD31) is an adhesion molecule that is expressed on a variety of cells, including platelets, monocytes, neutrophils and endothelial cells. It is clustered at cell-cell junctions as it enables homophilic binding of cells to their neighbors. Vascular endothelial cell cadherin (VE-Cadherin) is another adhesion molecule located at points of cell-cell contact specifically in endothelial cells. It is connected with the cytoskeleton through the adhesion molecule, ß-catenin. VE-Cadherin is required for VEGF-dependent cell survival, vessel remodeling and maturation of the vascular network (Carmeliet et al., 1999). VEGF works by binding to its receptor (VEGFR), more specifically VEGFR2 in endothelial cells. It is an important signaling molecule involved in both the formation of the circulatory system and angiogenesis (Carmeliet et al., 1999).

CD31 itself has been reported to act as a mechanotransduction molecule. Rapid tyrosine phosphorylation of CD31 and extracellular signal-regulated kinases (ERK) activation has been reported after application of shear stress (Osawa, 2002). Furthermore, stretch- and flow-induced CD31 tyrosine phosphorylation in intact endothelial cells is abolished when Fyn kinase, a member of the src family of kinases, is down-regulated (Chiu et al., 2008). Data suggest that Fyn kinase and CD31 are essential components of a mechanosensory complex. Shear stress has also been reported to cause the redistribution of both VE-Cadherin and VEGFR2 on the plasma membrane of endothelial cells (Chen et al., 1999; Noria et al., 1999). It is reported that flow evokes VEGFR2 to form clusters on the plasma membrane. It in turn binds to the adaptor protein Shc, recruits phosphatidylinositol-4,5-

bisphosphate 3-kinase (PI3K) and activates AKT and subsequent eNOS phosphorylation (Chen et al., 1999).

CD31, VE-Cadherin and VEGFR2 have been described to comprise a mechanosensory complex (Tzima et al., 2005). Authors suggest that in this model CD31 directly transmits mechanical force, VE-Cadherin acts as an adapter and VEGFR2 activates PI3K/AKT signaling. They report that disruption of this complex by either knocking-down CD31 or VE-Cadherin causes a disruption of the alignment of endothelial cells in the direction of flow as well as decreasing integrin $\alpha_v ß_3$ activation and the AKT and PI3K phosphorylation (Tzima et al., 2005). Investigation into the role of CD31 in flow-induced inflammation revealed a role for CD31 in disturbed flow responses *in-vivo*. Nuclear factor kappa-light-chain-enhancer of activated B cells (NF-kB) activation evoked by oscillatory flow was blunted in endothelial cells from CD31 knockout mice (Chen and Tzima, 2009). Furthermore, the increase in intercellular adhesion molecule 1 (ICAM-1) and VECAM-1 expression induced by prolonged oscillatory flow was suppressed in CD31 knockout mice (Chen and Tzima, 2009). Thus, this suggests that this triad complex is involved in endothelial shear stress sensing of both laminar and disturbed flow.

1.4.1.2 Integrins

Integrins are suggested to be downstream of the triad mechanosensory complex. VE-Cadherin and CD31 knockout endothelial cells failed to show activation of integrins after the onset of flow (Tzima et al., 2005). Integrins are a family of transmembrane receptors comprising α and β subunits. They interact with extracellular matrix and are involved in the transmission of mechanical signals. The discovery that shear stress activates integrins in endothelial cells opened up a new avenue of research on the importance of the extracellular matrix in shear stress signalling. Shear stress stimulates conformational activation of integrins that is followed by increased binding to extracellular matrix proteins and an inactivation of Rho. This inactivation of Rho is reported to be necessary for the cytoskeletal alignment in the direction of flow (Tzima et al., 2001). The formation of connections between integrins and their specific extracellular matrix ligands is reported to be critical in shear stress evoked mechanotransduction (Jalali et al., 2001). *In-vivo*, flow-induced vasodilation is abolished by blocking antibodies targeting β3 subunits of integrin in isolated coronary arteries (Muller et al., 1997).

1.4.1.3 Caveolae

Caveolae are a type of lipid raft that are small flask-shaped invaginations of the plasma membrane that are present in various cell types but abundantly found in endothelial cells. Caveolae are rich in Cavs, cholesterol and sphingolipids. Evidence that caveolae are involved in mechanosensation was first described in lung endothelial cells. Application of shear stress to rat pulmonary vasculature induced protein tyrosine phosphorylation and translocation of signalling molecules primarily to caveolae, including eNOS (Rizzo et al., 1998). As well as evoking translocation of eNOS, shear stress also induces Cav1 translocation to the edge of endothelial cells that are exposed to high hydrostatic pressure which is consistent with studies suggesting that caveolae buffer cell membranes against high mechanical stress (Sun et al., 2002; Sinha et al., 2011). *In-vivo*, Cav1 knockout mice present with impaired arterial remodelling in response to flow and have resulted flow-induced vasodilation (Yu et al., 2006). It is likely however, that caveolae are shear stress regulated and do not act as direct sensors themselves, but more research would uncover their role in force sensing.

1.4.1.5 GPCRs and G proteins

G-protein coupled receptors (GPCRs) have been reported as mechanotransducers (Gudi et al., 1996; Chachisvilis et al., 2006). Reports suggest that onset of flow can rapidly trigger activation of G proteins that is independent of the cytoskeletal and cytosolic components of endothelial cells (Gudi et al., 1996). Further experiments by the same group using purified G proteins reconstituted into phospholipid vesicles demonstrate that shear stress is able to increase the activity of G proteins in the liposomes. Suggesting that the phospholipid bilayer mediates shear stress-induced activation of G proteins in the absence of their protein receptors. Inhibiting G proteins also suppressed flow-mediated downstream signalling to Ras (Gudi et al., 2003). Shear stress induces Gαq/11 activation independently of GPCR activation in endothelial cells (dela Paz et al., 2017). In mice with induced endothelium-specific P2Y2 or Gq/G11 deficiency lacked flow-induced vasodilation and developed hypertension (Wang et al., 2015). Perhaps this is due to the lack of ability to sense mechanosensation that arises from blood flow.

Heteromeric G-proteins also participate in shear stress signalling and may form mechanosensitive complexes with known mechanosensors. In unstimulated

endothelial cells the heterotrimeric G-protein Gαq/11 associates with CD31 (Otte et al, 2009). Upon application of shear stress this complex dissociates. *In-vivo,* Gαq/11 colocalises with CD31 in areas of laminar, but not disturbed flow (Otte et al., 2009; Delmas et al., 2002). These studies suggest that GPCRs and G proteins are involved in shear responses and may even be mechanosensors in their own right (Givens and Tzima, 2016).

1.4.1.6 Mechanical sensitive ion channels

Ca^{2+} has been described as a 'dynamic master' intracellular regulator of mammalian cell biology. It is involved in various cellular processes including; proliferation, migration, survival, exocytosis during synaptic transcription and gene expression and transcription. Shear stress itself has been reported to evoke Ca^{2+} entry into endothelial cells (Schwarz et al., 1992). Several ion channels have been reported to be involved in shear stress sensing, some of which will be discussed below.

1.4.1.6.1 TRPV4 channels

TRPV4 channels are members of the 'vanilloid' subfamily of TRP channels. They do not undergo classical activation; instead agonists of the channel include physical and chemical stimuli as well as mechanical and osmotic challenges namely, shear stress and osmotic stress resulting in cell swelling (Watanabe et al., 2002; Gu and Gu, 2014). Shear stress evokes an increase in intracellular Ca^{2+} in endothelial cells and TRPV4 overexpression in the otherwise null cell line, human embryonic kidney (HEK)-293 is able to reconstitute this Ca^{2+} response (Mendoza et al., 2010). Endothelial TRPV4 channels have also been reported to be involved in shear stress evoked vasodilation, of the carotid artery and small sized Gracilis arteries (Kohler et al., 2006). Furthermore, in-vivo TRPV4 knockout mice presented with a decrease in shear stress induced, NO-dependent vasodilation in carotid arteries (Hartmannsgruber et al., 2007).

1.4.1.6.2 P2X4 purinoceptors

The P2X4 receptor is a ligand gated Ca^{2+}-permeable cation channel that is activated by ATP. Knocking down P2X4 protein expression abolished shear stress dependent Ca^{2+} response in HUVECs (Yamamoto et al., 2000). Reconstitution of

P2X4 dependent shear stress evoked Ca^{2+} responses was found when P2X4 was overexpressed in HEK 293 cells (Yamamoto et al., 2000). P2X4 knockout mice present with impaired responses to flow. The shear stress evoked Ca^{2+} influx and NO production was almost abolished in endothelial cells isolated from P2X4 knockout mice which was rescued by overexpressing P2X4 (Yamamoto et al., 2006). Interestingly, P2X4 knockout mice also presented with impaired vasodilatory responses and hypertension (Yamamoto et al., 2006).

1.4.1.6.3 Piezo channels

Piezo1 and Piezo2 were discovered more recently to be a mechanically activated ion channels (Coste et al., 2010). They are reported to be involved in various physiological processes including touch sensation, proprioception, nociception, vascular development and blood pressure regulation (Ranade et al., 2014; Woo et al., 2015; Rode et al., 2017; Li et al., 2014; Kim et al., 2012). Moreover mutations in Piezo channels have also been linked to disease (Zarychanski et al., 2012; Coste et al., 2013; Lukacs et al., 2015). The rest of this chapter will provide an overview of Piezo1 functions and molecular mechanisms in health and disease.

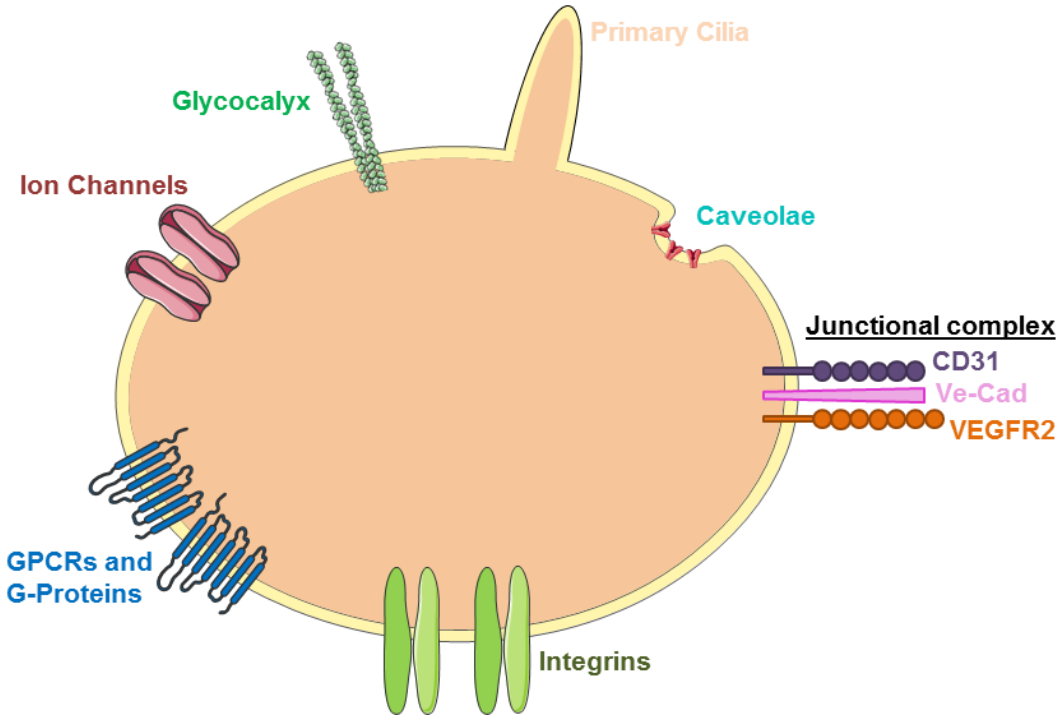

Figure 1.7 Overview of endothelial mechanosensors.

These sensors can be divided into luminal, junctional, and basal mechanosensors. Luminal mechanosensors include G-protein-coupled receptors (GPCRs, including the sphingosine 1-phosphate receptor 1, $S1P_1$, and the bradykinin B2 receptor) and heterotrimeric G-proteins (namely, Gαq/11), ion channels (including TRPV4, P2X4, Piezo1, and Piezo2), microtubule-based primary cilia, the glycocalyx and protein-coated membrane pits called caveolae (given structure by Caveolin 1–3 and Cavin 1–3). The known junctional mechanosensors, PECAM-1, VE-Cadherin, and VEGFR2, form a mechanosensory complex that elicits many signaling pathways as a response to shear. The basal mechanosensors consist of the integrins, which sense extracellular matrix type and substrate stiffness, all while integrating signaling pathways originating from other mechanosensors.

1.5 Piezo1

Piezo1 was discovered by the Patapoutian lab in 2010 and its name is based on the Greek word, πίεση, which means pressure (Coste et al., 2010). Microarray analysis was used to look for genes that spanned the membrane at least twice and siRNA targeting of each gene was undertaken. The FAM38A gene encoding Piezo1 was discovered to be responsible for the mechanically-activated current in the mouse neuroblastoma cell line, Neuro 2A, in response to prodding with a blunt glass pipette (Coste et al., 2010). Furthermore, when Piezo1 was overexpressed in the Piezo1 null cell line, HEK 293, an extremely rapid non-selective cationic current was recorded in response to mechanical stimulation (Coste et al., 2010). The Piezo

family consists of two members, Piezo1 and Piezo2. Both proteins assemble to form functional channels which independently confer mechanically activated non-selective cationic current. It is now known that Piezo1 channels can respond to various forms of mechanical stimulation including, poking, stretching and shear stress (Li et al., 2014; Coste et al., 2010; Cox et al., 2016). The ion permeation selectivity of mouse and human Piezo1 has been shown to be typical of non-selective cationic channels (Gnanasambandam et al., 2015). Piezo1 is permeable to monovalent and some divalent cations, particularly Ca^{2+} and Mg^{2+}. Piezo1 is not Ca^{2+} selective like Orai or voltage-gated Ca^{2+} channels. However, Coste *et al.*, (2010) suggested that Piezo1 prefers Ca^{2+} over other divalent cations.

1.5.1 Piezo1 structure

The structure of Piezo1 compared to other channels is striking. It does not possess much sequence and structural homology to any known classes of ion channels. There is loose structural similarity of the Piezo1 pore region to trimeric acid-sensing ion channel (ASIC) and ATP-gated P2X4 receptors that essentially contain two transmembrane (TM) domains and a large extracellular domain in each promoter (Gonzales et al., 2009; Kawate et al., 2009). Initially cross-linking studies suggested that Piezo1 forms a tetramer (Coste et al., 2012). However, using cryo-electron microscopy (EM), the full-length structure (2547 amino acids) of mouse Piezo1 was resolved (4.8A˚) (Ge et al., 2015). It was revealed that Piezo1 is around 900 kilodaltons and forms a trimeric propeller-like structure (Ge et al., 2015). The C-terminal regions are reported to come together to form the extracellular cap and the peripheral N-terminal regions are blades that form propeller-like structures (Figure 1.8). The extracellular blades are connected to the intracellular domain by three long beams (Figure 1.8). Recently, higher resolution cryo-EM structures report that Piezo1 consists of 38 transmembrane domains with 9 repetitive units consisting of 4 transmembrane domains forming the blades (Zhao et al., 2018; Saotome et al., 2018; Ge et al., 2015).

The combination of structural and functional characteristics proposed that mouse Piezo1 is divided into the peripheral blade structures that directly sense force to gate ion permeation through the central ion-conducting pore (Ge et al., 2015; Zhao et al., 2016). Experiments involving patch clamp on mutated and chimeric Piezo1 channels revealed that the C-terminal region of Piezo1 is important for the channel gating and ion selectivity, whereas, the N-terminal blade structure are important for

sensing force and mechanical activation (Coste et al., 2015; Zhao et al., 2016). An interesting experiment suggested that chimeric expression of the N-terminal region of Piezo1 with the otherwise mechanically insensitive ASIC confers sensitivity to mechanical force (Zhao et al., 2016). However, competing reports suggest that this could be due to endogenous Piezo1 expression in the heterologous system used (Dubin et al., 2017). It has been suggested that the beam structures of Piezo1 possess a dome structure and that this flattens upon channel opening without the application of force, lateral membrane tension alone is enough to confer this conformational change (Guo and MacKinnon, 2017). Furthermore, it is reported that Piezo1 might use its curved blades and beams as a pivot to form a lever-like structure (Zhao et al., 2018). Mechanosensation might evoke a large conformational change of the distal blades, forming propeller-like machinery, to slightly open the central pore to allow cation-selective permeation.

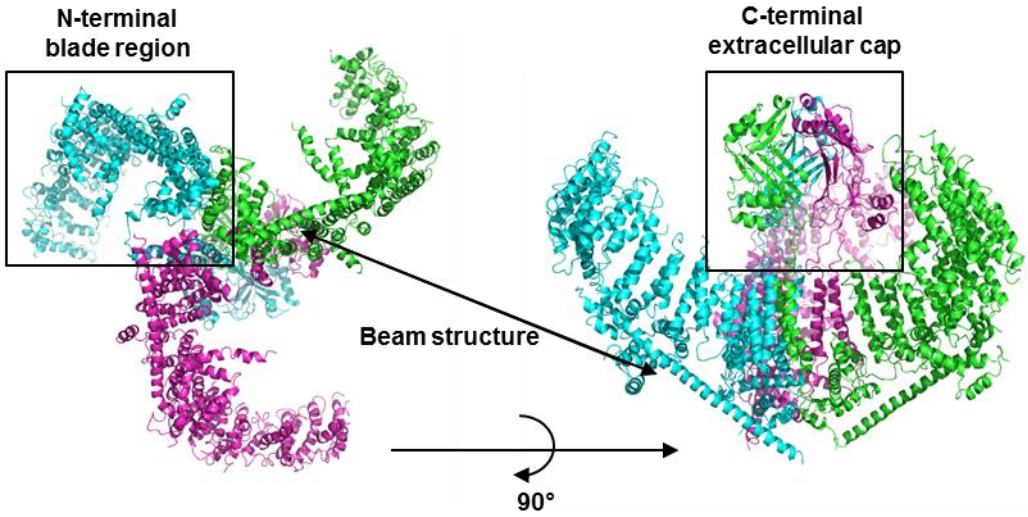

Figure 1.8 Cryo-EM structure of Piezo1 trimer.

Left: Intracellular view of the structure of Piezo1 to present the beam structures. Right: as on the left but rotated 90° around the x-axis to present the beam, blade and extracellular structures. PDB: 5Z10, 3.97 Å (Zhao et al., 2018).

1.5.2 Piezo1 pharmacology

1.5.2.1 Inhibitors of Piezo1 channels

To date the best small molecule inhibitors of Piezo1 channels are ruthenium red and gadolinium (Coste et al., 2010). However, they are blockers of many mechanically activated and other cationic and Ca^{2+}-selective channels, including Piezo2. Ruthenium red is a voltage dependent blocker of Piezo1 (IC_{50}: 5.4 µM) that is reported to block purified Piezo1 reconstituted into lipid bilayers (Coste et al., 2012). When applied to the extracellular solution of HEK 293 cells over expressing mouse Piezo1, ruthenium red inhibited inward mechanically activated currents without affecting outward currents. Moreover, when applied to the intracellular pipette solution ruthenium red had no effect, suggesting that it acts via the extracellular side of the channel, perhaps directly blocking the pore (Coste et al., 2012).

GsMTx4 (Grammostola Spatulata Mechanotoxin 4) is a 34 amino acid peptide that was isolated from the venom of a tarantula and was suggested to inhibit endogenous stretch channels (Suchyna et al., 2000). Further investigation indicated that both enantiomers of GsMTx4 inhibited endogenous mechanically activated currents suggesting that the inhibition occurred by positioning itself between the ion channel and lipid bilayer (Suchyna et al., 2004). In outside-out patch configuration, GsMTx4 inhibited both human wildtype and mutated Piezo1 (R2456K non-inactivating mutant) currents in overexpression systems, suggesting that the peptides ability to inhibit Piezo1 does not involve the protein region that is needed for Piezo1 inactivation (Bae et al., 2013).

1.5.2.2 Activators of Piezo1 channels

In physiology Piezo1 channels are activated by mechanical force. Recently, the Patapoutian group developed a high throughput screen to assess the function of Piezo1 and Piezo2 using Ca^{2+} imaging. A library of ~3 million compounds was screened for their ability to activate Piezo1 or Piezo2 and they identified the first small molecule activator of Piezo1, a synthetic substance called Yoda1 (Syeda et al., 2015). Yoda1 rapidly activated Ca^{2+} entry via Piezo1 and not Piezo2 without evoking internal Ca^{2+} release. Yoda1 activates purified Piezo1 present in lipid bilayers and thus activates Piezo1 in a membrane-delimited fashion, suggesting that Yoda1 binds to Piezo1 directly. Patch clamp experiments revealed that the

biophysical properties of chemically-activated Piezo1 were altered compared to mechanically activated Piezo1; Yoda1-actiavted Piezo1 presented with slower channel inactivation compared to mechanically activated Piezo1 channels. These alterations in properties are consistent with the changes found in mutations of Piezo1 that are associated with hereditary xerocytosis (Bae et al., 2013). The similarities between the biophysical properties of Yoda-activated Piezo1 and Piezo1-activation with C-terminal mutations suggests that perhaps Yoda1 works by binding to the C-terminus of Piezo1, near the channel pore. Furthermore, Yoda1 has been used as an agonist of Piezo1 to examine functional physiological roles of Piezo1 channels. Similarly to shear, application of Yoda1 to HUVECs evokes activation of downstream eNOS signalling and relaxation of mesenteric arteries (Wang et al., 2016). Moreover, similar to mechanical activation of Piezo1, Yoda1 causes Ca^{2+} influx and dehydration of red blood cells and can even cause Piezo1-dependent pancreatitis (Cahalan et al., 2015; Romac et al., 2018). The discovery of Yoda1 will facilitate the role of Piezo1 channels in human physiology and disease to be examined.

Recently, during structure-function relationship studies a second small molecule activator of Piezo1 was discovered, termed Jedi (Wang et al., 2018). Jedi1 and Jedi2 both dose-dependently activate Ca^{2+} entry in HEK 293 cells overexpressing Piezo1 but not Piezo2 independently of intracellular mediators. Jedi-evoked currents had a more rapid onset and faster decay compared to Yoda1 currents suggesting distinct activation mechanisms (Wang et al., 2018). Jedi-induced Piezo1 channel activation depended on the extracellular loops in the distal blade structures and two leucine residues in the proximal end of the beam but it remains unclear whether Jedi directly binds to Piezo1 (Wang et al., 2018). As of yet Jedi has not been examined in functional assays to examine the biology of Piezo1.

1.5.3 Functional roles of Piezo1

Since the discovery of Piezo1, studying the role of Piezo1 in biology has been a hot topic. Even though the pharmacology is poor, groups have used current tools to examine the function of Piezo1 channels in various body systems. Our lab is particularly interested in endothelial Piezo1 of the cardiovascular system. However, Piezo1 is widely expressed throughout the human body, including in the brain, lung and adipose tissue (Pathak et al., 2014; Li, 2015; Sugimoto et al., 2017).

Mechanical stimulation occurs in many ways throughout the body and diverse roles for Piezo1 in various body systems are beginning to unravel.

1.5.3.1 Piezo proteins: non vascular functions

Transduction of mechanical stimuli by receptor cells is essential for senses such as hearing, touch and pain. Piezo2 has mainly been studied in the sensory system where it is important for light touch, pain and proprioception (Woo et al., 2014; Woo et al., 2015; Dubin et al., 2017). However, roles for Piezo1 in mechanical nociception are beginning to emerge (Kim et al., 2012). Piezo1 knockout drosophila melanogaster (*d*Piezo1) were produced and their avoidance in response to von Frey filaments was examined. *d*Piezo1 knockout larvae presented with a severe deficit in their behavioural response to von Frey filaments (45 mN) compared to wildtype larvae. Responses to noxious heat and light touch were unaffected between wild-type and knockout larvae. These data demonstrate physiological roles for Piezo1 in mechanosensory nociception *in-vivo*. Furthermore, in the kidneys changes in urinary flow alters intraluminal pressure which is sensed by Piezo1 (Miyamoto et al., 2014). Piezo1 is abundantly expressed in mouse bladder urothelium. In epithelial cells isolated from mouse proximal convoluted tubes Piezo1 inhibition reduced stretch-activated currents and Ca^{2+} entry. Suggesting that Piezo1 channels sense extension of the bladder urothelium. Red blood cells experience mechanical forces while recirculating. Red blood cells exhibit Piezo1-dependent Ca^{2+} entry in response to mechanical stretch (Cahalan et al., 2015). Piezo1 knockout mouse red blood cells are overhydrated and present with increased fragility *in-vivo*. Treatment with Yoda1 was protective, mimicking the gain of function mutation, promoting dehydration due to Ca^{2+} influx and subsequent dehydration of RBCs via downstream activation of the KCa3.1. These data suggest that Piezo1 plays an important role in red blood cell volume homeostasis. Recently, Piezo1 modulation has been examined as a therapy for pressure-induced iatrogenic pancreatitis. Functional Piezo1 channels are expressed in pancreatic acinar cells (Romac et al., 2018). Yoda1 evokes Piezo1-mediated Ca^{2+} entry that induces cell death. GsMTx4 was administered to mice by intraperitoneal injection and this reduced the severity of pancreatitis. This result was mimicked with genetic deletion of Piezo1 in acinar cells (Romac et al., 2018). Consistent with Piezo1 activity promoting development of pancreatitis, infusion of Yoda1 into the pancreatic duct of mice induced Piezo1 dependent pancreatitis (Romac et al., 2018).

It is well established that Ca^{2+} mediates cell proliferation and migration (Clapham, 2007; Berridge et al., 2000). Interestingly Piezo1 has been reported to mediate migration of gastric cancer cells (Yang et al., 2014). The C-terminal portion of the Piezo1 protein was reported to interact with Trefoil factor family 1 that is involved in epithelial cell motility. Piezo1 knockdown in commercial gastric cancer cells attenuated wound healing in an *in-vitro* assay suggesting that Piezo1 is important for cell migration (Yang et al., 2014). Furthermore, inhibition of Piezo1 with the GsMTx4 toxin reduced motility of the MCF-7 breast cancer cell line, suggesting a possible role for Piezo1 in development and metastasis of breast cancer. Conversely, studies of Piezo1 depletion in small cell lung cancer cell lines suggest a role for Piezo1 in decreasing cell migration and metastasis (McHugh et al., 2012). Knockdown of Piezo1 evoked cell detachment and increased migration. Furthermore, Piezo1 knockdown in HeLa cells, a cell line derived from cervical cancer, evoked a decrease in cell adhesion (McHugh et al., 2010). Opposing roles for Piezo1 might suggest that Piezo1 mediates differential signalling pathways in specialised cells.

1.5.3.2 Piezo1 in the vascular system

Vascular systems are crucial for the early development and survival of mammals. In the embryo, initially vasculogenesis occurs, where endothelial cells migrate, differentiate and form tube-like structure which remodel to form blood vessels. Angiogenesis then occurs, developing new vessels from those pre-existing. The physiological force evoked by the flow of blood, creating laminar frictional force on endothelial cells, governs these processes. Endothelial cells sense this force which triggers downstream signalling events and this is important for vascular functions, from development to maintaining vascular homeostasis. To date there have been many proposed mechanisms by which endothelial cells can sense shear stress. However, Piezo1 channels have been discovered as direct shear stress sensors and are important for many endothelial cell functions (Li et al., 2014; Ranade et al., 2014).

1.5.3.2.1 Piezo1 in vascular development

Piezo1 has been reported to be essential for vascular development in mice (Li et al., 2014; Ranade et al., 2014). Global Piezo1 knockout results in embryonic lethality in mice at day E9.5-11.5. This is a critical time for vascular development as

it is around the time that the heart is starting to beat. Piezo1$^{-/-}$ yolk sacs presented with less prominent vasculature, with embryos exhibiting disorganised vasculature and fewer large vessels compared to those expressing Piezo1 (Li et al., 2014). Heterozygote Piezo1 knockout mice survived to adulthood, but again it caused reduced alignment of endothelial cells but had no major phenotype. This was mimicked in endothelial specific Piezo1 knockout mice (Li et al., 2014). Without stopping the heartbeat, endothelial Piezo1 knockout also caused developmental vascular defects. The data demonstrate the importance of endothelial Piezo1 to this process. *In-vitro* assays using Piezo1 siRNA in HUVECs supressed VEGF induced endothelial tube formation and migration (Li et al., 2014). These data suggest a critical role for Piezo1 in vascular development and embryonic survival.

1.5.3.2.2 Endothelial cell alignment

Endothelial cells align in the direction of laminar flow, and this is important for their function and maintenance of a healthy vasculature. As previously stated, areas of low and disturbed shear stress, i.e. at areas of bifurcations in arteries, endothelial cells present in a much more disorganised, cobblestone like structure (Figure 1.6). In HUVECs knockdown of Piezo1 abolishes flow-mediated alignment (Li et al., 2014). Mice with systemic knockdown of Piezo1 or heterozygote knockdown of Piezo1 present with the same disorganised endothelial structure (Li et al., 2014). The mechanism behind this is suggested to be mediated by calpain. Calpain is reported to be important in the structure of the actin cytoskeleton and focal adhesions and blocking calpain suppresses the flow-mediated alignment of HUVECs (Lebart and Benyamin, 2006; Li et al., 2014). Embryos with global Piezo1 knockout have reduced calpain activity. It is suggested that shear stress activates endothelial Piezo1 channels promoting Ca^{2+} entry which activates calpain to promote alignment (Li et al., 2014). Recently, endothelial cells have been isolated from human placenta and Piezo1 is expressed and functional in these cells (Morley et al., 2018). Application of Yoda1 evokes Piezo1-mediated Ca^{2+} entry and alignment. Investigation into the role of Piezo1 in placental vascular disease would be interesting.

1.5.3.2.3 Downstream signalling; eNOS regulation

eNOS activity is important for endothelial function and dysregulation of eNOS is reported to mediate endothelial dysfunction (Fleming, 2010). The first link between

Piezo1 and eNOS was described where VEGF-induced phosphorylation of eNOS was reduced in HUVECs treated with Piezo1 siRNA and haploinsufficient endothelial cells (Li et al., 2014). In addition, knockdown of Piezo1 led to a reduction in eNOS expression (Li et al., 2014). More recently, reports suggest that Piezo1 channels are important for relaxation of vessels. Yoda1-activation of Piezo1 activates downstream eNOS phosphorylation and subsequent relaxation of mesenteric arties in mice (Wang et al., 2016). The link between Piezo1 and eNOS is important, not only for endothelial cell migration and tube formation promoting vascular development but also for the control of blood pressure.

1.5.3.2.4 Piezo1 in cardiovascular homeostasis during exercise

Piezo1 has been reported to be important for the elevation of blood pressure during whole body physical activity by redistributing blood flow (Rode et al., 2017). As Piezo1 global knockout is embryonically lethal, in order to study the role of Piezo1 in blood pressure regulation a conditional endothelial knockout mouse model was developed. This involved using Cre-Lox mediated deletion driven by the endothelial specific Tie2 promoter (Piezo1$^{\Delta EC}$). The mice appeared healthy with normal body and organ weights and gained weight similar to the control littermates (Rode et al., 2017). Isometric tension recordings from mouse second-order mesenteric arteries suggested that Piezo1 channels have an anti-EDHF effect. Normally Ca^{2+} entry drives membrane potential depolarization which in-turn activates Ca^{2+} sensitive K^+ channels on endothelial cells. This causes hyperpolarisation which in turn spreads to neighbouring vascular smooth muscle cells to cause EDHF mediated relaxation (Khazaei et al., 2008). Toxin inhibitors of two K^+ channels slightly inhibited the acetylcholine evoked relaxation in wild-type mice (Rode et al., 2017). In Piezo1$^{\Delta EC}$ mice the inhibitors had a much stronger effect, suggesting that Piezo1 channels oppose EDHF *in-vivo*.

Given that mesenteric arteries are important for peripheral resistance blood pressure recordings took place. Blood pressure was monitored continuously for 6 days, encompassing periods of rest and physical exercise. At rest there was no difference in the blood pressure between wild-type and Piezo1$^{\Delta EC}$ mice (Rode et al., 2017). But, striking effects on blood pressure were recorded during exercise. Piezo1$^{\Delta EC}$ mice had a reduction in the increase of blood pressure after the onset of exercise compared to wild-type mice.

Investigating the mechanism influencing the blood pressure changes revealed that this was due to changes in membrane potential (Rode et al., 2017). Application of flow to endothelial cells freshly isolated from mesenteric arteries resulted in depolarisation. This depolarisation evoked subsequent activation of voltage-gated Ca^{2+} channels in vascular smooth muscle cells resulting in vasoconstriction. This process was blocked in the Piezo1$^{\Delta EC}$ mesenteric endothelial cells.

During exercise, mesenteric arteries constrict to allow a redistribution of blood flow to the skeletal muscles. The role of Piezo1 in the mesentery suggested that Piezo1 is involved in the redistribution of blood from the gut to skeletal muscles during exercise. Piezo1$^{\Delta EC}$ mice exercised less, suggesting that they were struggling (Rode et al., 2017). However, in saphenous and carotid arteries, which would normally dilate to provide more blood flow to skeletal muscles and the brain during exercise, Piezo1 did not have an anti-EDHF effect. This suggests that Piezo1 functions differ depending on the vascular bed.

1.5.4 Piezo1 in human disease

As Piezo1 global knockout is embryonic lethal and as Piezo1 channels have such important functions in human physiology it seemed almost certain that they will be involved in human disease. Recently various mutations that alter the activation properties of Piezo1 have been reported to be present in human patients with lymphatic dysplasia and hereditary xerocytosis. Therefore, targeting Piezo1 might be an important novel therapy for their treatment.

1.5.4.1 Lymphatic dysplasia

Autosomal recessive generalised lymphatic dysplasia has been linked to Piezo1 loss-of-function mutations (Fotiou et al., 2015; Lukacs et al., 2015). The lymphatic system is a network of vessels that is important for extracellular fluid homeostasis. Its role is to deliver lymph fluid, containing antigens, to the lymph nodes as part of the immune system. Similar to blood vessels, endothelial cells line lymphatic vessels and the surrounding smooth muscle cells are important to conduct lymph flow. A failure of lymphatics to drain interstitial fluid from the extracellular space back into the blood leads to lymphodema. Two reports have described mutations in

human *PIEZO1* in families with nonimmune hydrops fetalis, secondary to generalised lymphatic dysplasia (Lukacs et al., 2015; Fotiou et al., 2015). So far 12 mutations, the majority resulting in early stop codons, have been found in human patients with this disease and all are documented to be loss-of-function. While erythrocytes from healthy patients had robust Ca^{2+} responses to pressure and Yoda1, those from a patient carrying the disease exhibited significantly blunted responses (Lukacs et al., 2015). The mutation causing the disease was examined, (G2029R). HEK 293 cells expressing Piezo1-G2029R had a strongly diminished Ca^{2+} response and current to Yoda1 compared to wild-type which the authors suggest to be due to reduced channel abundance at the plasma membrane (Lukacs et al., 2015).

1.5.4.2 Hereditary Xerocytosis

Hereditary xerocytosis, also known as dehydrated somatocytosis, is an autosomal dominant haemolytic anaemia characterised by primary erythrocyte dehydration and has been linked to gain-of-function mutations of Piezo1 (Zarychanski et al., 2012). Currently 24 mutations of Peizo1 have been reported in patients with hereditary xerocytosis, but M2225R and R2456H are the most characterised. Both mutations have been shown to slow the inactivation of Piezo1 channel current as measured by whole cell and cell attached patch clamp (Bae et al., 2013). As in the disease state, deletion of Piezo1 in mouse red blood cells resulted in their severe dehydration (Cahalan et al., 2015). These cells were larger and more fragile than normal cells due to cell swelling, suggesting that Piezo1 is a negative regulator of red blood cell volume. Furthermore, Piezo1 can functionally respond to mechanical stretch, as this promoted a Piezo1-dependent increase in Ca^{2+} levels (Cahalan et al., 2015). The group suggest that Piezo1-evoked Ca^{2+} entry activates KCa3.1 mediating K^+ efflux and H_2O efflux resulting in dehydration. Thus, in patients with hereditary xerocytosis that have a gain-of-function mutation in Piezo1, this would be exaggerated. Recently, a group confirmed this phenotype in a mouse model expressing the R2482H (R2456H in human) gain-of-function mutation (Ma et al., 2018). Indeed the mouse model mimicked the human phenotype, the red blood cells that had Piezo1 gain-of-function showed reduced osmotic fragility and they were deformed and dehydrated. Interestingly, this mutation caused protection against cerebral complications of malaria (Ma et al., 2018).

1.6 Summary

In summary, endothelial cells perform a range of vital physiological functions but they are also implicated in a variety of pathological settings. Endothelial dysfunction is a hallmark of cardiovascular disease and is regarded as a key event in the initiation of a variety of life-threatening disease states. Ca^{2+} signalling is crucial to endothelial cell function and is regarded as the key signalling mechanism in non-excitable cells such as endothelial cells. An important physiological parameter governing endothelial function, vascular development and vascular homeostasis is shear stress, which in the vasculature is the frictional force arising from blood flow along the endothelial cells.

Recent years have seen the identification of Piezo1 channels as direct sensors of shear stress in endothelial cells. The Piezo1 channel has been implicated as a driver of embryonic vascular development and recently roles in vessel relaxation and regulation of blood pressure during full body physical activity have been described. With increasing knowledge of Piezo1 channel function in the cardiovascular system new opportunities are arising to examine roles of Piezo1 downstream signalling in endothelial cells.

The recent discovery of Yoda1, as a tool to mimic shear activation of Piezo1, enables a more targeted approach to investigate Piezo1. Piezo1 has been linked to eNOS phosphorylation in the literature. However, how Yoda1-activated Piezo1 phosphorylates eNOS at short time points remains elusive. The fact that Piezo1 mutations are reported in human disease is revolutionises Piezo1 channel research. Better understanding of Piezo1 channel signalling and function in endothelial cells will enable the development of more targeted therapies for Piezo1-mediated cardiovascular diseases.

1.7 Aims and Objectives

Overall aim

The overall aim of this project is to examine Piezo1-mediated downstream signalling pathways and examine Piezo1 partner proteins; aided by the novel chemical selective Piezo1 activator Yoda1 and to determine the mechanism by which Yoda1 mediates S1177 eNOS phosphorylation.

Hypothesis

Piezo1 channels couple to specific molecular pathways to importantly determine responses to blood flow.

Objectives

1. Determine the effect of Yoda1 on intracellular Ca^{2+} levels in human endothelial cells expressing endogenous Piezo1.
2. Examine whether Yoda1-mediated Ca^{2+} entry in human endothelial cells is dependent on Piezo1.
3. Examine whether Yoda1 can be used as a tool compound to mimic shear stress-activated downstream signalling.
4. Characterise Yoda1-mediated S1177 eNOS phosphorylation.
5. Examine whether Yoda1-mediated eNOS phosphorylation is Piezo1 dependent in human endothelial cells and mouse liver endothelial cells.
6. Examine the effect of Yoda1 analogues on Ca^{2+} entry and S1177 eNOS phosphorylation.
7. Investigate the effect of Yoda1 on other eNOS phosphorylation sites; S615, Y657, T495.
8. Determine the mechanism by which Yoda1-evokes eNOS phosphorylation by screening relevant candidate kinases.
9. Generate a suitable high-throughput system for examining hypotonic-activation of Piezo1.
10. Examine the relationship between Piezo1 and the mechanosensory triad comprising CD31, VE-Cadherin and VEGFR2.
11. Develop a FLIM/FRET system to examine Piezo1 protein interactions.

Chapter 2 Material and Methods

2.1 Ionic Solutions

Standard Bath Solution (SBS)

SBS contained (mM): NaCl 134, KCl 5, $MgCl_2$ 1.2, $CaCl_2$ 1.5, HEPES 10, D-Glucose 8; pH was titrated to 7.4 with 4 M NaOH.

Ca^{2+}-free SBS was prepared by omitting $CaCl_2$ and adding 0.4 mM EGTA.

Dulbecco's Phosphate Buffered Saline (DPBS)

DPBS without magnesium (Mg^{2+}) and Ca^{2+} (Lonza) contained (mM): KCl 2.68, KH_2PO_4 1.47, NaCl 136.89 and Na_2HPO_4-$7H_2O$ 8.06. DPBS was used for cell culture purposes including washing of cells during passage.

2.2 Chemicals and Reagents

All general salts and solutions were purchased from Sigma. Other chemicals are summarised in Table 2.1.

2.2.1 Yoda1 analogues

Analogues of Yoda1 were synthesised by Kevin Cuthbertson, School of Chemistry, University of Leeds. All synthesised chemicals were purified by column chromatography or trituration and determined as >97% pure by 1H NMR (proton nuclear magnetic resonance) and 13C NMR (carbon-13 nuclear magnetic resonance). Structures of Yoda1 and analogues of Yoda1 that have been used in this thesis are displayed in Figure 2.1.

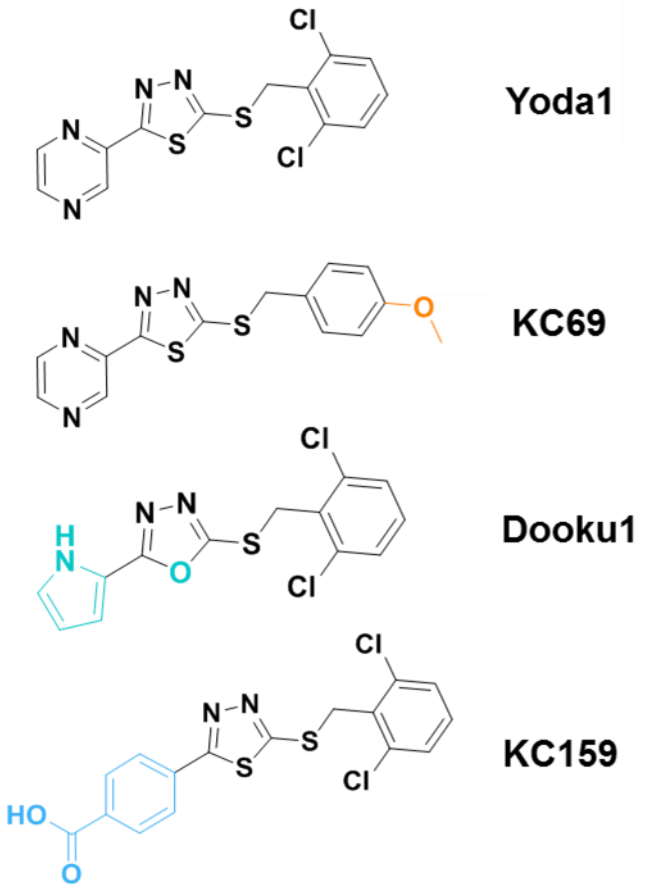

Figure 2.1 Structures of Yoda1 and analogues used in this thesis.

Modifications from the Yoda1 structure are highlighted in colour in each of the analogues.

Chemical	Company	Solvent	Storage	Working conc	Cat #
Apyrase	Sigma	H_2O	-20°C 10 mg/ml	10 µg/ml	A7646
ATP	Sigma	H_2O	-20°C 20 mM	20 µM	FLAAS
BIM	CalBiochem	DMSO	-20°C 10 mM	10 µM	203290
CK59	CalBiochem	DMSO	-20°C 100 mM	100 µM	208922
CNO	Abcam	H_2O	-20°C 10 mM	10 µM	ab141704
Gadolinium	Sigma	H_2O	Room Temp 100 mM	30 µM	439770
H89	LKT Laboratories	DMSO	-20°C 10 mM	10 µM	H0003
Ionomycin	Sigma	DMSO	-20°C 1 mM	5 µM	10634
KN93	Sigma	DMSO	-20°C 10 mM	10 µM	K1385
Mannitol	Sigma	H_2O	Room Temp 0.5 M	50 – 270 mM	M4125
Pluronic Acid F-127	Sigma	DMSO	Room Temp 10%	0.01%	P2443
Rotlerin	Sigma	Ethanol	-20 °C 10 mM	10 µM	R5648
Ruthenium red	Sigma	H_2O	Room Temp 30 mM	30 µM	R2751
Suraminutes	CalBiochem	H_2O	-20°C 10 mM	10 µM make fresh	574625
VEGF	Sigma	H_2O	-20°C 30 µg/ml	30 ng/ml	V7259
W7	Sigma	DMSO	-20°C 10 mM	30 µM	681629
Yoda1	Tocris	DMSO	-20°C 10 mM	10 µM	5586

Table 2.1 List of reagents.

List of reagents used throughout this thesis presented with their company and catalogue number and solvent/storage instructions.

2.3 Cell culture

2.3.2 Commercially available cell lines

Human Umbilical Vein Endothelial Cells

HUVECs from pooled donors were purchased from Lonza and maintained in Endothelial Cell Basal Medium (EGM-2) supplemented with 2% Fetal Calf Serum (FCS) and the following growth factors (supplied as a bullet kit; Lonza): 10 ng/ml VEGF, 5 ng/ml human basic fibroblast growth factor, 1 µg/ml hydrocortisone, 50 ng/ml gentamicin, 50 ng/ml amphotericin B, 10 µg/ml heparin and 10 µg/ml ascorbic acid. Cells were grown to 95% confluence before passage and utilised at 95% confluence for experiments. Cells were used from passage 2–6.

Human Embryonic Kidney 293 cells

HEK 293 cells (Invitrogen, UK) were cultured in Dulbecco's modified Eagle's medium (DMEM) GlutaMAX (Gibco) containing 4.5 $g.L^{-1}$ D-glucose and pyruvate (Invitrogen, U.K.). Media was supplemented with 10% fetal bovine serum (FBS), penicillin (50 $units.mL^{-1}$) and streptomycin (0.5 $mg.mL^{-1}$) (Sigma-Aldrich).

Piezo1 Tetracycline-Inducible Human Embryonic Kidney-293 cells (HEK P1)

Piezo1-green fluorescent protein (GFP) (Li et al., 2014) was used as a polymerase chain reaction (PCR) template to clone the human Piezo1 coding sequence into pcDNA™4/TO between HindIII and EcoRI restriction sites. Piezo1 was amplified as two fragments using the following primers:

HindIII-Piezo1-Fw: 5' AATAAGCTTATGGAGCCGCACGTG 3'
BamHI-Int.Piezo1-Rv: 5' AATGGATCCCCCTGGACTGTCG 3'
BamHI-Int.Piezo1-Fw: 5' AATGGATCCTCCCCGCCACGGA 3'
EcoRI-Piezo1-Rv: 5' AATGAATTCTTACTCCTTCTCACGAGT 3'

The two fragments were fused using a BamHI restriction site, resulting in the full length Piezo1 coding sequence with the C4182A silent mutation. T-REx™-293 cells were transfected with pcDNA4/TO-Piezo1 using Lipofectamine 2000 (Thermo Fisher Scientific). Subsequently, cells were treated with 10 µg/mL blasticidin (Invitrogen) and 200 µg/mL zeocin (Invitrogen) to select stably transfected cells. Single cell clones were isolated and analysed individually. Expression was induced by treating the cells for 24 hours with 10 $ng.mL^{-1}$ tetracycline (Sigma) and analysed

by real time quantitative PCR (RT-qPCR) and western blotting (Evans et al., 2018; Rode et al., 2017).

HEK P1 cells were maintained in DMEM supplemented with 10% FBS, penicillin (50 units.mL^{-1}) and streptomycin (0.5 mg.mL^{-1}), 200 µg.ml^{-1} zeocin and 10 µg.ml^{-1} blasticidin. Cells were grown to 95% confluence before passage and utilised at 95% confluence for experiments.

T-REx^{TM}-293 (HEK TREx)

T-REx^{TM}-293 cells without transfection with pcDNA4/TO-Piezo1 were used as a Piezo1 null control. Similarly to HEK P1 cells, T-REx^{TM}-293 cells were maintained in DMEM supplemented with 10% FBS, penicillin (50 units.mL^{-1}) and streptomycin (0.5 mg.mL^{-1}) and 10 µg.ml^{-1} blasticidin. Cells were grown to 95% confluence before passage and utilised at 95% confluence for experiments.

All cells were maintained in a 5% CO_2 incubator at 37°C unless stated otherwise.

2.3.1 Endothelial cell isolation

Human Liver Endothelial Cells

Human Liver Endothelial cells (LEC) were isolated from patients undergoing liver resection for colorectal metastases at St James's University Hospital, Leeds Teaching Hospitals NHS Trust. Ethical approval was provided by the Leeds Teaching Hospitals Local Research Ethics Committee (Ref: 14/YH/1001). Tissue was collected immediately following resection. A section of normal liver tissue was taken from a macroscopically normal area of the surgical specimen at least 2.5 cm away from any tumours. The samples were stored and transported in cold EBM-2 growth medium supplemented with EGM-2 bullet kit (Lonza) on ice. Briefly, 1 g of tissue was minced in a Petri dish. The tissue was resuspended in 9 mL 0.1% collagenase and 1 mL 2.5 U.mL^{-1} dispase solution and incubated for 45 minutes at 37°C under continuous agitation. Subsequently, the sample was passed through 100 µm and 40 µm cell strainers to remove major debris. This was followed by 2 washes in MACS buffer (PBS, 2 mM EDTA and 0.1% bovine serum albumin (BSA); pH 7.2). The pellet was resuspended in 20 mL of red blood cell lysis buffer (17 mM TRIS base, 140 mM NH_4Cl; pH 7.2) for 10 minutes at room temperature.

Following a final wash in MACS buffer, cells were incubated with 200 µl of dead cell removal paramagnetic microbeads per $1x10^7$ cells (Miltenyi Biotec) at room temperature for 15 minutes . The suspension was then passed through a LS cell separation column in a magnetic field to retain apoptotic cells, dead cells and debris. The live cell fraction was eluted and incubated with 25 µL FcR blocking reagent and 25 µL anti-CD31-conjugated paramagnetic microbeads per $1x10^7$ cells at 4°C for 15 minutes . This suspension was then passed through a MS column in a magnetic field and the unbound cells eluted with buffer. Once removed from the magnetic field, the MS column was washed with MACS buffer to elute CD31-positive cells. The approach was validated by western blot. Cells were used up to passage 4 and validated (Webster et al., 2017).

LECs were maintained in EGM-2 supplemented with 2% FCS and the bullet kit containing growth factors.

Mouse Liver Endothelial Cells (mLECs)

Mouse liver sinusoidal endothelial cells were isolated using an immunomagnetic separation technique. A whole mouse liver was minced using 2 scalpel blades and resuspended in a dissociation solution consisting of 9 ml 0.1 % collagenase II, 1 ml 2.5 U ml^{-1} dispase, 1 µM $CaCl_2$ and 1 µM $MgCl_2$ in Hanks Buffer solution. The tissue-dissociation mix was incubated at 37 °C for 50 minutes in a MACSMix Tube Rotator (Miltenyi Biotech) to provide continuous agitation. At the end of enzymatic digestion the sample was passed through 100 and 40 µm cell strainers to remove any undigested tissue. Cells were washed twice in PEB buffer consisting of PBS, EDTA 2 mM and 0.5% BSA, pH 7.2. The washed pellets were resuspended in 1 ml of PEB buffer and 200 µl of dead cell removal paramagnetic microbeads per 1×10^7 cells (Miltneyi Biotec) at room temperature for 15 minutes . After incubation the cells were passed through an LS column prepared with 1 × binding buffer (Miltenyi Biotec) in a magnetic field (Minutes iMACS Separator, Miltenyi Biotec). The eluate was then incubated with 20 ml red blood cell lysis buffer consisting of 17 mM Tris base, 140 mM NH_4Cl in PBS pH to 7.2. Cells were washed again in PEB buffer, and the pellet was resuspended in 1 ml PEB buffer and 30 µl CD146 microbeads (Miltenyi Biotec) at 4 °C for 15 minutes under continuous agitation. CD146 is a specific membrane protein marker for endothelial cells and is highly expressed in mouse endothelial cells. After incubation this solution was passed through an MS column prepared with PEB

buffer. CD146 positive cells were retained in the column and CD146 negative cells passed through as eluate. CD146 positive cells were washed through with warm EGM-2 media and the CD146 selection process was repeated a second time. After a second purification cells were plated and grown in a 5 % CO_2 incubator at 37 °C. Media were changed at 3 h and then every 24 h until confluent.

mLECs were maintained in EGM-2 supplemented with 2% FCS and the bullet kit containing growth factors.

2.4 Transfections

2.4.1 Short-interfering RNA transfection

HUVECs were transfected at 90% confluency in a 6 well plate. In brief, 20 nM short-interfering RNA (siRNA) (Table 2.2) was added to 200 µl Opti-MEM (Gibco) and 3 µl Lipofectamine™ 2000 (Invitrogen). This was incubated at room temperature for 20 minutes prior to adding to each well containing 800 µl EGM-2. Fresh EGM-2 growth medium was added after 4 hour of transfection and the cells were used for experimentation 48 hour after transfection.

2.4.2 Plasmid DNA transfection

HEK cells were transfected using Lipofectamine™ 2000 transfection reagent according to the manufacturer's protocol when 70% confluent in a 6 well plate. In brief, 3 µl Lipofectamine and 250 ng DNA were added to 200 µl Opti-MEM medium and this was incubated at room temperature for 20 minutes prior to addition to cells with 800 µl DMEM. Experiments were performed 48 hours post-transfection.

siRNA	Gene	Sequence (5'-3') sense	Supplier	ID
Scrambled	N/A	UGGUUUACAUGUCGACUAA UGGUUUACAUGUUGUGUGA UGGUUUACAUGUUUUCUGA UGGUUUACAUGUUUUCCUA	Dharmacon	001810
AKT	AKT1	CAUCACACCACCUGACCAA ACAAGGACGGGCACAUUAA CAAGGGCACUUUCGGCAAG UCACAGCCCUGAAGUACUC	Dharmacon	003000
AMPK1	PRKAA1	CCAUACCCUUGAUGAAUUA GCCCACAGGUAGAUAUAUG GAGGAUCCAUCAUAUAGUU ACAAUUGGAUUAUGAAUGG	Dharmacon	005027
AMPK2	PRKAA2	CGACUAAGCCCAAAUCUUU GAGCAUGUACCUACGUUAU GACAGAAGAUUCGCAGUUU GUCUGGAGGUGAAUUAUUU	Dharmacon	005361
CaMKI	CAMK1	AGAUACAGCUCUAGAUAAG GAAGAUAAGAGGACGCAGA UGAAAUACCUGCAUGACCU GAAUGAUGCCAAACUCUUU	Dharmacon	004940
CaMKIIδ	CAMK2D	GCUAGAAUCUGCCGUCUUU AAACCAAUCCACACUAUUA UCACCUAAAUGGCAUAGUU GCGACUUCAUGAUAGCAUA	Dharmacon	004042
CaMKIIγ	CAMK2G	CAGGAGAUCAUUAAGAUUA GCUCGGAUAUGUCGACUUC GUACACAACGCUACAGAUG GGAGAGUGUUAACCACAUC	Dharmacon	004536
CD31	PECAM1	CAAAUGAUCCUGCGGUAUU CCACUGAAGACGUCGAAUA GCAACACAGUCCAGAUAGU UGAAGAGCACAGAGAGUUA	Dharmacon	017029
Fyn #1	FYN	CGGAUUGGCCCGAUUGAUA GGACUCAUAUGCAAGAUUG GAAGCCCGCUCCUUGACAA GGAGAGACAGGUUACAUUC	Dharmacon	003140
Fyn #2	FYN	GGACUCACCGUCUUUGGAG	Ambion	1442
HRas	HRAS	GAACCCUCCUGAUGAGAGU GAGGAUGCCUUCUACACGU AGACGUGCCUGUUGGACAU GGAAGCAGGUGGUCAUUGA	Dharmacon	004142
Piezo1	FAM38A	GCCUCGUGGUCUACAAGAU	Ambion	4392422
PKA	PRKACA	CGGAGAAUCUGCUCAUUGA CAAGGACAACUCAAACUUA GAACCACUAUGCCAUGAAG CCUGCAAGCUGUCAACUUU	Dharmacon	004649
PKCα	PRKCA	UAAGGAACCACAAGCAGUA UUAUAGGGAUCUGAAGUUA GAAGGGUUCUCGUAUGUCA UCACUGCUCUAUGGACUUA	Dharmacon	003523

PKCβ	PRKCB	GGUCAUGCUUUCAGAACGA CCUGUCAGAUCCCUACGUA GAUUUGGGAUUGGGAUUUG UCAUUGUCCUCGUAAGAGA	Dharmacon	003758
PKCδ #1	PRKCD	CCAUGUAUCCUGAGUGGAA CCAAGGUGUUGAUGUCUGU AAAGAACGCUUCAACAUCG CCGCACCGCUUCAAGGUUC	Dharmacon	003524
PKCδ #2	PRKCD	GGUCACAAAUGCAGGCAAU	Ambion	103600
PKCδ #3	PRKCD	GGUGUUGAUGUCUGUUCAG	Ambion	773
PKCγ	PRKCG	GCCCGUAACCUAAUUCCUA GGAGGGCGAGUAUUACAAU GGGAGCGGCUGGAACGAUU CAGAAGACCCGAACGGUGA	Dharmacon	004654
RRas	RRAS	ACGAAGAUCUGCAGUGUGG CGACUUCCCCGUUGUGUUG GAACAAGAGCUCCCACCGA AGUCCUACUUCGUGUCUGA	Dharmacon	010352
VeCadherin	CDH5	GGACAUAACACCACGAAAC GAGCCCAGGUCAUUAUCAA CGAUAAUUCUGGACGUAUU UGACGUGGAUUACGACUUC	Dharmacon	003641
VEGFR2	KDR	GGGCAUGUACUGACGAUUA CUACAUUGUUCUUCCGAUA GGAAAUCUCUUGCAAGCUA GCGAUGGCCUCUUCUGUAA	Dharmacon	003148

Table 2.2 List of siRNA sequences.

siRNAs with 4 sequences are Dharmacon ON-TARGET plus SMARTpool siRNAs with a mixture of 4 siRNAs as a single reagent.

2.5 RNA isolation, cDNA preparation and real time quantitative polymerase chain reaction

2.5.1 RNA isolation

Total RNA was isolated from cells using a phase-separation technique. TRI-reagent was utilised for processing the tissue cells to enable isolation and purification of RNA. Cells were grown to confluence in a 6-well culture plate prior to lysis with ice-cold TRI-reagent (1 ml). The solution containing the lysed cells was transferred to a sterile 1.5 ml eppendorf tube and used immediately or stored at -80°C. All subsequent steps were performed using dedicated pipettes, sterile filter tips and autoclaved plastics.

100 µl bromochloropropane was added to all samples. The solution was vortexed thoroughly (x3) before undergoing centrifugation (12,000 rpm, 15 minutes) to separate the phases – RNA found in the top aqueous layer, DNA found in the middle layer and protein in the bottom layer. The RNA-containing phase was transferred to a new eppendorf and the RNA precipitated with an equal volume of ice-cold isopropanol, thoroughly vortexed (x3) and left on ice for 15 minutes. The sample was then centrifuged (13,000 rpm, 4°C, 20 minutes) to pellet the RNA followed by a wash step with fresh 75% ethanol. Following thorough vortexing to wash the pellet, a final spin (13,000 rpm, 4°C, 5 minutes) was undertaken followed by ethanol removal and the pellet was air-dried for 5 minutes at room temperature. The RNA was dissolved in 10 µl nuclease-free water before DNase digestion to remove any contaminating genomic DNA.

2.5.2 DNase digestion

RNase-free DNase 10 x reaction buffer (1.2 µl, Ambion) and DNase enzyme (0.5 µl) were added to the sample and incubated at 37°C for 1 hour. 2 µl inactivation agent (Ambion) was then added and the sample incubated at room temperature for 5 minutes. A final spin (13,000 rpm, 4°C, 2 minutes) enabled collection of the RNA supernatant and this was transferred to a fresh tube prior to RNA quantification. RNA was quantified using the Nanodrop (ThermoScientific) and stored at -80°C.

2.5.3 Reverse transcription

Complimentary DNA (cDNA) was synthesised using a High Capacity RNA-to-cDNA RT kit (Applied Biosystems). 1 µg of RNA was mixed with 5 µl 2x RT buffer, 0.5 µl 20x enzyme mix and nuclease-free water to make a 10 µl total reaction volume. Non-reverse transcribed (-RT) control solutions were prepared and tested in parallel. The solutions were mixed, centrifuged and incubated for 1 hour at 37°C followed by 5 minutes at 95°C. This produces cDNA that is ready for use in real-time qPCR application or short-term storage at 4°C.

2.5.4 Real-time quantitative polymerase chain reaction

RT-qPCR was carried out using SYBR Green I (Roche) on a LightCycler (Roche). SYBR Green I intercalates with double stranded DNA and fluoresces when excited at 470 nm. The emission of light at 530 nm is significantly enhanced in the DNA bound compared to the unbound state. Each reaction had a 10 µl total volume and contained the following: 5 µl of 2x iTaq™ Universal SYBR® Green Supermix (containing antibody-mediated hot-start iTaq DNA polymerase, dNTPs, $MgCl_2$, SYBR® Green I dye, enhancers and stabilizers), 0.75 µl of forward primer (0.375 µM), 0.75 µl of reverse primer (0.375 µM), 1 µl cDNA and 2.5 µl nuclease-free water. Primer sequences and information are displayed in Table 2.3. DNA amplification started with 10 minutes at 95°C, followed by 40 cycles with 10 seconds at 95°C and 60 seconds at 60°C. The relative abundance of target genes amplified by RT-qPCR were calculated relative to the housekeeping gene, ß actin.

2.5.5 Agarose gel electrophoresis

Reaction products were loaded onto a 2% agarose 1x TAE gel (Tris acetate EDTA) containing SYBR™ Safe (1:10,000) (Invitrogen), which binds DNA and allows visualisation of products upon exposure under ultraviolet light, and analysed by gel electrophoresis. PCR reaction solutions were mixed with 6 x loading buffer containing the following: 2.5% Ficoll-400, 11 mM EDTA, 3.3 mM Tris-HCl (pH 8.0), 0.017% SDS and 0.015% bromophenol blue (New England Biolabs). Gels were run at 80 volts for 50 minutes in 1 x TAE buffer. To test newly designed primers human Brain (*h*Brain) RNA was purchased from Ambion (ref: AM7962) and used as a positive control. PCR products were sent for sequencing to check the correct sequence is being amplified and run on a gel to check the product size is correct. Primer efficiencies were >90%.

Gene	Primer sequence (5' to 3')	Product size (base pairs)
AMPK1	Fwd: TGTCACAGGCATATGGTGGT Rv: GTGCAGCATAGTTGGGTGAG	157
AMPK2	Fwd: CGCCTCTAGTCCTCCATCTG Rv: TCGGATTCCAAGATGCCACT	196
ß Actin	Fwd: TCGAGCAAGAGATGGC CATCCAACGAAACTACCTTCA	132
Blk	Fwd: CTCTCAGGCTGGTCAGGAAA Rv: CAGAGCCTTCATCACGTTGG	155
CAMK1	Fwd: CATCTTGCTCTGCGGTTACC Rv: TTCTCCATCAAGTGCCGGAT	150
CaMKII a	Fwd: CACACCACCATCCTGAATC Rv: GATCTGTGGAAGTGGACGAT	179
CaMKII b	Fwd: GGGCATATTCGTCTGATGAT Rv: CTGAGACAAGGGTCTGTGCA	132
CaMKII d	Fwd: CAGTACATGGATGGCAGTGG Rv: TTCAACAGTGCCACTTCTGC	188
CaMKII g	Fwd: GTAAAGTCTCGCGGTGCTG Rv: GTCTCCTCCTCTTGCTCCCT	59
Fgr	Fwd: TGGCTTCCTTGATAGTGGCA Rv: CTGGGAATGCAGCCAGTTTT	201
Fyn	Fwd: TCACCAAAGGAAGAGTGCCA Rv: CAAAAGTGGGGCGTTCTTCA	162
Hck	Fwd: CCACAGAGAGCCAGTACCAA Rv: TTCCAGTCCAACCTACCCAC	201
Lck	Fwd: CAACCTGGTTATCGCTCTGC Rv: TGGCCACAAAATTGAAGGGG	164
Lyn	Fwd: CCACTATAGCTGGGAGGGTG Rv: GGCAAGAGAAGGCGGTATTg	209
Piezo1	Fwd: AGATCTCGCACTCCAT Rv: GGACTCGTGAGAAGGAG	182
PKA	Fwd: CTTCCAACTCCAGCGATGTG Rv: TTCCCGGTCTCCTTGTGTTT	214
PKCa	Fwd: CCAATGCCCTGGAGCTTGTA Rv: CCTCTGGATGGGGGACACTA	246
PKCb	Fwd: CTGCAAAGGGCTGATGACCA Rv: TTCAGCATTTCGCCCACAAG	167
PKCd	Fwd: CAGACCAAGGACCACCTGTT Rv: GCATAAAACGTGGCACGGTA	110
PKCg	Fwd: CACGAAGTCAAGAGCCACA Rv: TAGCTATGCAGGCGGAACTT	233
Src	Fwd: AAACCCTGCCCTCCTTAGAC Rv: TCCTGAGGATGACAGAGGGA	170

Yes	Fwd: GCTGGTTGATATGGCTGCTC Rv: CGACCATACAGTGCAGCTTC	228

Table 2.3 List of RT-qPCR primers.

Table includes sequences of forward and reverse primers used to amplify genes of interest in RT-qPCR experiments along with their predicted product size.

2.6 Immuno-precipitation

2.6.1 GFP Trap

HEK 293 cells were grown to confluence and transfected with the appropriate plasmids for 48 hours (Table 2.6). Cells were lysed as in section '2.72 Cell treatment and lysis'. GFP trap is coupled to agarose beads. These beads are advantageous as they do not possess an antibody so no heavy and light chains will be present on the western blot, they have a very high affinity binding even to low abundant proteins and they only need a short incubation time with lysate. 25 µl GFP-Trap bead 50% slurry (Chromotech) was used and all wash steps were performed with dilution buffer containing 10 mM Tris/Cl pH 7.5, 150 mM NaCl and 0.5 mM EDTA.

GFP-Trap beads were washed 3x with dilution buffer prior to addition to cell lysate. Beads were incubated with cell lysate at 4°C for 2 hours following another wash step (x3). To elute the proteins off the beads 40 µl sample buffer (2.7.1 Solutions) was added and samples were boiled at 95°C for 5 minutes. Western blotting was used for analysis (2.7 Western Blotting).

2.6.2 Active G-Protein

This assay was set up by Dr Keiichiro Tanaka (University of Yale) and taught during an external lab visit. All plasmids were a gift from Professor Martin Schwartz's lab, Yale University. A schematic describing the pulldown techniques is presented in Figure 2.2 Active G Protein pull down assay.

2.6.2.1 GINIP-GST purification

10 ml terrific broth (ThermoFisher Scientific) supplemented with ampicillin was inoculated with Bl21(DE3) competent *E.Coli* (ThermoFisher Scientific) containing the GST-GINIP plasmid (Table 2.6) and the bacteria grown overnight under constant agitation at 37°C. This culture was then added to 300 ml terrific broth (+ampicillin) and grown for a further 3 hours before addition of 100 µM Isopropyl β-D-1-thiogalactopyranoside (IPTG). IPTG mimics allolactose, a lactose metabolite that triggers transcription of the lac operon to induce protein expression. After a further 5 hours incubation under constant agitation at 30°C the bacteria were pelleted (6,000 g, 15 minutes) and stored at -80°C.

Bacteria were lysed in lysis buffer containing, 10 mM Tris-HCl (pH 7.5), 150 mM NaCl, 1% Triton X-100, 5 mM DTT, protease inhibitor cocktail (1:500) and 1 $mg.ml^{-1}$ lysozyme and re-suspended on ice. Sonication was used to lyse the bacteria (30 seconds, 50% duty, 50% output, 30 second break x3) and lysed bacteria were centrifuged (20,000 xg, 30 minutes, 4°C). The supernatant was mixed with glutathione beads (GE Healthcare Life Sciences) and rotated at 4°C for 2 hours to allow the induced GST-GINIP protein to bind to the beads via its GST tag. Following this incubation beads were washed (4x) in lysis buffer. GST-tagged protein was eluted using elution buffer containing 10 mM Tris-HCl (pH 7.5), 150 mM NaCl, 1% Triton X-100, 5 mM DTT, 50 mM Glutathione (pH to 7.2) overnight at 4°C. Samples were snap frozen in liquid nitrogen and stored at -80°C long term.

2.6.2.2 Active G protein pull down assay

Purified GST-GINIP protein was bound to new glutathione beads for 2 hours. HUVECs were grown to confluence and transfected with appropriate constructs for 48 hours. Prior to lysing, cells were treated with applicable test compounds. Cells were lysed and snap frozen in liquid nitrogen immediately to maintain G proteins in their active state. Cell lysates were quickly thawed in warm water and centrifuged (10,000 xg, 5 minutes, 4°C). 50 µl Glutathione beads bound to GST-GINIP were added to HUVEC cell lysate and samples were rotated for 20 minutes at 4°C. Following this incubation, the beads were washed in lysis buffer (x4) and bound proteins eluted in 40 µl sample buffer (95°c, 5 minutes) (Figure 2.2). Western Blotting was used for pull down analysis.

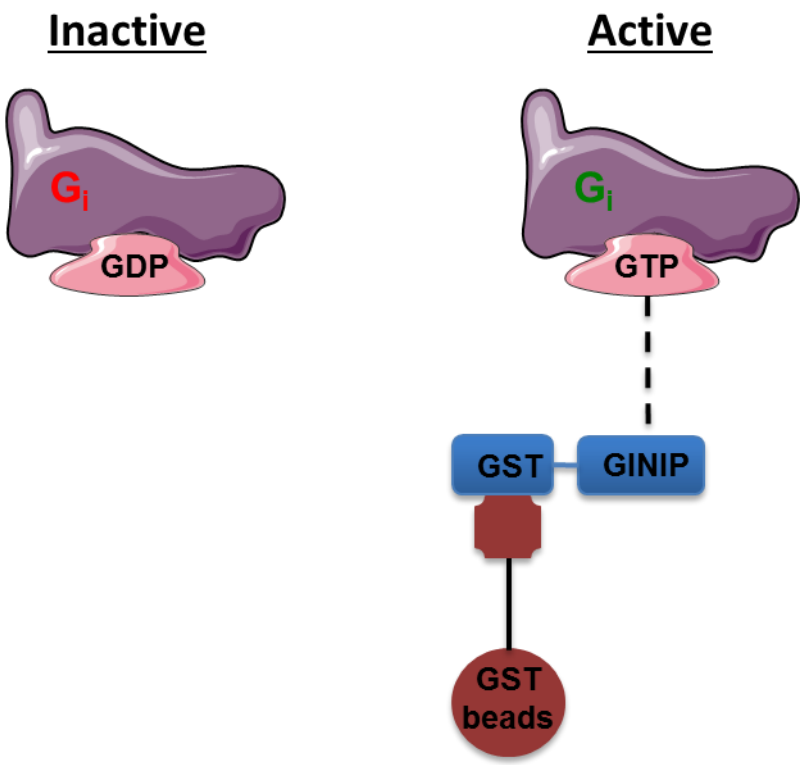

Figure 2.2 Active G Protein pull down assay.

Inactive G Proteins are bound to GDP. Activation of G Proteins is associated with the conversion of GDP to GTP. GINIP binds specifically to GTP on activated Gα proteins. A GINIP-GST fusion protein was utilised to facilitate the purification, and so detection, of GINIP-active G protein complexes using glutathione tagged beads.

2.6.3 Endogenous eNOS immunoprecipitation

HUVECs were plated in a 10 cm dish and lysed at 95% confluency as in '2.7.2 Cell treatment and lysis' section and 1 mg of protein as used in the assay. Protease and phosphatse inhibitors were present at a 1:500 dilution throughout all stages of the immunoprecipitation (IP). 1 mg of protein was mixed with 4 µg anti-eNOS antibody or a control IgG antibody and incubated overnight at 4°C under continuous agitation. The following day 50 µl Protein G sepharose beads (GE Healthcare Life Sciences) were washed in ice cold PBS to remove the 20% ethanol in which they are stored in (1000 g centrifugation). Beads were added to the protein mixed with antibody and further incubated overnight at 4°C under continuous agitation. Beads were washed again in ice cold PBS and protein that was bound to the beads was eluted in 40 µl 4x sample buffer (2.7.1 solutions) (95 °c, 5 minutes).

2.7 Western Blotting

2.7.1 Solutions

Lysis buffer:

10 mM Tris, pH 7.4, 150 mM NaCl, 0.5 mM EDTA, 0.5 % NP-40. Minutes iComplete protease inhibitors (Roche 1:500), and PhosSTOP phosphatase inhibitors (Roche 1:500) were added just before lysing

Sample (loading) buffer (4x):

200 mM Tris pH 6.8, 8% SDS, 40% glycerol, 8% mercaptoethanol, 0.1% bromophenol blue

Running (electrophoresis) buffer (BioRad):

25 mM Tris, 192 mM glycine and 0.1% SDS, pH 8.3

Semi-dry transfer buffer:

48 mM Tris, 39 mM glycine and 20% methanol.

TBS-T:

145 mM NaCl, 20 mM Tris-base, 0.5% Tween 20, pH 7.5.

Stripping buffer:

0.1% SDS, 0.2 M Glycine, pH 2.5

2.7.2 Cell treatment and lysis

Cells were grown to confluence in a 6 well plate and harvested in lysis buffer. Prior to treatment with an agonist cells were serum starved to dampen basal phosphorylation of proteins in 1.5 mM Ca^{2+} SBS for 1 hour. Treatment with Yoda1, Yoda1 analogues or VEGF was performed at room temperature and shear stress was carried out at 37°C with 5% CO_2. Immediately after treatment cells were washed twice in ice cold PBS to stop all phosphorylation/dephosphorylation events. 80 µl ice cold lysis buffer was then added to each well. Cells were scraped off the dish and lysate was left on ice for 30 minutes prior to centrifugation for 20 minutes (10,000 xg) at 4 ºC. The supernatant containing the soluble protein was kept for experimentation and pellet containing nuclei and cell debris was disposed of.

2.7.3 Protein Quantification

Protein quantification was performed on the supernatant (DC Protein Quantification (BioRad). This is a dye-binding assay in which a differential colour change occurs in response to various concentrations of protein. Absorbance was measured in a

microtitre plate reader at 570 nm wavelength. Comparison was made to a BSA standard curve and the protein concentrations were derived from this.

2.7.4 Western Blotting

20 µg of the protein sample was mixed with sodium dodecyl sulphate (SDS) reducing sample buffer and heated to 90°C for 5 minutes to ensure complete denaturation of the proteins. Samples were loaded alongside molecular weight markers (Bio-Rad) onto 4-20% gradient SDS polyacrylamide gels (Bio-Rad) and electrophoresis was carried out for 60-90 minutes at 175 volts. SDS is an anionic detergent that disrupts the secondary structures of proteins to create linear, negatively charged structures. Application of an electrical charge across the gel results in the movement of negatively charged proteins towards the positively charged electrode. The distance each protein travels is inversely proportional to its size and molecular weight.

Following gel electrophoresis, samples were transferred to a polyvinylidene fluoride membrane (PVDF) membrane (Immobilon) by semi-dry transfer at constant current of 50 mA for 90 minutes per membrane in transfer buffer. The membrane was then incubated for 1-2 hours in TBS-T containing 5% milk to block non-specific background binding. Membranes were then labelled overnight with primary antibodies in TBS-T containing 5% non-fat milk or 5% BSA for phospho-antibodies at 4°C. Table 2.4 lists all of the antibodies and appropriate dilutions used in this thesis. After three 10 minutes washes with TBS-T, the membrane was incubated with secondary horse radish-peroxidase (HRP) donkey anti-mouse, rabbit or goat secondary antibodies (1:5,000) (Jackson ImmunoResearch) in TBST-T containing 5% milk for 1 hour at room temperature prior to final washes with TBS-T.

2.7.5 Protein Visualisation

SuperSignal Femto detection reagents (Pierce Science) were used to detect protein bands. Membranes were imaged using a G:BOX (Syngene) with genesis software. Data were analysed using Image J software (NIH, Bestheda, Maryland, USA) measuring the mean grey intensity of each band and normalising it to that of β-actin or total protein loading control from the same sample. If membranes were re-probed, stripping buffer was applied for 20 minutes at room temperature and the protocol was repeated from the blocking stage.

2.8 Immunocytochemistry

Briefly, cells were seeded on cover slips (Thermo Scientific, thickness 0.15 mm) in 24-well plates 24 hours before experiments at 80 % confluence. Cells were washed in DPBS, fixed with 4% paraformaldehyde (PFA) for 10 minutes at room temperature and washed again with Tris Saline to quench the PFA. For permeabilization, 0.1 % TritonX-100 in DPBS was applied to cells for 10 minutes. To prevent non-specific antibody binding, permeabilized cells were blocked using 5% donkey serum (Gibco) for 1 hour. Primary antibodies were prepared at appropriate concentrations (Table 2.4) in DPBS containing 1% BSA and applied to cells following blocking for 1 hour at room temperature. After washing with PBS, cells were incubated with the relevant species specific fluorescent dye-conjugated secondary antibodies (1:300; Jackson ImmunoResearch Laboratories, Inc) for 30 minutes at room temperature before being mounted on slides with Prolong Gold Antifade Reagent containing DAPI (4',6-diamidino-2-phenylindole) to label the nuclei (Invitrogen). Slides were kept at room temperature overnight to allow the mounting media to set. Images were collected at room temperature using a Roper Cool SNAP HQ CDD camera with SoftWoRx acquisition and analysis software. A Zeiss LSM880 inverted microscope with an Airyscan attachment

Target	Dilution (IF)	Dilution (WB)	Company	Species antibody raised in	Cat #
BEEC4 (DLAKGGTVEYANEKHMLALA)	N/A	1:1000	Cambridge Biosciences	Rabbit	N/A
Active β-integrin	N/A	N/A	Milipore	Mouse	20792
AKT	N/A	N/A	BD Bioscience	Mouse	810860
Beta Actin	N/A	1:2000	Santa Cruz	Mouse	sc47778
CD31	1:200	1:1000	Dako	Mouse	MO823
eNOS	N/A	1:1000	BD Bioscience	Mouse	610296
ERK	N/A	1:1000	Cell Signalling	Mouse	4696S
GluGlu	N/A	1:1000	BioLegend	Mouse	901801
GST	N/A	1:1000	Cell Signalling	Rabbit	26225
HRas	N/A	1:1000	Santa Cruz	Rabbit	sc520
phosho-p44/42 ERK (T202/Y204)	N/A	1:1000	Cell Signalling	Rabbit	4370S
phospho-AKT (S473)	N/A	1:1000	Cell Signalling	Rabbit	4060S
phospho-eNOS (S1177)	N/A	1:1000	BD Bioscience	Mouse	612393
phospho-eNOS (S615)	N/A	1:1000	Abcam	Rabbit	138458
phospho-eNOS (T495)	N/A	1:1000	Cell Signalling	Rabbit	95745
phospho-eNOS (Y657)	N/A	1:1000	ECM Bioscience	Rabbit	NP4031
RRas	N/A	1:1000	Santa Cruz	Rabbit	sc523
VeCadherin	N/A	1:1000	R&D Systems	Mouse	9381
VEGFR2	N/A	1:1000	R&D Systems	Goat	AF357
β-integrin	N/A	1:1000	Bethyl	Rabbit	303735

Table 2.4 Summary of primary antibodies.

2.9 Endothelial Nitric Oxide Synthase Activity Assay

HUVECs were incubated at 37°C for 20 minutes in SBS buffer. 0.5 µCi.ml^{-1} L-[14C] arginine was then added for 5 minutes and cells stimulated with Yoda1 (2 µM) or its vehicle control for 20 minutes, or 30 ng.ml^{-1} VEGF or its vehicle before the reaction was stopped with cold PBS containing 5 mmol.L^{-1} L-arginine and 4 mmol.L^{-1} EDTA, after which cells were denatured in 95% ethanol. The soluble cellular components were dissolved in 20 mmol.L^{-1} HEPES-Na^{+} (pH 5.5) and applied to a well-equilibrated DOWEX (Na^{+} form) column. The L-[14C] citrulline content of the eluate was quantified by liquid scintillation counting and normalized against total protein content of the cells used.

2.10 Intracellular Ca^{2+} Measurement

The changes in the intracellular ionized Ca^{2+} (Ca^{2+}_i) concentration upon agonist evoked channel activation were measured using the fura-2 (Grynkiewicz et al., 1985) Ca^{2+} indicator dye and the FlexStationII^{384}.

2.10.1 Fura-2 acetoxymethyl ester (Fura-2 AM)

Fura-2 AM (Invitrogen, USA) is a ratiometric Ca^{2+} indicator dye that enables measurement of Ca^{2+}_i. The ratiometric property of fura-2 is advantageous as it allows accurate measurement of changes in Ca^{2+}_i whilst minimising the detrimental effects of factors that could cause measurement disturbance, such as dye concentration, leakage of the dye, photobleaching and varying cell thickness, delivering more reproducible results.

The –AM form is the membrane permeable, yet Ca^{2+} insensitive form of fura-2. Once inside the cell, the AM group is cleaved by intracellular non-specific esterases generating the charged and active form (fura-2) which is able to bind to Ca^{2+} with high affinity. Fura-2 is excited at wavelengths of 340 and 380 nm and emitted light is collected at 510 nm. Upon Ca^{2+} binding the excitation spectrum shifts, resulting in an increase in fluorescence emission at 340 nm and a decrease in fluorescence

emission at 380 nm (Figure 2.3). Fura-2 fluorescence is recorded as a ratio of 340/380. Thus, there is an overall increase in the ratio (ΔF ratio) that indicates an increase in intracellular Ca^{2+}.

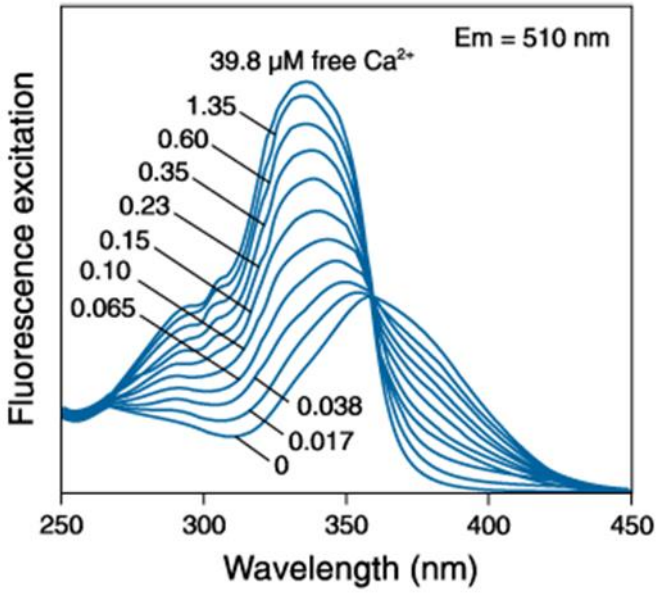

Figure 2.3 Fluorescence excitation spectra of fura-2 in varying free Ca^{2+} concentrations.

An increase in intracellular Ca^{2+} will cause the fura-2 fluorescence emission intensity at 510 nm to increase at excitation wavelength 340 nm and decrease at 380 nm. Image taken from (*http://www.lifetechnologies.com*).

2.10.2 High throughput Ca^{2+} measurement using the FlexStation II^{384}/FlexStation III^{384}

Intracellular Ca^{2+} measurements were made using either the FlexStation II^{384} or the FlexStation III^{384} (Molecular Devices) (Figure 2.4). The FlexStation is a bench-top high throughput fluorescence plate reader that can be utilised for kinetic fluorescence experiments using either a 96 or 384 well based assay. The FlexStation provides integrated fluid transfer from a compound plate to an assay plate whilst taking measurements of fluorescence. The FlexStation has three draws; the tip box draw (upper), the compound plate draw (middle) and the assay plate draw (lower). The automated device has a built-in 8-head dispenser that can be

programmed to add compounds from a compound plate into a prepared assay plate containing cells at designated time points and measure any subsequent changes in fluorescence. Softmax Pro 4.7.1 software (Molecular Devices) was used in order to select the desired excitation wavelengths (340 nm and 380 nm), the emission wavelength (510 nm), the time course of the experiment, the timing of compound addition and sampling frequency. Experiments were performed at room temperature (RT: 21 ± 2°C).

2.10.3 Experimental Protocol

24 hours prior to experimentation cells were seeded at 80-90 % confluence into 96-well plates. 96-well clear-bottomed poly-D-lysine-coated black plates (Greiner Bio-One, UK) were utilised for HEK P1 and HEK TRex cells, the poly-D-lysine improving adherence of the HEK cells throughout the assay. Clear-bottomed NUNC plates (NUNC, Thermo scientific, UK) were used for endothelial cells, which are inherently more adherent than HEK cells. Seeding densities of 60,000 HEK cells per well and 25,000 endothelial cells per well was used throughout. All cells were grown to confluence overnight at 37°C in a 5% CO_2 incubator. HEK P1 cells were pre-treated with 10 $ng.ml^{-1}$ tetracycline for 18 hours prior to experimentation to induce Piezo1 expression.

On the day of experimentation cells were incubated in 1.5 mM Ca^{2+} SBS containing fura-2 AM (2 µM) and 0.01% pluronic acid for 1 hour at 37°C protected from light. Pluronic acid is a mild detergent that was used to facilitate the solubility of the dye. After fura-2 loading, cells were washed (x3) in 1.5 mM Ca^{2+} SBS and incubated at room temperature prior to recordings to allow the de-esterification of the fura-2 AM. Pre-incubation solutions depended on the experiment being. All pre-incubations were carried out protected from the light.

The compound plate contained 1.5 mM Ca^{2+} SBS for all experiments. Automated compound transfer from the compound plate into the assay plate involved a 1:1 dilution. For experiments that involved the addition of a fresh compound to the assay plate (without prior incubation of the compound), the compound was prepared at 2x the desired final concentration for addition to the test plate, where it underwent a 1:1 dilution to the final required concentration. Its vehicle was present at the same concentrations in the assay plate solution. The FlexStation was

programmed to transfer 80 µl from the compound plate to the assay plate wells containing 80 µl (hence, a 1:1 dilution). For experiments involving pre-treatment with test compounds, it was important to maintain the concentration of the compound in the 1.5 mM Ca^{2+} SBS in the compound plate in line with that in the assay plate. This enabled the concentration of all compounds to be maintained in the assay plate.

After pre-incubation, the assay plate, compound plate and FlexStation tips were loaded into the FlexStation. Baseline fluorescence ratios were recorded before addition of the compound solution to the assay plate after 60 seconds. ΔF ratio values at peak Ca^{2+} entry were used for statistical comparison, unless stated otherwise. 'Zero baseline' traces are displayed throughout where baseline Ca^{2+} levels are consistent. Ca^{2+} traces displaying 'absolute' values are used only when the baseline Ca^{2+} level is altered.

2.10.3.1 Compound pre-incubation protocol

For experiments examining the effect of the pre-treatment of drugs, following fura-2 AM loading cells underwent incubation in 1.5 mM Ca^{2+} SBS containing the drug of interest or its vehicle for 30 minutes at room temperature. The compound plate contained the channel agonist e.g. Yoda1 along with the compound/control present in the pre-treatment to maintain its concentration.

2.10.3.2 Hypotonic assay

Following fura-2 AM loading cells underwent a SBS wash step and 30-minutes incubation in SBS at room temperature. The compound plate contained solutions of varying hypotonicity. In the compound plate SBS was used where Na^{+} was replaced with mannitol to allow control of the osmolarity of the solution. 270 mM mannitol was used as an isotonic control and mannitol was tested at decreasing concentrations (150 – 50 mM) to make solutions increasingly hypotonic. The hypotonic solutions induce movement of water into the cells by osmosis, consequently causing the cells to swelling. The increase in membrane tension that results from this swelling should evoke Piezo1 channel activation.

Figure 2.4 The Flexstation II384 bench-top microplate reader.

The FlexStation III^{384} (Molecular Devices) was used for Ca^{2+} measurement assays using the 96 well plate format. The temperature can be controlled and there are designated drawers for the tips, compound plate and assay plate to be inserted prior to experimentation. The FlexStation was controlled by Softmax Pro 4.7.1 (Molecular Devices) software which is displayed on the screen.

2.11 Whole Cell Electrophysiology

Whole-cell voltage-clamp electrophysiology was used to analyse the currents evoked by Yoda1 in HEK cells overexpressing Piezo1.

Borosilicate glass capillaries with an outside diameter of 1 mm and an inside diameter of 0.58 mm (Harvard Apparatus, USA) were used as the basis for patch pipettes. Pipettes were pulled using a PP-830 vertical 2-stage pipette-puller (Narishige, Tokyo, Japan) to a tip diameter of approximately 1 µm. Pipette resistances with pipette solution were 3-6 MΩ. Pipettes were mounted on a CV-4 head-stage (Molecular Devices, Sunnyvale, CA, USA) connected to a 3-way coarse manipulator and micromanipulator (Mitutoyo, Japan). The electrode was comprised of an Ag/AgCl wire. Electrical signals were amplified and recorded using an Axopatch 200B amplifier and pCLAMP 10.6 software (Molecular Devices, LLC). Data were filtered at 1 kHz and sampled digitally at 3 kHz via a Digidata 1440A analogue-to-digital converter (Molecular Devices).

The cells were bathed in SBS and intracellularly dialyzed with the standard patch pipette solution containing (mM): 145 CsCl, 2 $MgCl_2$, 10 Hepes, 1 EGTA, 5 Na_2ATP and 0.1 Na_2GTP, titrated to pH 7.2 with CsOH. The whole-cell voltage clamp mode was held at 0 mV, and a voltage ramp pulse from −100 mV up to +100 mV over 500 msec that were generated by the pCLAMP program were repeatedly applied to the cell every 5 sec. Drugs were applied extracellularly by perfusion of an external solution with drug-containing SBS. 24 hours prior to experimentation cells were plated on 13-mm glass cover slips at low density (~20-30%). Recordings were made after at least 5 minutes after break through to whole cell to allow the cell to recover.

Analysis was performed off-line using Clampfit 10.2 (Molecular Devices) and Origin 8.6 software (OriginLab, Northampton, MA).

2.12 Generation of Endothelial Specific Piezo1 Knockout Mouse Model

All animal work including organ harvesting was performed by Dr Baptiste Rode (University of Leeds). Animal work was approved by the University of Leeds Animal Ethics Committee and by The Home Office, UK (Ref: 40/3557 and P606320FB). Animals were maintained in GM500 individually ventilated cages (Animal Care Systems), at 21°C 50–70% humidity, light/dark cycle 12/12 hrs on RM1 diet (SpecialDiet Services, Witham,UK) *ad libitum* and bedding of Pure'o Cell® (Datesand, Manchester, UK). All animal use was authorised by the University of Leeds Animal Ethics Committee and The Home Office, UK. Genotypes were determined using RT-PCR with specific probes designed for each gene (Transnetyx, Cordova, TN).

To generate tamoxifen inducible deletion of the Piezo1 gene in endothelial cells of adult mice, C57BL/6 Piezo1^{flox} mice were crossed with C57BL/6 mice expressing cre recombinase under the Cadherin5 promoter (Tg(Cdh5-cre/ERT2)1Rha) and inbred to obtain C57BL/6 Piezo1$^{flox/flox}$/Cdh5-cre mice. Tamoxifen (Sigma-Aldrich) was dissolved in corn oil (Sigma-Aldrich) at 20 mg.mL-1. Adult male mice (aged 12 to 16 weeks) were injected intra-peritoneal with 75 mg.kg-1 tamoxifen for 5

consecutive days and liver tissues was harvested 10 to 14 days following the last tamoxifen injection. Piezo1$^{flox/flox}$/Cdh5-cre mice that received tamoxifen injections and therefore had Piezo1 deleted from their endothelial cells were referred as Piezo1$^{\Delta EC}$. Piezo1$^{flox/flox}$ littermates that received tamoxifen injections and therefore retained endothelial cell Piezo1 were referred as wildtype control.

2.13 Shear stress

For generating shear stress using an orbital shaker, endothelial cells were plated on a 6-well plate. At 100% confluency cells were subjected to shear stress generated by the orbital shaker (SSM1, Stuart) rotating at 153 rpm with an orbit of 16 mm for 24 hours. Cells were cultured in 2 mL medium, so that the shear stress at the edge of the wells was ~10-15 dyn.cm^{-2} (Dardik et al., 2005; Warboys et al., 2014). Cells were then imaged using the Incucyte^{TM} Kinetic Imaging System (Essen Bioscience, Michigan) in phase-contrast mode using a x10 objective.

2.13.1 Cell alignment analysis

To estimate the orientation of endothelial cells relative to flow images were analysed using ImageJ software (NIH, Bestheda, Maryland, USA). Images were processed using a 'Difference of Gaussian' operator to highlight the edge of individual cells. This was achieved by using the 'Difference of Gaussians' ImageJ plugin from the University of Sussex (http://www.sussex.ac.uk/gdsc/intranet/microscopy/imagej/utility). The settings used for phase contrast images were Sigma1=20, Sigma2=1.5. Enhance Contrast was applied. Automated quantification of cell orientation relative to flow was determined using an ImageJ plugin, OrientationJ, as described by (Rezakhaniha et al., 2012). OrientationJ produced a histogram of local angles. Using OriginPro 2017 Gauss distribution curves were fitted the histograms. The baseline-adjusted frequency at the mode of each curve compared between experimental groups. OrientationJ software is available for download from http://bigwww.epfl.ch/demo/orientation/. The protocol for analysis is summarised in Figure 2.5.

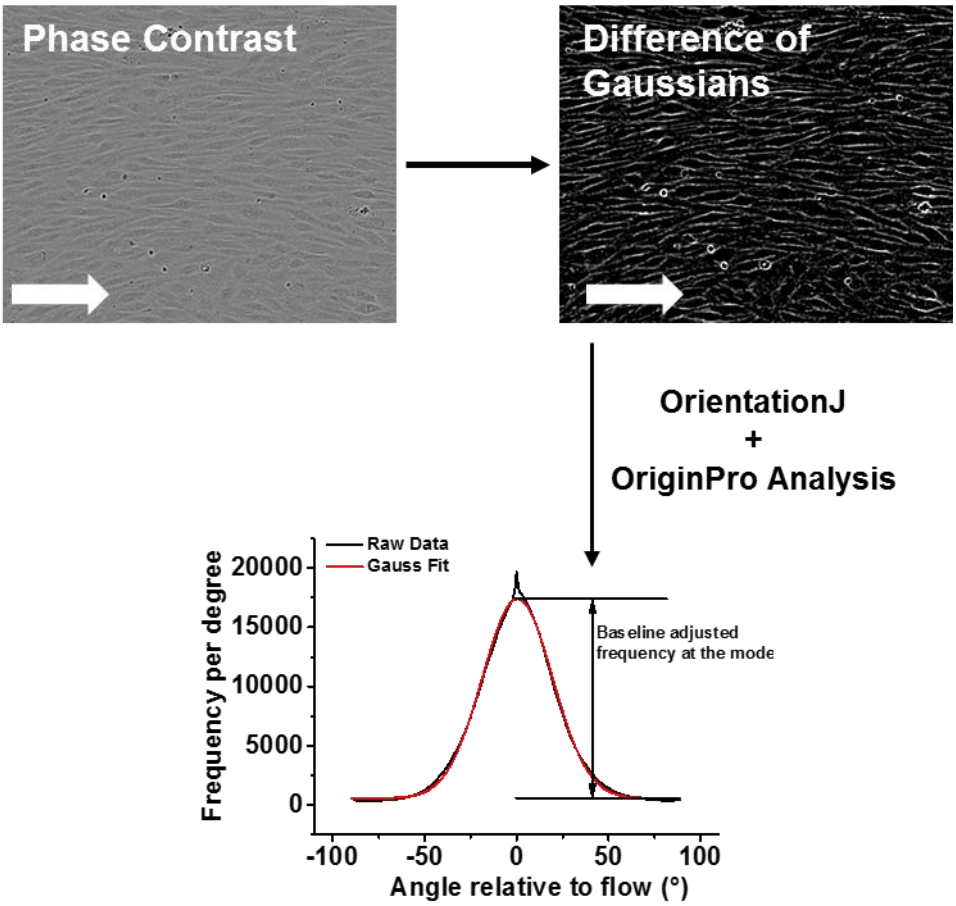

Figure 2.5 Method for cell alignment analysis.

Phase-contrast image is processed using Difference of Gaussians function in ImageJ software to define the cell edge. Orientations of the HUVECs are quantified using OrientationJ software, a plugin for ImageJ. The software returns the frequency of cells at each degree. The frequency of the aligned edges in the direction of flow are used for comparison.

2.14 Plasmids and construct assembly

A list of plasmids used throughout this thesis can be found in Table 2.6. mEmerald-VEGFR2-N was purchased from addgene (Table 2.6), however, it contained a CT insertion between T1303 and A1304. Dr Melanie Ludlow (University of Leeds) performed site-directed mutagenesis to remove this insertion. The sequence contained both the well-studied V297I and H472Q SNPs and they were mutated back to V and H respectively and cloned into pcDNA4/TO. mVenus-VE-Cadherin-N-10 was also purchased from addgene (Table 2.6) and Dr Melanie Ludlow (University of Leeds) removed the mVenus tag. Piezo1-GFP was previously published by our lab (Li et al., 2014) and Dr Melanie Ludlow (University of Leeds)

removed the GFP tag from this construct. The methods for cloning Piezo1 and CD31 tagged constructs will be described in more detail below.

2.14.1 Linearization of plasmids

The aim was to generate constructs containing Piezo1-sYFP2 or mTurquoise2 (mT) and CD31-sYFP2 or mTurquoise2 in the pcDNA6 expression vector. Using the Piezo1-YFP plasmid in the pcDNA6 vector as a template, the 720 bp YFP sequence was removed using inverse PCR with the Phusion® DNA polymerase (New England Bio Labs). Primers were designed so that the forward primer (Piezo1_Fwd) bound just after the 3' end of the YFP sequence and the reverse primer (Piezo1_BamH1_Rv) bound just prior to the 5' end of the YFP sequence (Figure 2.6; Table 2.5). Thus, only Piezo1 and the vector backbone were amplified. To clone the plasmid expressing CD31-mTurq2/sYFP2 the same principle was followed, using CD31-CFP as the template plasmid. The inverse PCR reaction utilised the CloneAmp DNA polymerase (Clonetech) with primers CD31_Fwd and CD31_HindIII_Rv (Table 2.5) in order to amplify CD31 and the vector backbone (minutes us CFP) (Figure 2.6). psYFP2-C1 and mTurquoise2-C1 plasmids were purchased from addgene (Table 2.6). The sYFP2/mTurq2 sequence was amplified from their corresponding plasmids using forward and reverse primers designed to overlap with the sequence on the Piezo1/CD31 PCR products (Piezo1_BamH1_mTurq2_Fwd, mTurq2_Rv (Piezo1), CD31_HindIII_mTurq2_Fwd and mTurq2_Rv (CD31) (Table 2.5; Figure 2.6). BamHI or HindIII restriction sites were introduced between Piezo1 or CD31 respectively and the fluorophores to facilitate future cloning steps.

PCR reaction mixes were prepared as per the manufacturer's protocol and reactions were set as follows:

Phusion PCR reaction protocol

98°C 30 sec
x25 [98°C 30 sec
57°C 30 sec
72°C 4 min (Piezo1)/30 sec (mT/sYFP2)]
72°C 8 min (Piezo1)/1 min (mT/sYFP2)

CloneAmp PCR reaction protocol

98°C 10 sec
x32 [98°C 10 sec
55°C 10 sec
72°C 1.5 min (CD31)]
72°C 3 min (CD31)

The subsequent PCR product was resolved on a 1 % agarose gel at 80 V for 1 hour, excised and extracted from the gel using a ZymocleanTMGel DNA Recovery Kit (Zymo Researched).

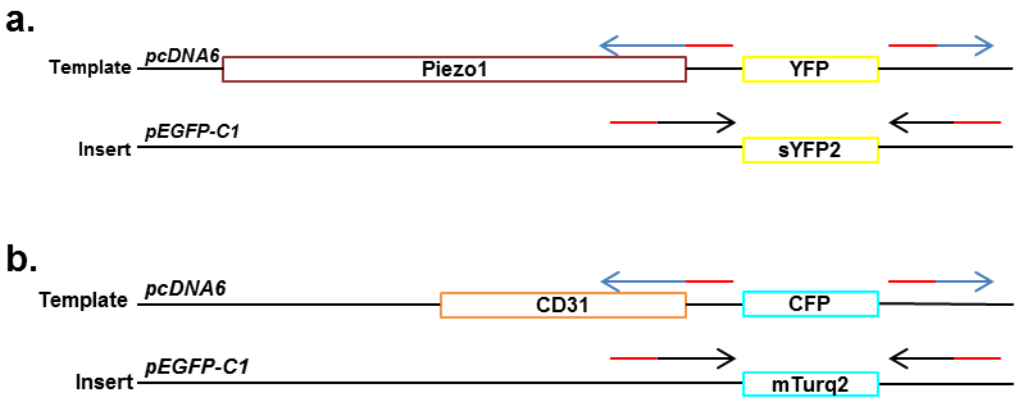

Figure 2.6 Linearization of template and amplification of insert.

a-b) Schematic of cloning strategy for Piezo1-sYFP2. a) and CD31-mTurq2 b). Template, insert and vector are as labelled. Arrows mimic primer design, red indicates the overlap that will be used for infusion, the template sequence is in blue and vector sequence in black.

Primer	Primer sequence (5' to 3')
Piezo1_Fwd	TGCAGATATCCAGCACAG
Piezo1_BamH1_Rv	GGATCCCTCCTTCTCAC
Piezo1_BamH1_mTurq2_Fwd	GAGAAGGAGGGATCCATGGTGAGCAAGGGC
mTurq2_Rv (Piezo1)	CTGGATATCTGCATTACTTGTACAGCTCGTCC
CD31_Fwd	GAATTCTGCAGATATCCAGC
CD31_HindIII_Rv	AAGCTTAGTTCCATCAAGG
CD31_HindIII_mTurq2_Fwd	CCTTGATGGAACTAAGCTTATGGTGAGCAAGGGC
mTurq2_Rv (CD31)	CTGCAGAATTC TTACTTGTACAGCTCGTCC
Piezo1-L4-sYFP2/mTurq2-Fwd	CGTGAGAAGGAGGGATCCGCCAGCGCATCCGCTA GCGCCTCTGCCAGCGCTAGTGCCTCTGCATCCGCT TCA
Piezo1-L4-sYFP2/mTurq2-Rv	CTTGCTCACCATGGATCCGCTAGCACTTGCGCTTG CACTGGCAGAGGCGGAGGCTGAAGCGGATGCAGA
CD31-L4-sYFP2/mTurq2-Fwd	CCCTTGATGGAACTAAGCTTGCCAGCGCATCCGCT AGCGCCTCTGCCAGCGCTAGTGCCTCTGCATCCGC TTCA
CD31-L4-sYFP2/mTurq2-Rv	CCTTGCTCACCATAAGCTTGCTAGCACTTGCGCTTG CACTGGCAGAGGCGGAGGCTGAAGCGGATGCAGA

Table 2.5 List of primers used for cloning constructs.

2.14.2 Infusion reaction to generate Piezo1-sYFP2/mTurq2 and CD31-sYFP2/mTurq2 constructs

The small overlaps on the sYFP2/mTurq2 primers were used to combine both the Piezo1/CD31 templates with the sYFP2/mTurq2 inserts using an infusion HD cloning (Clonetech) reaction. The infusion reaction is a ligation independent cloning method. The infusion enzyme has 3'-5' exonuclease activity and attacks exposed ends of broken double stranded DNA resulting in single stranded stretches of the template vector and sYFP2/mTurq2 insert allowing complementary paring during the infusion reaction. For this reaction 4 µl of template, 4 µl insert and 2 µl 5x Infusion HD enzyme premix (Clonetech) were mixed and incubated at 50 °c for 20 minutes.

2.14.3 Linker Design

Additional constructs were designed encompassing an extended series of amino acids, or a "linker", between Piezo1/CD31 and their corresponding fluorophore. Linker 4 (L4) was created using a series of Alanine and Serine amino acid repeats.

DNA:5'GCCAGCGCATCCGCTAGCGCCTCTGCCAGCGCTAGTGCCTCTGCATC
CGCTTCAGCCTCCGCCTCTGCCAGTGCAAGCGCAAGTGCTAGC 3',

Protein:ASASASASASASASASASASASASASASAS

This paring of amino acids was chosen as we predicted that it would give a good combination of flexibility and rigidity due to the differing charges of alanine and serine. Computer modelling predicts L4 to have a 5 nm linear structure.

Each linker was flanked with either a BamH1 (Piezo1) or a HindIII (CD31) restriction enzyme site to facilitate subsequent cloning and alterations of linkers. The linkers were inserted into either a BamH1 digested vector (Piezo1-mTurq2/sYFP2) or a HindIII digested vector (CD31-mTurq2/sYFP2) using the In-fusion method described above with primers displayed in Table 2.5. Final plasmids are displayed in (Figure 2.7 & Figure 2.8).

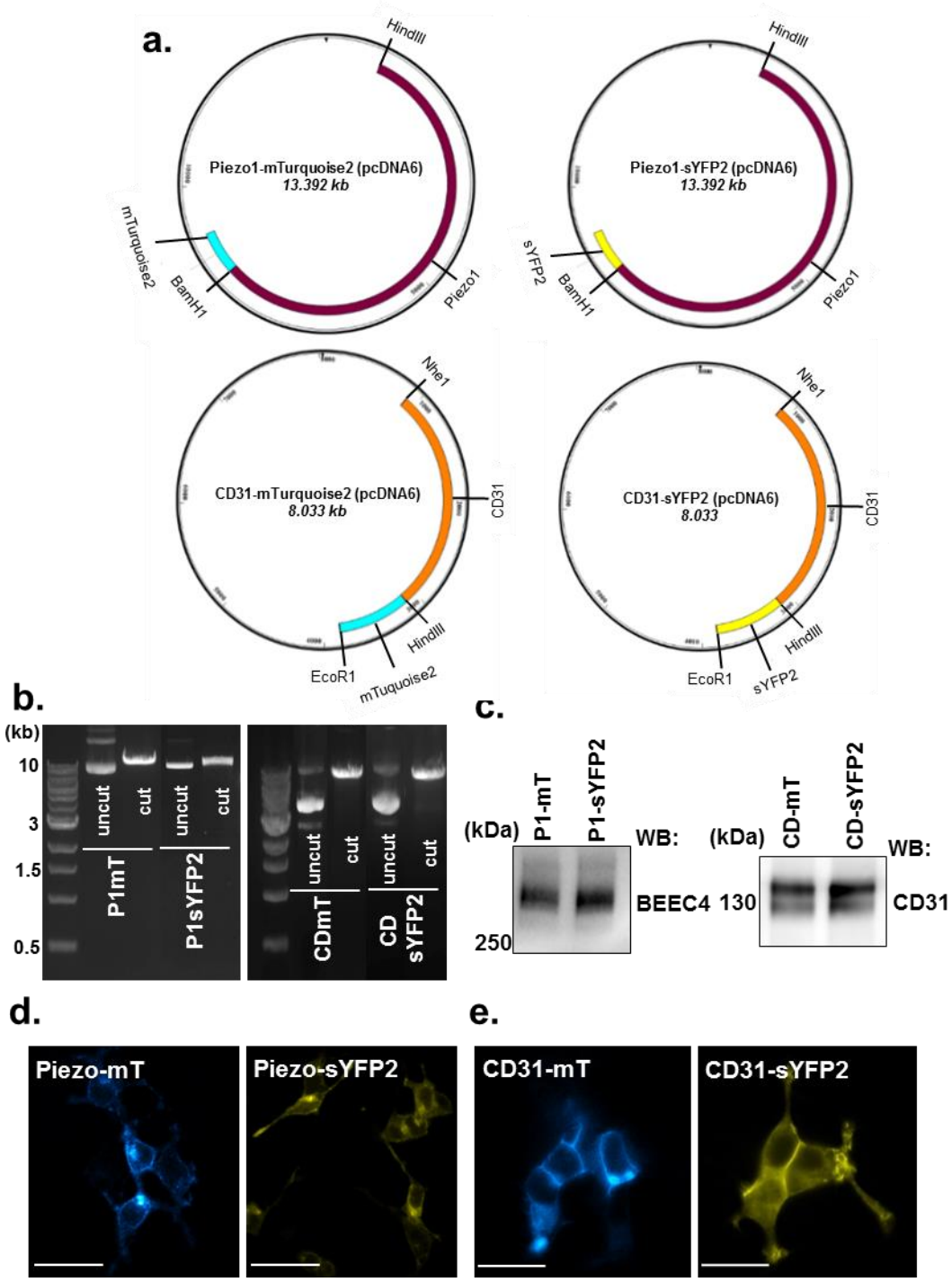

Figure 2.7 Piezo1 and CD31 construct design and validation

a) Construct maps for plasmids expressing Piezo1-mTurquoise2, Piezo1-sYFP2, CD31-mTurquoise2 or CD31-sYFP2 in the pcDNA6 vector. b) Electrophoresis gel of a restriction digest using restriction enzymes BamH1 (P1mT/P1sYFP2) or HindIII (CDmT/CDsYFP2). c) Example western blots for Piezo1 (anti-BEEC4 antibody) or CD31 (anti-CD31 antibody) expressed in HEK 293 cells transfected with Piezo1-mT, Piezo1-sYFP2, CD31, CD31-mT or CD31-sYFP2. d) HEK 293 cells transfected with Piezo1-mT (blue) or Piezo1-sYFP2 (yellow). e) HEK 293 cells transfected with CD31-mT (blue) or CD31-sYFP2 (yellow).

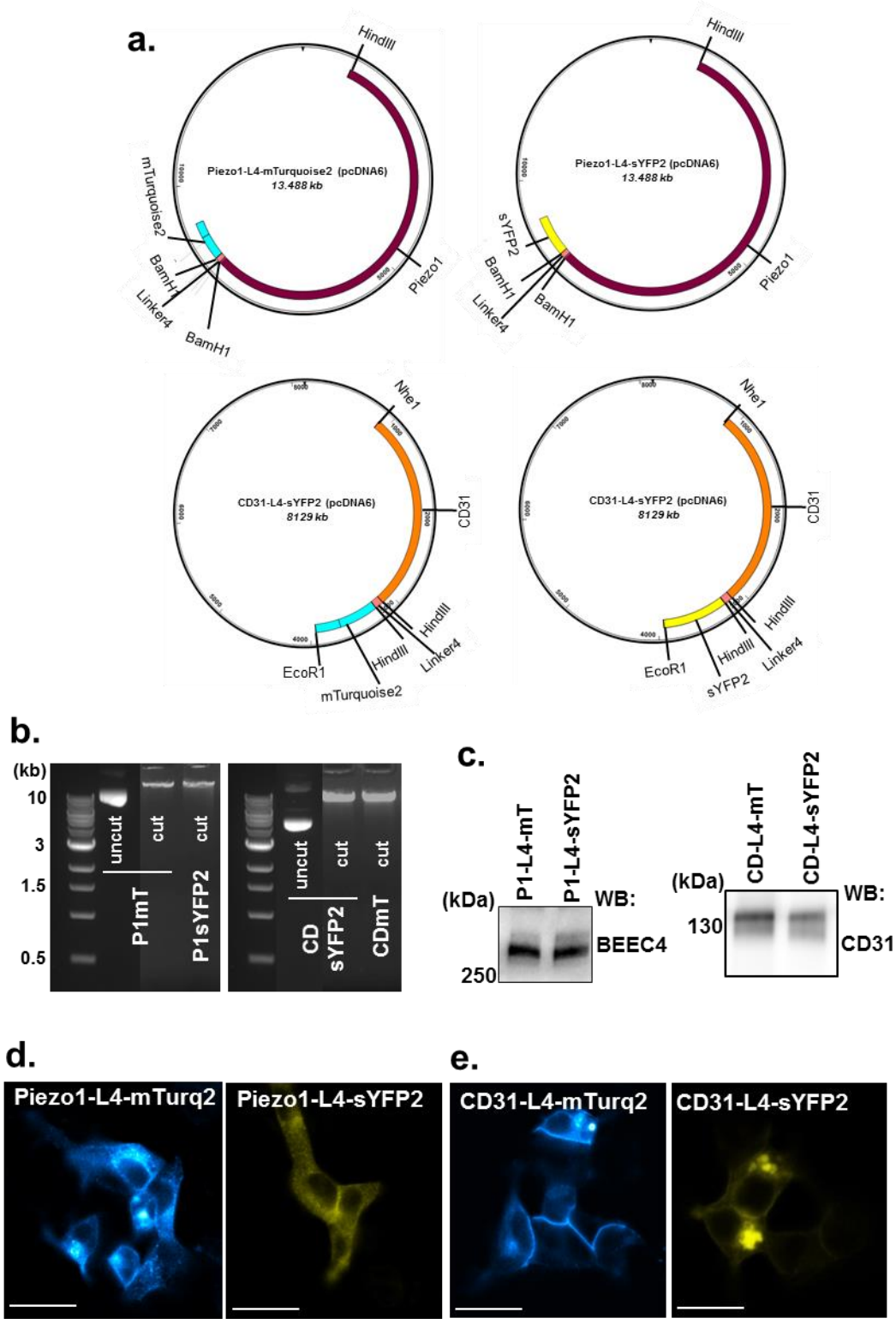

Figure 2.8 Piezo1 and CD31 linker 4 construct design and validation.

a) Construct maps for plasmids expressing Piezo1-L4-mTurquoise2, Piezo1-L4-sYFP2, CD31-L4-mTurquoise2 or CD31-L4-sYFP2 in the pcDNA6 vector. b) Electrophoresis gel of a restriction digest using restriction enzymes BamH1 (P1mT/P1sYFP2) or HindIII (CDmT/CDsYFP2) c) Example western blots for Piezo1 (anti-BEEC4 antibody) or CD31 (anti-CD31 antibody) expressed in HEK 293 cells transfected with Piezo1-L4-mT, Piezo1-L4-sYFP2, CD31-L4-mT or CD31-L4-sYFP2. d) HEK 293 cells transfected with Piezo1-L4-mT (blue) or Piezo1-L4-sYFP2 (yellow). e) HEK 293 cells transfected with CD31-L4-mT (blue) or CD31-L4-sYFP2 (yellow).

Plasmid	Vector	Selection Antibiotic	Notes
CD31	pcDNA6	Ampicillin	Cloned by Dr Bing Hou
CD31-L4-mT	pcDNA6	Ampicillin	Cloning as described in methods
CD31-L4-sYFP2	pcDNA6	Ampicillin	Cloning as described in methods
CS31-mT	pcDNA6	Ampicillin	Cloning as described in methods
Cd31-sYFP2	pcDNA6	Ampicillin	Cloning as described in methods
pRK5 c-Fyn	pRK5	Ampicillin	pRK5 c-Fyn was a gift from Filippo Giancotti (Addgene plasmid # 16032)
pRK5 FynΔSH3	pRK5	Ampicillin	pRK5 Fyn deltaSH3 was a gift from Filippo Giancotti (Addgene plasmid # 16034)
G_{i2}EE	pCSC-SP-PW-GFP	Ampicillin	Gift from Yale University
G_{i2}EE Q/L	pCSC-SP-PW-GFP	Ampicillin	Gift from Yale University
GST-GINIP	pCSC-SP-PW-GFP	Ampicillin	Gift from Yale University
hM4d	pCSC-SP-PW-GFP	Ampicillin	Gift from Yale University
mTurquoise2-C1	pEGFP-C1	Kanamycin	Gift from Michael Davidson & Dorus Gadella (Addgene plasmid # 54842)
Piezo1	pcDNA6	Ampicillin	Cloned from Piezo1-GFP (Li et al., 2014)
Piezo1-L4-mT	pcDNA6	Ampicillin	Cloning as described in methods
Piezo1-L4-sYFP2	pcDNA6	Ampicillin	Cloning as described in methods
Piezo1-mT	pcDNA6	Ampicillin	Cloning as described in methods
Piezo1-sYFP2	pcDNA6	Ampicillin	Cloning as described in methods
pSYFP2-C1	pEGFP-C1	Kanamycin	Gift from Dorus Gadella (Addgene plasmid # 22878)
VE-Cadherin*	mVenus-N1	Ampicillin	Cloned from mVenus-VE-Cadherin-N-10 which was a gift from Michael Davidson (Addgene plasmid # 56340)
VEGFR2*	pcDNA4/TO	Ampicillin	Cloned from mEmerald-VEGFR2-N which was a gift from Michael Davidson (Addgene plasmid # 54298)

Table 2.6 List of plasmids.

*More info can be found in section ‘2.14 Plasmids and construct assembly’

2.15 Fluorescence Lifetime Imaging Microscopy (FLIM) / Fluorescence Resonance Energy Transfer (FRET)

Fluorescence lifetime images were acquired using a confocal laser scanning microscope (Zeiss LSM 710) equipped with a time-correlated single photon counting module (SPC 150, Becker & Hickl). For detection of sYFP2 or mTurquoise2, the samples were excited using a 514 nm or 458 nm diode laser, respectively, at 40 MHz repetitions. Emitted light was spectrally filtered using a narrow 482/25 Brightline Bandpass filter 25mm (Zeiss). FLIM analysis was performed on SPC image (Becker & Hickl).

2.16 Data analysis

All data are presented as mean ± SEM. Data were analysed and figures formatted using OriginPro 9.1 software (OriginLab Corporation). Paired data were compared statistically using a paired Students' *t*-test. Data sets with more than 2 groups were compared using one-way ANOVA with a post-hoc Bonferroni correction. Statistical significance is indicated by * ($p<0.05$), ** ($p<0.01$) and *** ($p<0.001$). No significant difference is indicated by NS ($p>0.05$). The number of independent experiments is indicated by 'n'. For multiwell assays, the number of replicate wells is indicated by 'N'.

Chapter 3 Chemical Activation of Piezo1 is Tightly Coupled to eNOS Phosphorylation

3.1 Introduction

The literature suggests that endothelial cells possess a plethora of mechanosensors that are modulated by shear stress. These mechanosensors sense blood flow and translate physical force into biochemical signalling events (Givens and Tzima, 2016). The mechanosensory ion channel, Piezo1, is just one of the many proteins that shear stress regulates (Li et al., 2014; Givens and Tzima, 2016). The complexity of the shear stress response renders it challenging to study and understanding the mechanisms by which shear stress is sensed in endothelial cells requires an integrated approach. Studying the role of Piezo1 alone demands a more direct method. Pharmacological compounds that selectively modulate Piezo1 channels are attractive laboratory tools to overcome such difficulties as they would allow isolation of Piezo1-mediated responses. The pioneering discovery of the first chemical activator of Piezo1, Yoda1, in 2015 has provided an important new way to selectively stimulate this channel without mechanical force (Syeda et al., 2015). This opened up new possibilities for specific Piezo1 channel studies. Yoda1 was discovered during a high-throughput Ca^{2+} imaging screen and is reported as an agonist of both human and mouse Piezo1 when over-expressed in otherwise Piezo1 null cells.

The main aims of this chapter were to investigate whether Yoda1 could activate endogenous endothelial Piezo1 channels. Furthermore, it was important to examine whether a Piezo1-mediated downstream effect of shear stress, namely, eNOS phosphorylation, could be mimicked with Yoda1 application. Understanding this mechanism could be important for achieving better appreciation of how shear stress regulates cardiovascular structure and function. Intracellular Ca^{2+} measurement assays were carried out to examine whether Yoda1 could activate endothelial Piezo1 in HUVECs. Immunoblotting was undertaken to address whether Yoda1 could mimic shear stress evoked Piezo1 mediated eNOS phosphorylation. Chemical antagonists, siRNA targeting Piezo1 and an inducible endothelial Piezo1 knockout mouse model were used to assess the involvement of the Piezo1 channel in Yoda1-mediated eNOS phosphorylation.

3.2 Yoda1 activates endogenous human Piezo1 in HUVECs

In 2015 a library of ~3.25 million compounds was screened as activators of Piezo1 or Piezo2 channels. Yoda1 was identified as the first chemical agonist of the Piezo1 channel (Syeda et al., 2015). Yoda1 was described to be specific for human and mouse Piezo1 over Piezo2 and did not evoke any response in CRISPR/Cas9-manipulated Piezo1 null HEK 293 cells. Yoda1 activated purified Piezo1 channels reconstituted in an artificial bilayer, suggesting that Yoda1-evoked Piezo1 channel activation was membrane delimited. Application of the Ca^{2+} chelator, EGTA, suppressed the response confirming that Yoda1 activated plasma membrane Piezo1 to evoke Ca^{2+} entry. Here, Yoda1-mediated Piezo1 activation was examined in human endothelial cells endogenously expressing Piezo1 channels.

3.2.1 Yoda1 activates human Piezo1 overexpressed in a Piezo1 null cell line

In order to confirm that Yoda1 can activate human Piezo1 channels a HEK cell line expressing Piezo1 under a tetracycline inducible promoter (HEK-P1), which had previously been created in the laboratory (Rode et al., 2017), was utilised. Immunoblotting was used to validate the cell line. Commercially available anti-Piezo1 antibodies are fairly non-specific. Together with Cambridge Biosciences a range of anti-Piezo1 antibodies targeting various regions of the extracellular loop of Piezo1 were created with anticipation that they will have improved specificity. The antibody, BEEC4, was developed and was able to detect over-expressed Piezo1. As expected, application of tetracycline induced expression of Piezo1 (Figure 3.1a). The parent HEK-TRex cell line expressed little or no Piezo1. Next, intracellular Ca^{2+} was measured before and after application of Yoda1 using the FlexStation to record intracellular Ca^{2+} events. In keeping with the literature, Yoda1 increased the levels of intracellular Ca^{2+} in the HEK-P1 cells (Figure 3.1b) (Syeda et al., 2015). This was absent in the HEK-TRex cells, consistent with Piezo1 expression only in the HEK-P1 cells (Figure 3.1b). Application of DMSO, the vehicle of Yoda1, had no effect (Figure 3.1b). This result is in line with a previous publication suggesting that Yoda1 can activate human Piezo1 (Syeda et al., 2015).

3.2.2 Yoda1 activates Ca^{2+} entry in HUVECs

To examine whether Yoda1 could be useful to study endogenous Piezo1 channels the ability of Yoda1 to activate endothelial Piezo1 channels was examined in HUVECs. Due to poor aqueous solubility the maximum working dose of Yoda1 is 10-20 µM (Syeda et al., 2015). Application of a maximal dose of 10 µM Yoda1 increased intracellular Ca^{2+} levels compared to application of its vehicle alone (Figure 3.2a). Application of increasing concentrations of Yoda1 up to 10 µM dose-dependently increased intracellular Ca^{2+} levels (Figure 3.2b). Within the concentration range tested a maximal response was not achieved, which, along with the poor solubility likely causing some degree of precipitation, limits meaningful interpretation of the EC_{50} value. However, based on the data it is predicted that in HUVECs Yoda1 activates endogenous Piezo1 channels with an EC_{50} of 1.5 µM which closely matches that of HEK-P1 cells (Evans et al., 2018; Rode et al., 2017). Henceforth, Yoda1 was used at a sub-maximal dose of 2 µM, which we estimate to be around the EC_{80}.

In order to confirm that Yoda1 was activating plasma membrane Piezo1 channels and inducing Ca^{2+} entry and not causing Ca^{2+} release from intracellular stores, HUVECs were pre-treated with either 0 mM extracellular Ca^{2+} or physiological levels of extracellular Ca^{2+} (1.5 mM). In the absence of extracellular Ca^{2+} the activation observed with Yoda1 was dramatically reduced (Figure 3.3a & b). As a positive control to prove that the cells treated with 0 mM Ca^{2+} were alive a second application of Yoda1 in the presence of physiological Ca^{2+} was applied. Cells previously treated with 0 mM Ca^{2+}_{ex} were able to respond to application of Yoda1 in the presence of Ca^{2+} (Figure 3.3a & c). This was larger than cells earlier treated with vehicle in the presence of Ca^{2+} (Figure 3.3a & c). One explanation for the amplification of this response could be due to an additional contribution of SOCE. Pre-treatment with 0 mM Ca^{2+}_{ex} could have led to depletion of Ca^{2+} in the intracellular endoplasmic reticulum stores and addition of extracellular Ca^{2+} could activate SOCE, on top of the Yoda1-medaited Ca^{2+} entry. A second addition of Yoda1 in the presence of Ca^{2+} had no effect, perhaps due to Yoda1 not being washed out.

These data confirm that Yoda1 can activate Ca^{2+} entry in HUVECs. However, as the response is not fully abolished in the absence of extracellular Ca^{2+} it raises the

possibility that some functional Piezo1 channels could be present on intracellular membranes.

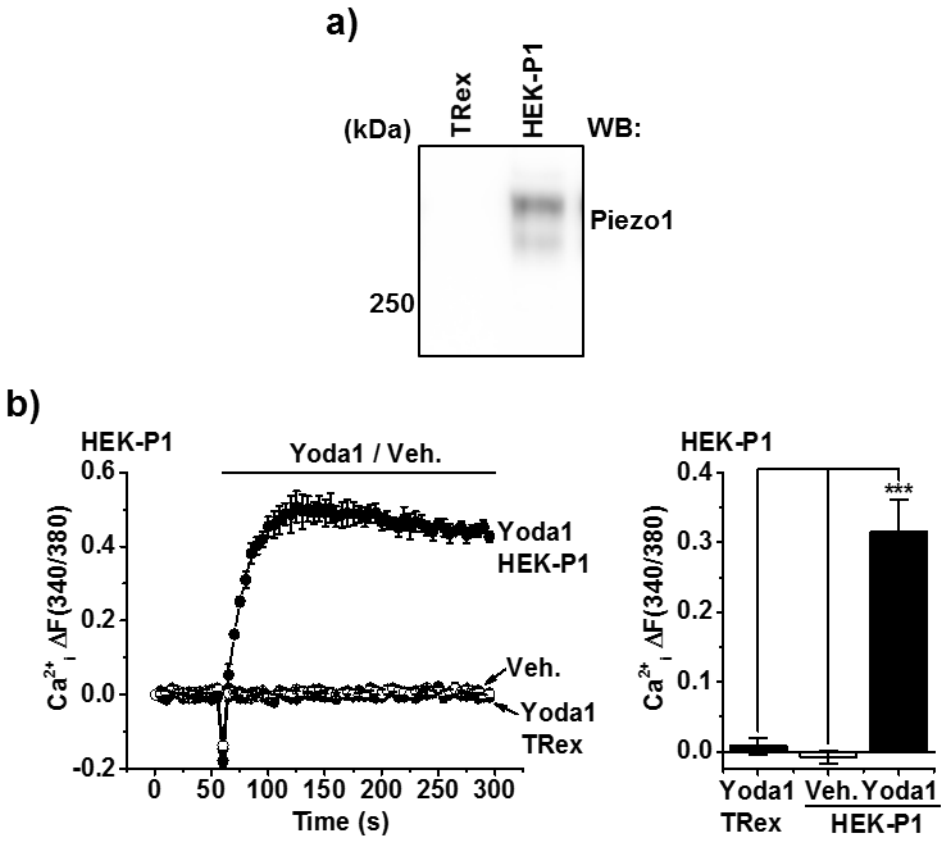

Figure 3.1 Yoda1 activates human Piezo1 when overexpressed in an otherwise null cell line.

a) Representative immunoblot for anti-Piezo1 (BEEC4) in HUVECs expressing Piezo1 under a tetracycline inducible promoter (HEK-P1) or not (TRex) after 24 hour treatment with 10 ng.ml^{-1} tetracycline. b) Left: example Ca^{2+} measurements in response to application of 2 µM Yoda1 or its vehicle (Veh.) in HEK-P1 or TRex control cells. Right: Mean data for the type of experiments shown on the left (n/N=3/12).

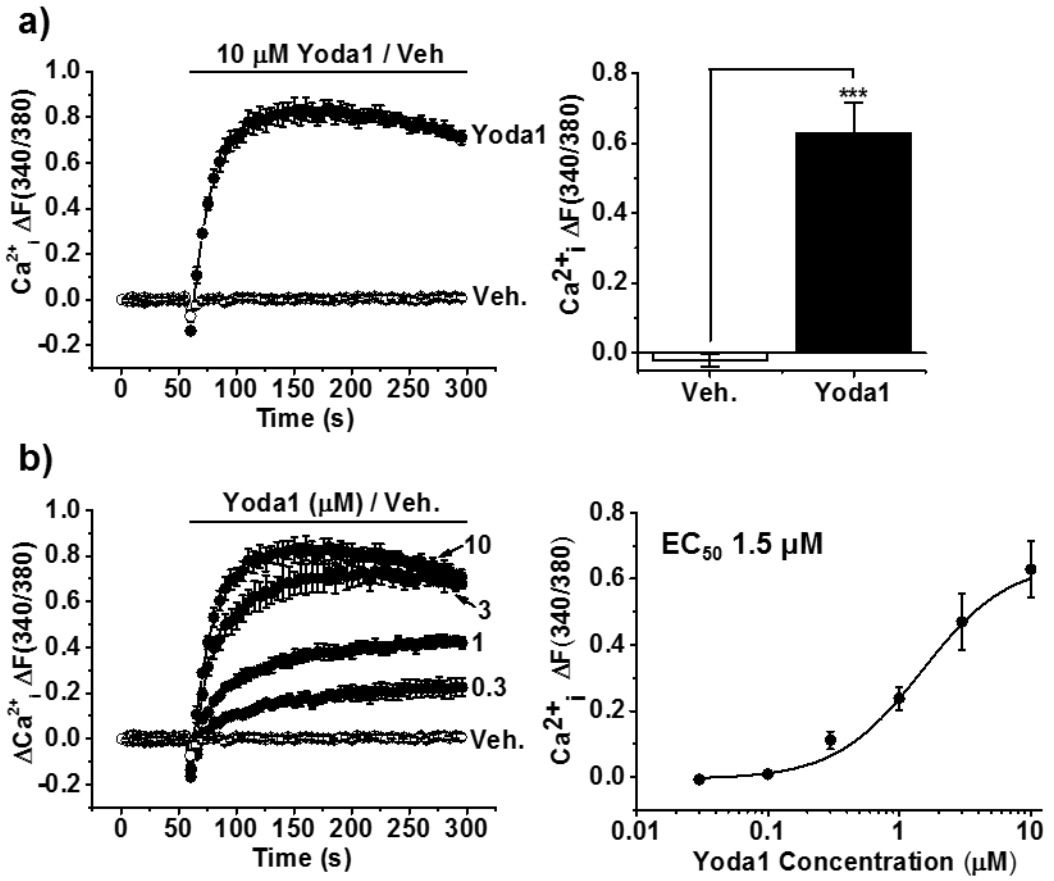

Figure 3.2 Yoda1 activates an increase in intracellular Ca^{2+} in HUVECs.

a) Left: Example Ca^{2+} measurement trace in HUVECs during application of 10 µM Yoda1 or its vehicle (Veh.). Right: Mean data for the type of experiments displayed on the left (n/N=3/12) b) Example Ca^{2+} measurement traces in response to increasing concentrations of Yoda1 (0.3 – 10 µM) or its vehicle (Veh.). Right: Concentration-response data for Yoda1 from the type of experiments on the left (n/N=3/12). The fitted curve is a Hill equation indicating the 50% maximum effect (EC_{50}) at 1.5 µM.

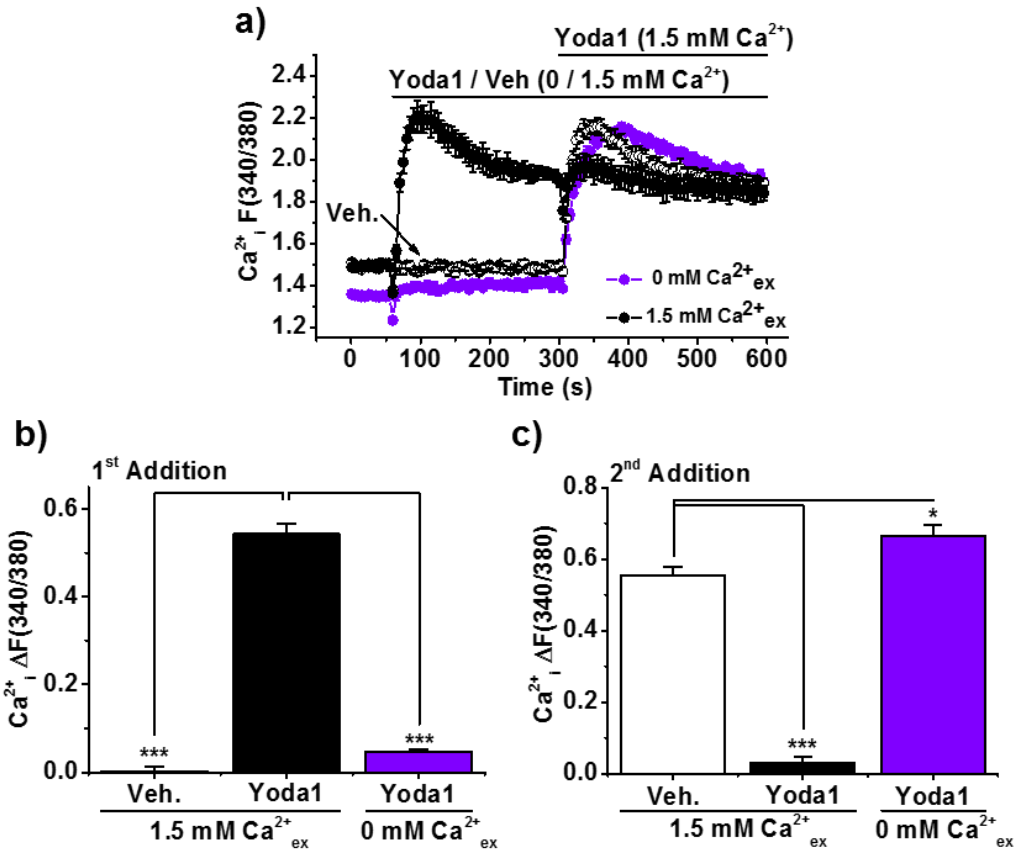

Figure 3.3 Yoda1 primarily activates Ca^{2+} entry in HUVECs.

a) Example Ca^{2+} measurement traces in response to 2 µM Yoda1 or its vehicle (Veh.) with or without 20-minutes pre-treatment with 0 mM extracellular Ca^{2+} (Ca^{2+}_{ex}) followed by a second addition of 2 µM Yoda1 in the presence of 1.5 mM Ca^{2+}_{ex}. b) Mean data for the type of experiment in (a) taking amplitude measurements during the first addition (100 seconds). c) Mean data for the type of experiment in (a) taking baseline measurements initially before the second addition and taking amplitude measurements during the second addition (400 seconds) (n/N=3/10-12).

3.2.3 Yoda1 activates Piezo1 mediated Ca^{2+} entry and current in HUVECs

After confirming that Yoda1 evokes Ca^{2+} entry in HUVECs it was important to test if this was Piezo1 mediated. Firstly, acute chemical inhibition of Piezo1 was examined. Gadolinium and ruthenium red are both widely used non-selective antagonists of non-selective cationic channels, including Piezo1 (Coste et al., 2012; Coste et al., 2010). Pre-treatment with either gadolinium or ruthenium red dose-dependently inhibited the Yoda1 evoked Ca^{2+} entry with IC_{50}'s of 7 μM and 2.6 μM respectively (Figure 3.4a & b). As they are Piezo1 channel antagonists this is consistent with Piezo1 channels mediating the response.

To further test if Yoda1 was activating Piezo1 channels, patch-clamp experiments were performed in HUVECs to examine the Yoda1-mediated current. These experiments were performed by Dr Yasuyuki Tanahashi, a visiting research fellow from Kyoto Sangyo University. Yoda1 increased both an inward and outward current that was sensitive to inhibition by ruthenium red, consistent with the Ca^{2+} imaging data (Figure 3.5a & c). The current (*I*) voltage (*V*) relationship represents that of a non-selective cation current with a reversal potential close to 0 mV (Figure 3.5b).

Even though it was important to examine acute blockade of Piezo1 channels, ruthenium-red and gadolinium are non-selective cation channel pore inhibitors and thus it was imperative to investigate the role of the channels further using a more selective inhibitory strategy. As there are currently no selective small-molecule inhibitors of Piezo1 channels, siRNA targeting Piezo1 to genetically disrupt its expression was utilised. Treatment with Piezo1 siRNA knocked down Piezo1 mRNA levels by over 90 % compared to those treated with a scrambled control (Figure 3.6a). The agarose gel demonstrates that the size of the end products amplified during the PCR were as expected from the primer design (Beta Actin: 194bp and Piezo1: 182bp) (Figure 3.6a). As end products of the PCR reactions were run on the gel the band in Piezo1 knockdown samples was of the same intensity. The anti-Piezo1 antibody BEEC4, which was developed in our lab, can only detect overexpressed Piezo1 and there are no antibodies that can convincingly detect endogenous Piezo1. Therefore, Piezo1 protein expression could not be investigated. Piezo1 knockdown dramatically blunted the Yoda1 evoked Ca^{2+} entry in HUVECs, consistent with the level of Piezo1 mRNA knockdown (Figure 3.6b).

These data confirm that Yoda1 is activating endogenous Piezo1 in HUVECs. As a positive control to corroborate that the cells treated with Piezo1 siRNA are viable and have equivalent Ca^{2+} content, ionomycin was applied. Ionomycin is an ionophore that allows Ca^{2+} entry into cells independently of any endogenous Ca^{2+} handling mechanisms. Ionomycin evoked Ca^{2+} entry in both scrambled siRNA and Piezo1 siRNA treated cells to the same degree, confirming the viability of the cells (Figure 3.6c).

Taken together these data suggest that Yoda1 activates endogenous Piezo1 channels in HUVECs causing Ca^{2+} entry that can be blocked by either genetically disrupting Piezo1 channel mRNA expression or by chemically inhibiting channel function. Overexpression of Piezo1 in an otherwise Piezo1 null cell line can reconstitute this response. To further support that Yoda1 activates endothelial Piezo1 channels patch-clamp experiments confirmed that Yoda1 evokes a Piezo1 like current.

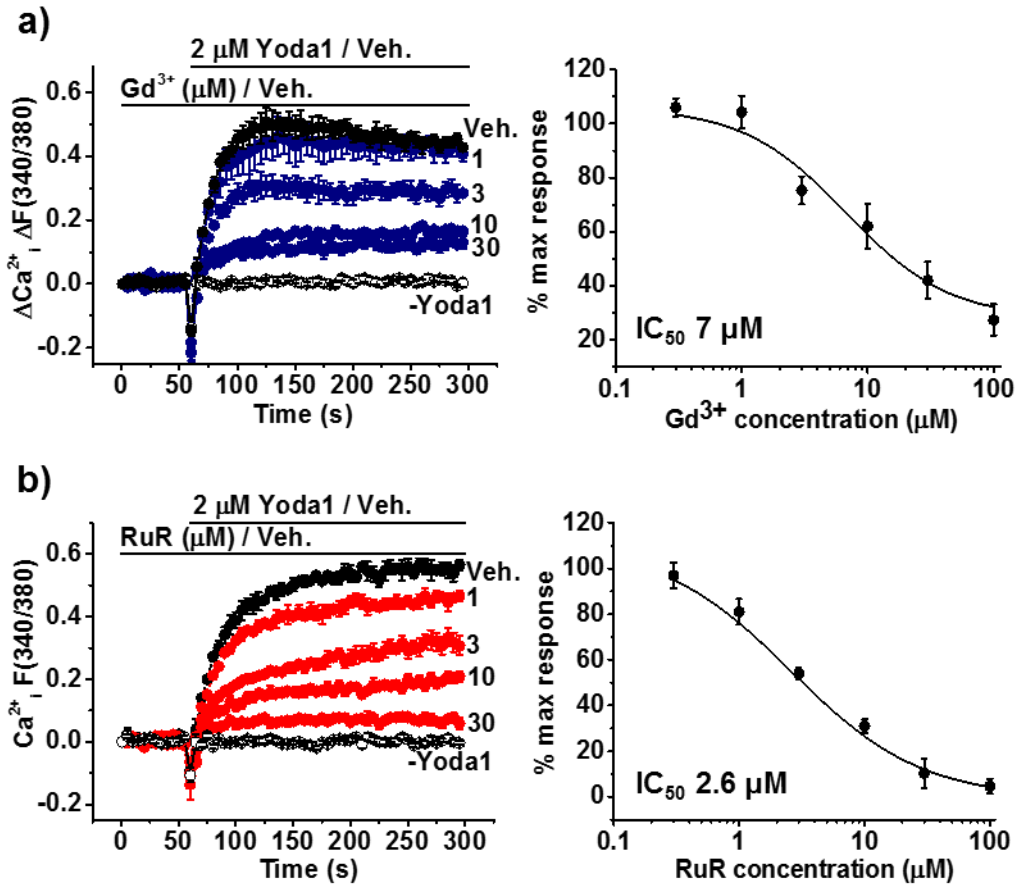

Figure 3.4 Yoda1 evoked Ca^{2+} entry is suppressed by classical ion channel inhibitors.

a) Left: example Ca^{2+} measurement trace showing Ca^{2+} entry in response to 2 µM Yoda1 in HUVECs after 20-minute pre-treatment with gadolinium at increasing concentrations (1-30 µM). Right: Concentration-response data for gadolinium (n/N=4/15-16). The fitted curve is a hill equation indicating the 50% inhibitory effect (IC_{50}) at 7 µM. b) Left: as in (a) but with increasing concentrations of ruthenium red (1-30 µM). Right: Concentration-response data for ruthenium red indicates an IC_{50} of 2.6 µM (n/N=3/10-11).

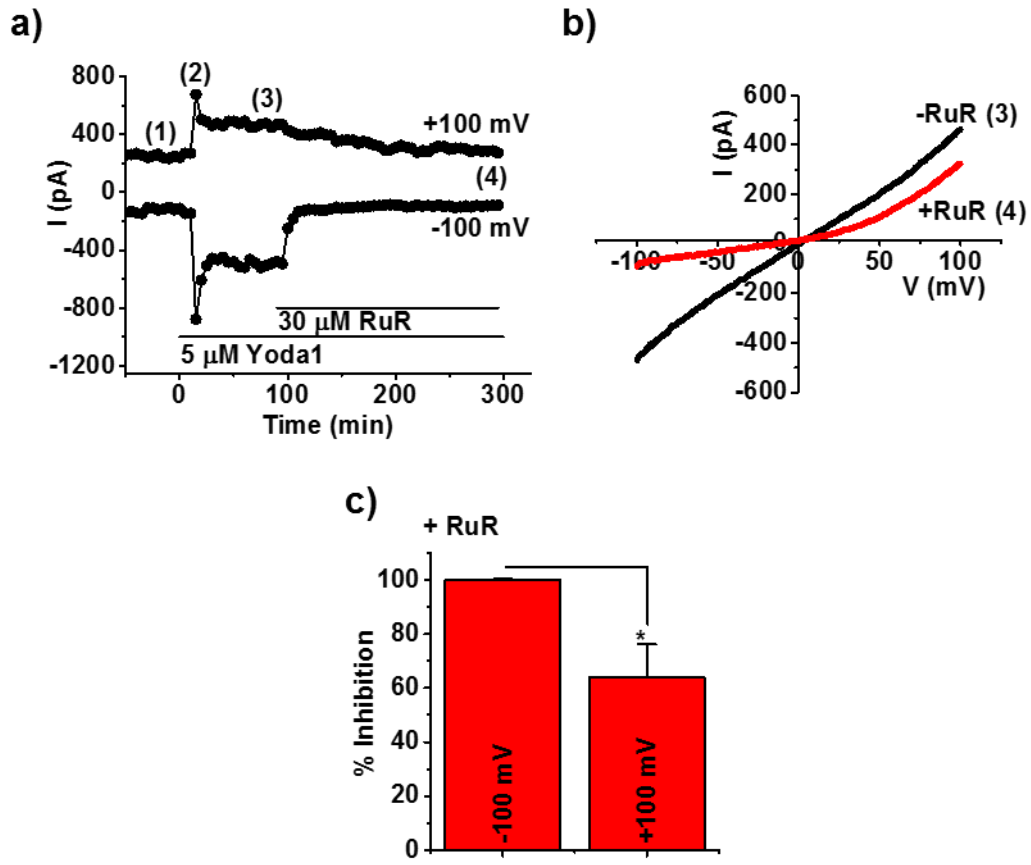

Figure 3.5 Yoda1 evokes a Piezo1 like current in HUVECs.

a) Whole-cell voltage-clamp recording of membrane current from a single HUVEC cell during ramp changes in membrane voltage from -100 to +100 mV applied every 10 s. Only current sampled at -100 and +100 is displayed. 5 µM Yoda1 and 30 µM ruthenium red are bath-applied as indicated by the horizontal bars. b) From the experiment shown in (a) displaying the current (*I*) voltage (*V*) relationship after Yoda1 treatment with (time point 4 in (a)) and without (time point 3 in (a)) ruthenium red application. c) Mean data for the type of experiment shown in a) demonstrating the % inhibition of ruthenium red at -100 and + 100 mV. Typical of n=3. All patch clamp experiments performed by Dr Yasuyuki Tanahashi on cells prepared by Hannah Gaunt.

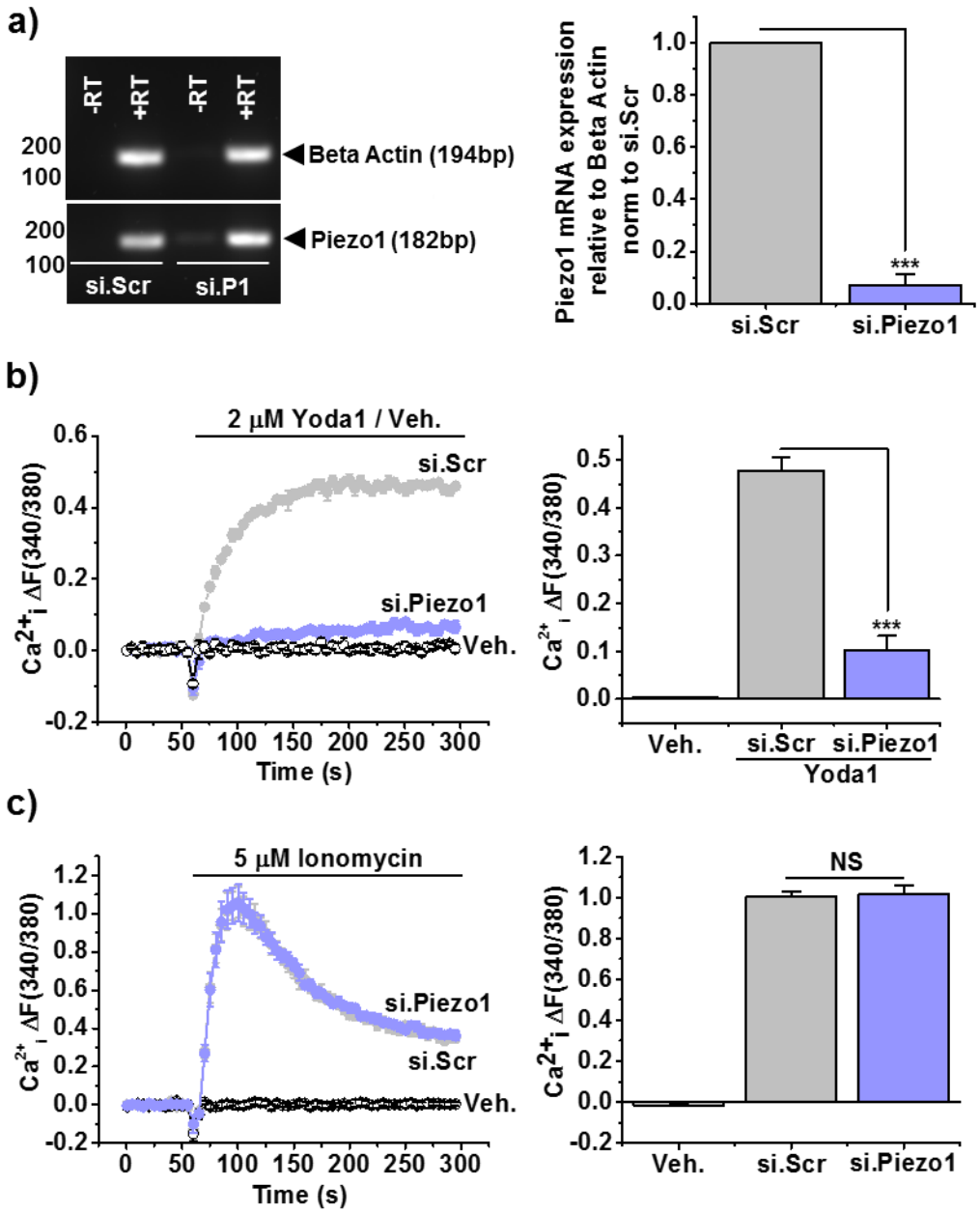

Figure 3.6 Yoda1 activates endogenous human Piezo1 in HUVECs.

a) Left: example agarose gel for end-point polymerase chain reaction products obtained with primers for Piezo1 and β-actin from HUVEC cDNA treated with either a scrambled siRNA (si.Scr) or Piezo1 siRNA (si.Piezo1/si.P1). A reverse transcriptase reaction was carried out (+RT [reverse transcriptase]) to generate cDNA. −RT denotes control reaction. Right: Mean data and analysis of Piezo1 mRNA relative to β-actin. (n = 3) b) Left: example Ca^{2+} measurement trace in the same cells treated with the same siRNA as in (a) during application of 2 µM Yoda1 or its vehicle (Veh.). Right: mean data for the type of experiment on the left (n/N=3/13). c) Left: As in (b) but with application of 5 µM Ionomycin or its vehicle (Veh.) Right: mean data for the type of experiment on the left (n/N=3/12).

3.3 Shear stress evokes Piezo1 mediated S1177 eNOS phosphorylation

Piezo1 channels are direct sensors of mechanical force that play critical roles in physiology (Li et al., 2014). Examining downstream signalling events that are associated with Piezo1's functions is very important to help us further understand its roles in cardiovascular physiology. Previous studies in our lab sought to investigate the downstream mechanisms evoked by shear stress mediated Piezo1 channel activation. Unbiased insight into downstream pathway analysis was obtained through titanium dioxide-trapping coupled with mass spectrometry to identify proteins affected by Piezo1 downregulation in static and shear stress conditions. In HUVECs, Piezo1-evoked shear regulation was linked to eNOS, also known as NOS3, a protein with very important roles in vascular biology and critical regulator of cardiovascular homeostasis (Li et al., 2014; Sessa, 2004).

Phospho-proteomic results identified that Piezo1 is important for eNOS phosphorylation at S114 but further work demonstrated a greater effect at S1177. Initially, the S1177 phospho site on eNOS was focused on as it is reported to be regulated by both Ca^{2+} and shear stress, two Piezo1 channel characteristics (Dimmeler et al., 1999; Fleming et al., 2001; Gallis et al., 1999). In order to validate these results follow-up immunoblotting experiments were performed measuring the protein level of S1177 phosphorylated eNOS compared to total eNOS. HUVECs treated with Piezo1 siRNA (si.Piezo1/si.P1), scrambled siRNA (si.Scr) or a mock transfection were subjected to 10 $dyn.cm^{-2}$ shear stress using the orbital shaker. Application of shear stress for 24 hours to control treated HUVECs (si.Scr / mock) evoked an increase in eNOS phosphorylation compared to static cells (Figure 3.7a). By comparison this response was blunted in cells with Piezo1 channel depletion (Figure 3.7a). Basal levels of peNOS were not affected by Piezo1 depletion (Figure 3.7b). Taken together, these data confirm that Piezo1 channels are crucial for shear stress mediated downstream signalling commanding S1177 eNOS phosphorylation.

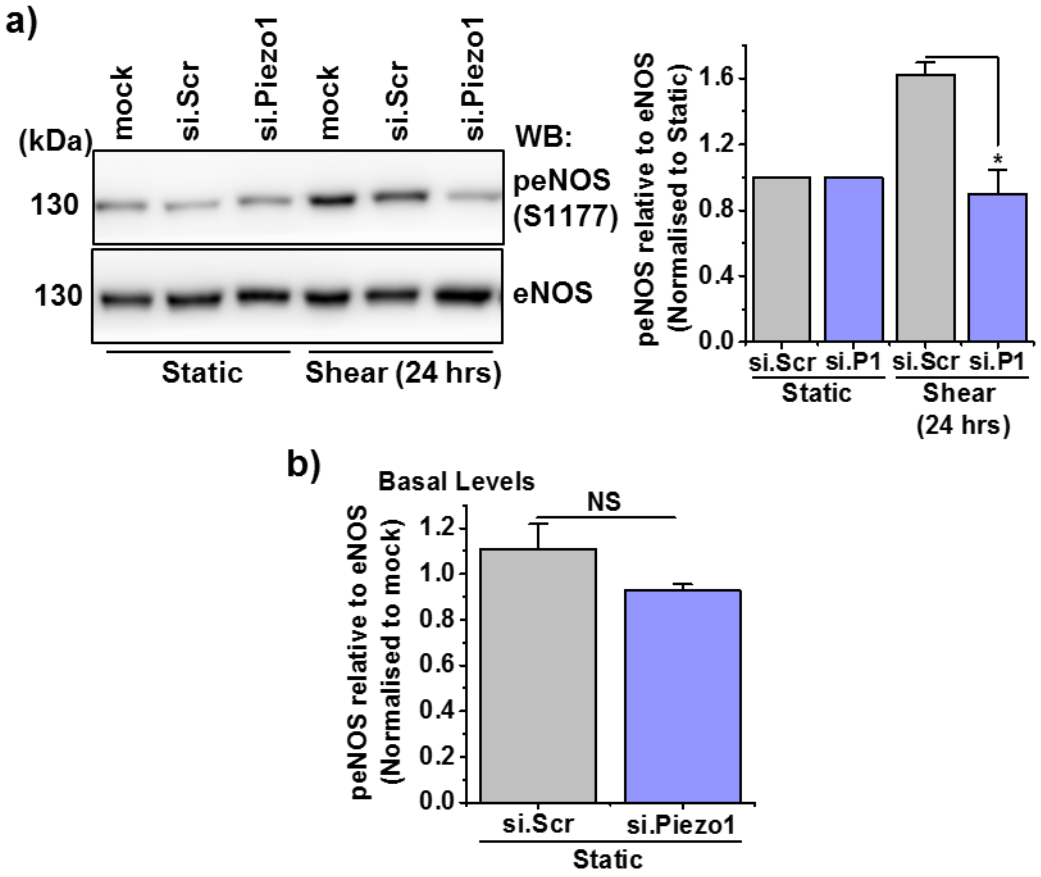

Figure 3.7 Piezo1 mediates shear stress induced eNOS phosphosylation in HUVECs

a) Left: representative immunoblot for anti-S1177 phospho-eNOS (peNOS) and anti-eNOS. HUVECs subjected to treatment with Piezo1 siRNA (si.Piezo1/si.P1), scrambed siRNA (si.Scr) or a mock transfection (mock). They are then exposed to 10 dyn.cm^{-2} shear stress or not for 24 hours using the orbital shaker. Right: mean data from n=3 independent experiments displayed as phospho-eNOS relative to total eNOS normalised to static control. b) Mean data from the type of experiments in (a) examining static phospho-eNOS expression relative to static eNOS (n=3).

3.4 Chemical activation of Piezo1 mimics shear stress induced S1177 eNOS phosphorylation and activation.

Physiological activation of Piezo1 channels mediated by shear stress leads to activation of downstream signalling, including eNOS phosphorylation. To determine whether the same phenomenon could be mimicked with selective chemical activation of the channels the small molecule Yoda1 was used.

3.4.1 Yoda1 mimics shear evoked downstream signalling in endothelial cells.

It is clear from intracellular Ca^{2+} measurement assays that the Yoda1 evoked Piezo1 activation is rapid. An increase in intracellular Ca^{2+} is induced within seconds of Yoda1 application and the response is sustained throughout the 5-minute measurement. In initial studies a 5-minute treatment of 5 µM Yoda1 was utilised but further on in the chapter studies of dose- and time-response relationships revealed that 1-minute treatment with 2 µM Yoda1 was sufficient to induce eNOS phosphorylation. In HUVECs 5-minute application of 5 µM Yoda1 evoked a clear increase in eNOS phosphorylation by 2.2 fold compared to that of vehicle control (Figure 3.8a).

To address the relevance to other endothelial cells, freshly isolated endothelial cells from human livers were studied. Healthy liver samples were taken from human patients during surgical liver resections and Dr Peter Webster (University of Leeds) isolated and cultured endothelial cells. These cells have previously been validated and are superficially similar to other types of endothelial cells (Webster et al., 2017). They express endothelial markers, VEGF treatment evokes Ca^{2+} signals and they align in the direction of flow. Similar to HUVECs, a 5-minute treatment with 5 µM Yoda1 was able to induce S1177 eNOS phosphorylation by 1.7 fold compared to vehicle (Figure 3.8b). Taken together, these data suggest that Yoda1 is able to mimic shear stress evoked eNOS phosphorylation in at least two types of human endothelial cells.

3.4.2 Yoda1 activates eNOS

NO is synthesised from the amino acid L-arginine by the NOS family of enzymes. Positive phosphorylation of eNOS activates the enzyme eNOS to lead to the generation of NO. In the cardiovascular system, NO has many cardio protective roles and is known to protect against endothelial cell dysfunction (Sessa, 2004).

As this study demonstrates that Yoda1 phosphorylates the positive regulatory site on eNOS, Ser1177, it was important to investigate whether this phosphorylation was sufficient to activate eNOS. To address this question, an eNOS activity assay measuring the biochemical conversion of L-arginine to L-citrulline was utilised. 20-minute application of Yoda1 was sufficient to evoke an increase in citrulline content, an indication of eNOS activation (Figure 3.9a). As a positive control VEGF was applied for 20-minutes. VEGF evoked a similar increase in citrulline content compared to Yoda1 (Figure 3.9b). These data suggest that Yoda1-evoked eNOS phosphorylation does indeed lead to eNOS activation, implicating Yoda1 as a useful tool to examine specific Piezo1 downstream pathway activation.

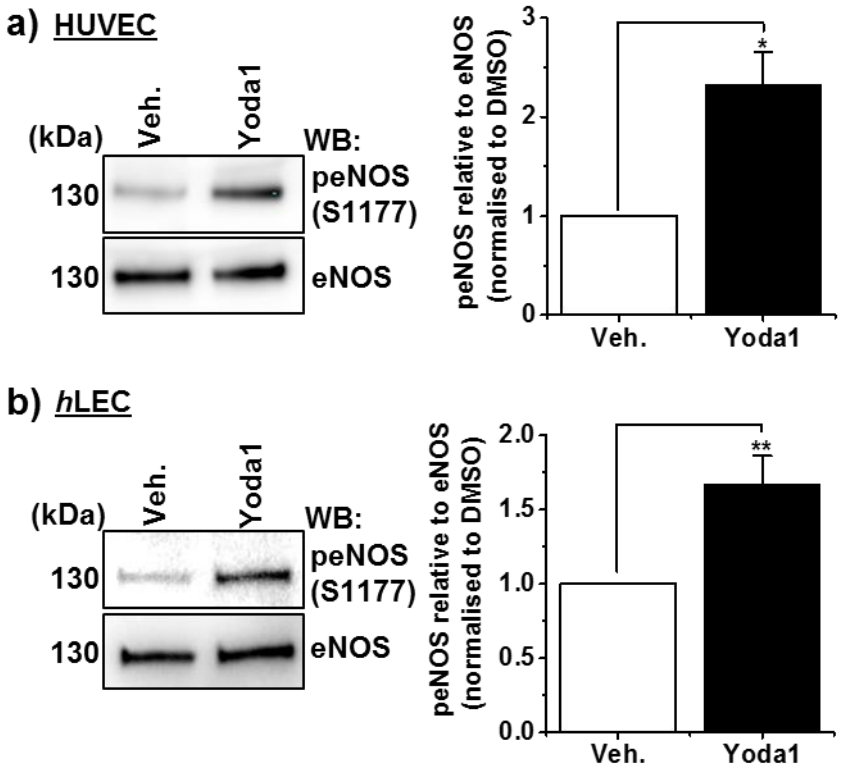

Figure 3.8 Yoda1 causes eNOS phosphorylation in two types of human endothelial cell.

a) Left: Representative immunoblot of HUVECs treated for 5-minutes with 5 μM Yoda1 or its vehicle (Veh.) for anti-S1177 phospho-eNOS or anti-eNOS. Right: Mean data from n=10 experiments displayed as S1177 phospho-eNOS relative to eNOS normalised to Veh. treatment. b) As in (a) but in endothelial cells isolated from human livers (hLEC) (n=4 patients).

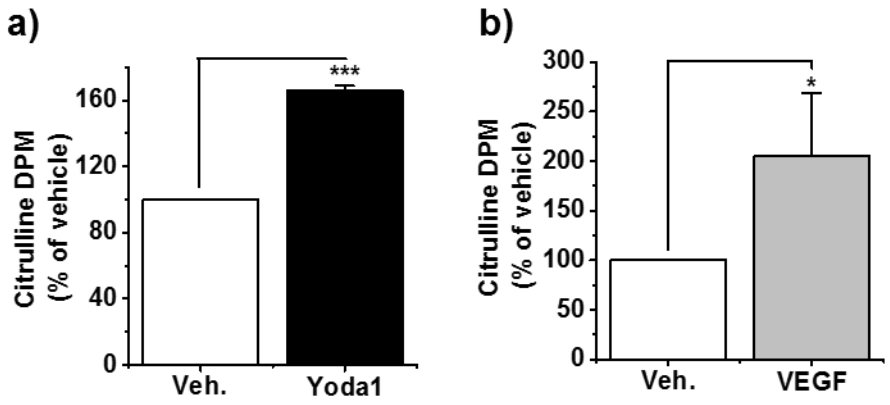

Figure 3.9 Yoda1 activates the eNOS enzyme.

a) Mean data for the biochemical L-arginine to L-citrulline conversion assay. HUVECs were treated with 2 µM Yoda1 or its vehicle (Veh.) for 20-minutes. Results are displayed as Citrulline disintegrations per minute (dpm) normalised to vehicle (Veh.) (n=3). b) As in (a) but in HUVECs treated with 30 $ng.ml^{-1}$ VEGF for 20-minutes (n=3). Experiments performed alongside Dr Hema Viswambharan (University of Leeds).

3.4.3 Yoda1 potently evokes a rapid increase in peNOS

So far it has been demonstrated that Yoda1 mimics shear stress mediated signalling to evoke eNOS phosphorylation. eNOS is a critical regulator of cardiovascular homeostasis. Its activation leads to the production of NO, which is an endogenous vasodilatory gas that regulates blood vessel diameter, blood pressure and maintains endothelial function. In order to further characterise Yoda1 mediated eNOS phosphorylation, dose-response experiments were carried out. In order to focus on early events 1-minute treatment was used. Yoda1 was applied to HUVECs for 1-minute at increasing concentrations (0.01 - 30 µM) and eNOS phosphorylation was examined. Even though the dose response curve was somewhat variable, there was a clear dose dependent increase in Yoda1 evoked eNOS phosphorylation (Figure 3.10). As before, the EC_{50} was predicted due to precipitation problems with Yoda1 at concentrations over 10 µM. Yoda1 phosphorylates eNOS with a predicted EC_{50} of 1.17 µM that plateaued at 3-10 µM (Figure 3.10). This EC_{50} is similar to that of the Ca^{2+} measurement response (Figure 3.2b).

In order to determine how rapidly Yoda1 evokes eNOS phosphorylation and to guide further experiments, time course experiments were carried out. HUVECs were treated with 2 µM Yoda1 for 10-300 seconds. 300-seconds was used as a maximum treatment time as direct downstream pathway activation was of interest. 60-second treatment with Yoda1 was sufficient to evoke an increase in eNOS phosphorylation and this was further amplified after 5-minutes (Figure 3.11). In some experiments eNOS phosphorylation was even seen after as little as a 10-second treatment with Yoda1.

Here onwards a submaximal dose of 2 µM Yoda1 with a treatment time of 1-minute was used throughout further experiments. This enabled robust yet immediate downstream signalling events evoked by Yoda1 to be examined.

3.4.4 Yoda1 phosphorylates eNOS to a similar degree as other physiological activators

Even though chemical activation of Piezo1 evoking eNOS phosphorylation is interesting it was important to examine whether the fold increase in eNOS phosphorylation was physiological. Yoda1 evoked eNOS phosphorylation was

compared to eNOS phosphorylation to known physiological activators: VEGF and shear stress (Papapetropoulos et al., 1997; Fleming, 2010). The eNOS phosphorylation induced by Yoda1 was comparable to both of the physiological responses (Figure 3.12); Yoda1, VEGF and shear stress evoked a 1.5, 1.4 and 1.7 fold increase in eNOS phosphorylation respectively.

These data suggest that Yoda1 is a useful tool to use to examine specific downstream signalling events and importantly, Yoda1 can rapidly and potently activate eNOS phosphorylation in line with established physiological agonists of eNOS.

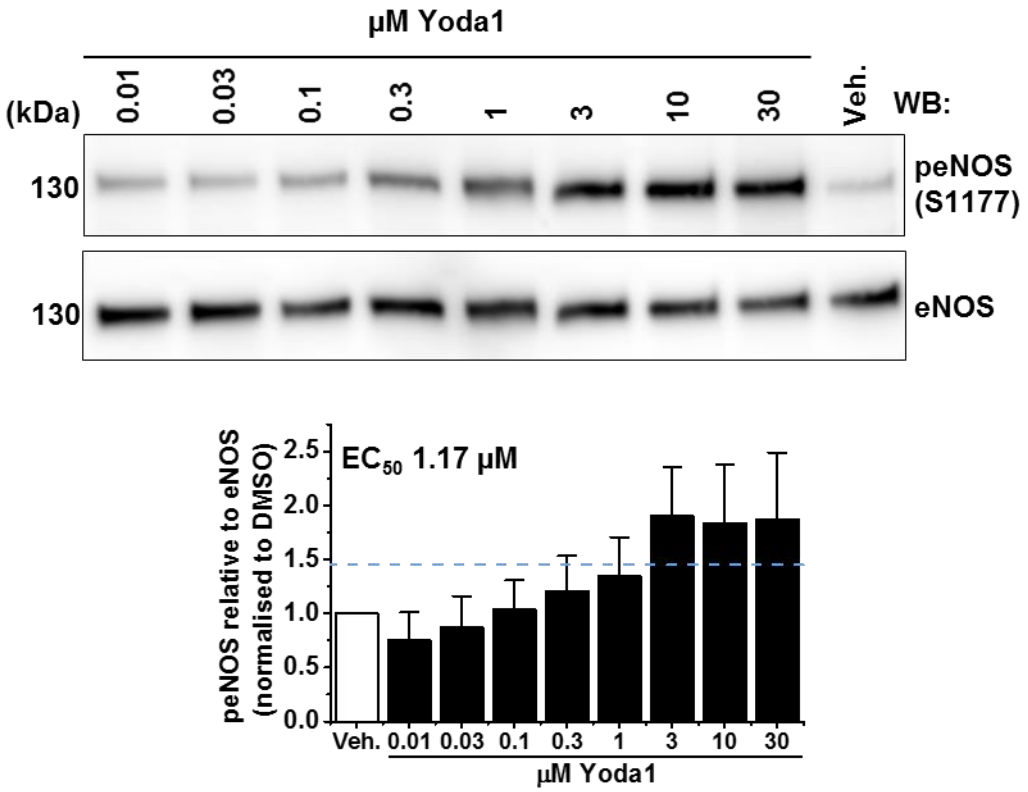

Figure 3.10 Yoda1 potently increases S1177 eNOS phosphorylation.

Upper: Representative immunoblots for anti-S1177 phospho-eNOS and anti-eNOS in HUVECs treated with increasing concentrations of Yoda1 (0.01-30 μM) or its vehicle (Veh.) for 1-minute. Lower: Mean data from 4-5 experiments. Data is displayed as peNOS relative to eNOS normalised to vehicle treated cells. 50% of the maximal response (EC_{50}) is estimated to be 1.17 μM.

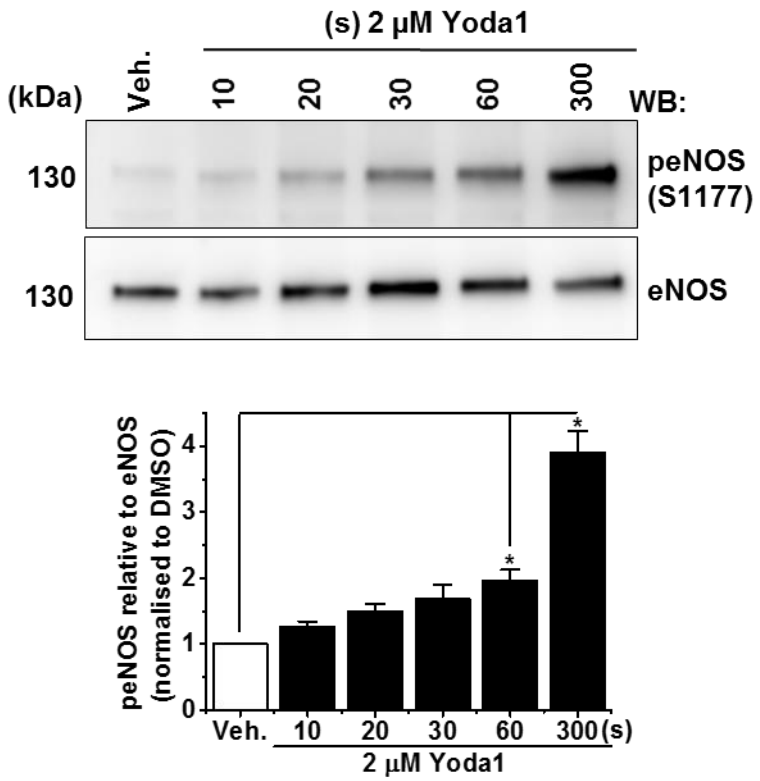

Figure 3.11 Yoda1 rapidly increases S1177 eNOS phosphorylation.

Upper: Representative immunoblots for anti-S1177 phospho-eNOS and anti-eNOS in HUVECs treated with 2 µM Yoda1 for 10-300 seconds or its vehicle (Veh.) Lower: Mean data from 3-4 experiments. Data is displayed as peNOS relative to eNOS normalised to vehicle.

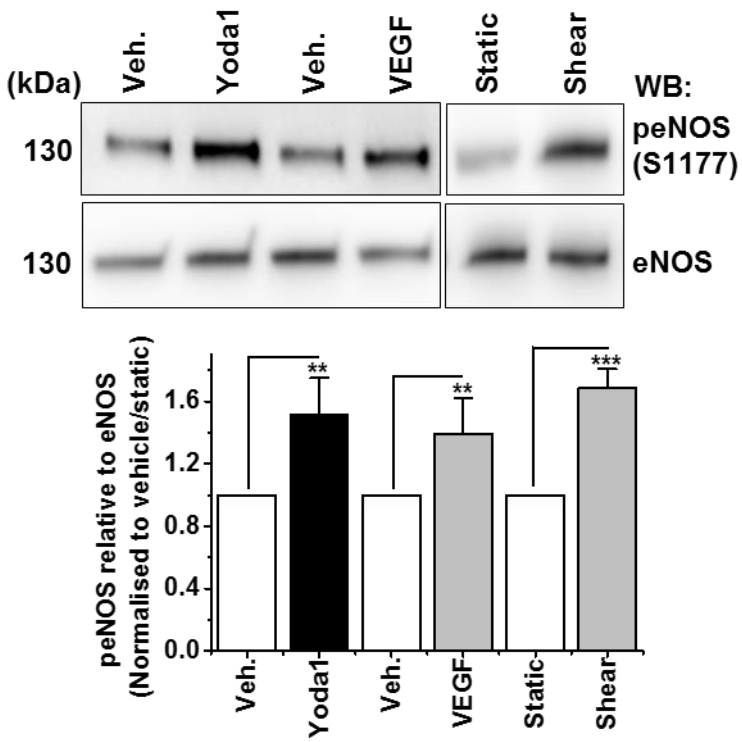

Figure 3.12 Yoda1 phosphorylates eNOS similar to physiological agonists.

Upper: Representative immunoblots for anti-S1177 phospho-eNOS and anti-eNOS in HUVECs treated with; 2 μM Yoda1 or its vehicle (veh.) for 1-minute, 20 ng.mL VEGF or its vehicle (Veh.) for 20-minutes or 10 dyn.cm^2 shear stress or static conditions for 20-minutes. Lower: Mean data from n=4-5 experiments. Data is displayed as peNOS relative to eNOS normalised to vehicle treated or static cells.

3.5 Chemical activation of Piezo1 mimics shear stress-mediated downstream pathways.

Results thus far demonstrate that Yoda1 is able to mimic shear stress to evoke eNOS phosphorylation and that a short 1-minute treatment of 2 μM Yoda1 is sufficient to evoke a physiological increase in eNOS phosphorylation. To examine whether Yoda1 could mimic other shear stress evoked endothelial signalling pathways, ERK 1/2 (p44/42 MAPK) and AKT phosphorylation events were investigated in HUVECs.

ERK and AKT are widely reported to be phosphorylated in response to shear stress (Dimmeler et al., 1999; Tseng et al., 1995). Firstly, as expected, treatment with 10 $dyn.cm^{-2}$ shear stress for 2-minutes evoked rapid p44/42 ERK phosphorylation (Figure 3.13a). Likewise, 2-minute treatment with 2 μM Yoda1 evoked an even larger increase in p44/42 ERK phosphorylation (Figure 3.13b). Furthermore, investigation into AKT phosphorylation revealed that both treatment with either 1-minute shear stress or Yoda1 was not able to evoke any increase in phospho-AKT (Figure 3.14a & b). However, a 10-minute treatment with either Yoda1 or shear stress was sufficient to evoke significant AKT phosphorylation (Figure 3.14a & b). Yoda1 and shear stress induced rapid ERK phosphorylation, however, the phospho-AKT that they induce occurs more slowly.

Taken together, these data suggest that Yoda1 acts similarly to shear stress and is able to mimic shear stress activation of downstream signalling pathways in endothelial cells.

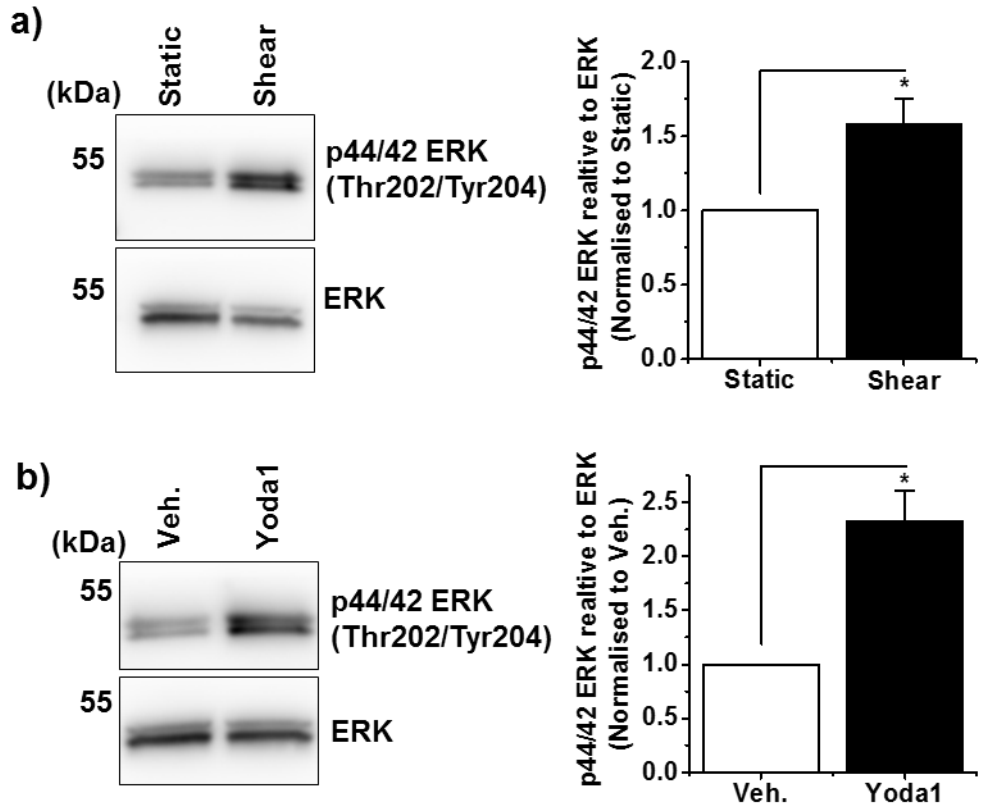

Figure 3.13 Treatment with either Yoda1 or shear stress evokes p44/42 ERK phosphorylation in HUVECs.

a) Left: Representative immunoblot of HUVECs treated for 2-minute with 10 dyn.cm^{-2} shear stress or not (static) for anti-Thr202/Tyr204 phospho-p44/42 ERK or anti-ERK. Right: Mean data from n=3 experiments displayed as Thr202/Tyr204 phospho-p44/42 ERK to ERK normalised to Veh. treatment. b) As in (a) but in HUVECs treated for 2-minutes with 2 µM Yoda1 or its vehicle (Veh.) (n=3).

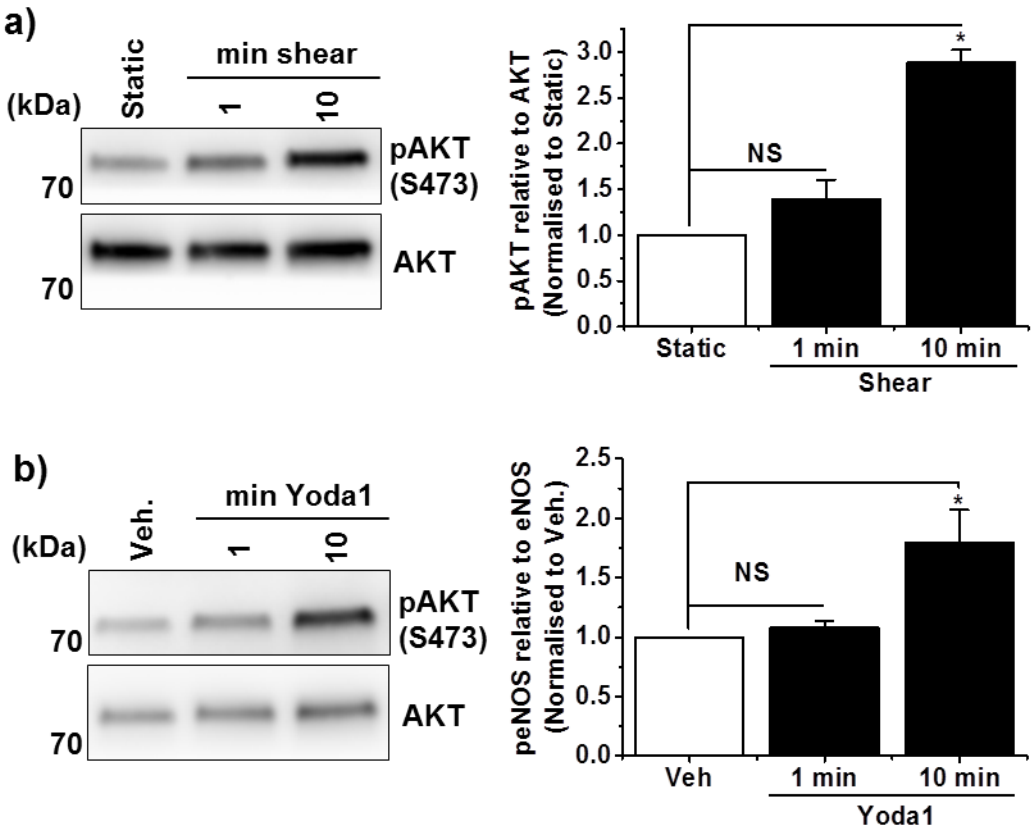

Figure 3.14 Treatment with either Yoda1 or shear stress similarly evoke delayed S473 AKT phosphorylation in HUVECs.

a) Left: Representative immunoblot of HUVECs treated with 10 dyn.cm^{-2} shear stress for either 1-minute, 10-minutes or not (static) for anti-S473 phospho-AKT or anti-AKT. Right: Mean data from n=3 experiments displayed as S473 phospho-AKT to AKT normalised to Veh. treatment. b) As in (a) but in HUVECs treated for either 1-minute or 10-minutes with 2 µM Yoda1 or its vehicle (Veh.) for 10-minutes (n=3).

3.6 Piezo1 is tightly coupled to eNOS phosphorylation

The data strongly suggest that Yoda1 treatment is sufficient for rapid phosphorylation of eNOS. However, it was essential to examine whether this phosphorylation was Piezo1 dependent. As Yoda1 seems to selectivity activate Ca^{2+} entry in HUVECs it was hypothesised that this phenomenon was Piezo1 dependent.

First it was important to prove that transfection with a scrambled siRNA (negative control) had no effect on the Yoda1 evoked eNOS phosphorylation itself. Indeed, Yoda1 evoked around a 1.5 fold increase in eNOS phosphorylation in both HUVECs treated with a mock transfection (-siRNA) and a scrambled transfection (si.Scr) (Figure 3.15). Since there was no difference between these two groups the control group for future analysis was scrambled siRNA treated cells.

3.6.1 Yoda1 evokes Piezo1 mediated eNOS phosphorylation in HUVECs

In order to examine the contribution of Piezo1 to Yoda1 evoked eNOS phosphorylation, HUVECs were treated with Piezo1 siRNA (si.Piezo1/si.P1). Treatment with Yoda1 evoked an increase in eNOS phosphorylation compared to treatment with its vehicle alone and this response was suppressed by over 90% in Piezo1 depleted HUVECs (Figure 3.16a). Piezo1 depletion had no effect on the basal levels of peNOS under vehicle treated conditions (Figure 3.16b).

In order to validate this result, gadolinium was used as a direct chemical inhibitor of Piezo1 channels. 30 µM gadolinium was utilised as this almost abolishes Yoda1 evoked Ca^{2+} entry in HUVECs (Figure 3.4b). HUVECs were subjected to 30-minute treatment with gadolinium prior to 1-minute application of 2 µM Yoda1. Similar to the result with Piezo1 genetic depletion, pre-treatment with gadolinium drastically suppressed Yoda1 evoked eNOS phosphorylation by 77% compared to cells pre-treated with vehicle (Figure 3.17).

Taken together, these data suggest that Yoda1 is indeed acting through Piezo1 channels to phosphorylate eNOS as this response can be suppressed by both Piezo1 siRNA, knocking down Piezo1 mRNA, and acute chemical inhibition.

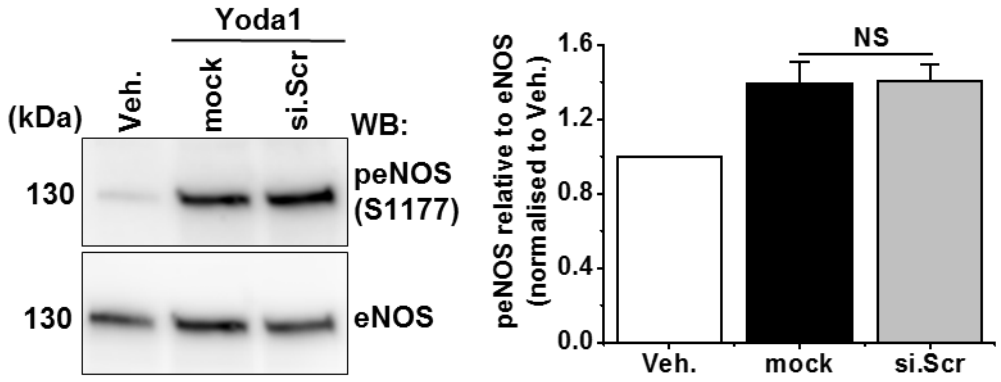

Figure 3.15 Scrambled siRNA has no effect on Yoda1 evoked eNOS phosphorylation in HUVECs.

Left: Representative immunoblots for anti-S1177 phospho-eNOS and anti-eNOS in HUVECs treated with 2 μM Yoda1 or its vehicle (veh.) for 1-minute. HUVECs were treated with either a mock transfection (-siRNA) or siRNA targeting a scrambled sequence (si.Scr). Right: Mean data from n=23 experiments. Data are displayed as peNOS relative to eNOS normalised to vehicle (Veh.) treated cells.

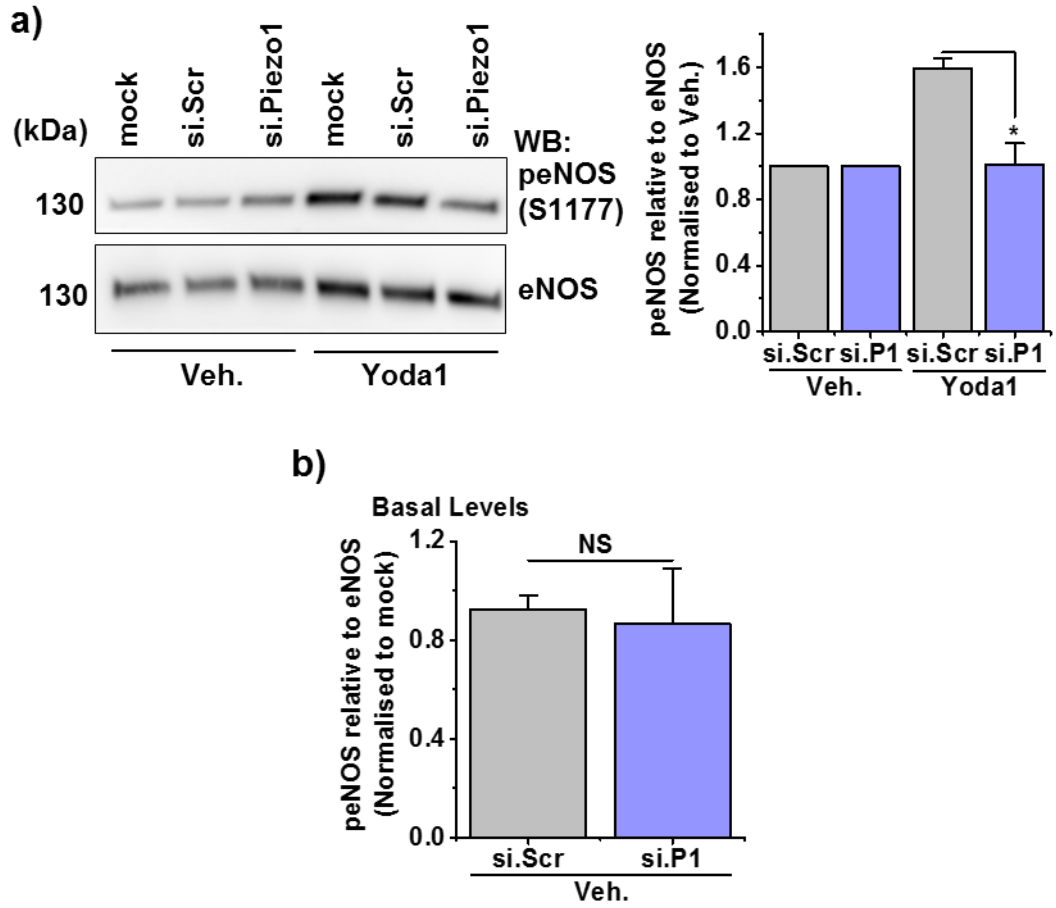

Figure 3.16 Yoda1 mediated eNOS phosphorylation is through Piezo1 activation in HUVECs.

a) Left: Representative immunoblots for anti-S1177 phospho-eNOS and anti-eNOS in HUVECs treated with 2 μM Yoda1 or its vehicle (Veh.) for 1-minute. HUVECs were treated with either a mock transfection (-siRNA) or siRNA targeting a scrambled sequence (si.Scr) or Piezo1 (si.Piezo1). Right: Mean data from 3 experiments. Data are displayed as peNOS relative to eNOS normalised to vehicle (Veh.) treated cells. b) Mean data from the type of experiments in (a) examining static phospho-eNOS expression relative to static eNOS (n=3).

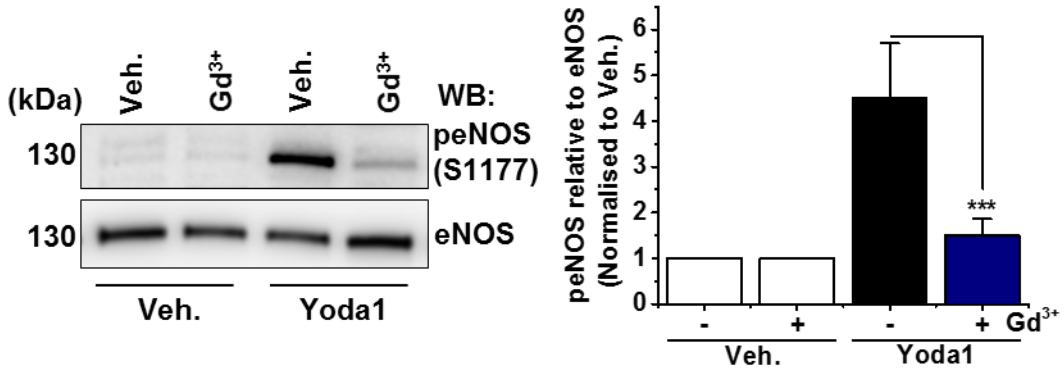

Figure 3.17 Yoda1 mediated eNOS phosphorylation is blocked by gadolinium.

Left: Representative immunoblots for anti-S1177 phospho-eNOS and anti-eNOS in HUVECs treated with 2 µM Yoda1 or its vehicle (Veh.) for 1-minute after pre-treatment with for 30-minutes with 30 µM gadolinium or its vehicle (Veh.). Right: Mean data from n=5 experiments. Data are displayed as peNOS relative to eNOS normalised to vehicle (Veh.) treated cells.

3.6.2 Yoda1 evokes Piezo1 mediated eNOS phosphorylation in mouse liver endothelial cells

In order to examine whether the results obtained in HUVECs could be replicated in mouse liver endothelial cells and to validate that Yoda1-mediated eNOS phosphorylation was Piezo1 dependent an endothelial Piezo1 knockout mouse model was used. Piezo1 global knockout is embryonic lethal (Li et al., 2014). In order to investigate the relevance of Piezo1 channels in the adult endothelium a tamoxifen inducible mouse model was created. These mice had a conditional Cre-Lox-mediated disruption of Piezo1 channels in the endothelium. Our lab has previously reported that these mice appeared normal and had normal body weights, weight gains and organ weights; gross anatomies and functions of the heart and aorta were also normal (Rode et al., 2017). Livers were harvested by Dr Baptiste Rode (University of Leeds) and endothelial cells were isolated from wild-type ($Piezo1^{Ctr}$) and endothelial Piezo1 knockout mice ($Piezo1^{\Delta EC}$) using a previously validated protocol (Rode et al., 2017). These cells are referred to as *m*LEC (mouse liver endothelial cells).

In order to validate that the *m*LECs isolated were of endothelial origin, immunocytochemistry was performed. CD31, a marker of endothelial cells, was indeed expressed in the *m*LECs (green staining) and this was not present when the cells were not incubated with the primary CD31 antibody (2° only control) (Figure 3.18a). Furthermore, immunoblotting confirmed expression of CD31 protein in both *m*LECs and HUVECs, the latter used as a positive control (Figure 3.18b).

A study from our lab previously reports that Yoda1 is able to activate an increase in intracellular Ca^{2+} in $Piezo1^{Ctr}$ endothelial cells and that this is abolished in $Piezo1^{\Delta EC}$ cells suggesting that Yoda1 specifically activates Piezo1 in these cells (Rode et al., 2017). Consistent with Yoda1 activating mouse Piezo1 (Rode et al., 2017; Syeda et al., 2015), Yoda1 evoked an increase in eNOS phosphorylation in endothelial cells isolated from control mice (Figure 3.19a). This was abolished in *m*LECs with genetic Piezo1 deletion (Figure 3.19a). Thus, Yoda1 selectively acts on Piezo1 to evoke eNOS phosphorylation. The level of total eNOS was not affected by Piezo1 deletion (Figure 3.19b). However, total basal phospho-eNOS was significantly decreased in $Piezo1^{\Delta EC}$ cells (Figure 3.19c). These data are interesting as they suggest that constitutive Piezo1 channel activity (i.e. without Yoda1) has a physiological role to phosphorylate eNOS. Taken together, these data confirm that

Yoda1 mediated eNOS phosphorylation is dependent on Piezo1 in both HUVECs and endothelial cells isolated from the endothelial cell specific, tamoxifen inducible mouse model. A physiological role for Piezo1 channels in eNOS phosphorylation *in-vivo* was also suggested since knocking out Piezo1 decreased basal phospho-eNOS levels.

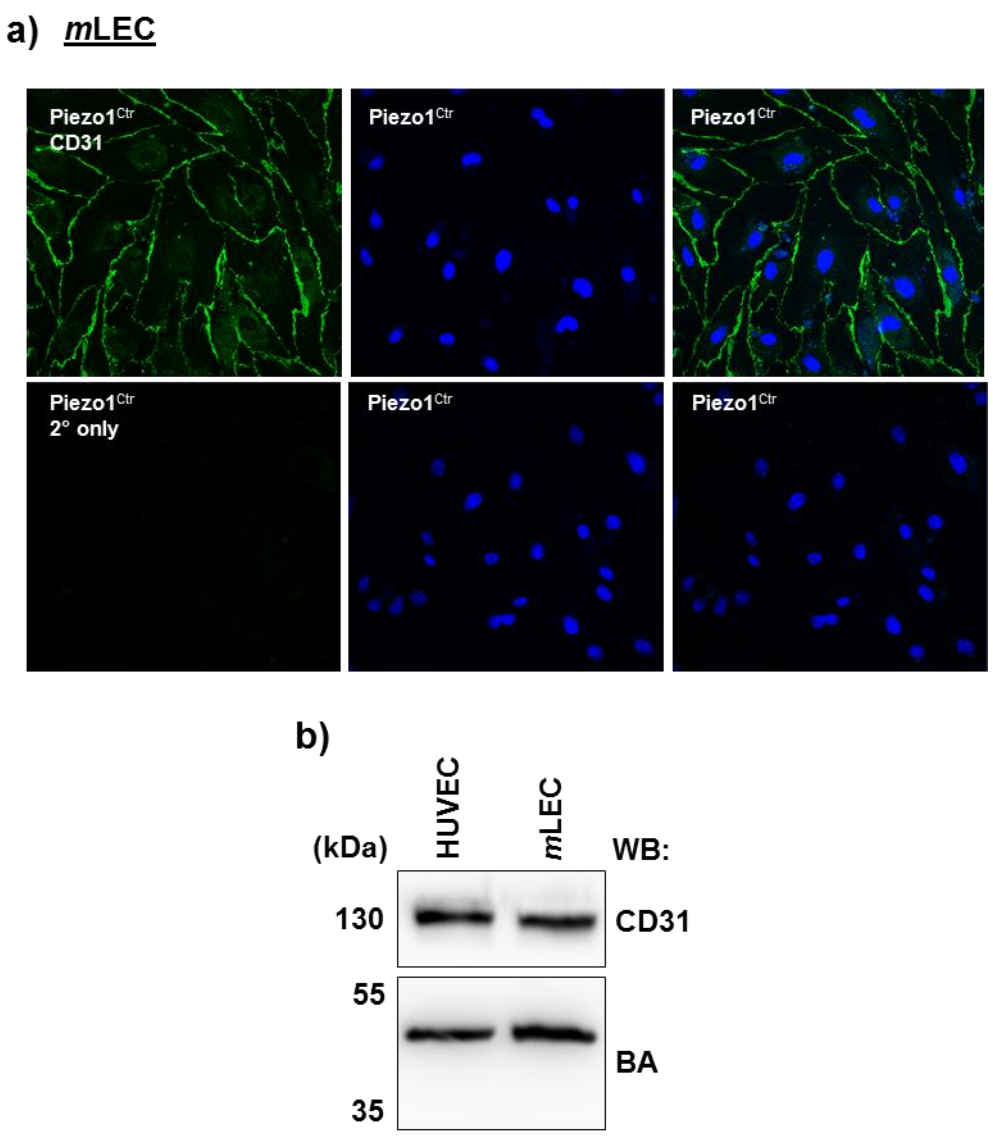

Figure 3.18 Validation of mouse liver endothelial cells (mLECs).

a) Immocytochemistry staining for anti-CD31 labelling the endothelial cells (green) and DAPI labelling the nuclei (blue) in mouse liver endothelial cells (*m*LECs). The bottom panel indicates control secondary only staining (without primary antibody). b) Representative immunoblots for anti-CD31 or anti-beta actin in HUVECs and *m*LECs

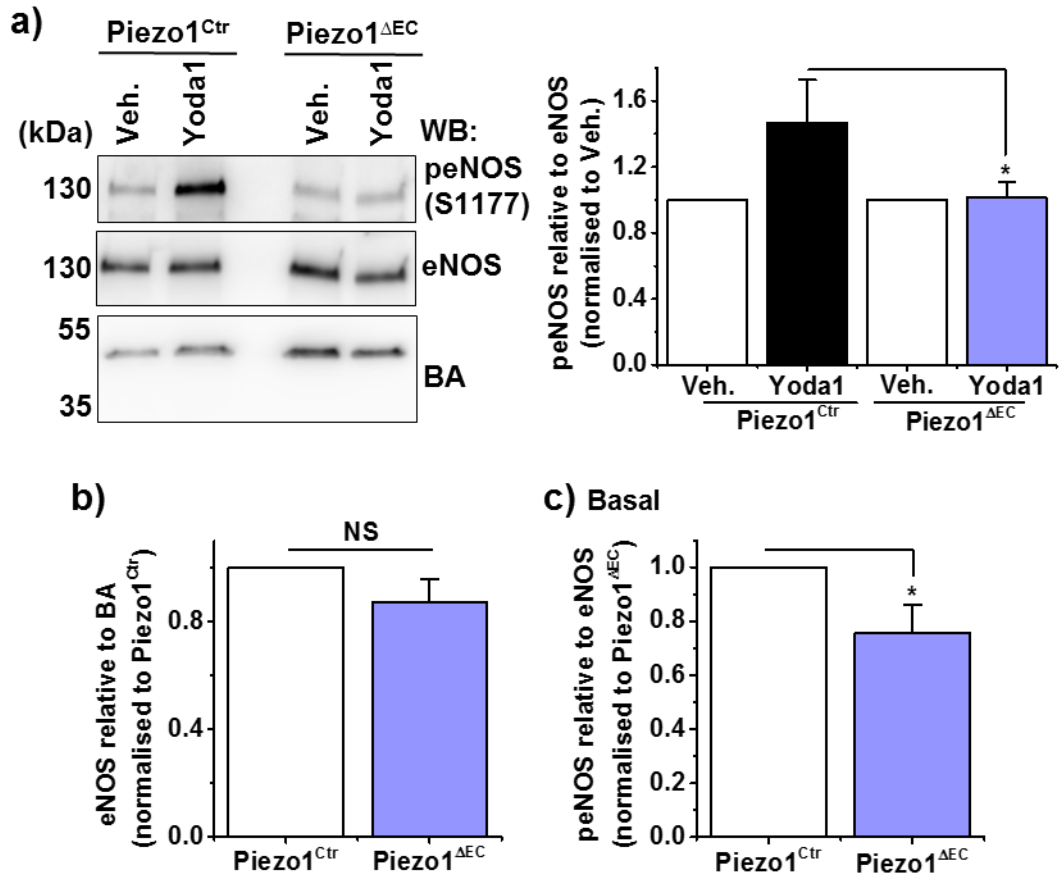

Figure 3.19 Endothelial knockout of Piezo1 *in-vivo* abolishes Yoda1 evoked eNOS phosphorylation.

a) Left: Representative immunoblots for anti-S1177 phospho-eNOS, anti-eNOS and anti-beta actin (BA) in Piezo1^{Ctr} or Piezo1$^{\Delta EC}$ *m*LECs treated with 2 µM Yoda1 or its vehicle (Veh.) for 1-minute. Right: mean data from n=3 experiments. Data are displayed as peNOS relative to eNOS normalised to their own Vehicle (Veh.). b-c) Data are from the type of experiments in (a). b) Data are displayed as eNOS relative to beta actin (BA) normalised to wild type cells to analyse eNOS expression. c) Data are displayed as peNOS relative to eNOS (vehicle treated cells) normalised to wild type cells to analyse basal peNOS expression.

3.7 Novel small-molecule modulators of Piezo1 channels

Genetic disruption of Piezo1 channels blocks Yoda1-mediated eNOS phosphorylation. Similarly, acute pre-treatment with gadolinium supresses this response. To confirm this result acute blockade of the channels was further examined. Yoda1 is a small-molecule agonist, but the pharmacology of these channels is otherwise limited. Known inhibitors of Piezo1 are generic cationic channel pore blocking agents e.g. gadolinium and ruthenium red (Coste et al., 2010; Coste et al., 2012).

3.7.1 KC159

The Yoda1 analogue, KC159, is an agonist of Piezo1 discovered during structure-activity relationship investigations of the Yoda1 compound series. KC159 has higher solubility compared to Yoda1, probably due to the addition of its carboxylic acid group Figure 3.20a). FlexStation analysis of intracellular Ca^{2+} levels revealed that similar to Yoda1, KC159 can activate Piezo1 but with slightly less efficacy (Figure 3.20b & c). Pre-treatment with KC159 for 30-minutes increased basal intracellular Ca^{2+} levels, consistent with results suggesting agonist properties. However, an additional application of Yoda1 could not increase the intracellular Ca^{2+} levels any further (Figure 3.20b & c). In order to investigate whether KC159 can activate Piezo1 mediated signalling pathways, immunoblotting analysis of eNOS phosphorylation was carried out. Excitingly, KC159, was also able to evoke an increase in eNOS phosphorylation similar to Yoda1 (Figure 3.20d) but the compound itself shows better physicochemical properties- making it more suited to further development as a lead candidate in the future.

3.7.2 Dooku1

Modifications of the pyrazine ring of Yoda1 led to the discovery of Dooku1 (Figure 3.21a). Dooku1 is a competitive inhibitor that specifically antagonises Yoda1 evoked activation of Piezo1 (Evans et al., 2018). Direct application of Dooku1 led to a slight, but non-significant, increase in intracellular Ca^{2+} levels. As reported previously, 30-minute pre-treatment with Dooku1 antagonised Yoda1 evoked Ca^{2+} entry in HUVECs (Figure 3.21b & c). Immunoblotting analysis revealed that pre-treatment with Dooku1 was sufficient to suppress Yoda1 evoked eNOS phosphorylation, consistent with Ca^{2+} measurement experiments (Figure 3.21d).

This compound demonstrates that chemical antagonism of Yoda1-evoked Piezo1 channel activity is possible.

3.7.3 KC69

Substitution of the dichloro-groups of Yoda1 to a methoxyl gave KC69 (Figure 3.22a). Intracellular Ca^{2+} analysis showed this compound had no effect on channel activity. Direct application of KC69 had no effect on intracellular Ca^{2+} levels compared to direct addition of Yoda1 (Figure 3.22b & c). Furthermore, pre-treatment with KC69 had no effect on both basal intracellular Ca^{2+} levels and the Yoda1 response (Figure 3.22b & c). Similarly, immunoblotting revealed that unlike Yoda1, KC69 had no effect on phospho-eNOS levels, consistent with FlexStation analysis (Figure 3.22d).

Taken together, these data suggest that chemical modifications of Yoda1 can alter its properties leading to the development of more soluble derivatives and also competitive antagonists. Compounds seem to act similarly in both Ca^{2+} measurement assays and downstream signalling analysis. For instance, KC69 is inactive in all experiments whereas, the agonist effects of KC159 are comparable to Yoda1 in both assays.

Investigating the structure-activity relationship of Yoda1 analogues and their physicochemical properties is crucial to the development of lead candidates with improved ADME properties for translational studies but is beyond the remit of this thesis.

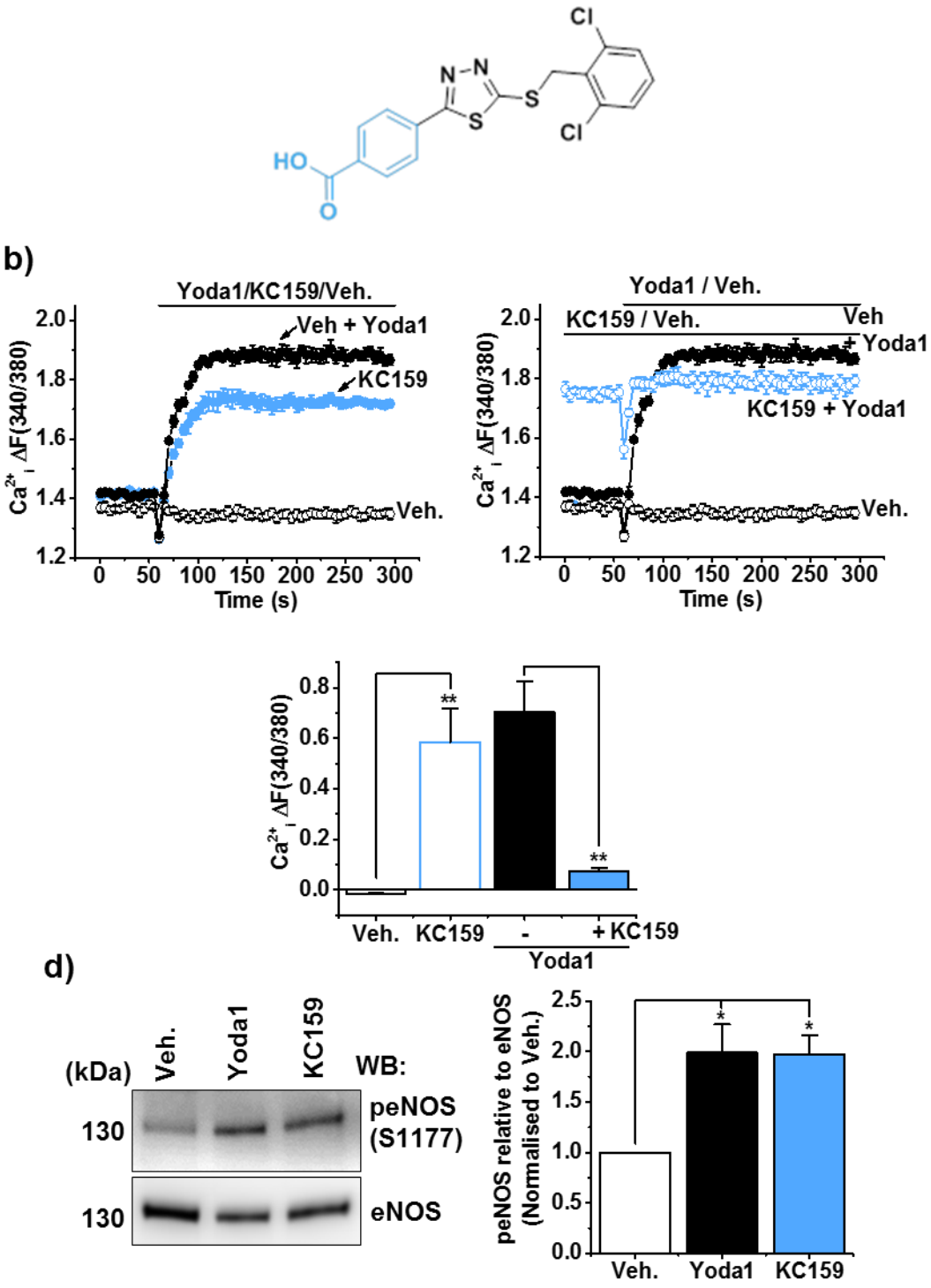

Figure 3.20 KC159, a novel Piezo1 agonist, evokes eNOS phosphorylation in HUVECs.

a) Chemical structure of KC159. b) Left: example Ca^{2+} measurement trace in HUVECs during application of 2 μM Yoda1, 10 μM KC159 or their vehicle (Veh.). Right: example Ca^{2+} measurement trace in HUVECs after pre-treatment for 30-minutes with 10 μM KC159 or its vehicle (Veh.) during application of 2 μM Yoda1 or its vehicle (Veh.). c) Mean data for the types of experiments in (b) (n/N=3/14-15). d) Left: Representative immunoblots for anti-S1177 phospho-eNOS and anti-eNOS in HUVECs treated with 2 μM Yoda1, 10 μM KC159 or their vehicle (Veh.) for 1-minute. Right: mean data from n=3 experiments. Data are displayed as peNOS relative to eNOS normalised to their own Vehicle (Veh.).

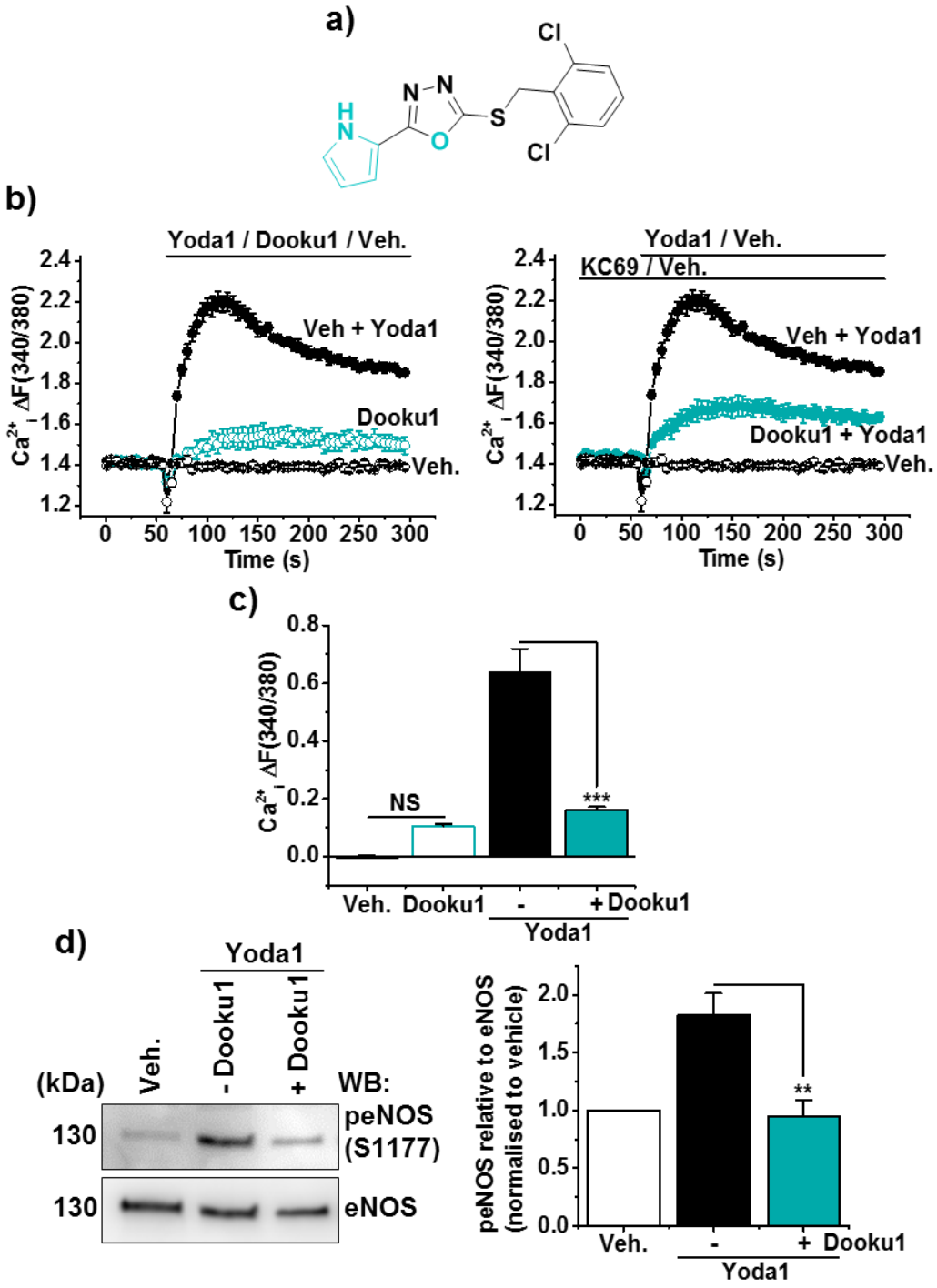

Figure 3.21 Dooku1, a competitive inhibitor of Yoda1 mediated Piezo1 activation, blocks Yoda1 evoked eNOS phosphorylation in HUVECs.

a) Chemical structure of Dooku1. b) Left: example Ca^{2+} measurement trace in HUVECs during application of 2 µM Yoda1, 10 µM Dooku1 or their vehicle (Veh.). Right: example Ca^{2+} measurement trace in HUVECs after pre-treatment for 30-minutes with 10 µM Dooku1 or its vehicle (Veh.) during application of 2 µM Yoda1 or its vehicle (Veh.). c) Mean data for the types of experiments in (b) (n/N=4/14-16). d) Left: Representative immunoblots for anti-S1177 phospho-eNOS and anti-eNOS in HUVECs treated with 2 µM Yoda1, 10 µM Dooku1 or their vehicle (Veh.) for 1-minute. Right: mean data from n=6 experiments. Data are displayed as peNOS relative to eNOS normalised to their own Vehicle (Veh.).

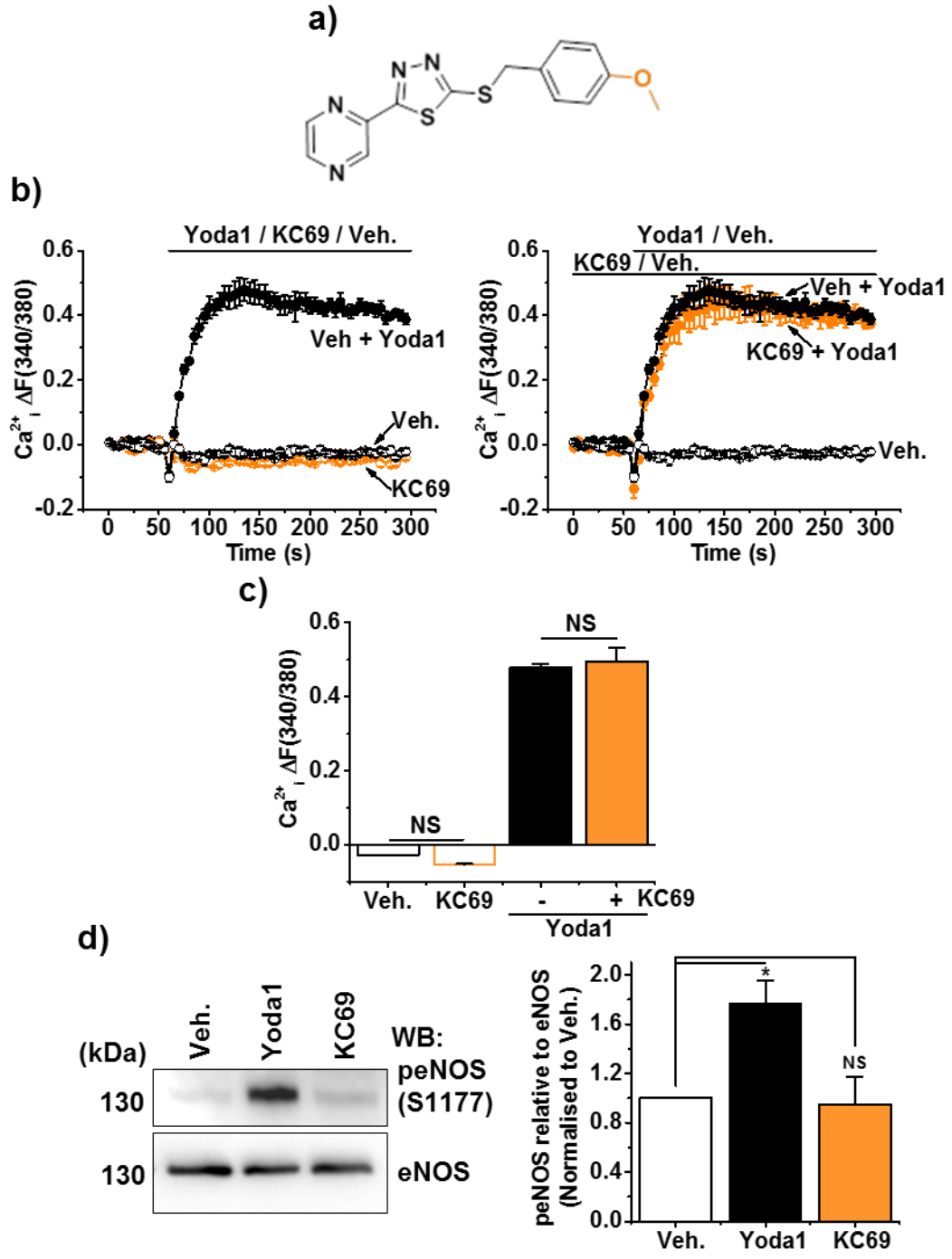

Figure 3.22 KC69, an inactive analogue of Yoda1, has no effect on phospho-eNOS levels.

a) Chemical structure of KC69. b) Left: example Ca^{2+} measurement trace in HUVECs during application of 2 µM Yoda1, 10 µM KC69 or their vehicle (Veh.). Right: example Ca^{2+} measurement trace in HUVECs after pre-treatment for 30-minutes with 10 µM KC69 or its vehicle (Veh.) during application of 2 µM Yoda1 or its vehicle (Veh.). c) Mean data for the types of experiments on the left (n/N=3/13). d) Left: Representative immunoblots for anti-S1177 phospho-eNOS and anti-eNOS in HUVECs treated with 2 µM Yoda1, 10 µM KC69 or their vehicle (Veh.) for 1-minute. Right: mean data from n=3 experiments. Data are displayed as peNOS relative to eNOS normalised to their own Vehicle (Veh.).

3.8 Yoda1 acts specifically on serine residues of eNOS

In order to examine the specificity of Yoda1 to the S1177 site on eNOS other phosphorylation sites were examined. Primarily the S1177 phospho-site on eNOS was focused on as it is reported to be regulated by both Ca^{2+} and shear stress, two Piezo1 channel characteristics (Dimmeler et al., 1999; Gallis et al., 1999; Fleming et al., 2001). However, eNOS possesses numerous phospho-sites and there are various molecular events that affect phospho-eNOS levels.

3.8.1 Ser615 phosphorylation site

The Ser615 phosphorylation site is reported to be activated by VEGF, hypoxia and adiponectin (Fleming, 2010). These stimuli in turn activate AKT, PKA and AMPK signalling leading to phosphorylation of this site, which has a positive effect on the activation of eNOS (Fleming, 2010) (Figure 3.23a). The effect of shear stress on this site remains unexamined. Application of 2 µM Yoda1 to HUVECs for 1-minute evoked an increase in levels of S615 phospho-eNOS (Figure 3.23b). This is consistent with the hypothesis of Yoda1 evoking activation of eNOS. Similar to S1177, Yoda1 is able to evoke a 1.8-fold increase in eNOS phosphorylation.

3.8.2 Tyr657 phosphorylation site

The Tyr657 site was interesting as it was initially linked to endothelial cells stimulated by shear stress, involving PYK2 to eNOS (Ayajiki et al., 1996; Tai et al., 2002). It is now known that insulin and angiotensin II also act on eNOS via this site (Figure 3.24a). This site is a negative regulatory site, its phosphorylation is associated with a decrease in enzyme activity. In contrast to reports suggesting activation by shear stress, Yoda1 at this fast time point had no effect (Figure 3.24b). Consistent with the hypothesis of Yoda1 evoking eNOS activation.

3.8.3 Thr495 phosphorylation site

The Thr495 residue on eNOS is constitutively phosphorylated in all of the endothelial cells investigated to date and again is a negative regulatory site where its phosphorylation ultimately leads to a decrease in eNOS activity (Fleming et al., 2001). This site can be activated by O_2^- and Ox-LDL, which phosphorylate Thr495

via PKC activation. (Figure 3.25a). As the antibody targeting this phospho-site is poor it was difficult to detect a band on the western blot. An eNOS IP experiment was performed to enrich the expression of eNOS. The IP was performed with an anti-eNOS antibody on cells treated with Yoda1 or its vehicle or an IgG control (Figure 3.25b). eNOS was able to be pulled out of HUVEC lysates and this was absent from the IgG control. As expected the input band for the lysates was blank for peNOS (T495) (Figure 3.25b). However, after pull down of eNOS a peNOS T495 band was detected and this was unchanged between treatment with Yoda1 or its vehicle (Figure 3.25b).

These data suggest that Yoda1-stimulated Piezo1 specifically signals to activating residues of eNOS. Both of the serine residues are reported to activate eNOS leading to nitric oxide production and protection against endothelial cell dysfunction.

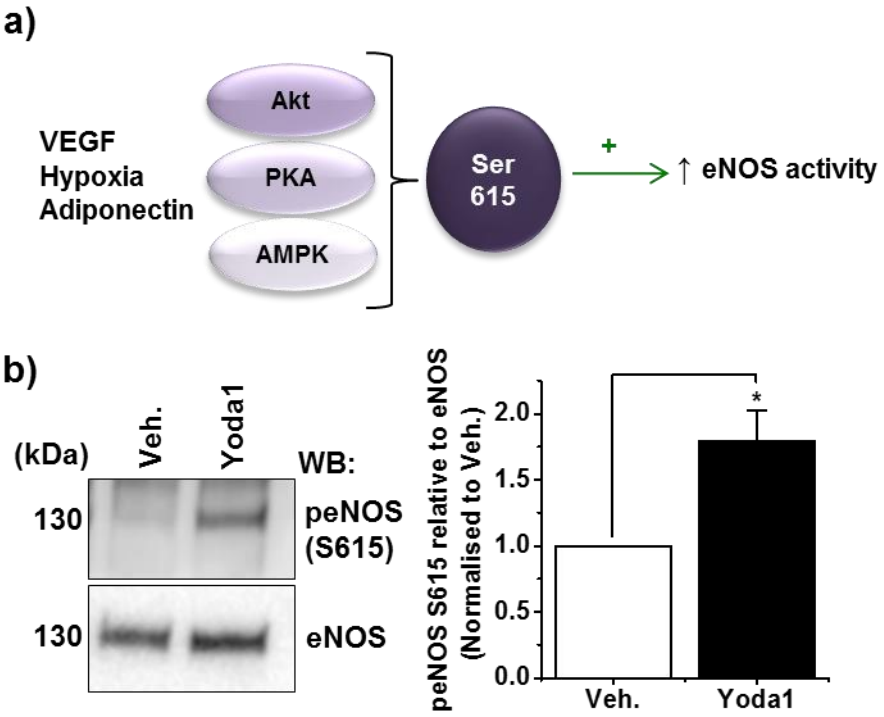

Figure 3.23 Yoda1 phosphorylates eNOS at S615.

a) Schematic diagram of how the Ser615 site can regulate both eNOS activity and be regulated. b) Left: Representative immunoblots for anti-S615 phospho-eNOS and anti-eNOS in HUVECs treated with 2 μM Yoda1 or its vehicle (Veh.) for 1-minute. Right: Mean data from n=3 experiments. Data are displayed as peNOS relative to eNOS normalised to vehicle (Veh.) treated cells.

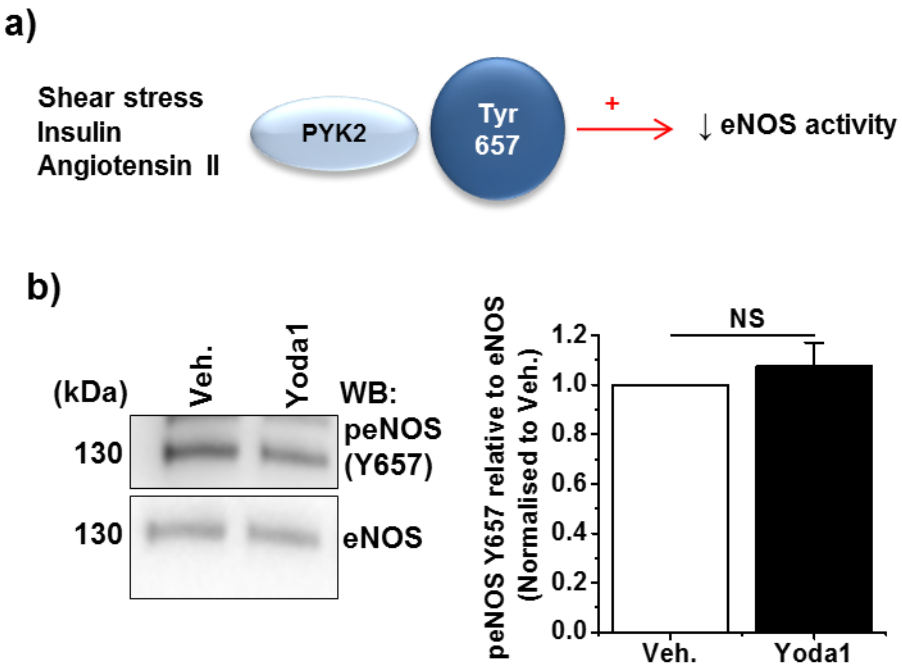

Figure 3.24 Yoda1 has no effect on eNOS at Tyr657.

a) Schematic diagram of how the Tyr657 site can regulate both eNOS activity and be regulated. b) Left: Representative immunoblots for anti-Y657 phospho-eNOS and anti-eNOS in HUVECs treated with 2 μM Yoda1 or its vehicle (Veh.) for 1-minute. Right: Mean data from n=3 experiments. Data are displayed as peNOS relative to eNOS normalised to vehicle (Veh.) treated cells.

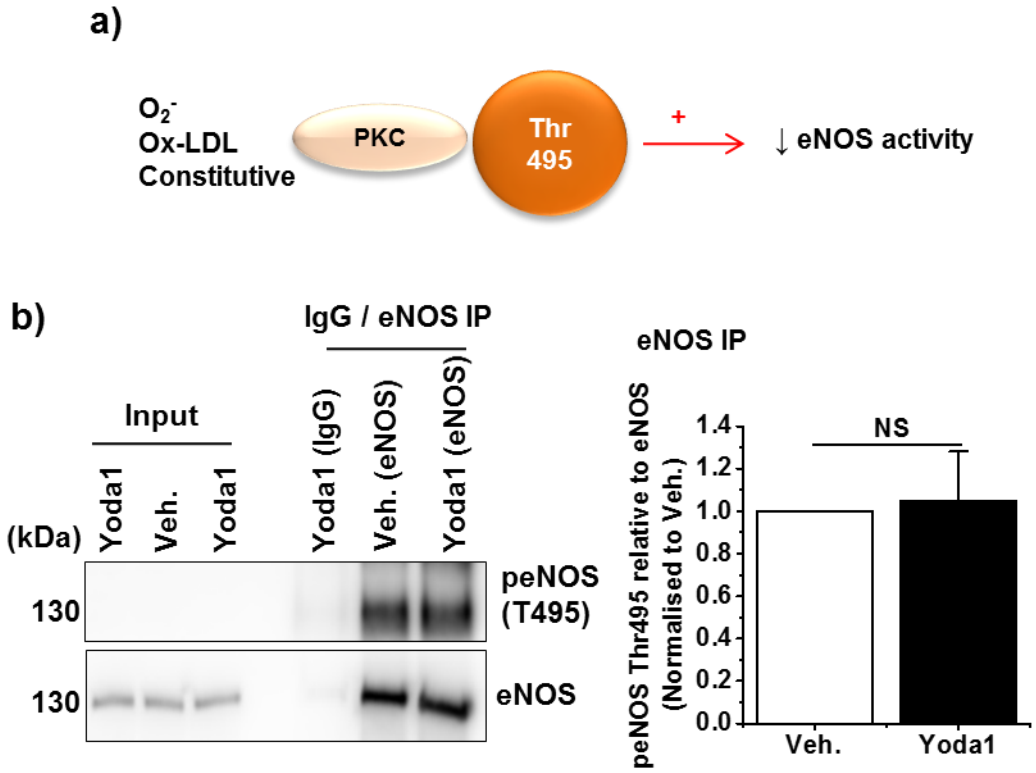

Figure 3.25 Yoda1 has no effect on the Thr495 residue on eNOS.

a) Schematic diagram of how the Thr495 site can regulate eNOS activity. b) Left: Representative immunoblots for anti-Thr495 phospho-eNOS and anti-eNOS in HUVECs treated with 2 μM Yoda1 or its vehicle (Veh.) for 1-minute. Input represents lysate before pull-down and after pull-down is denoted by (IgG) or (eNOS). Right: Mean data from n=3 experiments. Data are displayed as peNOS relative to eNOS normalised to vehicle (Veh.) treated cells after eNOS IP.

3.9 Discussion

Our laboratory is interested in endogenous endothelial Piezo1 as it is reported to be involved in the development of both the blood and lymphatic vessels and is important for cardiovascular function during exercise (Li et al., 2014; Lukacs et al., 2015; Rode et al., 2017). Consistent with this goal this study examined the chemical activation of endothelial Piezo1 channels, primarily focusing on their signalling to and activation of the crucial cardiovascular regulator eNOS.

The advantage of utilising a chemical agonist over shear stress is to achieve greater specificity, while the latter can activate a plethora of mechanosensors the former should activate only Piezo1. Therefore, it was imperative to initially verify that Yoda1 does show specificity for Piezo1 in endothelial cells. Application of Yoda1 to HEK 293 cells, a Piezo1 null cell line, did not have an effect on intracellular Ca^{2+} levels. However, when human Piezo1 was over-expressed in this cell line Yoda1 was able to evoke a rapid increase in intracellular Ca^{2+}. Yoda1 was also able to activate Ca^{2+} entry in HUVECs, consistent with activation of endogenous Piezo1 channels. Disruption of Piezo1 channel mRNA expression using siRNA targeting Piezo1 or acutely blocking Piezo1 channel activity using the non-selective cation channel pore blockers gadolinium and ruthenium red all supressed the Yoda1-evoked Ca^{2+} entry. In keeping with the literature, when HUVECs were pre-treated with 0 mM extracellular Ca^{2+} the Yoda1 response was blunted but not abolished. This suggests that the majority of the response is through plasma membrane Piezo1 channels (Syeda et al., 2015; Ilkan et al., 2017). The remaining response could be due to Yoda1 activating Piezo1 channels on membranes of internal stores, for example on the ER, activating store-release mechanisms, but there is no evidence for this. This would need to be investigated further. Nonetheless, the majority of the Yoda1 response is mediated by Ca^{2+} entry. Yoda1 treatment also evoked phosphorylation of eNOS in endothelial cells. Again, disruption of Piezo1 channel expression using siRNA targeting Piezo1 or blocking Piezo1 channel activity using the non-selective cation channel pore blockers gadolinium and ruthenium red all profoundly supressed this response in HUVECs. Moreover, mouse liver endothelial cells lacking Piezo1 showed no Yoda1-induced eNOS. Collectively these data confirmed that Yoda-1 is a specific agonist of Piezo1 in endothelial cells.

Shear stress initiates a plethora of signalling pathways in endothelial cells. While eNOS forms the primary target of interest within this work, whether Yoda-1 could mimic activation of other shear-evoked downstream signalling was investigated. The PI3K/AKT pathway and the ERK/MAPK pathways were examined. Treatment of HUVECs with shear stress is reported to activate the PI3K/AKT signalling pathway, leading to protection against apoptosis and promoting eNOS phosphorylation and nitric oxide production (Dimmeler et al., 1999; Fisslthaler et al., 2008; Fisslthaler et al., 2000). Data in this chapter confirm that 10-minute treatment with shear stress enhanced AKT phosphorylation in HUVECs. Encouragingly, treatment with Yoda1 is able to mimic this response. 1-minute treatment with neither shear stress nor Yoda1 had any effect on AKT phosphorylation. However, when this time point was increased to 10-minutes both agonists were able to evoke AKT phosphorylation markedly. It is widely reported that shear stress evokes p44/42 ERK phosphorylation leading to alterations in gene expression (Tseng et al., 1995; Li et al., 1996). A short 2-minute treatment of HUVECs with shear stress evoked an increase in p44/42 ERK phosphorylation and this was comparable to Yoda1 evoked p44/42 ERK phosphorylation. These data suggest that Yoda1 mimics shear stress activation of signalling pathways and is a useful tool compound to specifically investigate Piezo1 mediated signalling pathways.

Proteomic studies suggested that Piezo1 regulates shear-evoked eNOS phosphorylation. This was confirmed by immunoblotting. Specifically activating Piezo1 with Yoda1 treatment also potently evoked rapid phosphorylation of eNOS in HUVECs and in primary endothelial cells isolated from human and mouse livers. The phosphorylation was predominantly of the serine residues (S1177 & S615). Post completion of this study a manuscript was published by a competing group (Wang et al., 2016). Similar to work in this chapter, the Offermanns group suggest that Yoda1 activates Piezo1 mediated Ca^{2+} entry and eNOS phosphorylation in HUAECs and HUVECs (Wang et al., 2016). Utilising Yoda1 at 1 µM for a treatment time of 5-minutes, they suggest a mechanism of action involving Piezo1 activation coupling to ATP release and subsequent $P2Y_2/G_q/G_{11}$/AKT mediated phosphorylation of eNOS. Within my study eNOS phosphorylation was observed at a much quicker time point than that used by the Offeremans group, and indeed than the majority of shear stress signalling studies, exciting interest in the initial signalling events that take place directly after Piezo1 channel activation. Thus a shorter treatment time of 1-minute was examined. It is possible that Piezo1 activation can activate more than one signalling cascade to activate eNOS. The

Offermans group suggest activation of a moderately slow mechanism linking Piezo1 to eNOS phosphorylation involving activation of G-proteins. However, as Piezo1 channels are activated so rapidly a potential direct/tight coupling mechanism was investigated. In this chapter it is reported that in HUVECs the EC_{50} of Yoda1 was 1.5 µM and 1.17 µM in Ca^{2+} imaging and assays measuring S1177 phospho-eNOS respectively. Thus, 2 µM Yoda1 treatment was used throughout this study (~EC_{80}) to ensure a robust and consistent response. Under these conditions it is possible that the mechanism of action of Yoda1 could be different, it is important to investigate this further.

Blood pressure is controlled by the production of the vasodilating substance, nitric oxide, which is released from the endothelium in response to various agonists. VEGF and shear stress are physiological activators of eNOS that lead to nitric oxide dependent proliferation and angiogenesis of HUVECs and regulation of vascular tone (Papapetropoulos et al., 1997; Cooke, 2000). It was important to compare Yoda1-evoked eNOS phosphorylation to other physiological agonists to detect whether Yoda1-evoked enough eNOS phosphorylation to have an effect in physiology. Indeed, Yoda1-evoked eNOS phosphorylation was equivalent to that evoked by physiological activators. Furthermore, Yoda1-evoked eNOS phosphorylation was substantial enough to evoke eNOS activation and our lab report that it causes nitric oxide and dose-dependent relaxation of aortic rings (Evans et al., 2018). This is beneficial as treatment with Yoda1 could protect against hypertension. Loss of endothelial Piezo1 *in-vivo* led to a reduction in basal levels of phospho-eNOS, suggesting that the mechanosensing activity of Piezo1 channels is constantly operating and is required to maintain basal shear stress induced nitric oxide formation. Surprisingly however, knockout of endothelial Piezo1 has no effect on resting blood pressure of mice but strikingly it is required for elevated blood pressure during whole body physical activity in the animals (Rode et al., 2017). Data from our lab imply that the nitric oxide mechanism is naturally suppressed in mesenteric arteries, which usually constrict during whole body physical activity. Nonetheless, the vasodilatory effect might of course be important in other circumstances and this does not rule out a role for Piezo1 in regulating vascular tone and blood pressure in physiology. In fact, the role of endothelial Piezo1 has been studied in sedate mice where relevance of the nitric oxide mechanism has been suggested (Wang et al., 2016). The effect reported was however on systolic blood pressure and as vasodilatation should affect diastolic pressure the relevance of this is unclear. It remains to be clarified if endothelial

Piezo1 is important for vasodilation *in-vivo* in sedentary mice. Furthermore, biallelic mutations of Piezo1 that result in attenuated function have recently been described in patients with congenital lymphatic dysplasia, and Piezo1 global knockout mice fail to develop a vascular network (Lukacs et al., 2015; Li et al., 2014). Thus, lack of Piezo1 has profound effects on vascular and cardiovascular physiology. However, more work is needed to examine the role of Piezo1-mediated nitric oxide production *in-vivo*.

eNOS is constitutively expressed however, there are multiple physical and chemical stimuli activating various molecular events that affect eNOS levels (Fleming, 2010). eNOS possesses numerous phospho-sites that are phosphorylated by various stimuli. Throughout this study S1177 was examined as it reported to be activated by shear stress and Ca^{2+} which are in keeping with established Piezo1 characteristics (Dimmeler et al., 1999; Fleming et al., 2001). However, other phospho-sites were briefly examined. Fluid shear stress is also reported to activate the Y657 site via activation of PYK2 (Ayajiki et al., 1996; Tai et al., 2002). Yoda1 failed to phosphorylate this site. Likewise, Yoda1 failed to phosphorylate the constitutively active T495 inhibitory site. These data are consistent with Yoda1 activating eNOS and nitric oxide dependent relaxation of aortic rings (Evans et al., 2018). The angiogenic factor, VEGF is reported to phosphorylate the S615 site on eNOS to promote its activity (Fleming, 2010). Similar to S1177, Yoda1 evoked phosphorylation of the S615 site. However, further work is needed to examine whether this is Piezo1 dependent and this was out of the scope of this project.

Treatment with Yoda1 is able to mimic shear evoked downstream signalling. Medicinally, the Yoda1 drug series could be used to reduce vascular tone and blood pressure and increase endothelial function by increasing nitric oxide formation. One major disadvantage of the use of Yoda1 is its lack of druggable properties. Yoda1 has poor solubility, a short half-life and a high clearance rate. Notably however, Yoda1 can be chemically modulated to develop analogues with altered chemical properties. This is very important for the development of more druggable Piezo1 modulators. Yoda1 appears to have a very tight structure-activity relationship. Small changes to the molecule had drastic functional effects. Substitution of the dichloro group to a methoxy group to develop KC69 renders the compound inactive in both Ca^{2+} and phospho-eNOS measurement assays.

Moreover, modifying the pyrazine ring of Yoda1 led to the development of Dooku1 – a small-molecule which antagonises Yoda1-evoked Piezo1 channel activation (Evans et al., 2018). Even though this compound is not useful to block physiological Piezo1 channels (Evans et al., 2018) it provides a useful tool compound to study Yoda1-evoked Piezo1 channel activation and signalling. The major drawback of using Yoda1 *in-vivo* is its poor ADME properties. *In-vitro* ADME analysis suggested that compared to Yoda1, KC159 had much greater kinetic solubility and doesn't precipitate in aqueous solution until 76.6 µM. Furthermore, KC159 had a half-life almost 40-times greater than Yoda1 and the clearance of KC159 was around 35-times lower than Yoda1. Importantly, this more translationally-relevant Yoda1 analogue is still able to evoke Ca^{2+} entry and phospho-eNOS signalling. Overall, these characteristics would make KC159 a more desirable drug to use to analyse Piezo1 mediated signalling and to take forward to *in-vivo* assays

3.10 Summary

Arterial blood pressure is controlled under both normal and hypertensive conditions by various vasodilatory factors including nitric oxide. These are produced and released from the endothelium in response to fluid shear stress (Hahn and Schwartz, 2009). Piezo1 is one of the plethora of proteins that is activated by shear stress to produce the endothelial protective nitric oxide. Yoda1 is a useful research tool, not only mimicking mechanical stimulation of the channels but also facilitating study of Piezo1 channels from a practical perspective without the need for mechanical stimulation and importantly lacking effect on other channels (Cahalan et al., 2015; Lukacs et al., 2015; Wang et al., 2016; Rode et al., 2017). Yoda1 allows specific examination of Piezo1 mediated signalling and there is potential to discover and develop more translational analogues that evoke the same phenomenon that could have medicinal impact. The data indicate that Yoda1 evokes Piezo1 mediated Ca^{2+} entry in HUVECs and the existence of rapid and direct coupling between Piezo1 and eNOS activation (Figure 3.26). The mechanism by which Yoda1 mediated Piezo1 channel activation evokes eNOS phosphorylation remains unknown. This suggests that a chemical Piezo1 activator can not only reduce vascular tone but may also increase endothelial function by increasing nitric oxide

formation. Understanding this mechanism could be important for achieving better appreciation of how shear stress regulates cardiovascular structure and function.

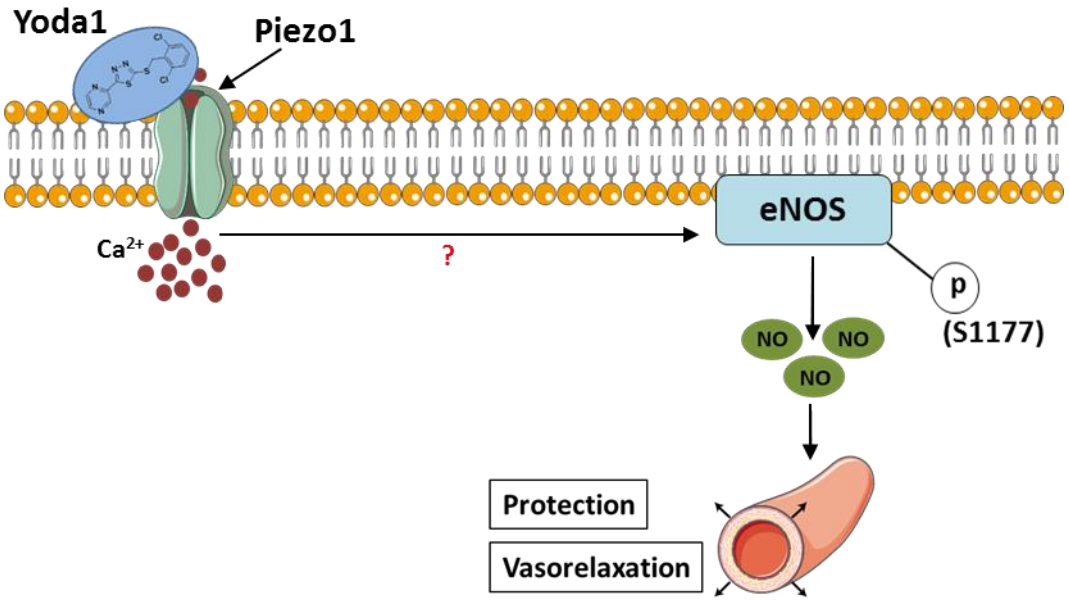

Figure 3.26 Schematic of Yoda1-mediated Piezo1 activation.

Yoda1 activates Piezo1 channels to evoke Ca^{2+} entry and eNOS phosphorylation. The mechanism that mediates this remains unknown.

Chapter 4 Piezo1 Cross-Talks with CD31 and VE-Cadherin Proteins of the Mechanosensory Triad Promoting eNOS Phosphorylation

4.1 Introduction

Furchgott elegantly demonstrated that endothelial cells play a pivotal role in acetylcholine mediated relaxation in isolated arteries including rabbit aorta (Furchgott and Zawadzki, 1980). Successively followed the observation of NO production by the endothelium (Palmer et al., 1987) and the discovery of the NO generating enzyme, NOS (Bredt et al., 1990). eNOS is reported to be constitutively expressed. However, numerous physical and chemical stimuli affect eNOS levels and phosphorylation. eNOS S1177 can be rapidly phosphorylated after the application of many stimuli including, fluid shear stress, VEGF, Ca^{2+} and small-molecules including Yoda1, as described in the previous chapter. There are a plethora of signalling pathways that are involved in S1177 eNOS phosphorylation and the mechanism by which vascular cells sense shear stress to evoke eNOS phosphorylation is incompletely understood.

In the last chapter it was demonstrated that Yoda1 induces Piezo1-induced S1177 eNOS phosphorylation. An important next step was to understand the signalling pathway mediating this. The Offermanns group described a mechanism by which Yoda1 mimicked shear stress to evoke Piezo1-mediated ATP release through pannexin channels that in turn acted on P2Y2 receptors activating G_q/G_{11} proteins which resulted in phosphorylation of AKT and eNOS leading to NO production and relaxation of mesenteric arteries (Wang et al., 2016). This group utilised a 5-minute Yoda1 treatment time point. However, as Yoda1 mediates rapid activation of Piezo1 (within seconds), in my study a shorter Yoda1 treatment time (1-minute) was exploited to examine initial downstream signalling events. One interesting finding that the Offermanns group didn't study in detail was the Piezo1 channel dependency of shear stress-mediated CD31 and VEGFR2 tyrosine phosphorylation.

CD31 is an adhesion molecule that is expressed on a variety of cells, inducing endothelial cells. It is clustered at cell-cell junctions to enable homophilic binding of cells to their neighbours. It is interesting as it has been described to be present in a

mechanosensory triad complex with VE-Cadherin and VEGFR2 (Tzima et al., 2005). In this model CD31 directly senses and transmits mechanical force. However, data suggesting an extremely rapid activation of Piezo1 in response to shear stress and the embryonic lethal phenotype that is reported in Piezo1 knock-out mice (Li et al., 2014) competes with previous reports and suggests that Piezo1 is the principal direct shear stress sensor.

Data in the last chapter demonstrated that Yoda1-mediates activation of Piezo1 channels to cause rapid Ca^{2+} entry and eNOS phosphorylation and activation. During this chapter the molecular basis of Yoda1-evoked eNOS phosphorylation was instigated. The main aim of this chapter was to understand the initial signalling pathways activated by 1-minute Yoda1 treatment in endothelial cells. Yoda1-mediated eNOS phosphorylation was examined in HUVECs using immunoblotting and Yoda1-mediated Piezo1 channel activation was investigated using the FlexStation to examine intracellular Ca^{2+} signals. An assay utilising hypotonic stress to induce activation of endogenous Piezo1 channels was developed to investigate mechanical Piezo1 activation. Furthermore the role of the mechanosensory CD31/VE-Cadherin/VEGFR2 triad in Yoda-1 evoked eNOS phosphorylation was investiagted. Finally the physical and biochemical partnership between Piezo1 and the triad in endothelial cells was examined using GFP-Trap pull down and FLIM/FRET microscopy. This will in turn enable us to better understand shear stress sensing in endothelial cells.

4.2 Yoda1 acts independently of ATP activated P2Y2 receptors and AKT to evoke eNOS phosphorylation

The Offermanns group recently suggested that Yoda1 evokes Piezo1 dependent ATP release through pannexin channels activating P2Y2 receptors to induce AKT mediated eNOS phosphorylation (Wang et al., 2016). Initially in this chapter work was carried out to examine whether this mechanism led to Yoda1-evoked eNOS phosphorylation after 1-minute treatment with Yoda1 or whether a more direct mechanism was involved.

4.2.1 Yoda1 acts independently of extracellular ATP and P2Y2 receptors to evoke eNOS phosphorylation

Firstly, it was important to examine the role of extracellular ATP in the coupling between Piezo1 channel activation and eNOS phosphorylation. In order to recapitulate work by the Offermanns group apyrase, an enzyme that catalyses the hydrolysis of ATP, was utilised. As a positive control in HUVECs, it was important to confirm that apyrase was able to breakdown ATP. Intracellular Ca^{2+} responses were measured during application of 20 µM ATP or its vehicle (Veh.). 30-minute pre-treatment with 10 $U.ml^{-1}$ apyrase abolished the ATP induced increase in intracellular Ca^{2+} (Figure 4.1a). These data suggest that the apyrase is sufficient to breakdown ATP. In order to examine whether extracellular ATP is involved in Yoda1 evoked Ca^{2+} entry, HUVECs were pre-treated with apyrase and intracellular Ca^{2+} was measured during application of Yoda1. There was no difference in the Yoda1 evoked Ca^{2+} response with or without apyrase pre-treatment (Figure 4.1b). Similarly, immunoblotting experiments suggested that pre-treatment with apyrase failed to suppress the Yoda1 evoked eNOS phosphorylation (Figure 4.1c).

In order to further investigate the role of ATP in Yoda1-evoked eNOS phosphorylation a direct application of ATP was examined. 1-minute treatment with ATP was used in order to replicate the short Yoda1 treatment time. It is widely reported that direct application of 100 µM ATP evokes S1177 eNOS phosphorylation and NO production (Silva et al., 2006; Silva et al., 2009). However, it is unclear if this occurs at such an early time point. As a positive control, as expected 1-minute treatment with Yoda1 evoked an increase in phospho-eNOS (Figure 4.2). Interestingly, 1-minute treatment with 100 µM ATP was insufficient to evoke eNOS phosphorylation (Figure 4.2). Taken together, these data suggest that

Yoda1 mediated eNOS phosphorylation can occur independently of extracellular ATP.

In order to further investigate the reported mechanism coupling Piezo1 to eNOS phosphorylation insight into the role of P2Y2 was sought. Suramin, a previously reported non-selective G-protein coupled P2Y2 receptor inhibitor that inhibits ATP induced NO production through P2 receptors, was utilised (Beindl et al., 1996; Silva et al., 2006). Firstly, we confirmed that suramin was indeed able to inhibit ATP induced P2Y2 evoked Ca^{2+} entry. 30-minute pre-treatment with 10 µM suramin was sufficient to suppress ATP evoked Ca^{2+} entry, consistent with its ability to block P2 receptors (Figure 4.3a). Suramin pre-treatment suppressed Yoda1 evoked Ca^{2+} entry by about 25% (Figure 4.3b). There appeared to be a similar small inhibitory effect on Yoda1 evoked eNOS phosphorylation but it did not reach statistical significance (Figure 4.3c).

These data suggest that short treatment with Yoda1 evokes eNOS phosphorylation independently of extracellular ATP and P2 receptors.

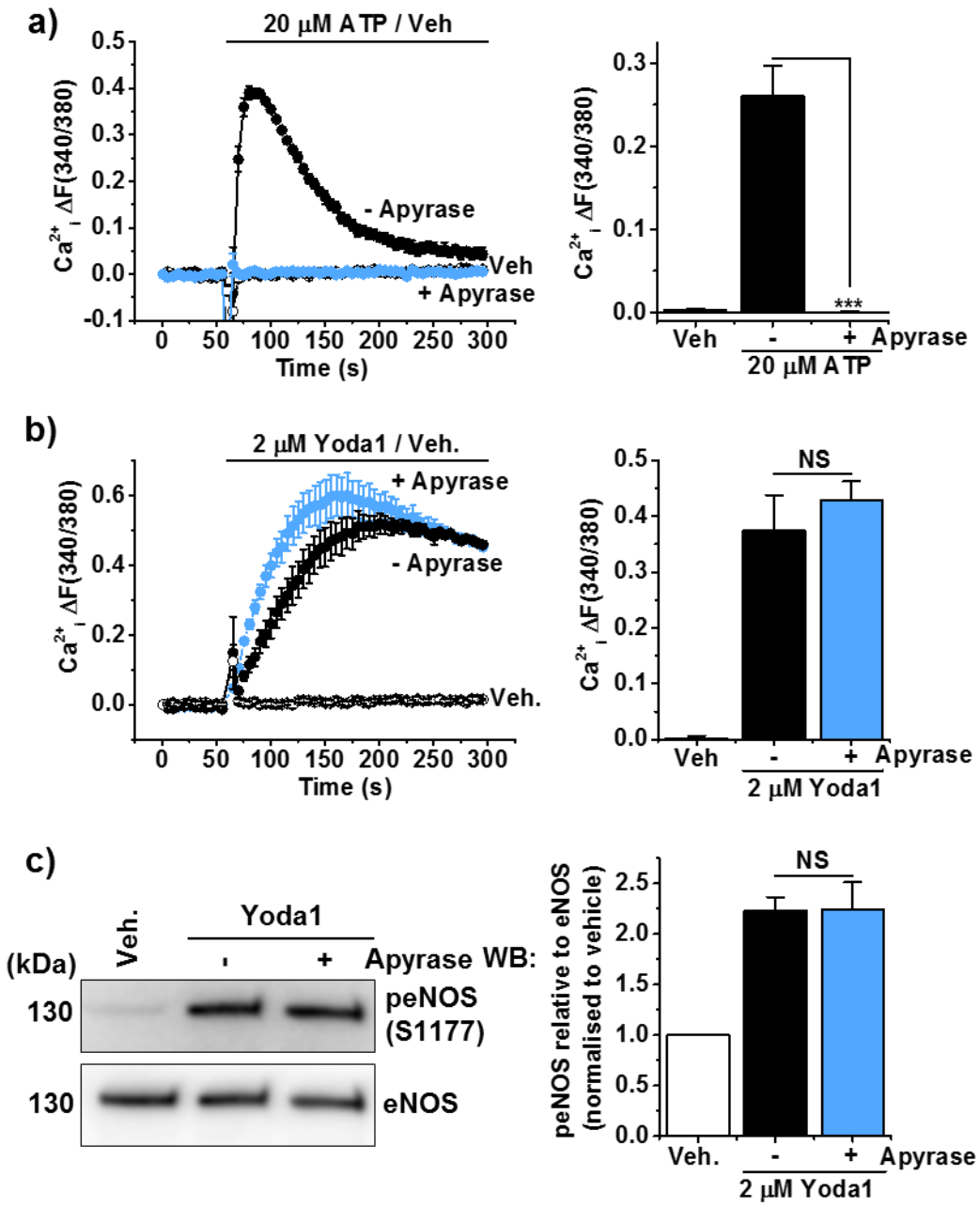

Figure 4.1 Apyrase pre-treatment does not affect Yoda1 evoked eNOS phosphorylation.

a) Left: example intracellular Ca^{2+} measurement trace in HUVECs during application of 20 µM ATP or its vehicle (Veh.). Cells are pre-treated for 30-minutes with 10 $U.mL^{-1}$ apyrase (+Apyrase) or its vehicle (-Apyrase). Right: Mean data for the type of experiment shown on the left n/N=4/24 b) Left: as in (a) but during application of 2 µM Yoda1 or its vehicle (Veh.). Right: Mean data for the type of experiment shown on the left n/N=7/30-34 c) Left: Representative immunoblot for anti-S1177 phospho-eNOS and anti-eNOS in HUVECs treated for 1-minute with 2 µM Yoda1 or its vehicle (Veh.). HUVECs were pre-treated with 10 $U.mL^{-1}$ apyrase or its vehicle (Veh.) for 30-minutes. Right: mean data from n=3 experiments displayed as phosphorylated eNOS relative to total eNOS (normalised to vehicle treatment).

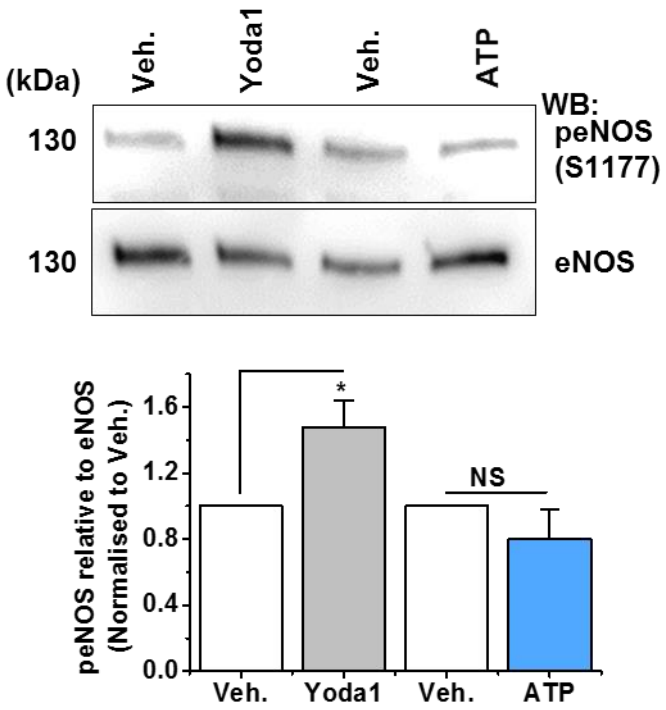

Figure 4.2 1-minute treatment with ATP is insufficient to evoke eNOS phosphorylation.

Upper: Representative immunoblot for anti-S1177 phospho-eNOS and total eNOS in HUVECs treated for 1-minute with 2 μM Yoda1, 100 μM ATP or their vehicles (Veh.). Lower: mean data from n=3 experiments displayed as phosphorylated eNOS relative to total eNOS (normalised to vehicle treatment).

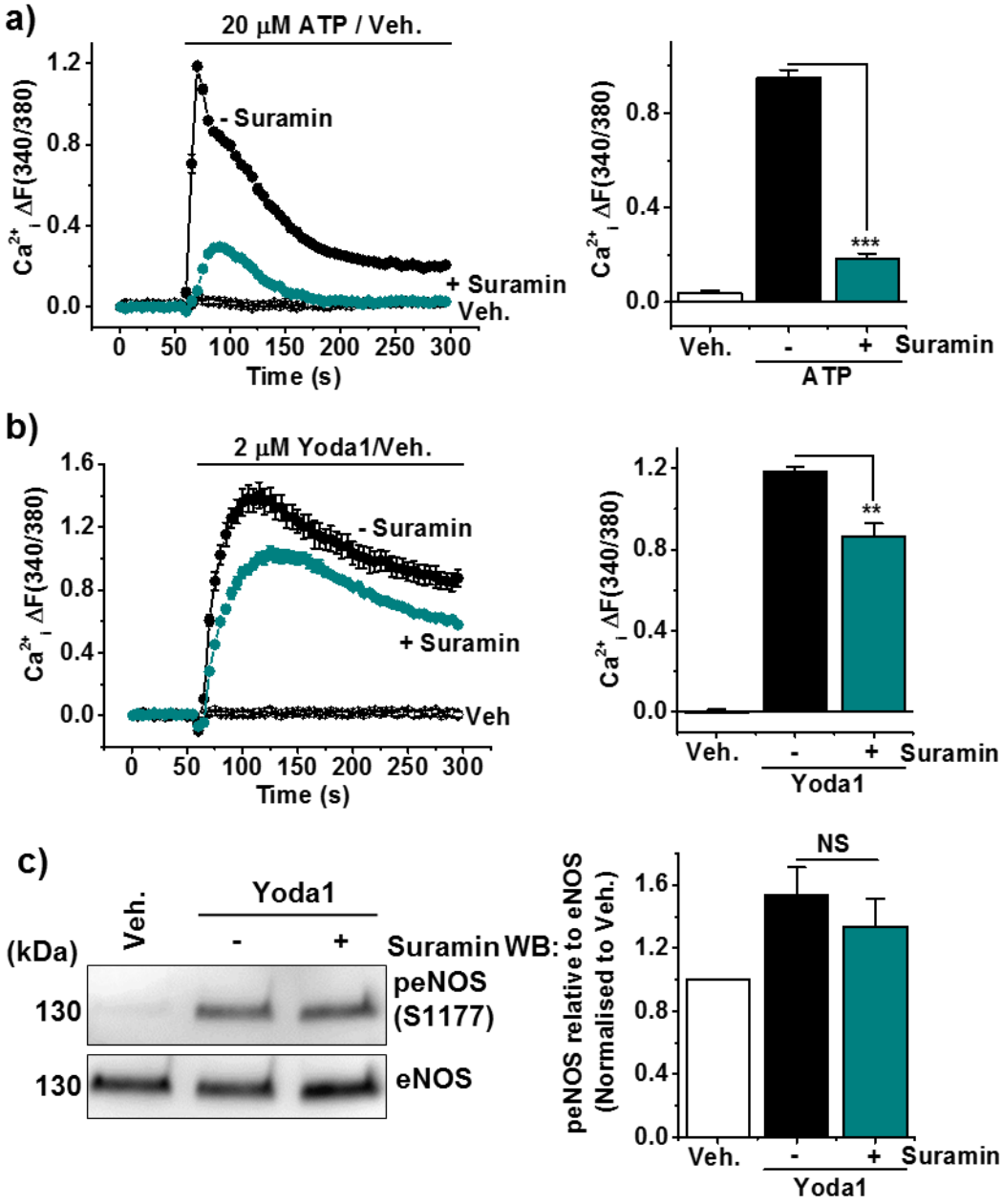

Figure 4.3 Suramin pre-treatment does not affect Yoda1-evoked eNOS phosphorylation.

a) Left: example intracellular Ca^{2+} measurement trace in HUVECs during application of 20 µM ATP or its vehicle (Veh.). Cells are pre-treated for 30-minutes with 10 µM suramin (+suramin) or its vehicle (-suramin). Right: Mean data for the type of experiment shown on the left n/N=3/12-18. b) Left: as in (a) but during application of 2 µM Yoda1 or its vehicle (Veh.). Right: Mean data for the type of experiment shown on the left n/N=3/12-18. c) Left: Representative immunoblot for anti-S1177 phospho-eNOS and anti-eNOS in HUVECs treated for 1-minute with 2 µM Yoda1 or its vehicle (Veh.). HUVECs were pre-treated with 10 µM suramin or its vehicle for 30-minutes. Right: mean data from n=3 experiments displayed as phosphorylated eNOS relative to total eNOS (normalised to vehicle treatment).

4.2.2 Yoda1 evoked eNOS phosphorylation is independent of AKT at short time points

It is widely reported that AKT signalling leads to S1177 eNOS phosphorylation. This was first described by the Pearson group in 1999 (Michell et al., 1999) whereby an inhibitor of AKT signalling reduced both VEGF and insulin-like growth factor 1 (IGF-1) induced AKT activity and eNOS phosphorylation in bovine aortic endothelial cells (BAECs). The same year the PI3K/AKT signalling pathway was reported to lead to Ca^{2+} independent eNOS phosphorylation (Dimmeler et al., 1999). It is now well established that activation of the PI3K/AKT pathway has physiological importance mediating NO-induced endothelial cell migration and angiogenesis induced by VEGF (Kawasaki et al., 2003). More recently, Piezo1 evoked eNOS phosphorylation has been suggested to be mediated by AKT signaling (Wang et al., 2016). In HUAECs and HUVECs 5-minute treatment with Yoda1 induced AKT phosphorylation. However they did not provide evidence that AKT mediated the phosphorylation of eNOS. Work in the previous chapter suggests that indeed 10-minute treatment with either shear stress or Yoda1 was able to evoke AKT phosphorylation in HUVECs, but that a 1-minute treatment time point was insufficient to induce this (Figure 3.14).

Although the data of Figure 3.14 did not suggest a role for AKT in the short-term action of Yoda1, the role of AKT in Yoda1-evoked eNOS phosphorylation was further examined. AKT genetic disruption was performed in HUVECs with siRNA targeting AKT (si.AKT). AKT knockdown was examined by western blotting. AKT protein was knocked down by 65% compared to that of the scrambled treated control (si.Scr) (Figure 4.4a). Next, the role of AKT in Piezo1 channel activity was considered. Intracellular Ca^{2+} measurements confirmed that knocking down AKT had no effect on Yoda1-evoked Piezo1 channel activation compared to cells treated with scrambled siRNA (Figure 4.4b). Furthermore, western blotting analysis of Yoda1 evoked eNOS phosphorylation revealed that genetic disruption of AKT had no effect on this response (Figure 4.4c). Taken together, these data suggest that at 1-minute Yoda1 evoked eNOS phosphorylation is independent of AKT.

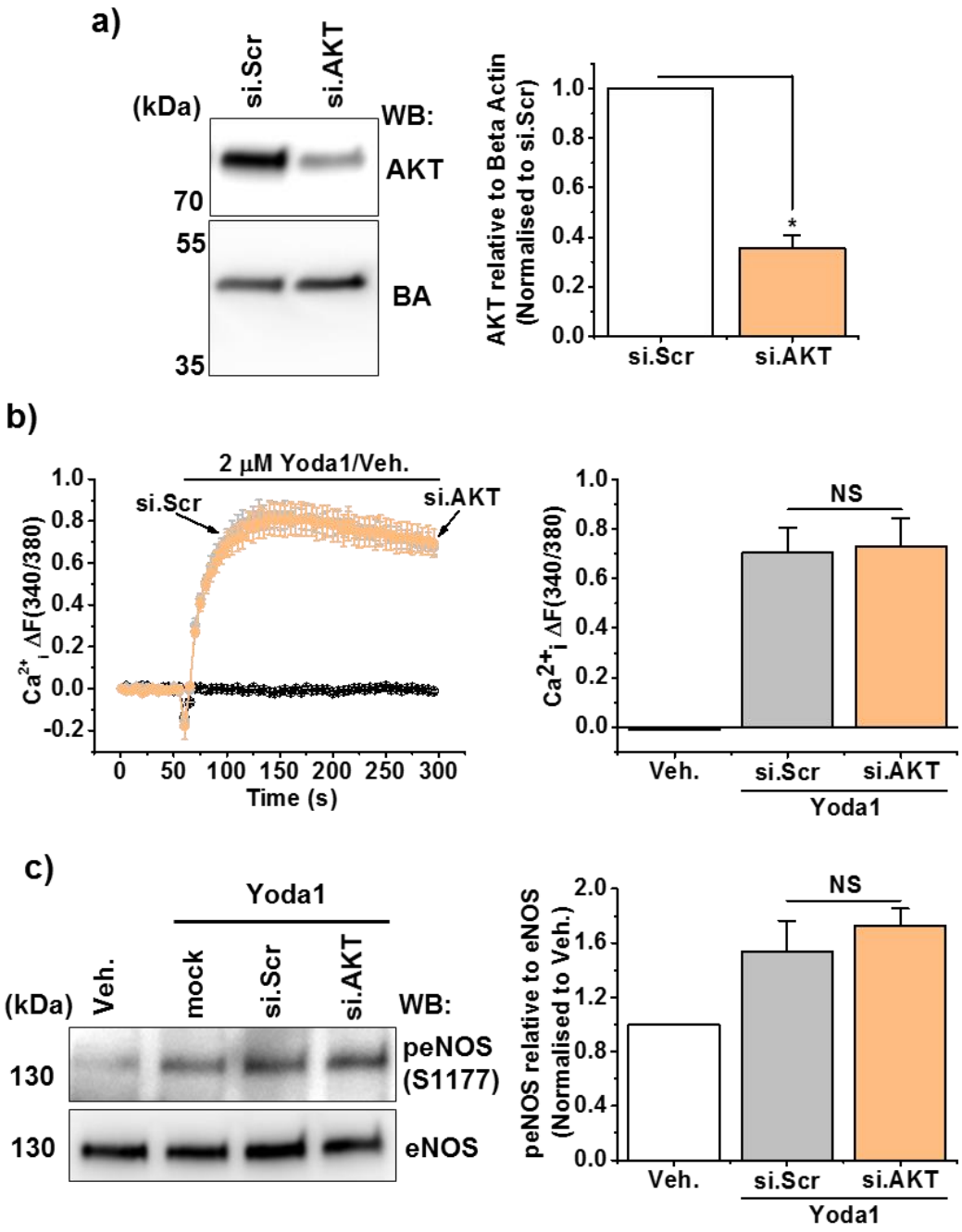

Figure 4.4 Yoda1-evoked eNOS phosphorylation is independent of AKT.

a) Left: Representative immunoblot for anti-AKT and anti-beta actin in HUVECs treated with a mock transfection (-siRNA), scrambled siRNA or AKT siRNA. Right: Mean data from n=3 experiments displayed as AKT relative to beta actin. b) Left: example intracellular Ca^{2+} measurement trace in HUVECs during application of 2 µM Yoda1 or its vehicle (Veh.). Cells are treated with siRNA targeting AKT or a scrambled control sequence. Right Mean data for the type of experiment shown in the left n/N=3/17-18. c) Left: Representative immunoblot for anti-S1177 phospho-eNOS and anti eNOS in HUVECs treated with 2 µM Yoda1 for 1-minute or its vehicle (Veh.). Cells are treated with a mock transfection (-siRNA) or siRNA targeting AKT or a scrambled control sequence. Right: Mean data from n=3 experiments displayed as phospho-eNOS relative to total eNOS normalised to vehicle treated HUVECs.

4.2.3 Yoda1 does not activate G_{i2} proteins in HUVECs

It is widely reported that shear stress evokes activation of G proteins and GPCRs are suggested to mediate primary mechanotransduction and NO production in endothelial cells (Kuchan et al., 1994; Chachisvilis et al., 2006). During an external visit to Professor Martin Schwartz's lab (Yale University), G-protein activation by Yoda1 was examined. Preliminary data from the Schwarz group suggested that G_{i2} and G_q proteins are important for flow induced alignment, AKT phosphorylation and cAMP activation of HUVECs. Dr Keiichiro Tanaka (University of Yale) developed an active G-protein pull down assay and G_{i2} proteins were studied.

As a positive control HUVECs were used expressing G_{i2} proteins, its constitutively active mutant (G_{i2} Q/L) or their vector. G-proteins were expressing a GluGlu (EE) tag to allow detection with immunoblotting. Purified GINIP-GST was used for the pull down. GINIP binds to active G-proteins (GTP) and glutathione beads were used in the pull down. The presence of GluGlu in the input suggests that both G_{i2} and G_{i2} Q/L were expressed in HUVECs compared to cells transfected with the vector alone (Figure 4.5a). GST was pulled down in all conditions but only G_{i2} Q/L was active (Figure 4.5a).

Next, HUVECs co-expressing G_{i2} (expressing GluGlu tag) and the G_i-protein coupled receptor, hM4D (modified from the human-M4-muscarinic (hM4) receptor) were used and active G_{i2} was pulled down using GINIP-GST (that binds to the GTP on active G-proteins). Clozapine-*N*-oxide (CNO) was used as a positive control as it is reported to activate GPCRs (Armbruster et al., 2007). A GST-GINIP pull down was performed after 30-second or 2-minute treatment with CNO or its vehicle (Veh.) and expression of GluGlu and GST was examined. Immunoblotting for GluGlu showed that G_{i2} was expressed equally in all samples and that 2-minute application of CNO was able to evoke G_{i2} activation (Figure 4.5b). These data suggest that the active G_{i2} pull down experiment was viable and that agonist activation of G_{i2} proteins can be detected in HUVECs. However, treatment with 30-second or 2-minute Yoda1 did not activate G_{i2} proteins. No active G_{i2} proteins were pulled down in any of the lysates (Figure 4.5c). This work is currently ongoing in Yale and Dr Keiichiro Tanaka has repeated this assay with both G_{i2} and G_q proteins.

Taken together these data suggest that short treatment with Yoda1 evokes eNOS phosphorylation independently of extracellular ATP, P2Y2, AKT and G_{i2} proteins.

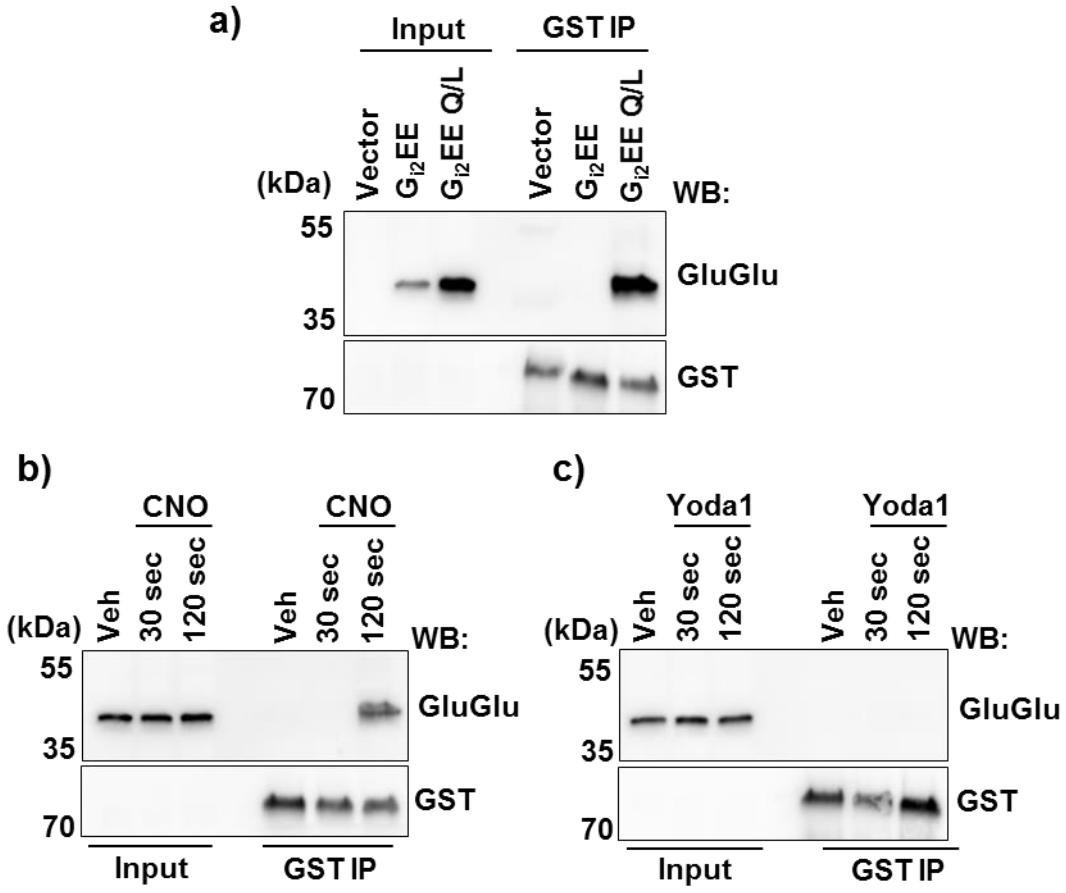

Figure 4.5 Yoda1 does not activate G_{i2} proteins.

a) Representative immunoblot for anti-GluGlu and anti-GST in HUVECs transfected with G_{i2} EE, its constitutively active mutant (G_{i2} EE·Q/L) or their vector. Input represents cell lysates and the IP is performed with GINIP-GST that binds to GTP on active G-proteins (n=2). b) as in (a) but HUVECs transfected with G_{i2} EE and hM4D. Cells were treated with 10 µM CNO for 30-seconds or 2-minutes or its vehicle (Veh) (n=2). c) as in (b) but HUVECs are treated with 2 µM CNO for 30-seconds or 2-minutes or its vehicle (Veh) (n=2).

4.3 The role of CD31, VE-Cadherin and VEGFR2 in Yoda1-evoked eNOS phosphorylation

The mechanosensory triad complex comprising CD31, VE-Cadherin and VEGFR2 has been associated with shear stress evoked eNOS phosphorylation. Shear stress is reported to tyrosine phosphorylate CD31 and VEGFR2 to activate PI3K/AKT-eNOS signalling (Fleming et al., 2005; Tzima et al., 2005; Bagi et al., 2005). *In-vivo* both CD31 and VEGFR2 have also been reported to be important for eNOS activation and NO dependent vasodilation (Bagi et al., 2005; Jin et al., 2003). More recently it has been reported that the shear stress induced tyrosine phosphorylation of CD31 and VEGFR2 is Piezo1 dependent (Wang et al., 2016). Thus, we investigated whether Piezo1 is acting in partnership to cross-talk with the previously reported mechanosensory triad to evoke Yoda1-mediated eNOS phosphorylation.

4.3.1 CD31 and VE-Cadherin are important for Yoda1-evoked eNOS phosphorylation

HUVECs were treated with siRNA targeting CD31 (si.CD31), VE-Cadherin (si.VeCad), VEGFR2 (si.VR2) and Piezo1 (si.P1) as a positive control. Application of 2 µM Yoda1 for 1-minute evoked an increase in eNOS phosphorylation in both mock (-siRNA) and scrambled siRNA (si.Scr) treated cells compared to its vehicle (Figure 4.6a). As expected, after Piezo1 knockdown Yoda1-induced eNOS phosphorylation was abolished (Figure 4.6a). Furthermore, knockdown of CD31 and VE-Cadherin also significantly suppressed this response (Figure 4.6a). siRNA targeting VEGFR2 appeared to reduce the response but statistical significance was not achieved (Figure 4.6a). These data suggest that Yoda1 evoked eNOS phosphorylation is dependent on CD31 and VE-Cadherin proteins of the triad.

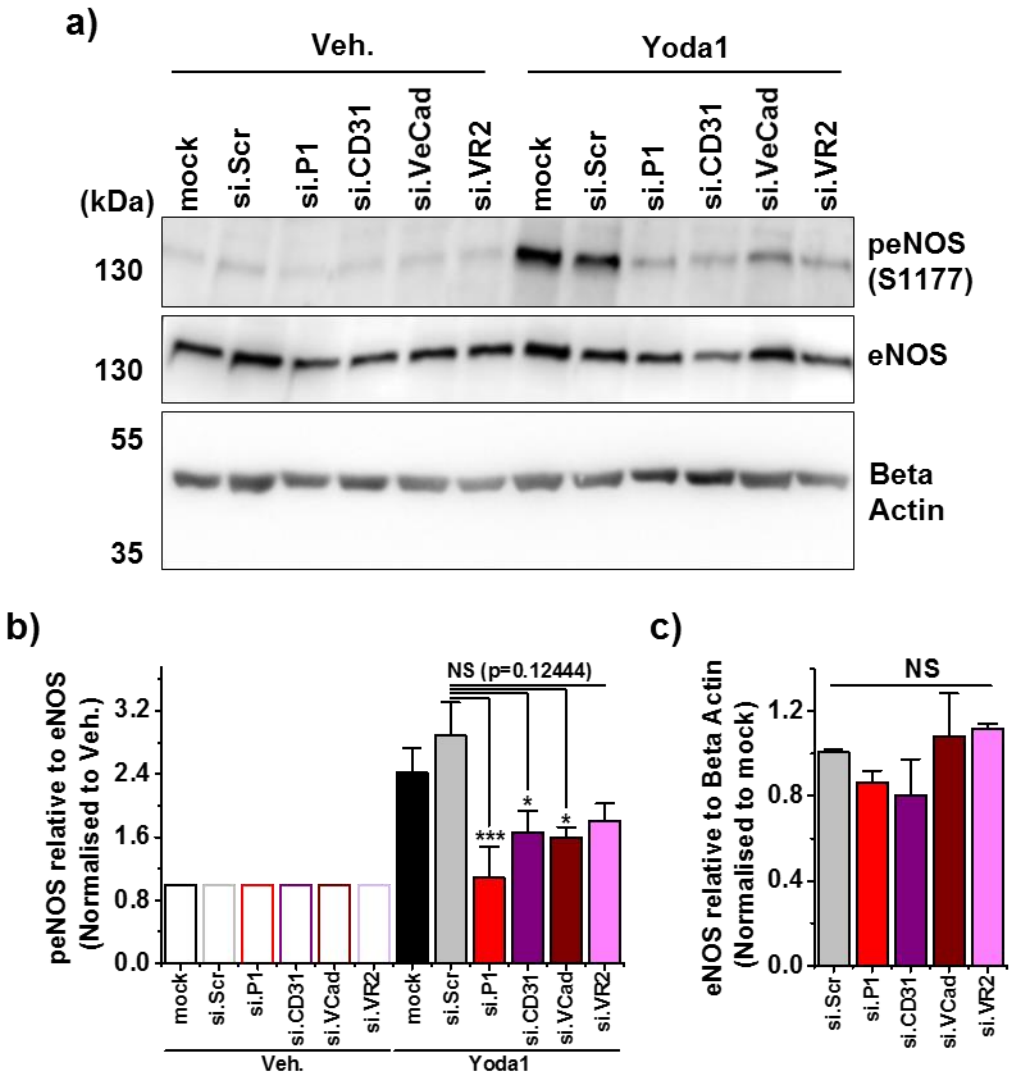

Figure 4.6 Piezo1 cross-talks with CD31, VE-Cadherin and VEGFR2 to evoke Yoda1-mediated eNOS phosphorylation.

a) Upper: Representative immunoblot for anti-S1177 phospho-eNOS and anti eNOS in HUVECs treated with 2 μM Yoda1 for 1-minute or its vehicle (Veh.). Cells are treated with a mock transfection (-siRNA) or siRNA targeting Piezo1, CD31, VE-Cadherin (VeCad), VEGFR2 (VR2) or a scrambled control sequence. b) Mean data from n=3 experiments displayed as peNOS relative to total eNOS normalised to vehicle treated HUVECs. c) Mean data from n=3 experiments displayed as eNOS relative to beta actin normalised to mock transfected cells.

4.4 The triad acts downstream of chemical Piezo1 activation

Knocking down CD31 and VE-Cadherin proteins of the triad strongly suppressed Yoda1-mediated eNOS phosphorylation. In order to investigate whether knockdown of the triad affects Piezo1 channel function or whether the triad is acting downstream of Piezo1 to mediate its signalling, intracellular Ca^{2+} measurement assays were carried out. HUVECs were treated with siRNA targeting each member of the triad individually and Yoda1-mediated Piezo1 channel activation was examined

For the next set of experiments the control scrambled siRNA response was common to all experiments but they are displayed separately for clarity. This was taken into account during the statistical analysis. siRNA targeting CD31 (si.CD31/si.CD) was able to knockdown CD31 protein expression in HUVECs by 85% compared to cells treated with siRNA targeting a scrambled control sequence (si.Scr) (Figure 4.7a). Yoda1-mediated Ca^{2+} entry was comparable with and without CD31 knockdown (Figure 4.7b). The amplitudes of the responses were similar and the EC_{50}s were 1.86 µM and 1.82 µM with and without CD31 knockdown respectively (Figure 4.7c & d). Analysis of the gradient of the Hill plots demonstrates no change with and without CD31 expression (Figure 4.7c & e). Similarly, knocking down VE-Cadherin by 90% (si.VeCad/siVC) (Figure 4.8a) had no effect on Yoda1 mediated Piezo1 activation (Figure 4.8b-d). The amplitude of the Ca^{2+} entry mediated by Yoda1 was similar. The EC_{50}s with and without VE-Cadherin knockdown were 1.81 µM and 1.82 µM respectively and the gradient of the dose-response curve was unchanged (Figure 4.8c - e). Investigation into the final member of the triad, VEGFR2, again demonstrated that VEGFR2 does not affect Yoda1-mediated Ca^{2+} entry. VEGFR2 was knocked down by 67% (siVEGFR2/siVR2) (Figure 4.9a). Yoda1 Ca^{2+} responses were similar with and without VEGFR2 knockdown (Figure 4.9b). The EC_{50} appears to be slightly higher without VEGFR2 expression (12.56 µM), but this can only be an estimate as maxima responses were not obtained (Figure 4.9c-d). The gradient of the dose-response curve was also slightly increased but this did not reach statistical significance (Figure 4.9e).

Taken together, these results suggest that the members of the triad are not involved in Yoda1-mediated Ca^{2+} entry. The data suggest that CD31 and VE-Cadherin are downstream of Yoda1 mediated Piezo1 channel activation.

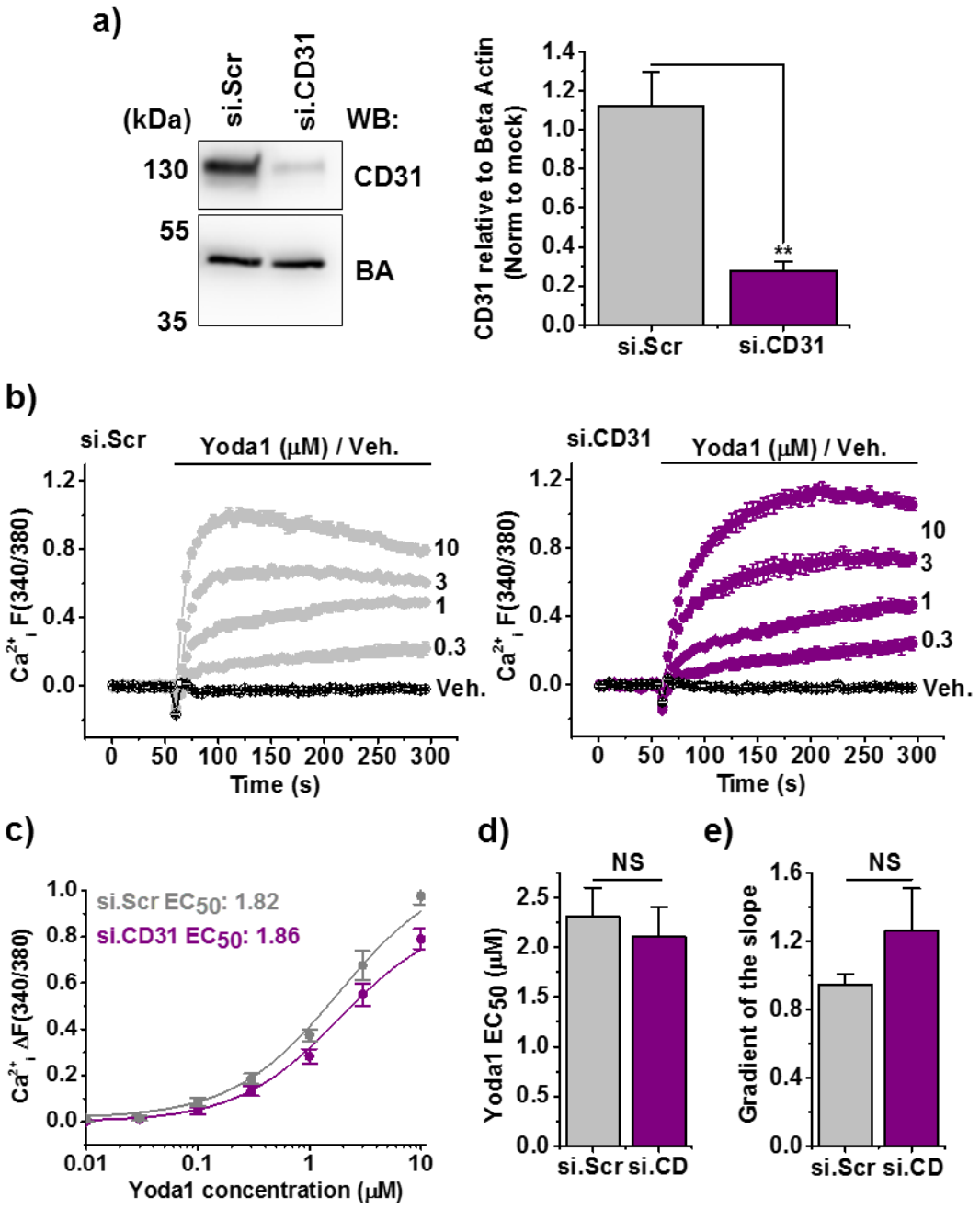

Figure 4.7 Yoda1-medated Ca^{2+} entry is CD31 independent.

a) Left: Representative immunoblot for anti-CD31 and anti-beta actin in HUVECs treated with siRNA targeting CD31 (si.CD31) or a scrambled control sequence (si.Scr). Right: Mean data from n=3 experiments displayed as CD31 relative to beta actin normalised to mock (-siRNA) treated HUVECs. b) Example intracellular Ca^{2+} measurement traces in HUVECs during application of a range of doses of Yoda1 or its vehicle (Veh.). On the left cells are treated with siRNA targeting a scrambled control sequence and on the right cells are treated with siRNA targeting CD31. c) Concentration-response data for Yoda1 from the type of experiments in b) (n/N=3-6/18-36). The fitted curves are Hill equations indicating the 50% maximum effect (EC_{50}) at 1.82 µM for scrambled siRNA treated cells and 1.86 µM for Piezo1 siRNA treated cells. d) Mean data for the type of experiment shown in (c) mean is an average of EC_{50}s from individual repeats n=3. e) Mean data for the type of experiment shown in c), mean is an average gradient of the line (n=3),

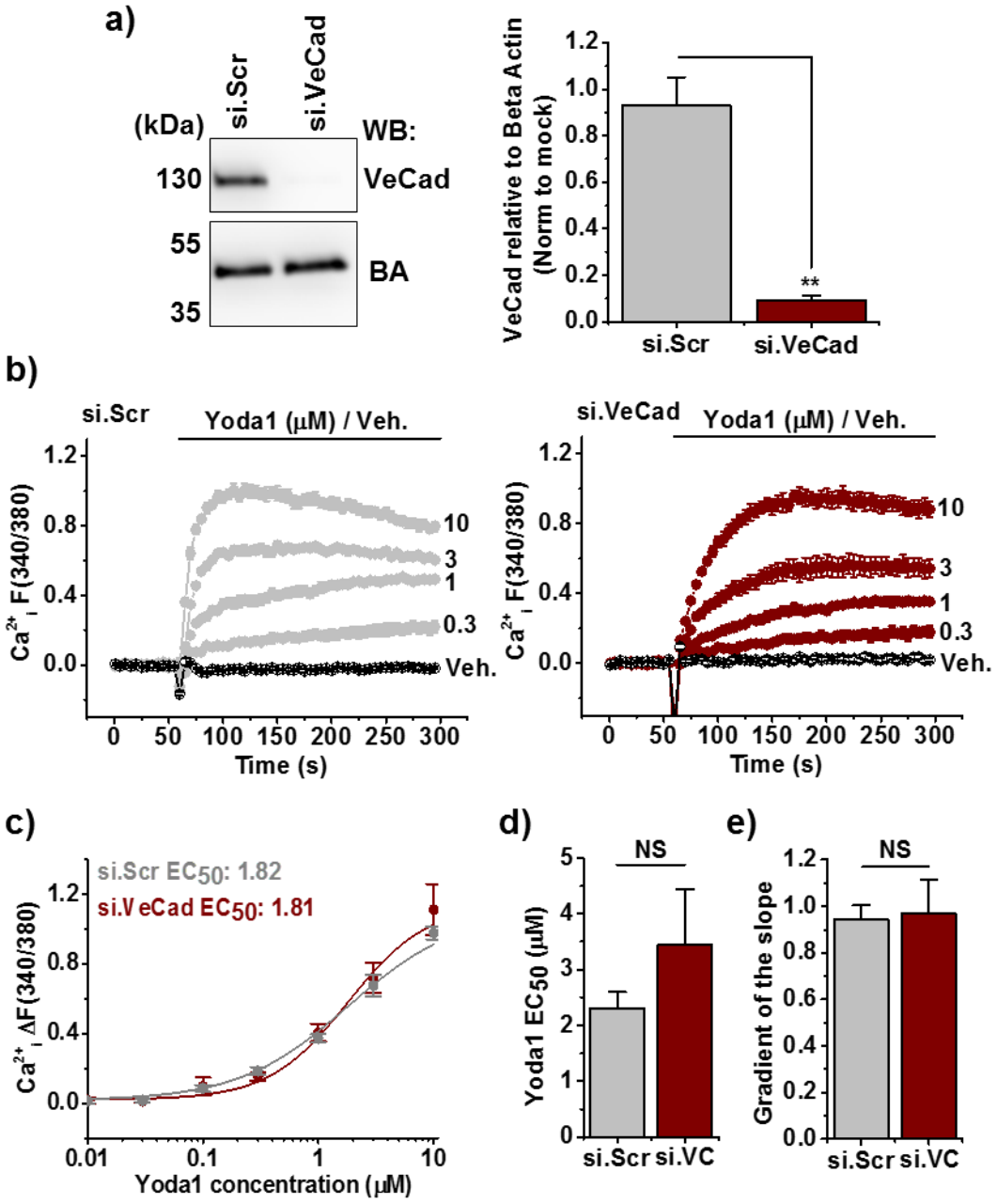

Figure 4.8 Yoda1-medated Ca^{2+} entry is VE-Cadherin independent.

a) Left: Representative immunoblot for anti-VE-Cadherin and anti-beta actin in HUVECs treated with siRNA targeting VE-Cadherin (si.VeCad) or a scrambled control sequence (si.Scr). Right: Mean data from n=3 experiments displayed as CD31 relative to beta actin normalised to mock (-siRNA) treated HUVECs. b) Example intracellular Ca^{2+} measurement traces in HUVECs during application of a range of doses of Yoda1 or its vehicle (Veh.). On the left cells are treated with siRNA targeting a scrambled control sequence and on the right cells are treated with siRNA targeting VE-Cadherin. c) Concentration-response data for Yoda1 from the type of experiments in (b) (n/N=3-6/18-36). The fitted curves are Hill equations indicating the 50% maximum effect (EC_{50}) at 1.82 µM for scrambled siRNA treated cells and 1.81 µM for VE-Cadherin siRNA treated cells. d) Mean data for the type of experiment shown in c) mean is an average of EC_{50}s from individual repeats n=3. e) Mean data for the type of experiment shown in (c), mean is an average gradient of the line (n=3).

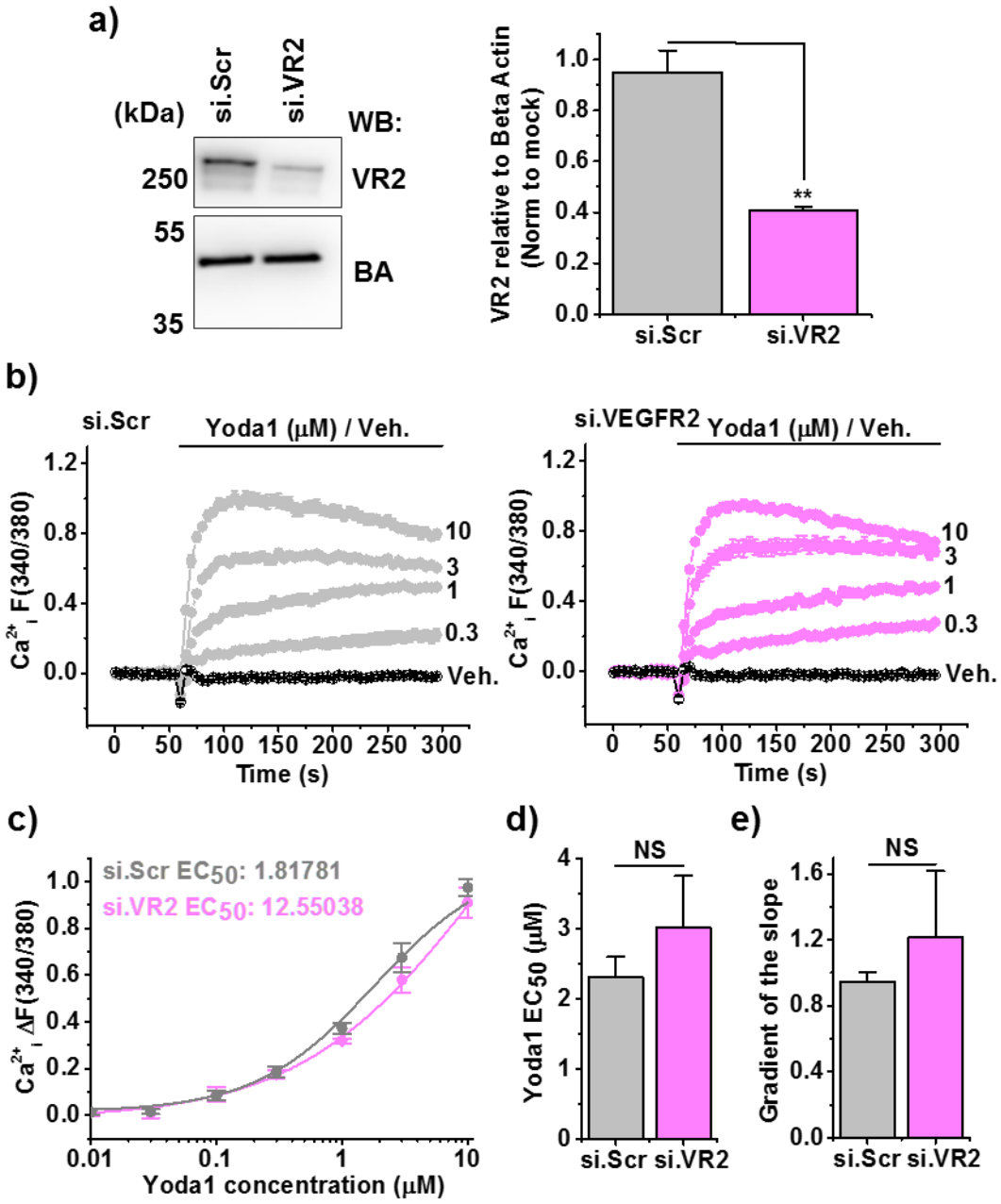

Figure 4.9 Yoda1-medated Ca^{2+} entry is VEGFR2 independent.

a) Left: Representative immunoblot for anti-VEGFR2 and anti-beta actin in HUVECs treated with siRNA targeting VEGFR2 (si.VR2) or a scrambled control sequence (si.Scr). Right: Mean data from n=3 experiments displayed as VEGFR2 relative to beta actin normalised to mock (-siRNA) treated HUVECs. b) Example intracellular Ca^{2+} measurement traces in HUVECs during application of a range of doses of Yoda1 or its vehicle (Veh.). On the left cells are treated with siRNA targeting a scrambled control sequence and on the right cells are treated with siRNA targeting VEGFR2. c) Concentration-response data for Yoda1 from the type of experiments in b) (n/N=3-6/18-36). The fitted curves are Hill equations indicating the 50% maximum effect (EC_{50}) at 1.82 µM for scrambled siRNA treated cells and 12.55 µM for VEGFR2 siRNA treated cells. d) Mean data for the type of experiment shown in c) mean is an average of EC_{50}s from individual repeats n=3. e) Mean data for the type of experiment shown in (c), mean is an average gradient of the line (n=3).

4.5 CD31 and VE-Cadherin proteins of the triad complex act downstream of Piezo1 channel activation by hypotonic stress

Data thus far suggest that the triad are not involved in Yoda1-evoked Piezo1-mediated Ca^{2+} entry. In order to examine mechanical activation of Piezo1 a 96-well plate assay to provoke hypotonic stress was developed. We assume that the activation of Piezo1 is due to mechanical force evoked by cell swelling, however as of yet there is no evidence for this. This assay was set up alongside Dr Melanie Ludlow (University of Leeds). The FlexStation was used to examine intracellular Ca^{2+} levels and buffer was used where Na^{+} was replaced with decreasing mannitol concentrations to make solutions increasingly hypotonic. The assay has been previously published in HUVECs where hypotonic stress was reported to mimic shear stress mediated ATP release (Hirakawa et al., 2004). Firstly, to examine whether HUVECs respond to hypotonic stress the FlexStation was used and intracellular Ca^{2+} responses were examined during application of hypotonic solutions. Application of decreasing concentrations of mannitol dose-dependently caused transient increases in the intracellular Ca^{2+} concentration (Figure 4.10a). The EC_{50} of mannitol was 86.69 mM (Figure 4.10b). 270 mM mannitol was used as an isotonic control throughout all experiments.

It is reported that suramin pre-treatment, to block ATP evoked activation of P2 receptors, suppressed the hypotonic response (Hirakawa et al., 2004). In order to validate the assay suramin pre-treatment was replicated. Application of 90 mM mannitol evoked an increase in intracellular Ca^{2+} levels compared to the control (270 mM mannitol) and this was blunted with pre-treatment with suramin (Figure 4.11). Consistent with the literature, these data suggest that hypotonic stress is able to evoke activation of suramin sensitive receptors or channels. P2 receptors are ligand-gated Ca^{2+} channels that are activated by ATP. P2X4 is reported to be important in shear stress evoked Ca^{2+} entry as this was abolished in endothelial cells from P2X4 deficient mice (Yamamoto et al., 2006). These data suggest that ATP is a major factor of this response, but, as the response is not fully abolished by suramin pre-treatment, perhaps Piezo1 channels also contribute.

4.5.1 Yoda1 strongly potentiates hypotonic responses

It is reported that in HEK 293 cells over-expressing human Piezo1 Yoda1 is able to modulate mechanical responses. Yoda1 pre-treatment potentiated mechanical Piezo1 activation and affected the sensitivity of the inactivation kinetics (Syeda et al., 2015). Next the effect of Yoda1 pre-treatment on the hypotonic response was examined. 0.03 µM Yoda1 was utilised to evoke minimal Piezo1 channel activation itself (Figure 4.12b). Baseline recordings demonstrate that 30-minute pre-treatment with 0.03 µM Yoda1 slightly activated Piezo1 channels compared to cells pre-treated with its vehicle (Veh.) (Figure 4.12). Application of 90 mM mannitol alone evoked a small increase in intracellular Ca^{2+} compared to that of the control (270 mM mannitol). After Yoda1 pre-treatment this response was strongly potentiated (Figure 4.12). These data are in keeping with the literature suggesting that Yoda1 can potentiate mechanical activation of Piezo1.

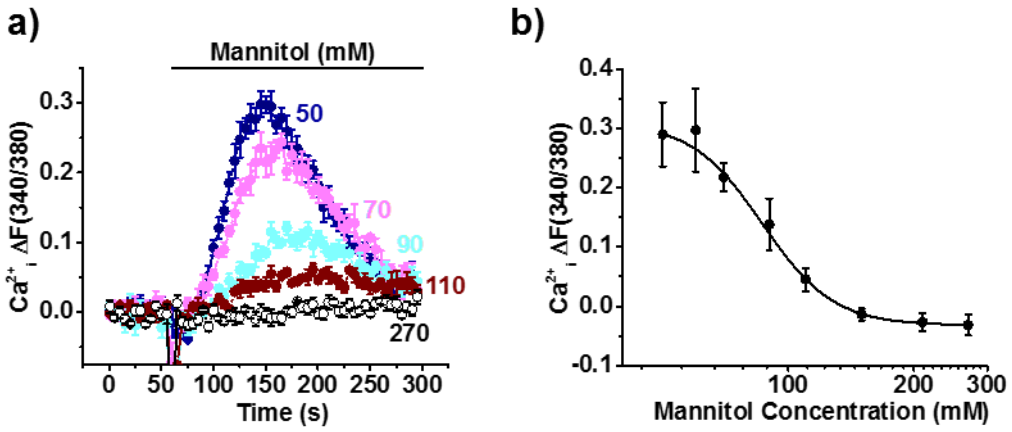

Figure 4.10 Hypotonic stress evokes an increase in intracellular levels of Ca^{2+} in HUVECs.

a) Example intracellular Ca^{2+} measurement traces in HUVECs during application of a range of doses of mannitol to evoke hypotonic stress or not (270 mM). b) Concentration-response data for mannitol from the type of experiments in (a) (n/N=4/15-16). The fitted curve is a hill equation indicating the 50% maximum effect (EC_{50}) at 86.69 mM mannitol.

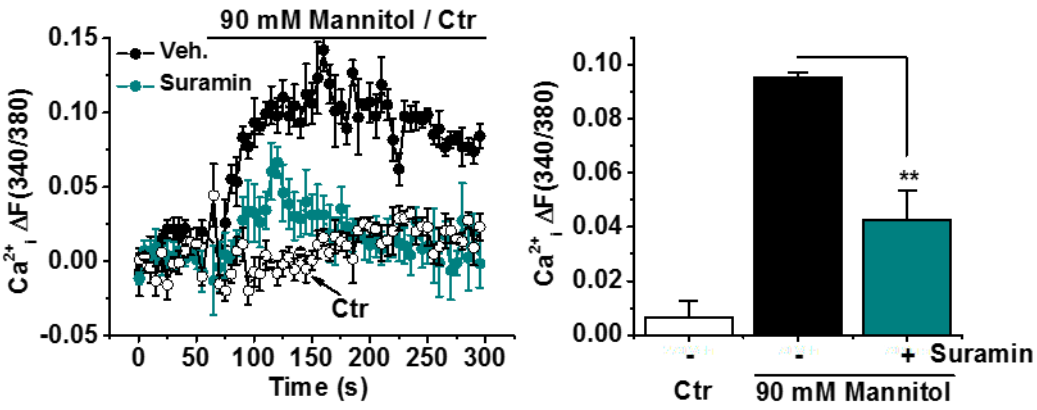

Figure 4.11 Hypotonicity mediated Ca^{2+} entry is blunted by suramin pre-treatment.

Left: Example intracellular Ca^{2+} measurement traces in HUVECs during application 90 mM mannitol or a control (270 mM) to evoke hypotonic stress or not. Cells are pre-treated with 10 µM suramin or its vehicle (Veh.) (n/N=3/12). Right: Mean data for the type of experiment shown on the left from n=3 individual repeats.

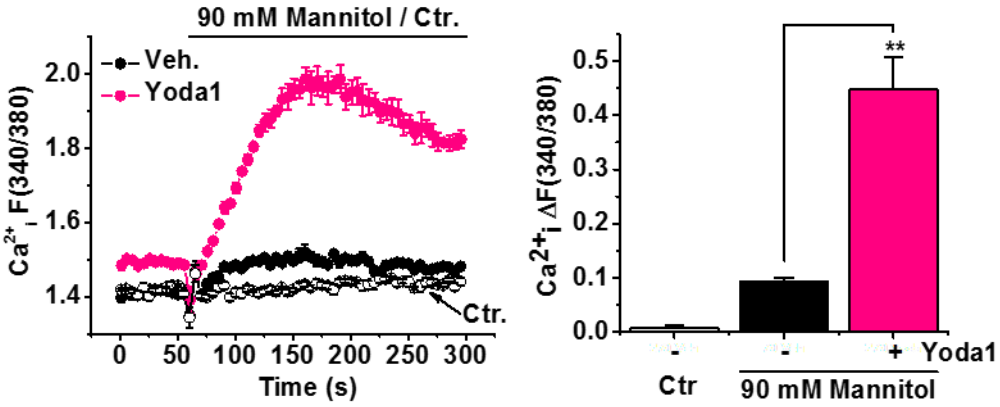

Figure 4.12 Yoda1 pre-stimulation potentiates hypotonicity induced activation.

Left: Example intracellular Ca^{2+} measurement traces in HUVECs during application 90 mM mannitol or a control (270 mM) to evoke hypotonic stress or not. Cells are pre-treated with 0.03 µM Yoda1 or its vehicle (Veh.) (n/N=3/11-12). Right: Mean data for the type of experiment shown on the left from n=3 individual repeats.

4.5.2 Hypotonic stress activates Piezo1 channels

It is clear that pre-treatment with suramin does not fully block hypotonicity induced Ca^{2+} entry suggesting that this response is not only mediated by P2 receptors but by other ion channels as well. Next, the involvement of Piezo1 channels in the Ca^{2+} entry evoked by hypotonic stress was investigated. The non-selective cation channel ion pore blocker, gadolinium was used. HUVECs were pre-treated for 30-minutes with 30 µM gadolinium (+Gd^{3+}) or its vehicle (-Gd^{3+}) and hypotonic induced Ca^{2+} entry was examined. In cells pre-treated with the vehicle of gadolinium normal dose-dependent hypotonic responses were observed (Figure 4.13a). These responses were blunted after gadolinium pre-treatment by 85% (Figure 4.13a & b). EC_{50}s with and without gadolinium pre-treatment were 93.67 mM and 90.27 mM mannitol respectively (Figure 4.13 b & c). These data suggest that mechanosensitive non-selective cation channels, including Piezo1 channels, are mediating the increase in intracellular Ca^{2+} evoked by cell swelling.

In order to more specifically examine whether Piezo1 channels can be studied with hypotonic cell swelling, siRNA targeting Piezo1 was utilised. Piezo1 genetic disruption blunted the hypotonic response by 45% (Figure 4.14a & b). The mannitol EC_{50} with and without Piezo1 knockdown is comparable; 77.44 mM and 86.67 mM respectively. These data suggest that the hypotonicity-evoked Ca^{2+} response is partially mediated by Piezo1. Suramin pre-treatment and Piezo1 siRNA effects are both relatively large and as suramin slightly inhibits Piezo1-mediated Ca^{2+} entry (Figure 4.3) the responses might be slightly overlapping.

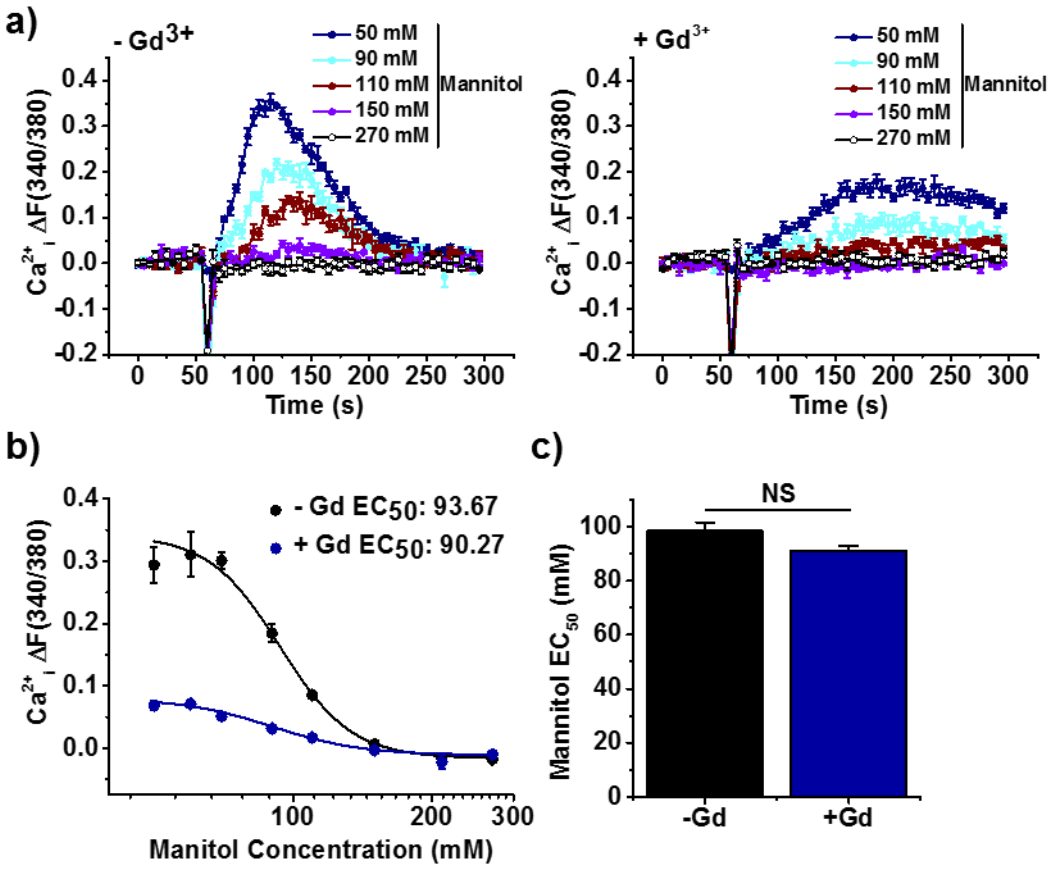

Figure 4.13 Gadolinium pre-treatment suppresses Ca^{2+} entry evoked by hypotonicity.

a) Example intracellular Ca^{2+} measurement traces in HUVECs during application of varying mannitol concentrations (50-270 mM). Left: after pre-treatment with the vehicle of gadolinium (-Gd^{3+}). Right: After pre-treatment with 30 µM gadolinium. (n/N=4/16). b) Concentration-response data for mannitol from the type of experiments in (a) (n=4). The fitted curve is a hill equation indicating the 50% maximum effect (EC_{50}) at 93.67 mM mannitol without gadolinium pre-treatment and 90.27 mM mannitol with gadolinium pre-treatment. c) Mean data for the type of experiment shown in (b) mean is an average of EC_{50}s from independent repeats n=4.

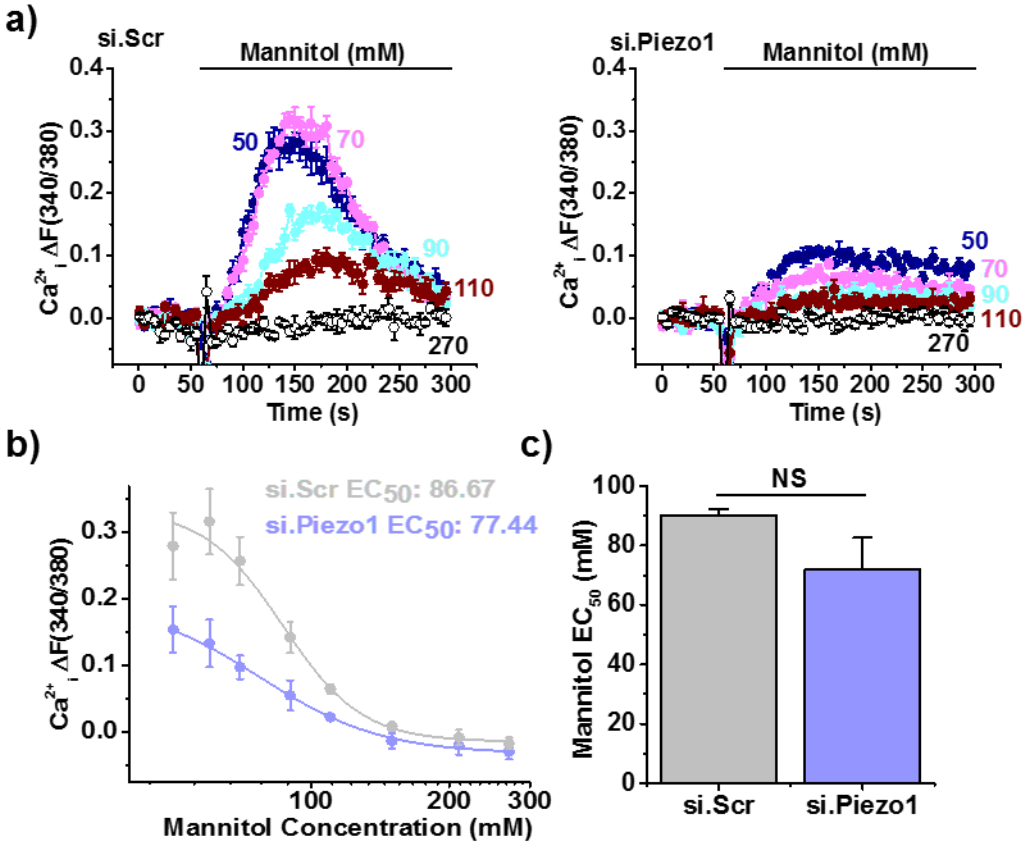

Figure 4.14 Piezo1 is activated by hypotonicity in HUVECs.

a) Example intracellular Ca^{2+} measurement traces in HUVECs during application of varying mannitol concentrations (50-270 mM). Left: in cells treated with siRNA targeting a scrambled control sequence (si.Scr). Right: in cells treated with siRNA targeting Piezo1 (si.Piezo1) (n/N=3-4/12-16). b) Concentration-response data for mannitol from the type of experiments in a) (n=3-4). The fitted curve is a hill equation indicating the 50% maximum effect (EC_{50}) at 86.67 mM and 77.44 mM mannitol with and without Piezo1 expression respectively. c) Mean data for the type of experiment shown in (b) mean is an average of EC_{50}s from independent repeats n=3-4.

4.5.3 Hypotonicity-evoked Ca^{2+} signals are independent of the CD31/VE-Cadherin/VEGFR2 complex

Data earlier in this chapter suggest that members of the triad are not involved in Yoda1-mediated Ca^{2+} entry but that CD31 and VE-Cadherin proteins are important for the integrity of Yoda1-mediated eNOS phosphorylation. In order to investigate whether the triad is involved in the hypotonicity-evoked Ca^{2+} response, each member was knocked down and hypotonic activation of HUVECs was examined. As before, for the next set of experiments the control scrambled siRNA response was common to all experiments but they are displayed separately for clarity. This was taken into account during the statistical analysis

Firstly, CD31 was knocked down in HUVECs (si.CD31/si.CD). Disruption of CD31 expression had no effect on Ca^{2+} entry evoked by hypotonicity (Figure 4.15a). Hypotonic stress induced comparable increases in intracellular Ca^{2+} in cells treated with CD31 siRNA (si.CD31) and siRNA targeting a scrambled control (si.Scr) (Figure 4.15a). The EC_{50} of mannitol is unchanged with and without CD31 expression; 86.67 mM and 80.39 mM respectively and the gradient of the dose-response curve was similar (Figure 4.15b - d). Next VE-Cadherin knockdown was examined. Again, VE-Cadherin knockdown had no effect on the amplitude of the Ca^{2+} entry evoked by hypotonic stress (Figure 4.16a). Furthermore, the EC_{50} of mannitol was similar with and without expression of VE-Cadherin (86.67 mM and 78.33 mM mannitol respectively) and the gradient of the slope was unchanged (Figure 4.16b - d). Finally, VEGFR2 was examined. Similarly, the Ca^{2+} entry evoked by cell swelling was similar with and without VEGFR2 expression and gradient of the curves and the EC_{50}s were equivalent (si.Scr: 86.67 mM and siVEGFR2: 75.35 mM) (Figure 4.17 a - d).

In brief, CD31 and VE-Cadherin were important for Yoda1 evoked eNOS phosphorylation but were not involved in the Ca^{2+} entry evoked by Yoda1. Furthermore, they were also not involved in the Ca^{2+} entry evoked by hypotonicity-evoked activation of Piezo1. Taken together, these data suggest that CD31 and VE-Cadherin do not affect Yoda1 mediated Ca^{2+} entry but are required in some way for Piezo1-evoked eNOS phosphorylation.

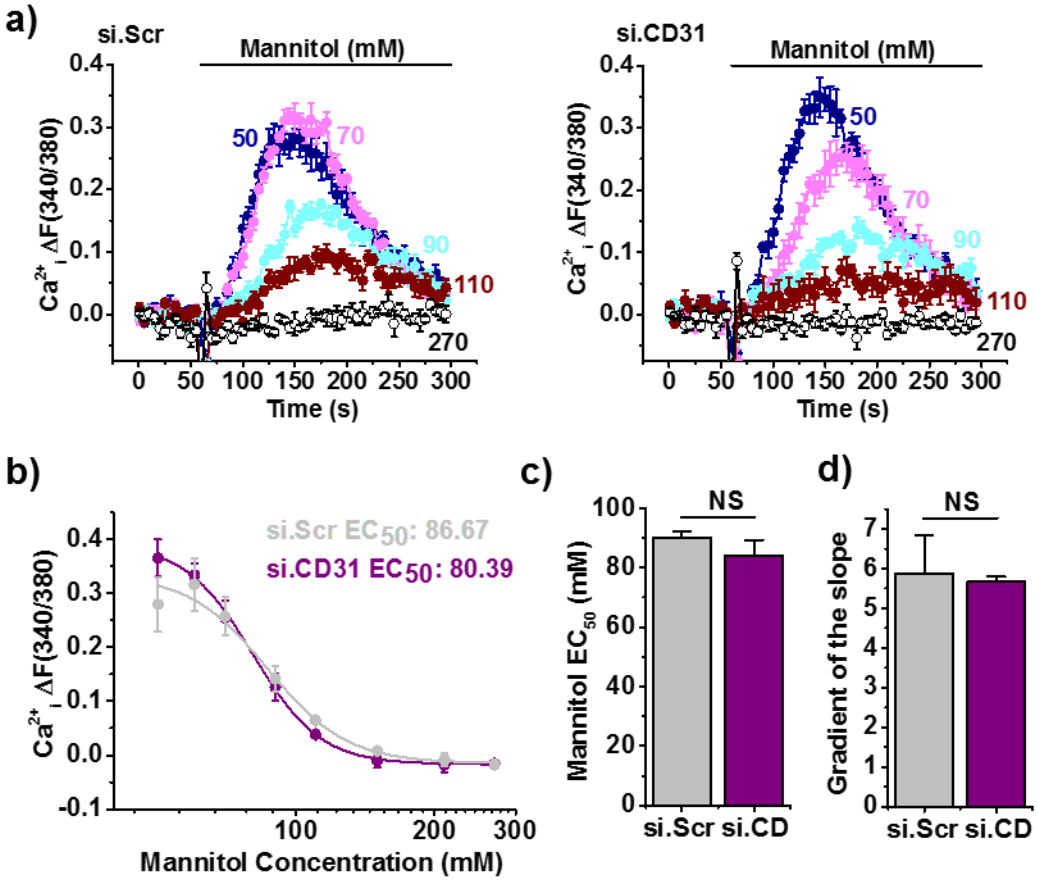

Figure 4.15 CD31 knockdown does not affect mechanical cation channel activation.

a) Example intracellular Ca^{2+} measurement traces in HUVECs during application of varying mannitol concentrations (50-270 mM). Left: in cells treated with siRNA targeting a scrambled control sequence (si.Scr). Right: in cells treated with siRNA targeting CD31 (si.CD31). (n/N=4/16). b) Concentration-response data for mannitol from the type of experiments in a) (n=4). The fitted curve is a hill equation indicating the 50% maximum effect (EC_{50}) at 86.67 mM and 80.39 mM mannitol with and without CD31 expression respectively. c) Mean data for the type of experiment shown in (b) mean is an average of EC_{50}'s from individual repeats n=4. d) Mean data for the type of experiment shown in (b) mean is an average of the gradient of the curves (n=3).

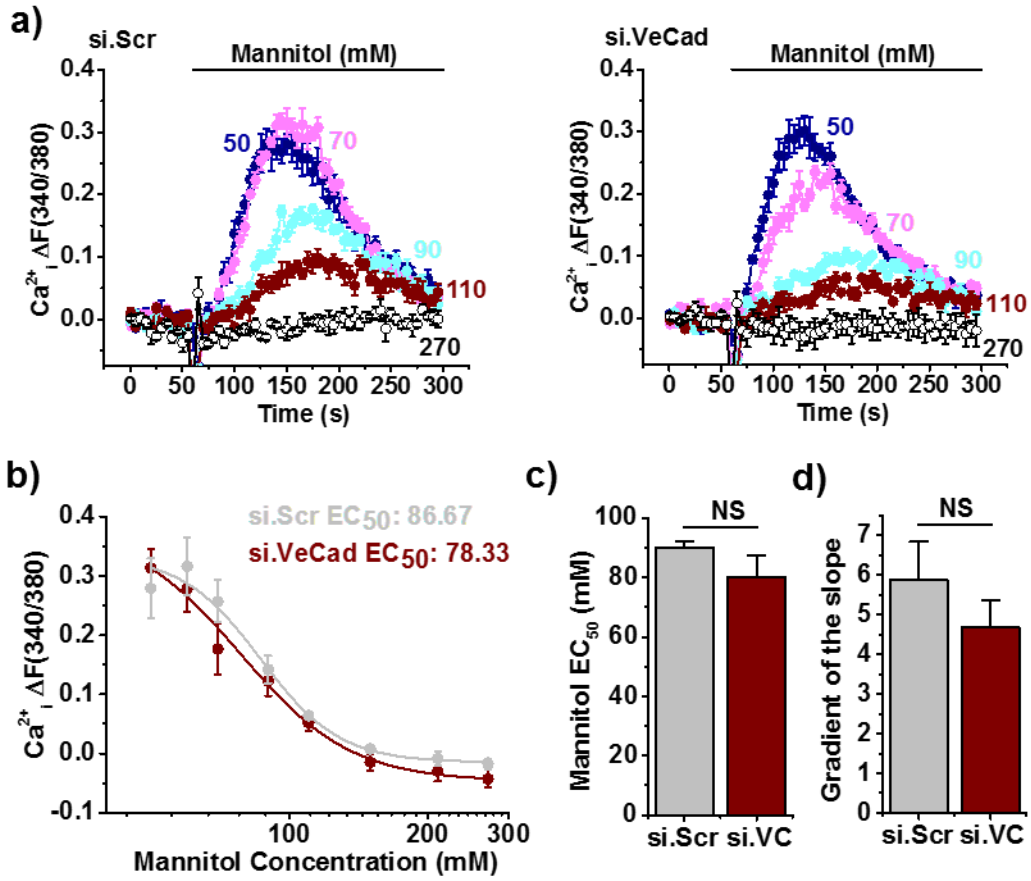

Figure 4.16 VE-Cadherin knockdown does not affect mechanical cation channel activation.

a) Example intracellular Ca^{2+} measurement traces in HUVECs during application of varying mannitol concentrations (50-270 mM). Left: in cells treated with siRNA targeting a scrambled control sequence (si.Scr). Right: in cells treated with siRNA targeting VE-Cadherin (si.VeCad). (n/N=4/16). b) Concentration-response data for mannitol from the type of experiments in a) (n=4). The fitted curve is a hill equation indicating the 50% maximum effect (EC_{50}) at 86.67 mM and 78.33 mM mannitol with and without VE-Cadherin expression respectively. c) Mean data for the type of experiment shown in (b) mean is an average of EC_{50}'s from individual repeats n=4. d) Mean data for the type of experiment shown in (b) mean is an average of the gradient of the curves (n=3).

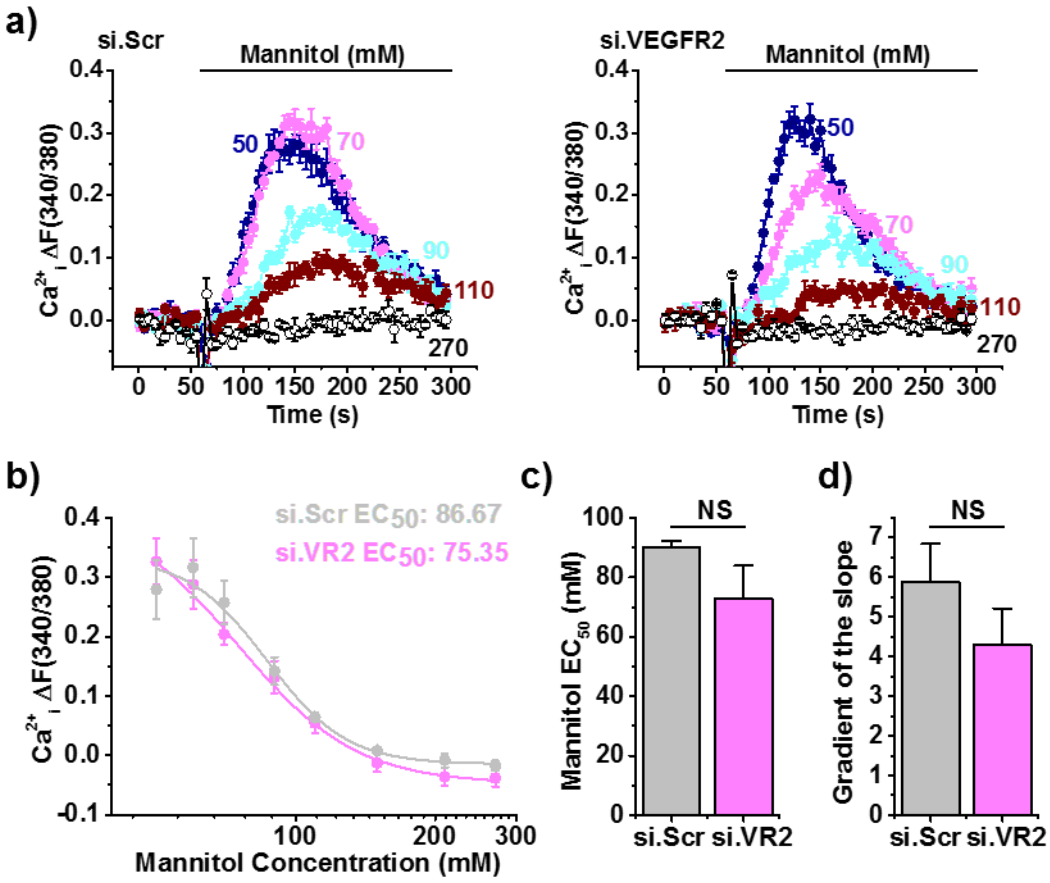

Figure 4.17 VEGFR2 knockdown does not affect mechanical cation channel activation.

a) Example intracellular Ca^{2+} measurement traces in HUVECs during application of varying mannitol concentrations (50-270 mM). Left: in cells treated with siRNA targeting a scrambled control sequence (si.Scr). Right: in cells treated with siRNA targeting VEGFR2 (si.VR2). (n/N=4/16). b) Concentration-response data for mannitol from the type of experiments in a) (n=4). The fitted curve is a hill equation indicating the 50% maximum effect (EC_{50}) at 86.67 mM and 75.35 mM mannitol with and without VEGFR2 expression respectively. c) Mean data for the type of experiment shown in (b) mean is an average of EC_{50}'s from individual repeats n=4. d) Mean data for the type of experiment shown in (b) mean is an average of the gradient of the curves (n=3).

4.6 Piezo1 knockdown does not affect CD31 activation of beta1-integrin

Data thus far demonstrates that the triad is not involved in the Ca^{2+} signalling of Piezo1 activated by either Yoda1 or hypotonic stress. In order to investigate whether Piezo1 knockdown affects CD31 signalling, active ß-integrin1 was examined. We chose to focus on CD31 as it is suggested to be the direct shear stress sensor in the triad (Tzima et al., 2005). CD31 is reported as a ligand for ß-integrin signalling involved in adhesion of leukocytes to endothelium (Piali et al., 1995). Furthermore, it has been reported that the signals required for integrin activation can be elicited by clustering of CD31 (Zhao and Newman, 2001).

Shear stress evoked activation of ß-integrin was examined in HUVECs as an indirect method to examine CD31 function. Firstly, 20-minute shear stress was able to evoke an increase in ß-integrin activation compared to static treated cells (Figure 4.18a & b). As expected, this was significantly suppressed after CD31 knockdown (si.CD31) compared to cells treated with a scrambled control (si.Scr) but Piezo1 knockdown (si.Piezo1/si.P1) did not alter shear stress evoked ß-integrin activation (Figure 4.18a & b). Furthermore, knockdown of CD31 or Piezo1 had no effect on the expression of total ß-integrin compared to cells treated with a scrambled control siRNA (Figure 4.18c). CD31 appeared to slightly decrease expression of total ß-integrin but this did not reach significance. These data suggest that Piezo1 does not affect CD31 signalling as measured by CD31-dependent ß-integrin activation after 20 min shear stress.

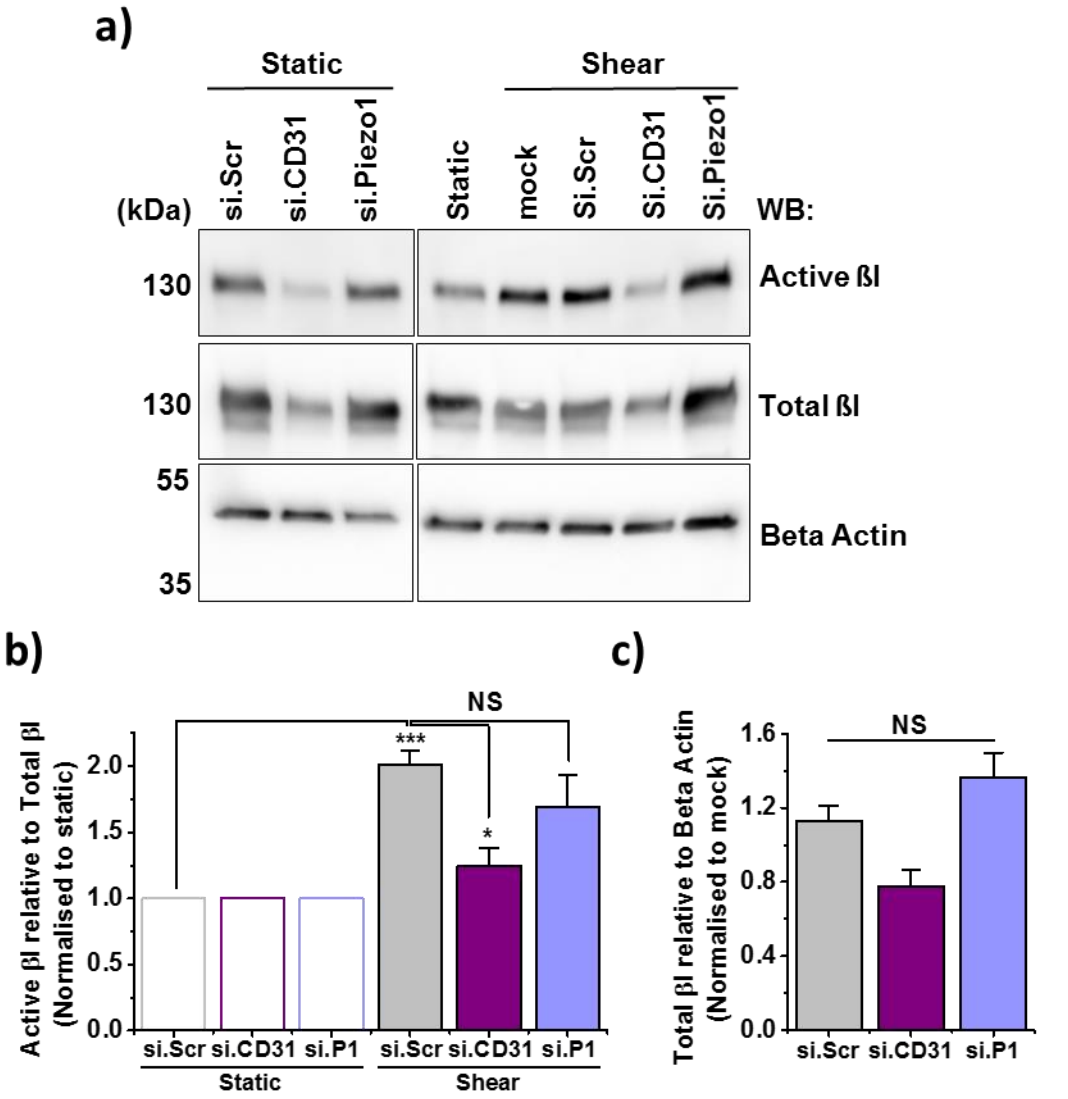

Figure 4.18 Shear-mediated ß1- integrin activation was CD31 but not Piezo1 dependent.

a) Representative immunoblot for anti-active ß-integrin, anti-ß-integrin and anti-ß-actin in HUVECs treated with 10 dyn.cm^{-2} for 20-minutes or not (static). Cells are treated with siRNA targeting CD31 (si.CD31), Piezo1 (si.Piezo1), a scrambled control sequence (si.Scr) or a mock transfection (-siRNA). b) Mean data from n=3 experiments displayed as active ß-integrin (ßI) relative to total ßI normalised to static treated HUVECs. c) Mean data from n=3 experiments displayed as total βI relative to ß-actin.

4.7 Biochemical characterisation of the relationship between Piezo1 and the triad

In order to determine whether Piezo1 and the triad are present within the same complex, co-immunoprecipitation experiments were performed. As there is no antibody that can reliably detect endogenous Piezo1, co-immunoprecipitation experiments were performed on HEK cells over expressing various constructs. HEK cells were co-transfected with either Piezo1 or Piezo1-mTurquoise2 alongside each member of the triad individually. GFP-Trap pull down of the mTurquoise2 tag (mTurquoise2 is a GFP mutant) was performed and immunoblotting was utilised to detect whether each triad member was co-pulled down. Firstly, the interaction between Piezo1 and CD31 was examined. In the input BEEC4 polyclonal anti-Piezo1 antibody detected that Piezo1 and Piezo1-mTurquoise2 were transfected equally, CD31 was also co-transfected in both (Figure 4.19a). GFP-Trap was able to pulldown Piezo1-mTurquoise2 (Figure 4.19a). CD31 was also present in the same sample, suggesting that both Piezo1 and CD31 interact in the same complex together (Figure 4.19a). The result was similar for both VE-Cadherin and VEGFR2. Both VE-Cadherin and VEGFR2 pulled down with Piezo1-mTurquoise2 (Figure 4.19b & c). For the first time, these data suggest that Piezo1 and the mechanosensory triad comprising CD31, VE-Cadherin and VEGFR2 are all interacting and are present in a complex together when over expressed in HEK cells.

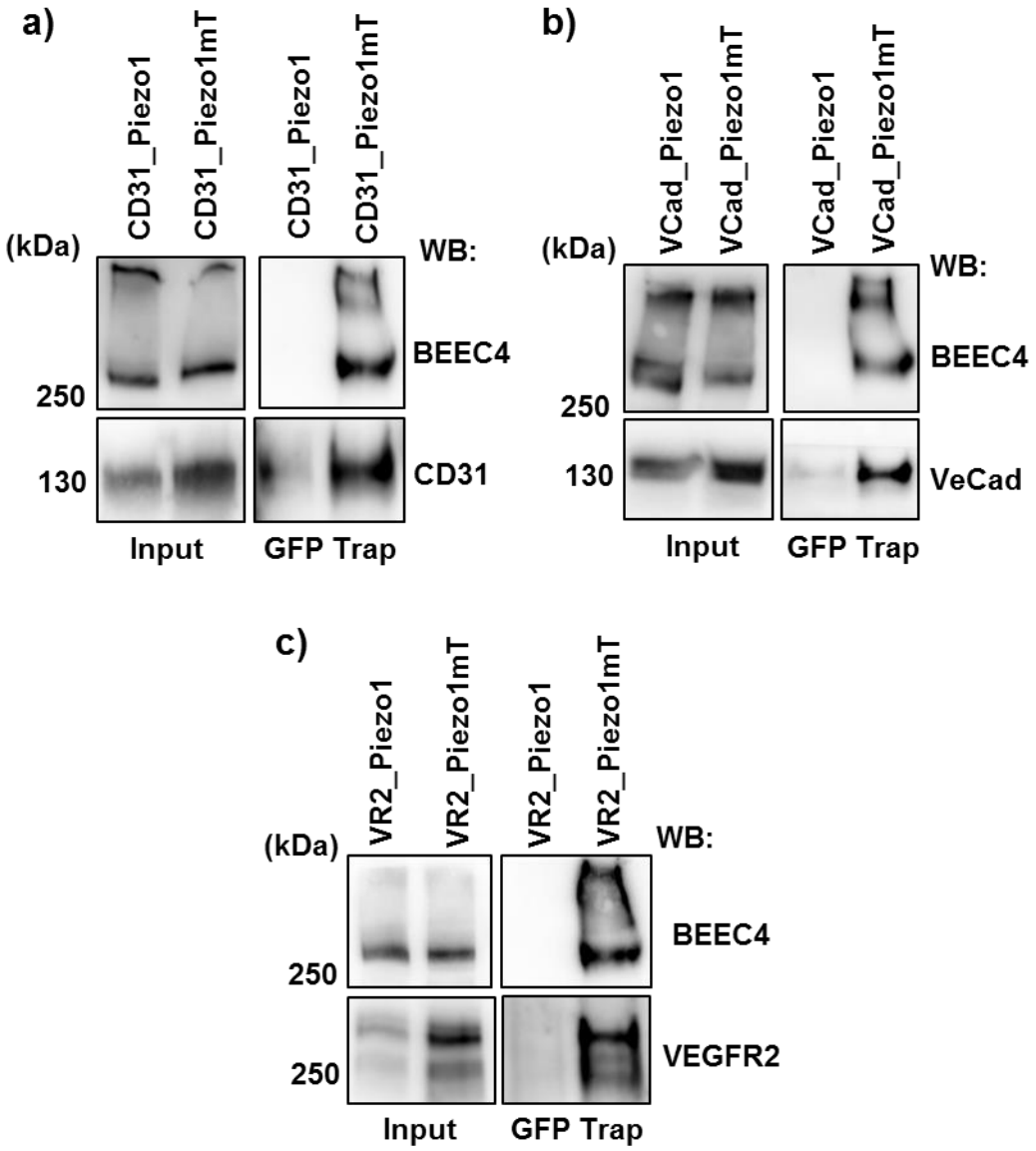

Figure 4.19 Piezo1 and the triad co-immunoprecipitate together when overexpressed in HEK cells.

a) Representative immunoblot for anti-BEEC4 (Piezo1) and anti-CD31. HEK cells were co-transfected with CD31 and Piezo1 or CD31 and Piezo1-mTurquoise2 (mT). Input represents total lysate and a GFP trap was performed to pull down the mT tag on Piezo1. b) as in (a) but immunoblot for anti-BEEC4 (Piezo1) and anti-VE-Cadherin. HEK cells were co-transfected with VE-Cadherin and Piezo1 or VE-Cadherin and Piezo1-mTurquoise2 (mT). c) as in (a) but immunoblot for anti-BEEC4 (Piezo1) and anti-VEGFR2. HEK cells were co-transfected with VEGFR2 and Piezo1 or VEGFR2 and Piezo1-mTurquoise2 (mT).

4.8 Examining Piezo1 and CD31 interaction using FLIM/FRET

So far work in this chapter has suggested that the rapid tight coupling of Piezo1 to eNOS phosphorylation depends on CD31 and VE-Cadherin triad proteins and that all three triad proteins are capable of close association to Piezo1. In order to test whether Piezo1 and CD31 not only form a complex but directly interact, Förster resonance energy transfer (FRET) experiments were carried out using fluorescence lifetime imaging microscopy (FLIM). FRET refers to the non-radiative, nanometer ranged process whereby if proteins are <10 nm apart energy from an excited donor fluorophore is transferred to an acceptor fluorophore.

4.8.1 Fluorescence lifetime imaging set up

Firstly, it was important to set up and calibrate our own FLIM/FRET system, the first time this technology has been developed in Leeds. Cyan variants of GFP are widely used as donors in FRET experiments. mTurquoise2 (mT) has been described as the preferable cyan variant of GFP for long-term imaging and as a donor for FRET to a yellow fluorescent protein (YFP). It has been reported to be brighter with faster maturation, higher photostability, longer mono-exponential lifetime and the highest quantum yield measured for a monomeric fluorescent protein (Goedhart et al., 2012). As determined by the spectral overlap, mTurquoise2 was a suitable FRET partner for sYFP2 (Figure 4.20a), In order to confirm the photo stability of mTurquoise2, bleaching experiments were carried out using the two-photon laser that will be used for FLIM experiments at a power of 3.5. 10-minutes of excitation evoked 5% bleaching of mTurquoise2, which was significantly less than cyan fluorescent protein (CFP) (Figure 4.20b & c). These data suggest that mTurquoise2 is a preferable donor fluorophore with sYFP2 as the accepter.

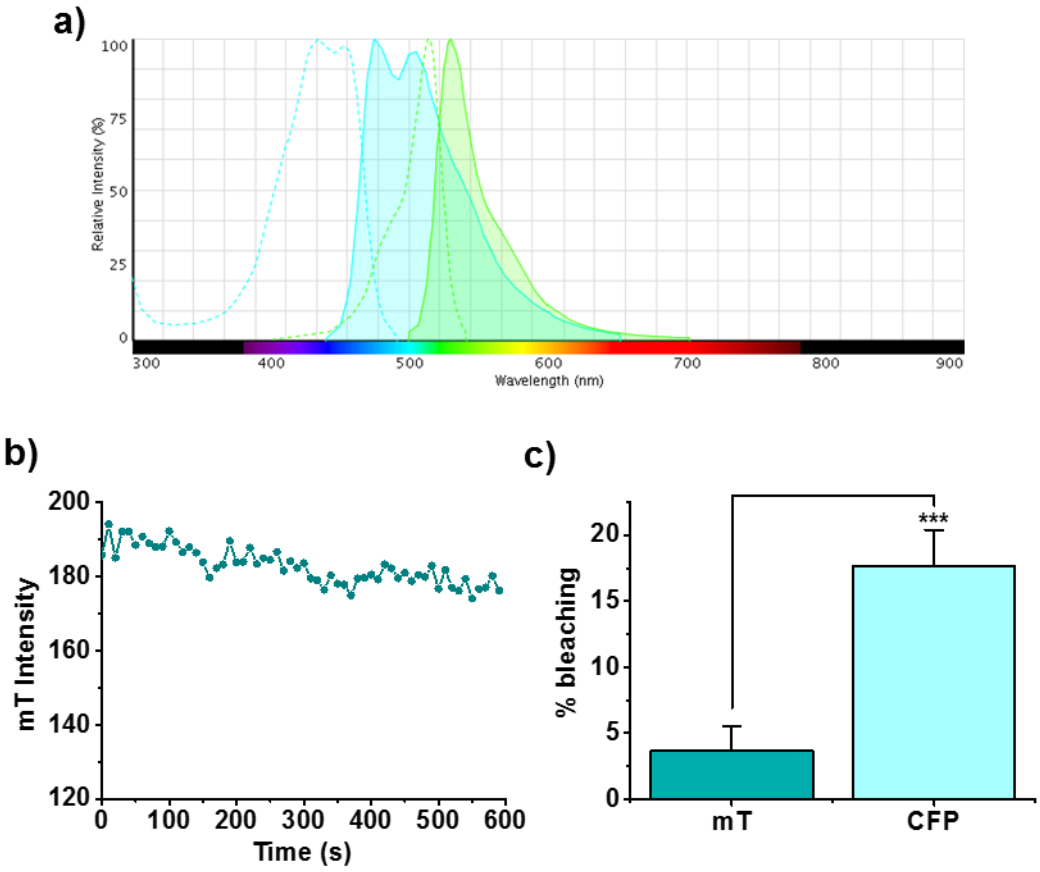

Figure 4.20 Förster resonance energy transfer and Fluorescence lifetime imaging set up.

a) mTurquoise2 and sYFP2 spectra. Excitation (dotted line) and emission (solid line) spectra of fluorescent proteins mTurquoise2 (donor; in cyan) and sYFP2 (acceptor; in yellow) molecules. The emission of mTurquoise2 overlaps with the excitation of sYFP2. b) Bleaching of mTurquoise2 over 10-minutes with laser power 3.5 (as used for FLIM experiments). c) Mean data for the time of experiment in (b) representing % bleaching over 10-minutes for mT and CFP n=3.

4.8.2 FRET detection in control constructs

In order to confirm that FRET was able to be detected with our system, control experiments were carried out. The donor only control for these experiments was mTurquoise2, a positive FRET control was a concatemer of mTurquoise2-sYFP2 and the negative control was mTurquoise-T2A-sYFP2 (the T2A mutation separates the two produced proteins to stop their interaction). Confocal images were taken analysing expression of both mTurquouse2 (mT) and sYFP2 for each (Figure 4.21a-c). Intensity and fluorescence lifetime images were also taken for each (Figure 4.21a-c). The lifetime of mTurquoise2 was 3.7 ns, similar to that previously reported suggesting that our system is calibrated correctly (Goedhart et al., 2012)(Figure 4.21a & d). There was a significant drop in lifetime in cells overexpressing the mTurquoise2-sYFP2 concatemer to 2.7 ns, indicating energy transfer and a FRET interaction (Figure 4.21b & d). The donor only result was reconstituted when the T2A mutation was present inhibiting the interaction of mTurquoise2 and sYFP2 (Figure 4.21c & d). These data suggest that the FLIM system is calibrated correctly and FRET can be detected.

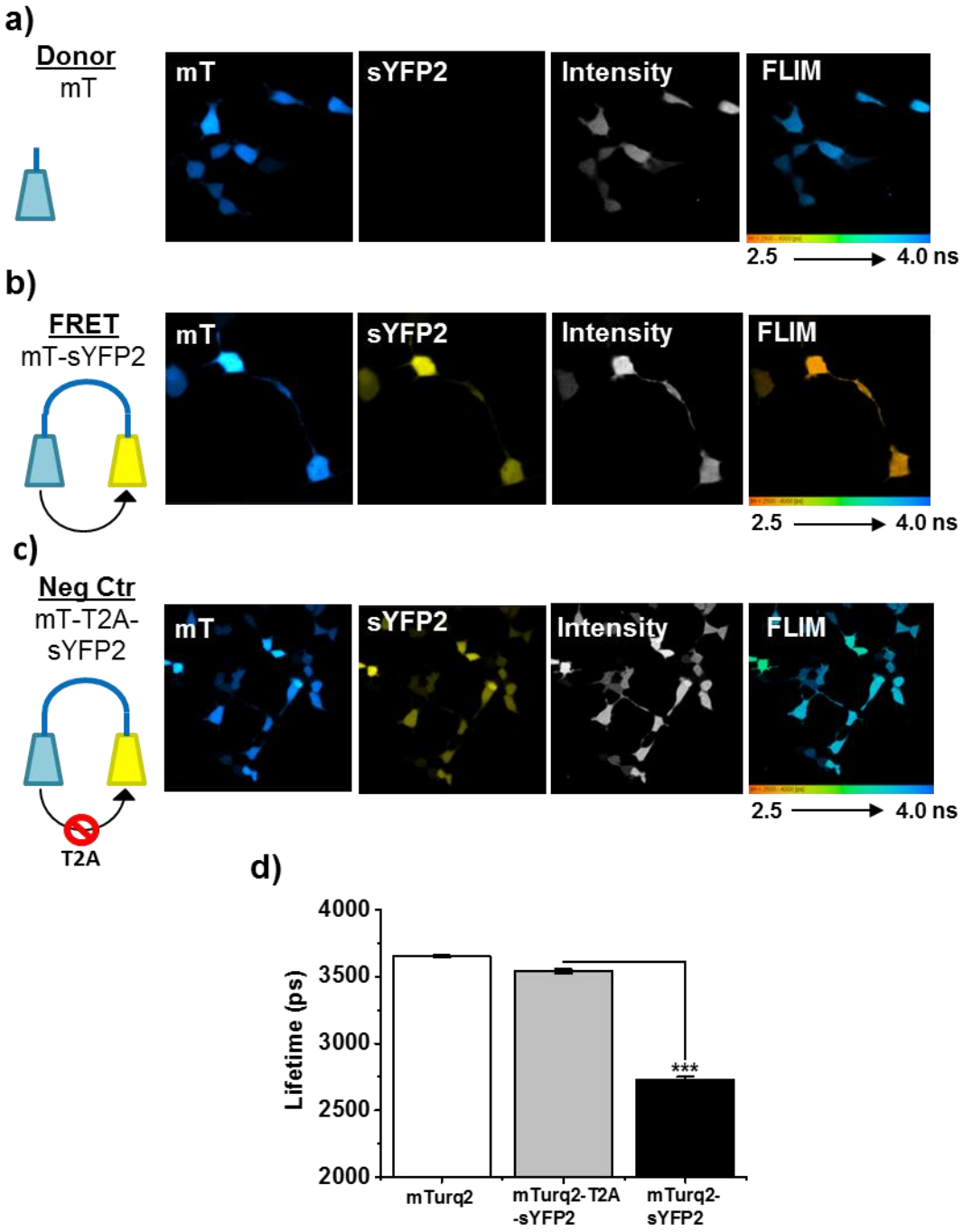

Figure 4.21 mTurquoise2 and sYFP2 are valid FRET pairs.

a-c) From left to right: images showing mTurquoise2 fluorescence, sYFP2 fluorescence, FLIM intensity and lifetime as indicated by the colour scale a) HEK cells transfected with mTurquoise2 (mT; donor). b) HEK cells transfected with mTurquoise2-sYFP2 concatemer. c) HEK cells transfected with the negative control mTurq2-T2A-sYFP2 construct. d) Mean data representing lifetimes of every pixel over the whole image. n/N=3/19-20.

4.8.3 Examining Piezo1 and CD31 interaction using FLIM/FRET

Following the successful set up of the FLIM system, we investigated whether CD31-mTurquoise2 and Piezo1-sYFP2 interact using FLIM/FRET. HEK 293 cells were transfected with either CD31-mTurq2 (donor only control) or co-transfected with both CD31-mT and Piezo1-sYFP2. FLIM measurements demonstrate that HEK cells transfected with the donor only control, CD31-mTurq2, have an average lifetime of 3.46 ns (Figure 4.22a & b). This is similar to what we previously found for mTurq2 alone (Figure 4.21d). When CD31-mT was co-expressed with Piezo1-sYFP2, there was no difference in lifetime compared to the donor only control (3.43 ns) (Figure 4.22a & b). These data suggest that with these constructs we cannot detect FRET between Piezo1 and CD31.

As we were unable to detect FRET between CD31-mTurq2 and Piezo1-sYFP2, a linker was inserted between Piezo1 and CD31 and their fluorophores to try to increase our FRET efficiency Constructs expressing Piezo1-L4-mTurq2 and CD31-L4-sYFP2 were created. Linker 4 (L4) was created using a series of Alanine and Serine amino acid repeats (GCC AGC GCA TCC GCT AGC GCC TCT GCC AGC GCT AGT GCC TCT GCA TCC GCT TCA GCC TCC GCC TCT GCC AGT GCA AGC GCA AGT GCT AGC, ASASASASASASASASASASASASASAS). This paring of amino acids was chosen as we predicted that it would give a good combination of flexibility and rigidity due to the differing charges of alanine and serine. Computer modelling of L4 suggested it to have a 5 nm linear structure. To determine whether CD31-mT and Piezo1-sYFP2 interact after addition of L4, FLIM/FRET experiments were carried out. HEK 293 cells were transfected with either Piezo1-L4-mTurq2 (donor only) or both Piezo1-L4-mT and CD31-L4-sYFP2. The FLIM image shows an average lifetime of 4 ns for the donor only construct (Figure 4.23a & b). When both plasmids were co-expressed the lifetime significantly dropped to 3.85 ns (Figure 4.23a). These data suggest that Piezo1 and CD31 directly interact when overexpressed in HEK 293 cells. More work is needed to examine other members of the triad.

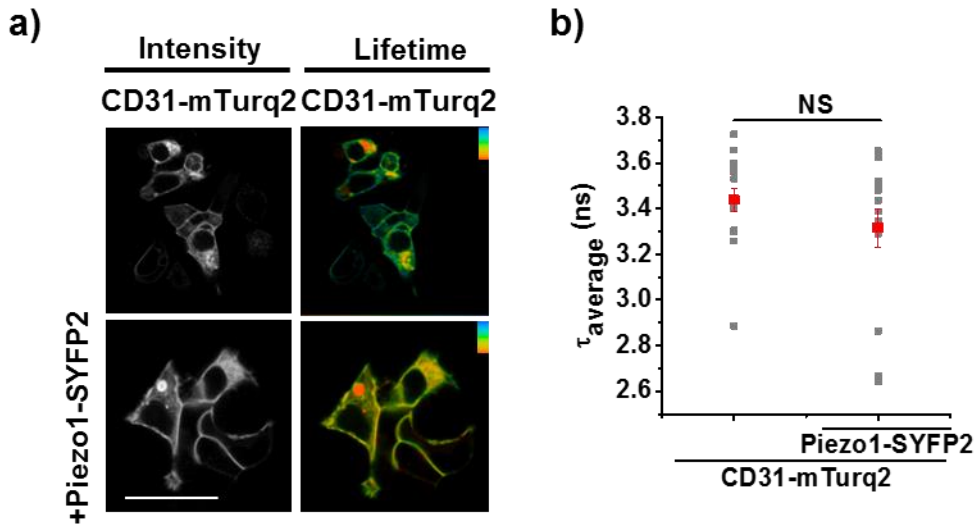

Figure 4.22 Piezo1-sYFP2 and CD31-mTurquoise2 do not interact when overexpressed in HEK 293 cells.

a) Upper: HEK cells expressing CD31-mTurquoise2 (Turq2) as the donor only control. Lower: HEK cells co-expressing CD31-mTurquoise2 and Piezo1-sYFP2. Left: FLIM intensity and right: FLIM lifetime images as indicated by the colour scale (3.5-4.1 ns). Scale bars are 50 µm. c) Mean data representing lifetimes of every pixel over the whole image. n/N=3/9-11. Cells prepared by Hannah Gaunt and experiments and analysis performed alongside Dr Eulashini Chuntharpursat (University of Leeds).

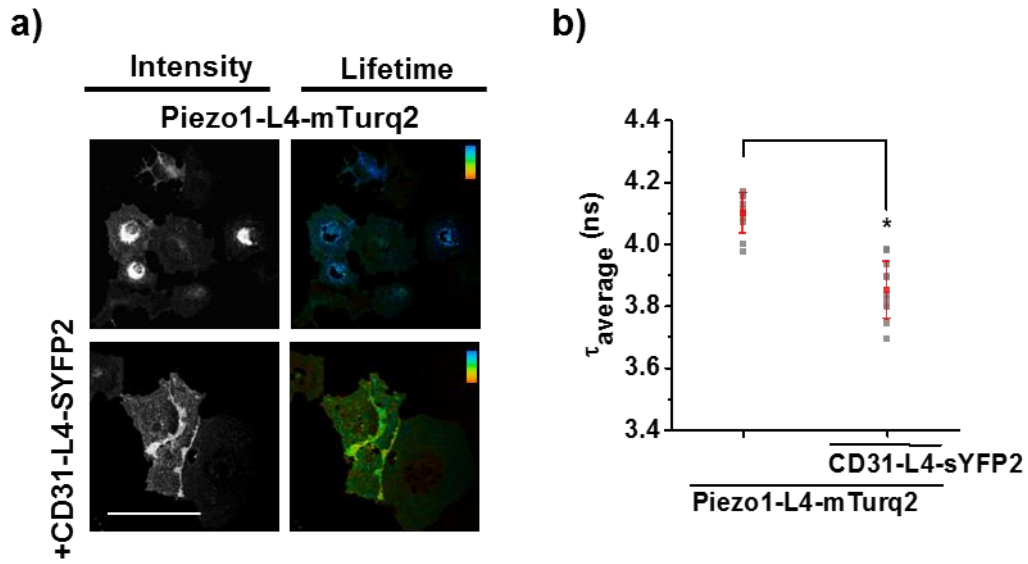

Figure 4.23 Piezo1-L4-sYFP2 and CD31-L4-mTurquoise2 interact when overexpressed in HEK 293 cells.

a) Upper: HEK cells expressing Piezo1-L4-mTurquoise2 (Turq2) as the donor only control. Lower: HEK cells co-expressing Piezo1-L4-mTurq2 and CD31-L4-sYFP2. Left: FLIM intensity and right: FLIM lifetime images as indicated by the colour scale (3.5-4.1 ns). Scale bars are 50 µm. c) Mean data representing lifetimes of every pixel over the whole image. n/N=3/9-11. Cells prepared by Hannah Gaunt and experiments and analysis performed alongside Dr Eulashini Chuntharpursat (University of Leeds).

4.9 Discussion

This chapter focussed on how Piezo1 channels couple rapidly to eNOS and the relevance of a previously described shear stress-sensing triad to this rapid coupling. In HUVECs, short 1-minute Yoda1 treatment evoked eNOS phosphorylation independently of extracellular ATP, P2Y2 receptors and AKT but dependently on the CD31 and VE-Cadherin proteins of the triad. The data suggest that knockdown of each member of the triad had no effect on Piezo1 channel activity evoked by Yoda1 or hypotonicity. Therefore, the triad must be involved downstream of Piezo1 in the Piezo1-mediated eNOS phosphorylation pathway. Over-expression studies using two independent methods for detecting protein-protein interaction provided evidence that Piezo1 is capable of interacting with CD31, the previously suggested master player of the triad. The data suggest that CD31 and VE-Cadherin are somehow required for the integrity of the rapid Piezo1 signalling to eNOS. Contrary to previously published work, this mechanism does not involve ATP or P2 receptors.

The Offermanns group suggest that chemical activation of Piezo1 induced ATP release through pannexin channels, the ATP subsequently acting on P2Y2 receptors to evoke AKT mediated phosphorylation of eNOS. This mechanism is activated after 5-minute treatment with Yoda1. Work in this chapter investigates direct signalling events mediated by Piezo1 channels so a short treatment time of 1-minute was used. Firstly, it was demonstrated that 1-minute treatment of HUVECs with extracellular ATP was not sufficient to phosphorylate eNOS and pre-treatment with apyrase, to catalyse the hydrolysis of ATP, did not inhibit Yoda1-mediated eNOS phosphorylation. Furthermore, blocking P2Y2 channels with suramin did not affect Yoda1-mediated eNOS phosphorylation. Thus, ruling out the involvement of extracellular ATP and P2Y2 channels at a short time point. AKT is widely reported to be involved in shear stress evoked eNOS phosphorylation (Dimmeler et al., 1999). Even though the Offermanns group suggest that Yoda1 mediates AKT phosphorylation they failed to examine the role of AKT in the Yoda1-mediated eNOS phosphorylation pathway. Treating HUVECs with siRNA targeting AKT had no effect on Yoda1-mediated eNOS phosphorylation. However, AKT levels were only knocked down by 65%. Thus, it is important that future work examines whether this level of knockdown is sufficient to block shear- or VEGF- evoked eNOS phosphorylation. Nonetheless, as our data suggest that at short 1-minute Yoda1

treatment the mechanism coupling Piezo1 to eNOS phosphorylation is independent of AKT other mechanisms were examined.

An interesting result from the Offermanns group suggested that CD31 and VEGFR2 are tyrosine phosphorylated by shear stress and that this is supressed with genetic disruption of Piezo1 channels (Wang et al., 2016). However, they did not follow this result up further. The past years have yielded many insights into the mechanisms behind shear stress sensing in endothelial cells including the identification of many putative endothelial shear stress sensors. Some of which include ion channels namely, Piezo1 and junctional mechanosensors including CD31. CD31 is an adhesion molecule that is expressed on a variety of cells, including endothelial cells. It is clustered at cell-cell junctions to enable homophilic binding of cells to their neighbours. Evidence suggests that CD31 acts in partnership with VE-Cadherin and VEGFR2 to mediate many more shear stress responses including activation of downstream signalling (Fleming et al., 2005). In fact, CD31, VE-Cadherin and VEGFR2 have been described to comprise a mechanosensory triad complex together in endothelial cells (Tzima et al., 2005). Disruption of this complex by knocking-down either CD31 or VE-Cadherin caused a disruption of the alignment of endothelial cells in the direction of flow (Tzima et al., 2005). However, maybe CD31 isn't a direct sensor of shear stress after all and could be acting downstream of the chief mechanosensor, Piezo1.

It is currently unclear if there is one direct shear stress sensor or whether the shear stress response is more integrated. Data suggesting an extremely rapid activation of Piezo1 channels in response to shear stress and the drastically lethal phenotype that is reported in Piezo1 knock-out mice (Li et al., 2014) led us to consider Piezo1 as the principle shear stress sensor and examine whether it works in partnership with CD31. When overexpressed in HEK 293 cells, without presence of other endothelial cell components shear stress is able to evoke a Piezo1-mediated current and Ca^{2+} entry. However, expression of Piezo1 alone is not sufficient to allow HEK 293 cell alignment in response to shear (Li et al., 2014), suggesting that Piezo1 might cross-talk with other endothelial cell components to achieve alignment. Reports have linked CD31 with activation of a non-selective cation current. H_2O_2 application to both HUVECs and endothelia-like cells overexpressing CD31 evoked a CD31 dependent non-selective cation current (Ji et al., 2002). The non-selective cation channel activity reported has many similar characteristics to

that of Piezo1 as it is a voltage independent non-selective cation current that is Ca^{2+}-permeant. Furthermore, in a separate study mechanosensation using a 'puffer pipette' evoked a very similar CD31 dependent non-selective cation current in both HUVECs and endothelia-like cells overexpressing CD31 (O'Brien et al., 2001). However, CD31 itself is not suggested to form a functional ion channel. It could be possible that Piezo1 channels are mediating the CD31 associated currents. Thus, we examined the relationship between Piezo1 and the CD31 expressing triad.

Data in this chapter suggest that knockdown of CD31 and VE-Cadherin proteins of the triad suppressed Yoda1-induced eNOS phosphorylation. To examine whether the triad was acting up or downstream of Piezo1 to evoke eNOS phosphorylation, Piezo1 activity was examined with and without expression of the triad. Knockdown of each member of the triad had no effect on Yoda1- or hypotonicity- induced Piezo1 channel activation suggesting that CD31 and VE-Cadherin proteins of the triad are acting downstream of Piezo1. Importantly Piezo1 knockdown did not affect the function of CD31 signalling to ß-integrin. Therefore, CD31 signalling can be both Piezo1 dependent and Piezo1 independent. Examining the role of Piezo1 and the triad in shear-mediated eNOS phosphorylation was out of the scope of this study but is an important next step.

VEGFR2 does not significantly suppress Yoda1-mediated eNOS phosphorylation. It is reported to be expressed alongside CD31 and VE-Cadherin in a mechanosensory triad. In this model it is suggested that CD31 directly transmits mechanical force, VE-Cadherin acts as an adapter and VEGFR2 activates PI3K/AKT signalling. Acute onset of flow is reported to trigger tyrosine phosphorylation of CD31 and VEGFR2 in endothelial cells and the activation of a number of signalling pathways and this has recently been reported to be Piezo1-dependent (Osawa, 2002; Chen et al., 1999; Wang et al., 2016). One pathway CD31 tyrosine phosphorylation is reported to modulate is shear stress evoked phosphorylation of AKT and subsequent eNOS phosphorylation in HUVECs (Fleming et al., 2005). Moreover, VEGFR2 has been reported to be important for flow- and VEGF- mediated PI3K/AKT-eNOS activation and NO dependent vasodilation *in-vivo* (Jin et al., 2003; Feliers et al., 2005). It is interesting that members of the triad are reported to signal to S1177 eNOS via the PI3K/AKT signalling pathway whereas data in this chapter suggest that Yoda1 mediated eNOS signalling was independent of ATK at a short 1-minute time point. It is important to note that the literature linking the triad to S1177 eNOS

phosphorylation is after longer treatment times, i.e. 10 minutes onwards. It remains unclear how Piezo1 channels signal to CD31 and VE-Cadherin proteins of the triad at shorter time points and furthermore, how Yoda1 stimulates these proteins to signal to eNOS. More work is needed to investigate the kinase or kinases involved in Yoda1-mediated cross-talk between Piezo1 and the triad and subsequent eNOS phosphorylation.

Biochemical characterisation of the relationship between Piezo1 and the triad suggests that when overexpressed in HEK 293 cells Piezo1-mTurquoise2 is present in a complex together with CD31, VE-Cadherin and VEGFR2. One criticism is that it is possible that overexpression of the proteins drives their interaction. Further work is needed to examine this interaction endogenously. One major limitation is the lack of antibodies that can detect endogenous Piezo1. If an antibody detecting endogenous Piezo1 is developed then endogenous pull down experiments could be carried out. Our lab is currently developing a Piezo1-HA mouse developed using CRISPR/Cas9 technology. This will be advantageous as endothelial cells isolated from these mice could be used in experiments using HA-conjugated beads to pull down the HA tag on Piezo1. Further work is needed to investigate this.

As CD31 is reported to be the direct mechanosensor in the triad the partnership between Piezo1 and CD31 was further investigated. Again, these experiments were on proteins overexpressed in HEK cells. Without addition of a linker between the proteins and fluorophores no FRET was detected suggesting no interaction. It is possible that the fluorophore is trapped near the beam of Piezo1 and not able to move freely. After addition of a flexible 5 nm linker between each protein and fluorophore FRET was detected, suggesting direct interaction between Piezo1 and CD31. It is unknown where CD31 might interact with Piezo1. As CD31 is membrane spanning we hypothesise that they interact near the blades towards the periphery of Piezo1, it is currently unknown whether they interact intracellularly or extracellularly. Cryo-EM is currently being carried out by a member of the group to examine the structure of Piezo1 and CD31 in partnership to reveal interaction sites. Further work is also needed to examine whether Piezo1 directly interacts with VE-Cadherin and VEGFR2 but importantly, the tools have been created and systems set up in order to allow further investigation of this relationship as well as other potential partner proteins.

4.10 Summary

For the first time we suggest that cross-talk between Piezo1 and CD31 and VE-Cadherin proteins of the triad is important for the integrity of Yoda1-mediated eNOS phosphorylation, but that this is independent of ATP and AKT. We propose a pathway whereby Yoda1 specifically activates Piezo1 which signals downstream to CD31 and VE-Cadherin to phosphorylate S1177 eNOS via a kinase (Figure 4.24). We report that even though both mechanosensors are able to work in partnership to activate phospho-eNOS they are also able to function in isolation of each other. It is currently unknown which tyrosine kinase is phosphorylating CD31 and how eNOS is phosphorylated at S1177, more work is needed to investigate this (Figure 4.24).

Flow-dependent vascular remodeling involves multiple genes, cell types and processes. Until now it is unclear whether mechanosensors function independently or together. The elucidation of a previously unrecognized partnership between Piezo1 and the mechanosensory triad expands our understanding of endothelial shear stress responses. These findings have important implications for understanding vascular physiology and could contribute to the development of novel therapeutic strategies.

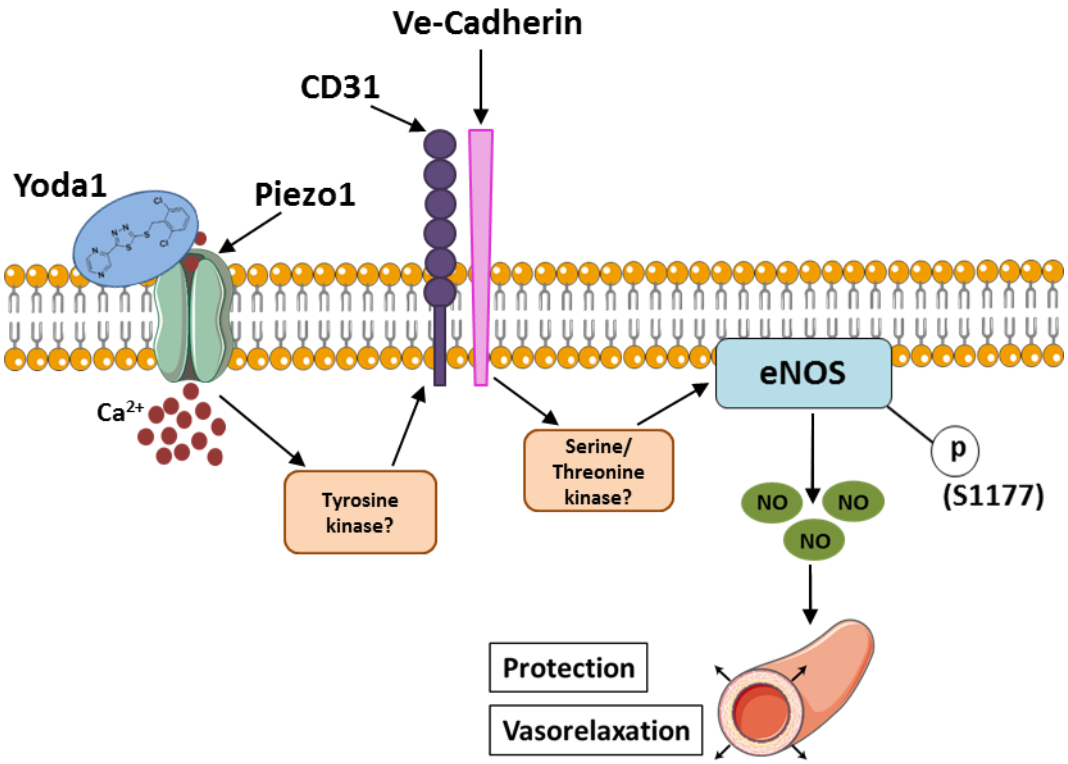

Figure 4.24 Schematic of the proposed mechanism linking Yoda1-mediated Piezo1 activation to S1177 eNOS phosphorylation.

Yoda1 activates Piezo1 channels to evoke CD31 and VE-Cadherin mediated S1177 eNOS phosphorylation, but it remains unclear which kinase or kinases is involved in this process.

Chapter 5 Tight Coupling of Yoda1-Activated Piezo1 to eNOS via Fyn and PKC-delta

5.1 Introduction

Data throughout this thesis suggest a rapid coupling between Yoda1-activated Piezo1 and S1177 eNOS phosphorylation and that CD31 and VE-Cadherin proteins of the mechanosensory triad are somehow required for the integrity of this response. Even though over-expression studies suggest that Piezo1 and CD31 directly interact it is currently unclear how they cross-talk and which kinase(s) links the signalling pathway together. Literature suggests that numerous stimuli evoke eNOS phosphorylation and the kinases involved in this process vary depending on the stimuli applied (Figure 5.1). The S1177 site on eNOS is unstimulated under basal conditions but is reported to be rapidly phosphorylated after the application of various agonists including, shear stress, VEGF and Ca^{2+}.

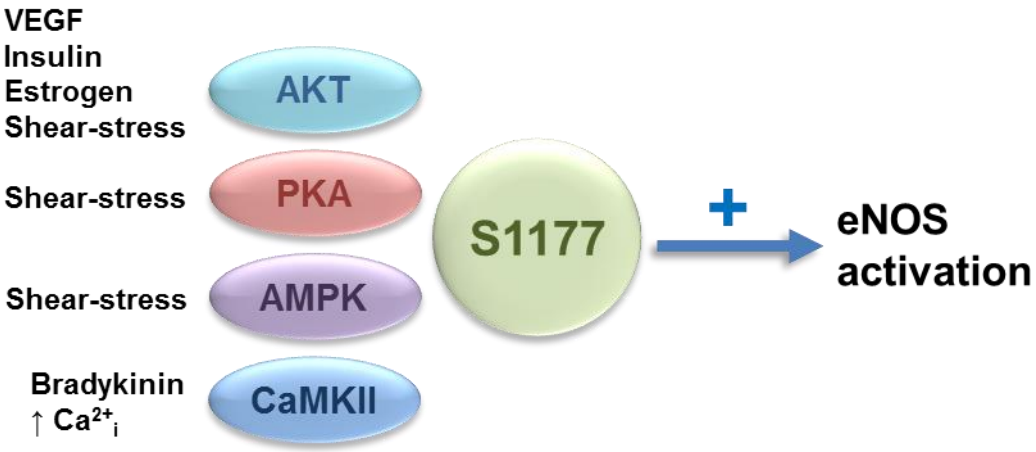

Figure 5.1 The regulation of the S1177 phosphorylation site on eNOS.

Schematic depiction of the kinases that regulate the eNOS S1177 phosphorylation site to promote eNOS activation.

eNOS was first described as a Ca^{2+}-CaM dependent form of NOS (Michel et al., 1997). Humoral ligands, including bradykinin, stimulate eNOS phosphorylation by raising the levels of intracellular Ca^{2+} to induce CaM to activate CaMKII. In rat

aortas the CaMKII inhibitor, KN93, suppressed bradykinin-induced eNOS activity and relaxation of rat aortic rings (Schneider et al., 2003). Moreover, in the case of VEGF, there is strong evidence supporting PI3K activation of AKT, which in turn is responsible for regulating the phosphorylation and activation of eNOS (Papapetropoulos et al., 1997). Furthermore, it is widely accepted that in cultured endothelial cells and isolated blood vessels shear stress evoked eNOS phosphorylation is dependent on AKT (Dimmeler et al., 1999; Fulton et al., 1999), protein kinase A (PKA) (Boo et al., 2002b) and AMPK (Fleming et al., 2005; Zhang et al., 2006). There are reports suggesting that a coordinated interaction between AKT and PKA are important for NO production whereas AMPK is reported to act independently of AKT to activate eNOS (Boo et al., 2002b; Zhang et al., 2009). Data in the previous chapter suggested that Yoda1 evoked eNOS phosphorylation is independent of the classical AKT/PI3K pathway. Thus, the molecular mechanisms by which Yoda1 regulates eNOS phosphorylation and NO production remain incompletely understood.

During this chapter considerable effort was made to further understand the molecular basis behind Yoda1-evoked eNOS phosphorylation and a screen for the kinase, or kinases, inducing fast Piezo1-mediated eNOS phosphorylation (i.e. within 1 minute) was carried out. Various candidate kinases were knocked down using siRNA to genetically disrupt their expression or chemically inhibited and the effect of this on both Piezo1 channel function and Yoda-mediated eNOS phosphorylation was examined. Kinase knockdown efficiency was examined by either RT-qPCR or western blotting, Piezo1 activation was measured using the FlexStation to measure intracellular Ca^{2+} levels and eNOS phosphorylation was examined using immunoblotting.

5.2 Fyn kinase is important for Piezo1-mediated eNOS phosphorylation

Data in the previous chapter demonstrated that disruption of CD31 by RNAi suppressed Yoda1-evoked S1177 eNOS phosphorylation. This suggested that Yoda1-activated Piezo1 is signalling via CD31 to evoke eNOS phosphorylation. It is widely reported that acute onset of physiological shear stress triggers tyrosine CD31 phosphorylation and recently this has been suggested to be dependent on the expression of Piezo1 (Osawa, 2002; Chen et al., 1999; Wang et al., 2016). Data in chapter 3 suggest that Yoda1 mimics shear stress signalling. Therefore, it is hypothesised that Yoda1 is evoking CD31 phosphorylation. However, the tyrosine kinase coupling Piezo1 to CD31 remains unidentified. Members of the Src family of kinases have been reported as strong candidates for mediating tyrosine phosphorylation of CD31 (Cao et al., 1998). Furthermore, it is reported that stretch- and flow-induced tyrosine phosphorylation of CD31 was dependent on Fyn tyrosine kinase expression (Chiu et al., 2008). These data led us to examine the role of Fyn in Yoda1-mediated eNOS phosphorylation.

5.2.1 Fyn tyrosine kinase is highly expressed in HUVECs

Firstly, mRNA expression levels of each member of the src family were examined in HUVECs. As a positive control, to test if the primers could amplify their target, *h*Brain mRNA was utilised. Indeed, primers for Fyn, Hck, Src, Fgr, Lyn, Yes and Lck each amplified a distinct single product of the correct size (Figure 5.2a). Primers for Blk amplified two products, with the smaller band being the correct size (Figure 5.2a). This could be due to expression of different isoforms or because the primers were amplifying an off-target product. mRNA expression of the src family was examined in HUVECs. Fyn, Src and Yes were all convincingly expressed in HUVECs (Figure 5.2b). Notably, the expression of Fyn was significantly higher than any other member of the src family (Figure 5.2b). Specifically, Fyn mRNA expression was around 50-fold higher than Src and 162-fold higher than Yes, the only other detectable members of the src-family. Thus, the role of Fyn was examined in further detail.

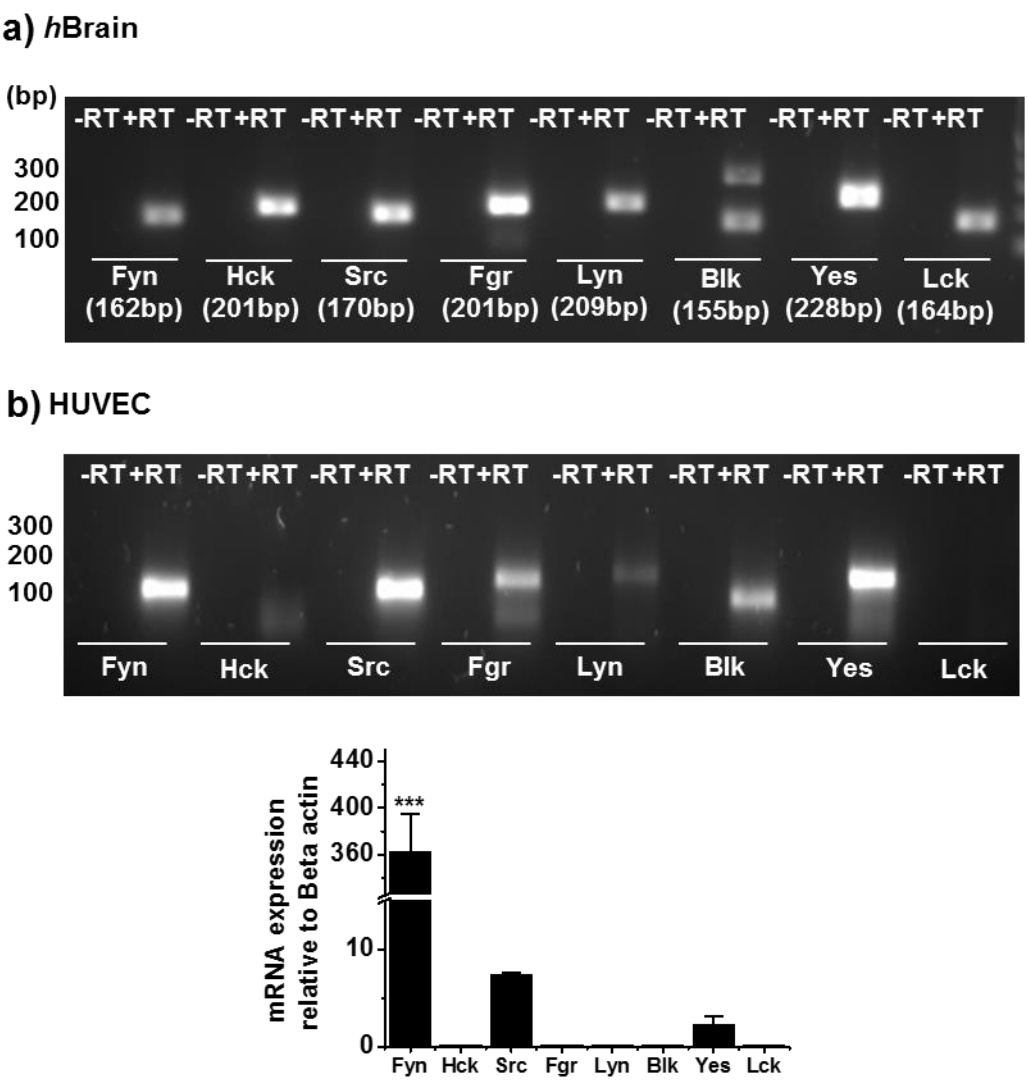

Figure 5.2 Fyn kinase is the highest expressed src family member in HUVECs.

a) End-point PCR products obtained with Fyn, Hck, Src, Fgr, Lyn, Blk, Yes and Lck primers for human (*h*) Brain mRNA after reverse transcriptase reaction (+RT) or not (-RT) to generate cDNA. b) Upper: as in (a) but for HUVEC mRNA. Lower: Mean data and analysis of Fyn, Hck, Src, Fgr, Lyn, Blk, Yes and Lck mRNA relative to beta actin (n=3).

5.2.2 Disruption of Fyn by RNAi blunts Yoda1-mediated S1177 eNOS phosphorylation

As Fyn is highly expressed in HUVECs and as reports have suggested that Fyn is involved in shear-evoked CD31 phosphorylation its role in Yoda1-mediated eNOS phosphorylation was studied. Fyn is a proto-oncogene tyrosine-protein kinase that codes for proteins that regulate cell growth. Fyn has been reported to be involved in estrogen evoked activation of NOS via the PI3K/AKT-dependent pathway (Haynes et al., 2003). To study the role of Fyn in Yoda1-evoked eNOS phosphorylation siRNA targeting Fyn was utilised. HUVEC samples were collected after treatment with a mock transfection (-siRNA), scrambled sRNA (si.Scr) and Fyn siRNA (si.Fyn) and mRNA expression was examined. End-point PCR products were run on a gel and indeed primers were able to specifically amplify Fyn, Piezo1 and beta actin mRNA (Figure 5.3). Treatment with Fyn siRNA was able to knockdown Fyn mRNA expression compared to a scrambled control by 62% in HUVECs without affecting expression of Piezo1 (Figure 5.3). In order to examine whether Fyn mRNA knockdown affects Piezo1 function intracellular Ca^{2+} measurements were carried out. Yoda1-evoked Ca^{2+} entry was not effected by Fyn siRNA when compared to the scrambled siRNA treated control (Figure 5.4a). Excitingly, Fyn mRNA knockdown suppressed Yoda1-evoked eNOS phosphorylation by 82% (Figure 5.4b). Thus, these data suggest a novel mechanism whereby Fyn kinase is involved in coupling Yoda1-mediated Piezo1 activation to S1177 eNOS phosphorylation.

In order to further test this idea, siRNA targeting a different nucleotide sequence on Fyn was utilised (si.Fyn #2). Similarly to before, Fyn siRNA #2 was able to knockdown mRNA expression of Fyn compared to scrambled siRNA (si.Scr) by 92% (Figure 5.5). Again, PCR reactions were clean and a band of the correct size was present, as expected from our primer design (Figure 5.5). Furthermore, knockdown of Fyn mRNA using siRNA #2 did not affect Yoda1 mediated Ca^{2+} entry (Figure 5.6a), but it abolished Yoda1-mediated eNOS phosphorylation (Figure 5.6b).

Taken together, these data suggest that Fyn kinase is mediating fast Yoda1-mediated eNOS phosphorylation. The data suggest a novel mechanism whereby Yoda1-activated Piezo1 is tightly coupled to S1177 eNOS phosphorylation via Fyn tyrosine kinase.

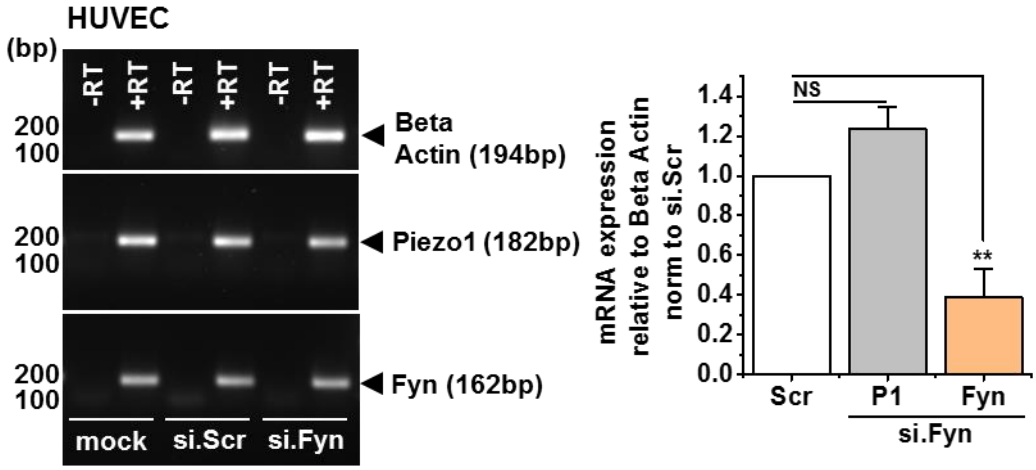

Figure 5.3 mRNA knockdown of Fyn does not affect Piezo1 expression.

Left: End-point PCR products obtained with primers for Beta actin, Piezo1 and Fyn for HUVECs treated with a mock transfection (-siRNA), scrambled siRNA (si.Scr) or Fyn siRNA (si.Fyn). mRNA obtained after reverse transcriptase reaction (+RT) or not (-RT) to generate cDNA Right: Mean data and analysis of Piezo1 and Fyn mRNA relative to beta actin after Fyn knockdown (si.Fyn) or not (si.Scr) normalised to si.Scr (n=4).

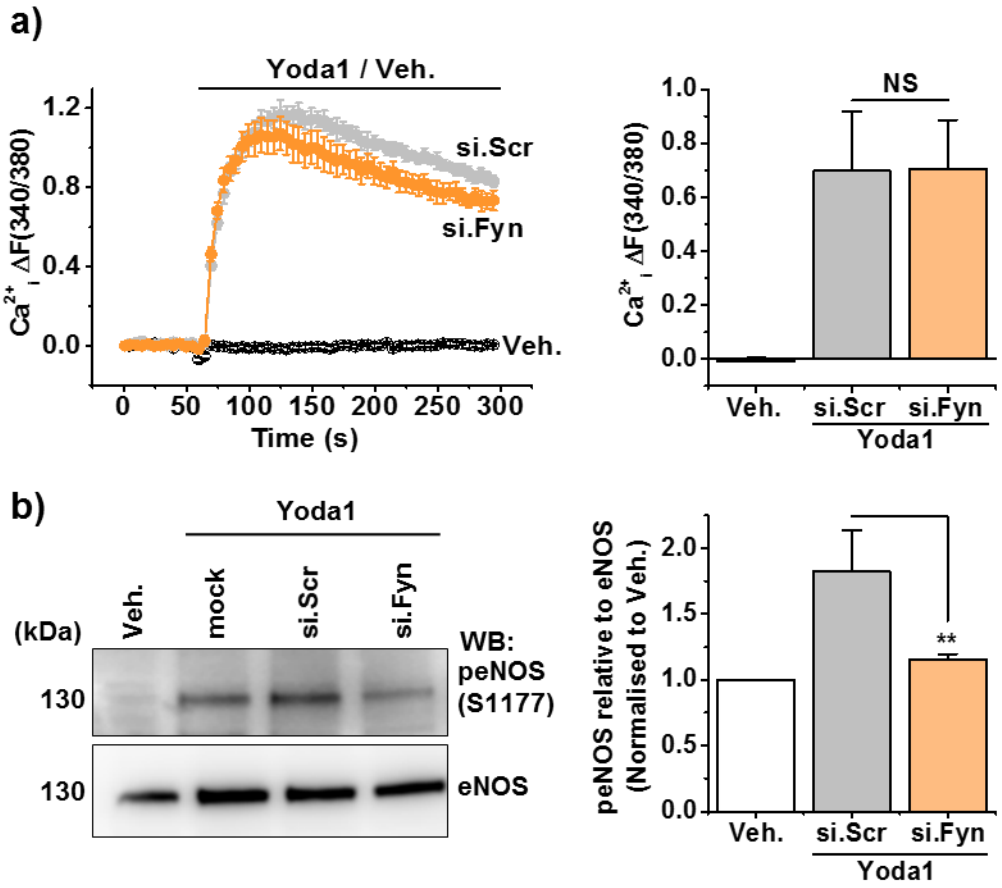

Figure 5.4 Genetic disruption of Fyn kinase blunts Yoda1-evoked eNOS phosphorylation.

a) Left: example intracellular Ca^{2+} measurement trace in HUVECs during application of 2 μM Yoda1 or its vehicle (Veh.). Cells are treated with a mock transfection (-siRNA) or siRNA targeting Fyn (si.Fyn) or a scrambled control sequence (si.Scr). Right: Mean data for the type of experiment shown on the left n/N=3/17 b) Left: Representative immunoblot for anti-S1177 phospho-eNOS and anti-total eNOS in HUVECs with and without Fyn genetic disruption treated for 1-minute with 2 μM Yoda1 or its vehicle (Veh.). Right: mean data from n=5 experiments displayed as phosphorylated eNOS relative to total eNOS (normalised to vehicle treatment).

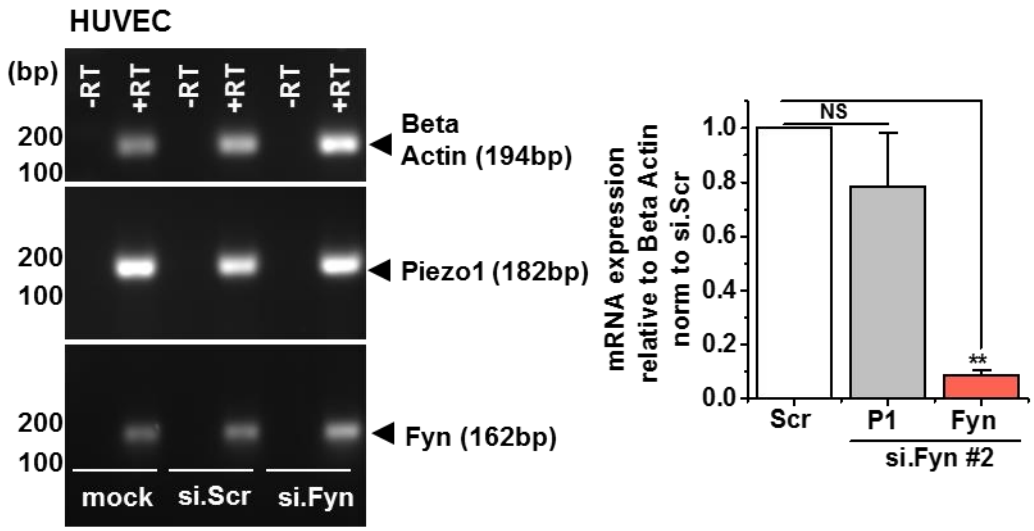

Figure 5.5 mRNA knockdown of Fyn does not affect Piezo1 expression.

a) End-point PCR products obtained with primers for Beta actin, Piezo1 and Fyn for HUVECs treated with a mock transfection (-siRNA), scrambled siRNA (si.Scr) or Fyn siRNA (si.Fyn). mRNA obtained after reverse transcriptase reaction (+RT) to generate cDNA or not (-RT). Right: Mean data and analysis of Piezo1 and Fyn mRNA relative to beta actin after Fyn knockdown (si.Fyn) or not (si.Scr) normalised to si.Scr (n=5).

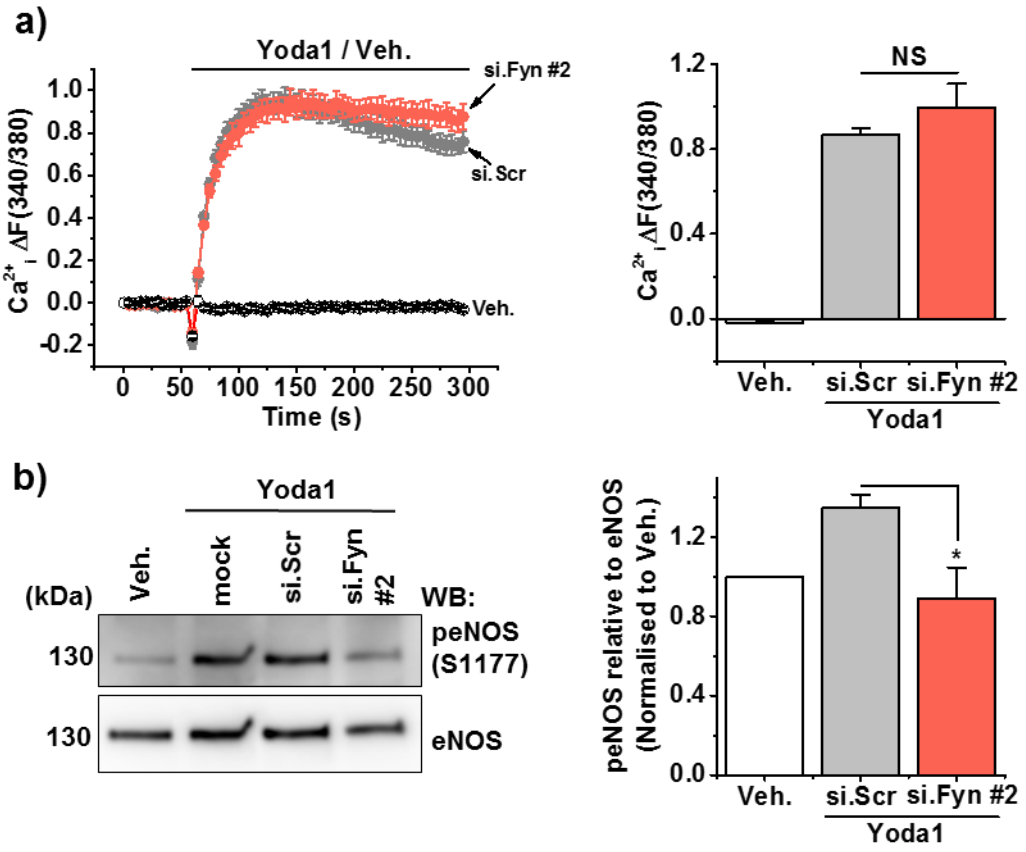

Figure 5.6 Treatment with a second Fyn siRNA validates previous results.

a) Left: example intracellular Ca^{2+} measurement trace in HUVECs during application of 2 µM Yoda1 or its vehicle (Veh.). Cells are treated with siRNA targeting Fyn (si.Fyn#2) or a scrambled sequence (si.Scr). Right: Mean data for the type of experiment shown on the left n/N=3/18 b) Left: Representative immunoblot for anti-S1177 phospho-eNOS and anti-eNOS in HUVECs with and without Fyn genetic disruption treated for 1-minute with 2 µM Yoda1 or its vehicle (Veh.). Right: mean data from n=3 experiments displayed as phosphorylated eNOS relative to total eNOS (normalised to vehicle treatment).

5.3 Investigation into classical kinases that regulate S1177 eNOS phosphorylation

The data so far suggest that Fyn kinase is mediating Yoda1-mediated eNOS phosphorylation. Perhaps, evoking tyrosine phosphorylation of CD31, mimicking shear stress. Fyn is a tyrosine kinase, thus is unable to phosphorylate S1177 on eNOS directly and data in Chapter 3 (Figure 3.24) rule out Yoda1-mediated Y657 phosphorylation of eNOS. Therefore, it is still unclear which kinase is directly phosphorylating S1177 eNOS. Next, kinases that are classically reported to phosphorylate S1177; namely AKT (Dimmeler et al., 1999; Fulton et al., 1999), PKA (Boo et al., 2002b) and AMPK (Fleming et al., 2005; Zhang et al., 2006) were examined. In the previous chapter a role for AKT was ruled out but PKA and AMPK remained yet to be investigated.

5.3.1 Disruption of PKA mRNA expression by RNAi has no effect on Yoda1-mediated S1177 eNOS phosphorylation

Shear stress evoked S1177 eNOS phosphorylation has been reported to be dependent on PKA activation (Figure 5.1) (Boo et al., 2002b). Chemically inhibiting PKA with the widely used inhibitor H89 is reported to inhibit shear stress dependent phosphorylation of eNOS and NO production (Boo et al., 2002b). In order to investigate the role of PKA in Yoda1-mediated S1177 eNOS phosphorylation HUVECs were pre-treated with H89 prior to Yoda1 addition. 30-minute pre-treatment with 10 µM H89 increased basal intracellular Ca^{2+} levels alone (Figure 5.7a). This suggests that H89 is somehow modulating a Ca^{2+} entry mechanism. Furthermore, the mean amplitude of the Yoda1 response was reduced suggesting that H89 inhibits endogenous Piezo1 channel activity or that the fura-2 signal had reached its maximum.

To investigate whether H89 is directly inhibiting Piezo1 channels or if H89 is activating other endothelial Ca^{2+} entry/release mechanisms the inducible Piezo1 overexpressing HEK 293 cell line was investigated. Cells were treated with tetracycline to induce Piezo1 expression (HEK-P1) or not (TRex). Application of 2 µM Yoda1 evoked an increase in intracellular Ca^{2+} in HEK-P1 cells compared to its vehicle but not in TRex cells lacking Piezo1 expression (Figure 5.7b). Pre-treatment with H89 did not affect this response or baseline intracellular Ca^{2+} levels

(Figure 5.7b). As baseline Ca^{2+} levels were not altered in HEK-P1 cells after H89 pre-treatment it is likely H89 was modulating Ca^{2+} handling in endothelial cells or endogenous Piezo1 channels in HUVECs, perhaps indirectly through an endothelial protein that is not expressed in HEK 293 cells. These data suggest that H89 does not inhibit Piezo1 channel activity and it is likely that the inhibitory effect reported in HUVECs is due to a technical artefact of fura-2 reaching its maximum (Figure 5.7a).

Pre-treatment with H89 had no effect on Yoda1-evoked eNOS phosphorylation (Figure 5.7c). Even though there appeared to be a decrease in the response, this failed to reach statistical significance. Taken together, these data suggest that chemical inhibition of PKA modulates intracellular Ca^{2+} levels in HUVECs but does not affect Yoda-mediated eNOS phosphorylation.

As H89 appears to modulate intracellular Ca^{2+} levels further work was needed to examine the role of PKA in Yoda1-medaited eNOS phosphorylation. siRNA targeting PKA was used to disrupt the expression of PKA. PKA knockdown was examined at the mRNA level using RT-PCR. *h*Brain cDNA was used as a positive control to ensure that our primers could specifically amplify PKA mRNA. End-point PCR products were run on a gel and one clear band was present of the correct size (Figure 5.8a). Indeed, PKA mRNA was amplified specifically using the primers designed. HUVECs treated with a mock transfection (-siRNA), PKA siRNA (si.PKA) or a scrambled control (si.Scr) were used and the expression of Beta Actin, Piezo1 and PKA mRNA was examined. Analysis of PCR products demonstrates that Beta Actin, Piezo1 and PKA can be detected and treatment with PKA siRNA was able to knockdown the expression of PKA without affecting Piezo1 levels (Figure 5.8b). Again one single band was present of the correct size suggesting specific PKA amplification. In order to examine the effect of disrupting PKA expression on Yoda1-evoked Piezo1 channel activity, intracellular Ca^{2+} experiments were carried out. PKA mRNA genetic disruption (si.PKA) had no effect on Yoda1-evoked Ca^{2+} entry compared to treatment with scrambled siRNA (si.Scr) (Figure 5.9a). Furthermore, PKA knockdown also had no effect on Yoda1 evoked eNOS phosphorylation (Figure 5.9b). These results argue against a role for PKA in the mechanism evoking fast Yoda1 mediated eNOS phosphorylation.

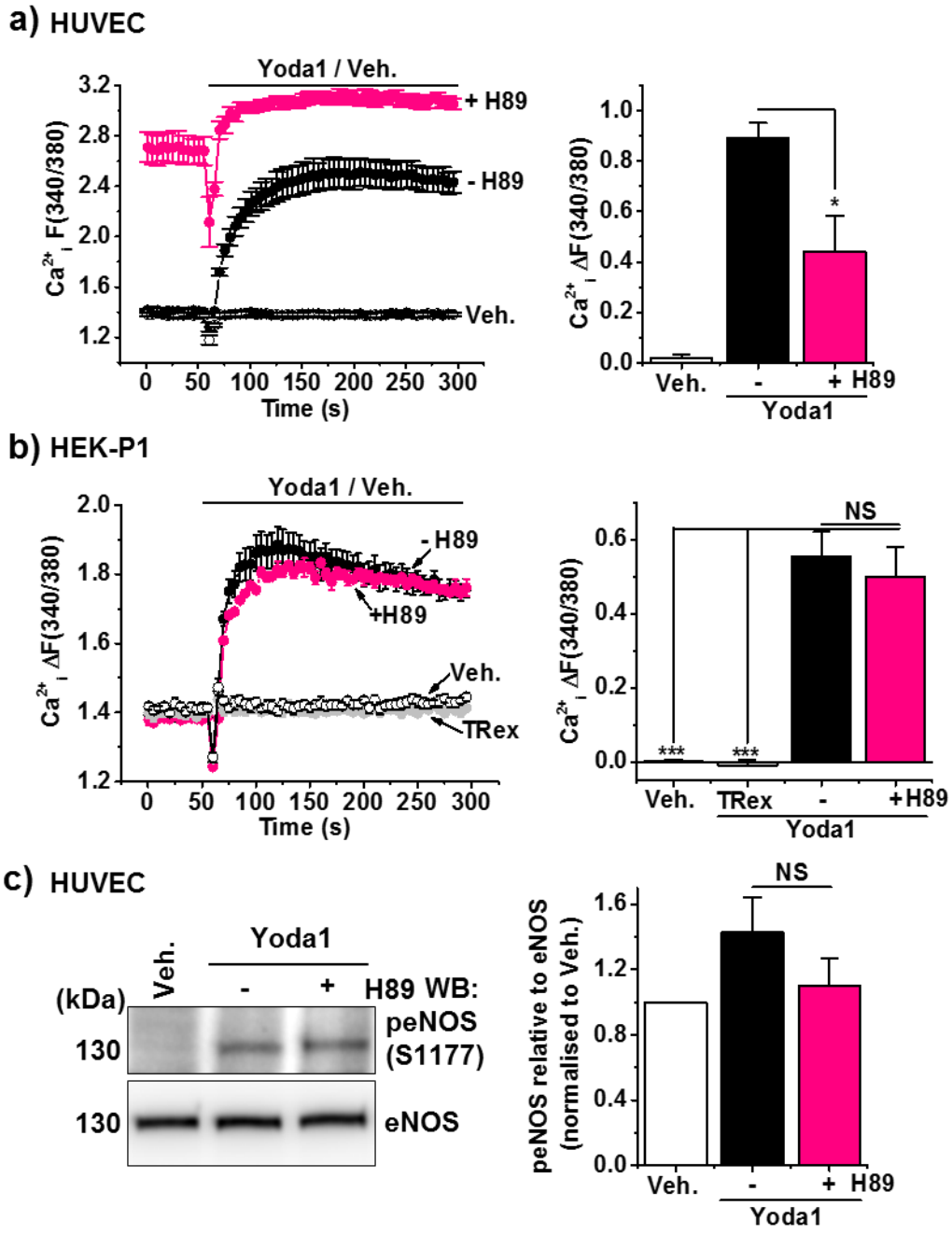

Figure 5.7 A chemical inhibitor of PKA has no effect on Yoda1 evoked eNOS phosphorylation.

a) Left: example intracellular Ca^{2+} measurement trace in HUVECs during application of 2 μM Yoda1 or its vehicle (Veh.). Cells are pre-treated for 30-minutes with 10 μM H89 (+H89) or its vehicle (-H89). Right: Mean data for the type of experiment shown on the left n/N=4/23-24. b) Left as in (a) but in HEK cells induced for 24-hours with 10 $ng.ml^{-1}$ tetracycline to over-express Piezo1 (HEK-P1) or not (TREx). Right: Mean data for the type of experiment shown on the left n/N=3/18 c) Left: Representative immunoblot for anti-S1177 phospho-eNOS and anti-eNOS in HUVECs after 1-minute treatment with 2 μM Yoda1 or its vehicle (Veh.) after pre-treatment for 30-minutes with 10 μM H89 (+H89) or its vehicle (-H89). Right: mean data from n=3 experiments displayed as phosphorylated eNOS relative to total eNOS normalised to vehicle treatment.

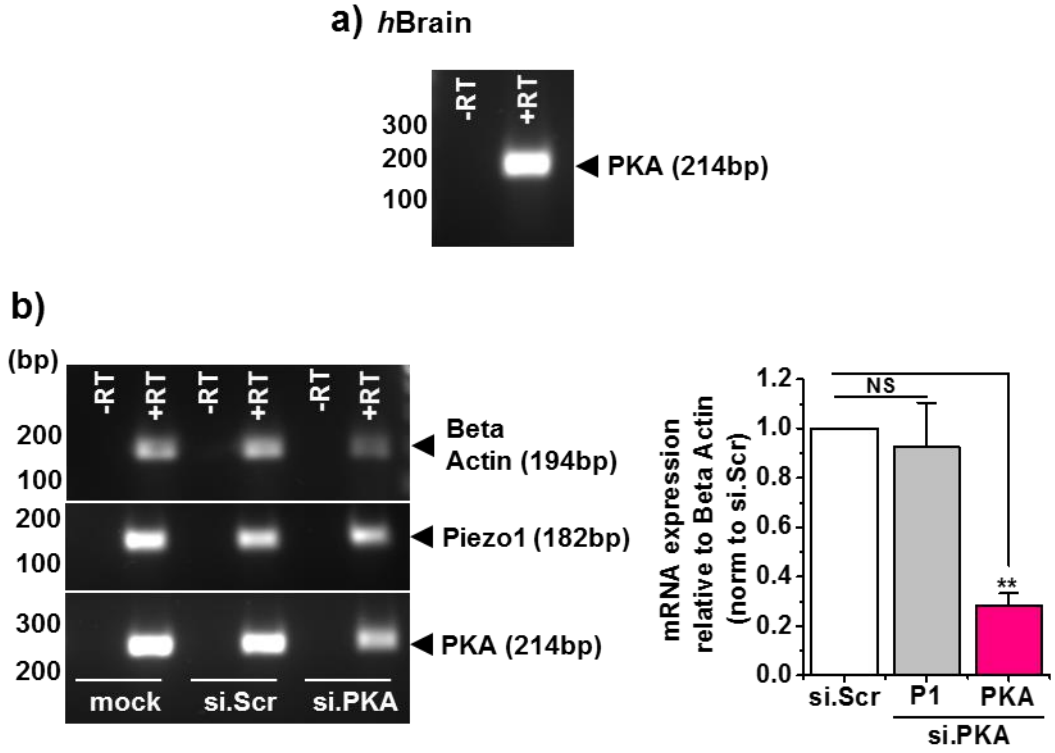

Figure 5.8 PKA siRNA knocks down PKA mRNA expression without disrupting Piezo1 expression.

a) End-point PCR products obtained with PKA primers for human (*h*) brain mRNA after reverse transcriptase reaction (RT) to generate cDNA. b) Left: as in (a) but with primers for Beta actin, Piezo1 and PKA for HUVEC cDNA treated with a mock (-siRNA), scrambled siRNA (si.Scr) or PKA (si.PKA) siRNA. Right: Mean data and analysis of Piezo1 and PKA mRNA relative to beta actin normalised to si.Scr (n=3).

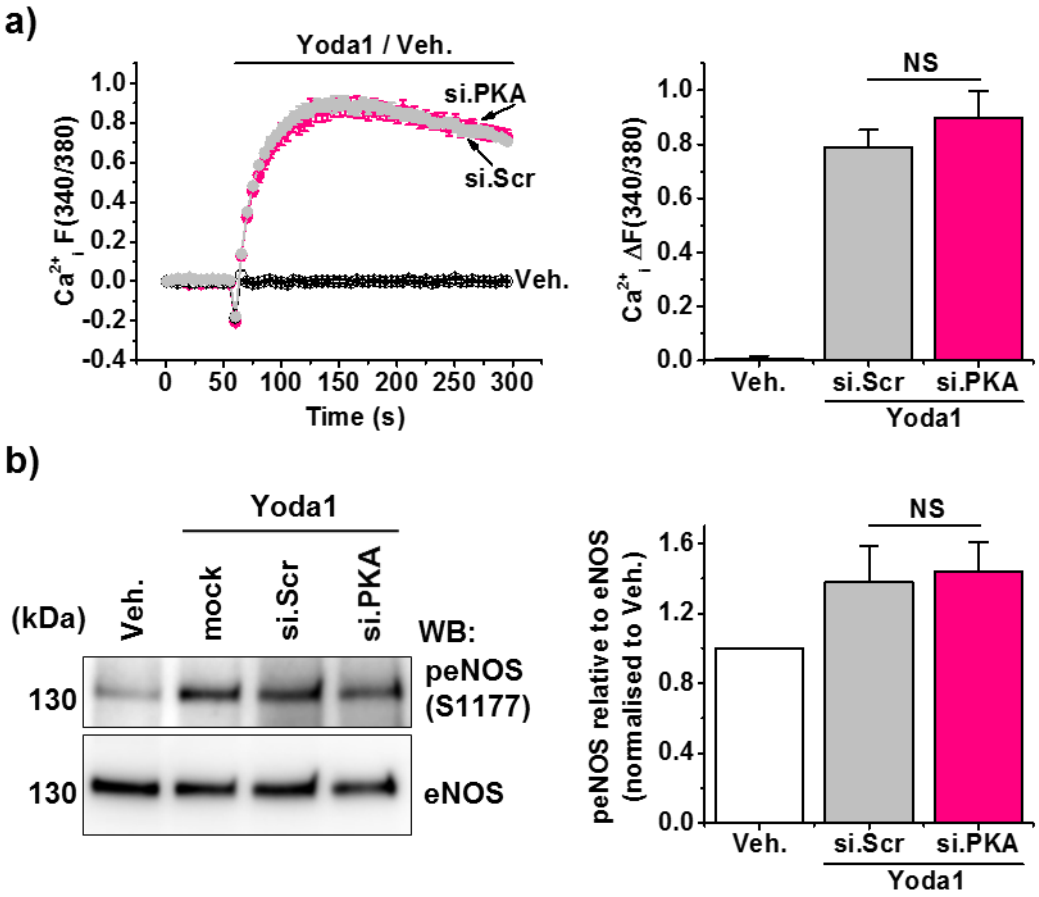

Figure 5.9 PKA siRNA has no effect on Yoda1-mediated Ca^{2+} entry or eNOS phosphorylation.

a) Left: example intracellular Ca^{2+} measurement trace in HUVECs during application of 2 µM Yoda1 or its vehicle (Veh.). Cells are treated with siRNA targeting PKA (si.PKA) or a scrambled sequence (si.Scr). Right: Mean data for the type of experiment shown on the left n/N=3/18 b) Left: Representative immunoblot for anti-S1177 phospho-eNOS and anti-eNOS in HUVECs treated with a mock transfection (-siRNA), scrambled siRNA or PKA siRNA after 1-minute stimulation with 2 µM Yoda1 or its vehicle (Veh.). Right: mean data from n=3 experiments displayed as phosphorylated eNOS relative to total eNOS normalised to vehicle treatment.

5.4 siRNA targeting AMPKα1 and AMPKα2 does not affect Yoda1-evoked eNOS phosphorylation

AMPK can phosphorylate eNOS on serine (S633 and S1177) and threonine (Thr496) residues (Chen and Tzima, 2009; Chen et al., 1999). *In-vivo* AMPK is reported to phosphorylate eNOS (S1177) independently of AKT in mice during treadmill running to evoke shear stress (Zhang et al., 2009). In keeping with this report, data in the previous chapter also exclude the involvement of AKT in Yoda1-mediated eNOS phosphorylation. Thus, AMPK was an important candidate kinase to consider.

To investigate the role of AMPK, siRNA targeting AMPKα1 (si.AMPK1) and AMPKα2 (si.AMPK2) was performed and the knockdown efficiency was analysed using RT-qPCR. End-point PCR reactions on *h*Brain samples suggest that our primers were able to successfully amplify both AMPKα1 and AMPKα2 mRNA without amplifying off-target products (Figure 5.10a). Similarly, in HUVECs end-point PCR reactions were run on a gel and the data suggested that the reactions were clean and primers were amplifying a product of the correct size, as expected from our primer design (Figure 5.10b). AMPKα1 siRNA knocked down AMPKα1 (A1) mRNA expression by 77% compared to HUVECs treated with a scrambled control siRNA (si.Scr) without affecting expression of Piezo1 or AMPKα2 (A2) (Figure 5.10c). AMPKα2 siRNA was less specific as it knocked down both AMPKα1 (A1) and AMPKα2 (A2) by 53% and 52% respectively (Figure 5.10d). Importantly, Piezo1 levels remained unchanged (Figure 5.10d). Thus, the data suggest that we are able to successfully knockdown both AMPKα1 and AMPKα2 in HUVECs.

Next, the effect of genetic disruption of AMPKα1 and AMPKα2 on Piezo1 activity was examined. Knocking down both AMPKα1 (si.A1) and AMPKα2 (si.A2) mRNA had no effect on Yoda1-evoked Piezo1 mediated Ca^{2+} entry compared to the scrambled control (si.Scr) (Figure 5.11a). Furthermore, both knockdowns also had no effect on Yoda1-evoked eNOS phosphorylation (Figure 5.11b). The data suggest that Yoda1 evokes eNOS phosphorylation independently of AMPK expression.

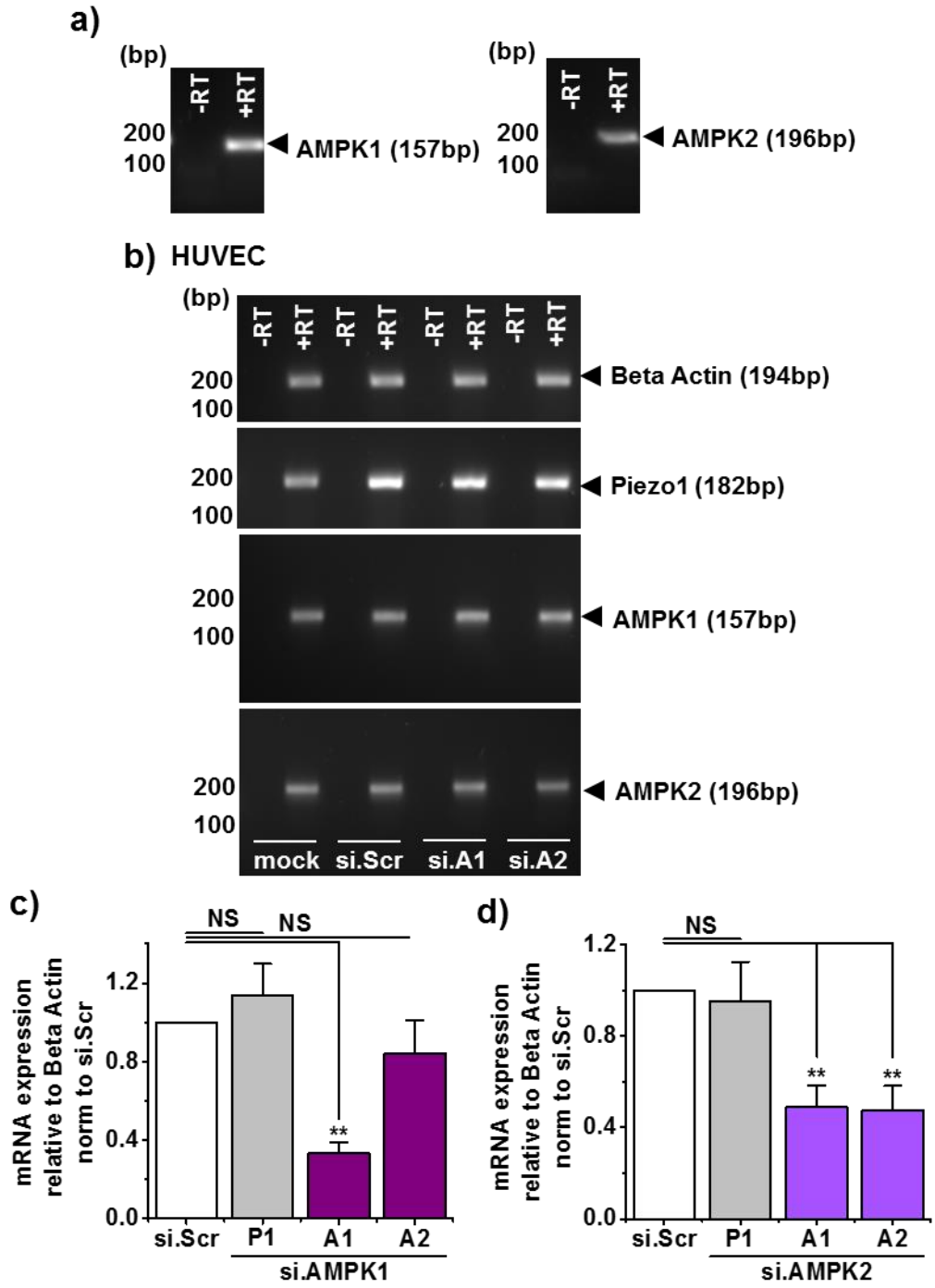

Figure 5.10 Genetic disruption of AMPK mRNA does not affect Piezo1 expression.

a) End-point PCR products obtained with AMPKα1 and AMPKα2 primers for human brain (*h*Brain) mRNA after reverse transcriptase reaction (+RT) or not (-RT) to generate cDNA. b) As in (a) but with primers for beta actin, Piezo1, AMPKα1 and AMPKα2 in HUVEC samples treated with AMPKα1 (si.A1), AMPKα2 (si.A2) or scrambled siRNA (si.Scr). c) Mean data and analysis of Piezo1 (P1), AMPKα1 (A1) and AMPKα2 (A2) mRNA expression relative to beta actin (normalised to si.Scr) after treatment with AMPKα1 siRNA or scrambled siRNA (n=6). d) As in (c) but relative mRNA expression after treatment with AMPKα2 siRNA (n=12).

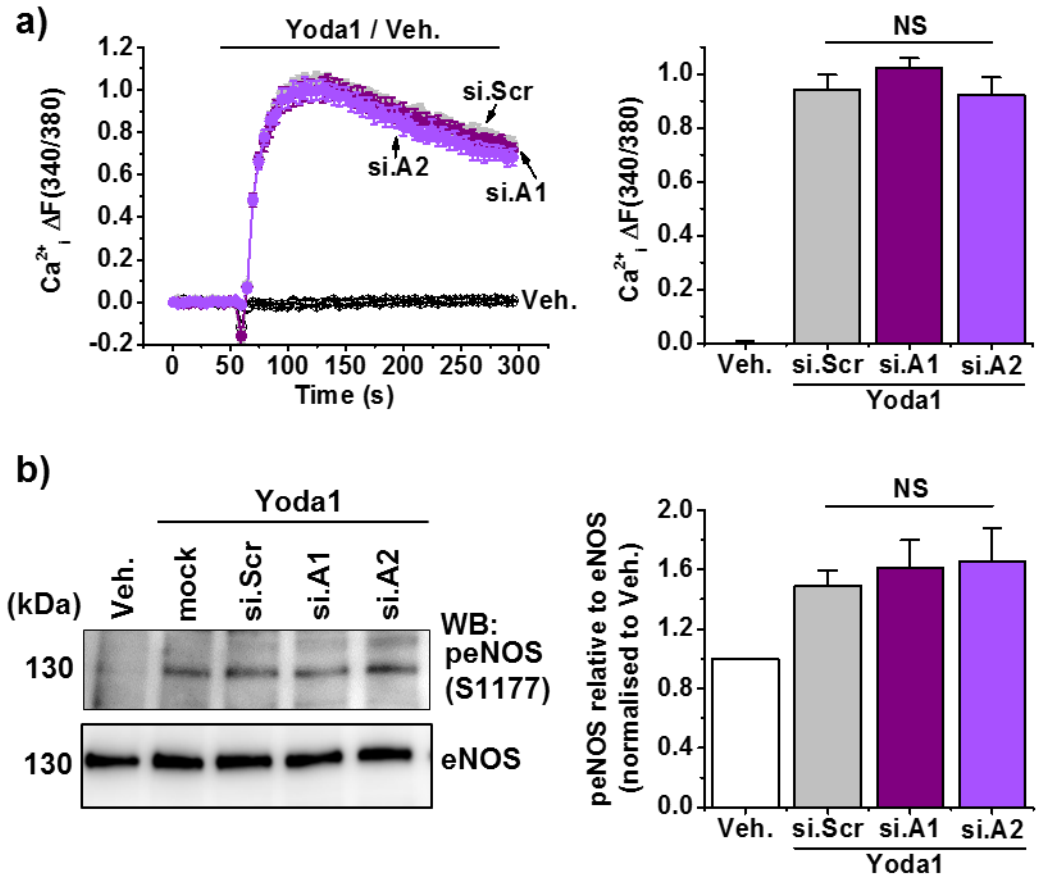

Figure 5.11 Knockdown of AMPKα1 and AMPKα2 mRNA does not affect Yoda1-mediated Piezo1 activation.

a) Left: example intracellular Ca^{2+} measurement trace in HUVECs during application of 2 μM Yoda1 or its vehicle (Veh.). Cells are treated with siRNA targeting AMPKα1 (si.A1), AMPKα2 (si.A2) or a scrambled sequence (si.Scr). Right: Mean data for the type of experiment shown on the left n/N=3/17-18 b) Left: Representative immunoblot for anti-S1177 phospho-eNOS, total eNOS in HUVECs with and without AMPKα1 or AMPKα2 genetic disruption treated for 1 minute with 2 μM Yoda1 or its vehicle (Veh.). Right: mean data from n=4 experiments displayed as phosphorylated eNOS relative to total eNOS normalised to vehicle treatment.

5.5 Yoda1-evoked S1177 eNOS phosphorylation is dependent on extracellular Ca^{2+} but independent of classical Ca^{2+} pathways

Functionally, eNOS was initially classified as a Ca^{2+}/CaM-dependent enzyme with low but measurable activity at resting levels of Ca^{2+} (Fleming, 2010). However, it is now widely accepted that eNOS can be phosphorylated both dependently and independently of Ca^{2+}. For example, a transient phosphorylation of eNOS is apparent under VEGF and shear stress stimuli when mediated by Ca^{2+} dependent cascades but a more sustained activation of eNOS is observed when Ca^{2+} independent kinases are involved (Devika and Jaffar Ali, 2013). As Piezo1 channel activation elicits a rapid increase in intracellular Ca^{2+} in HUVECs the next logical kinases to examine were the classical Ca^{2+} dependent kinases.

5.5.1 Yoda1 evoked eNOS phosphorylation is dependent on extracellular Ca^{2+}

Firstly, to examine the role of Ca^{2+} entry across the plasma membrane in Yoda1-evoked eNOS phosphorylation HUVECs were pre-treated with 0 mM extracellular Ca^{2+}. In contrast to the 2-fold increase in Yoda1 mediated eNOS phosphorylation in HUVECs under normal physiological levels of extracellular Ca^{2+}, pre-treatment with 0 mM Ca^{2+} drastically suppressed this response by 93% (Figure 5.12). Consistent with Piezo1 channels conducting Yoda-mediated Ca^{2+} entry, these data suggest that this Ca^{2+} entry is critical for Yoda- evoked eNOS phosphorylation. However, it is unclear how meaningful these data are as complete removal of Ca^{2+}_{ex} is highly non-specific and could drastically alter intracellular Ca^{2+} signalling. More work is needed to confirm this.

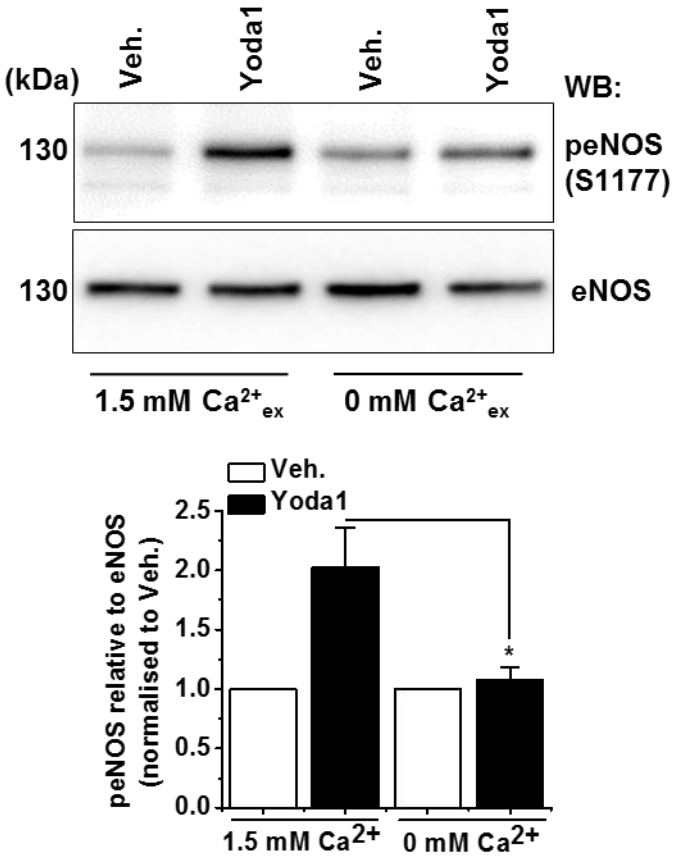

Figure 5.12 Omission of extracellular Ca^{2+} abolishes Yoda1-evoked eNOS phosphorylation.

Upper: Representative immunoblot for anti-S1177 phospho-eNOS and anti-eNOS in HUVECs treated for 1-minute with 2 μM Yoda1 or its vehicle (Veh.). HUVECs were pre-treated for 20-minutes with 1.5 mM extracellular Ca^{2+} (Ca^{2+}_{ex}) or 0 mM $Ca^{2+}_{ex.}$ Lower: mean data from n=5 experiments displayed as phosphorylated eNOS relative to total eNOS normalised to vehicle treatment.

5.5.2 Yoda1-evoked eNOS phosphorylation is blocked by chemical CAMKII inhibitors

As it is evident that Yoda1 evoked eNOS phosphorylation was Ca^{2+} dependent, classical Ca^{2+} pathways reported to mediate eNOS phosphorylation were investigated. CaM was the first reported eNOS-associated protein (Busse and Mulsch, 1990). CaM is a Ca^{2+}-binding protein. Once bound to Ca^{2+}, CaM acts as part of a Ca^{2+} signalling pathway that can modulate target proteins such as CaM kinase II (CaMKII). CaMKII is reported to be involved in Ca^{2+} dependent eNOS phosphorylation, eNOS activation and endothelial-dependent relaxation (Schneider et al., 2003).

In order to investigate the role of CaMKII the non-selective protein kinase inhibitors CK59 and KN93 were used that are reported to inhibit CaMKII. Firstly, CK59 was utilized. It is reported that pre-treatment of 25 µM CK59 does not affect alignment of HUVECs, suggesting that it does not affect Piezo1 channel function (Li et al., 2014). To further investigate this, intracellular Ca^{2+} measurement assays were carried out to assess Piezo1 channel activity. 30-minute pre-treatment of HUVECs with 100 µM CK59 slightly potentiated Yoda1-mediated Ca^{2+} entry compared to cells treated with its vehicle (Figure 5.13a). Importantly, pre-treatment with CK59 abolished Yoda1-mediated eNOS phosphorylation (Figure 5.13b). Similarly, KN93, a more potent CaMKII inhibitor, also suppressed Yoda1-mediated eNOS phosphorylation (Figure 5.14b) without affecting Piezo1 channel activity as measured using the Ca^{2+} measurement assay (Figure 5.14a). Taken together, these data suggest a role for CaMKII in Yoda1-mediated eNOS phosphorylation.

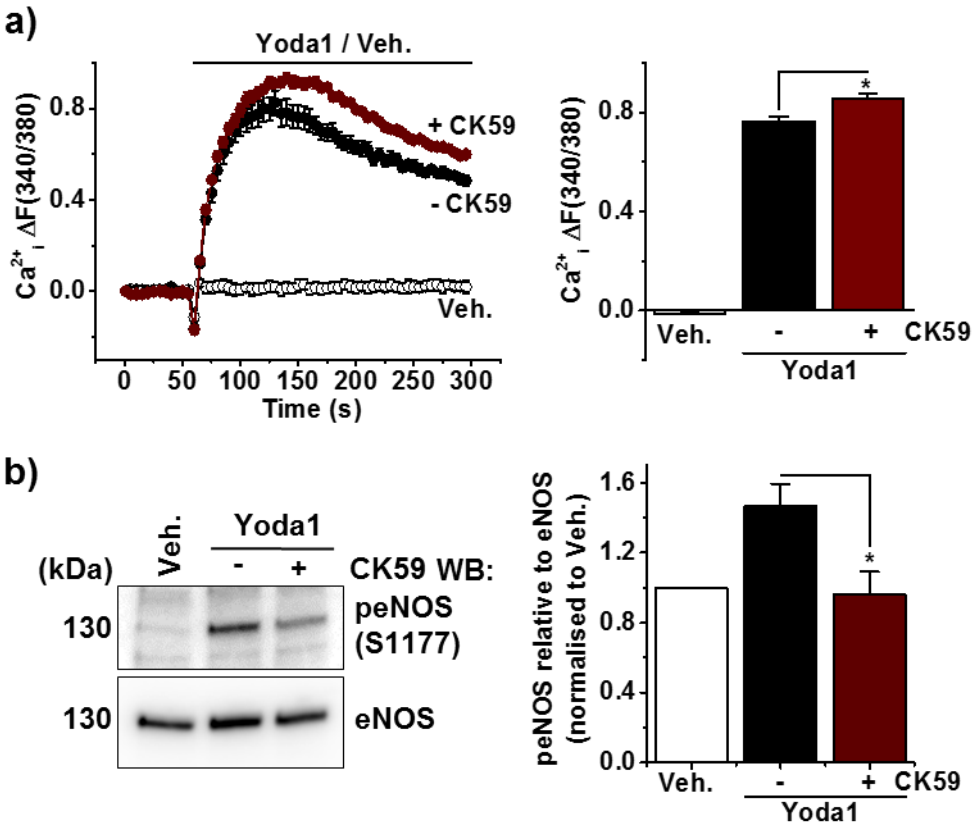

Figure 5.13 The CaMKII chemical inhibitor, CK59, inhibits Yoda1-evoked eNOS phosphorylation.

a) Left: example intracellular Ca^{2+} measurement trace in HUVECs during application of 2 μM Yoda1 or its vehicle (Veh.). Cells are pre-treated for 30-minutes with 100 μM CK59 (+ CK59) or its vehicle (- CK59). Right: Mean data for the type of experiment shown on the left (n/N=3/12-18). b) Left: Representative immunoblot for anti-S1177 phospho-eNOS and anti-total eNOS in HUVECs treated for 1-minute with 2 μM Yoda1 or its vehicle (Veh.). HUVECs were pre-treated as in (a). Right: mean data from n=3 experiments displayed as phospho-eNOS relative to total eNOS normalised to vehicle treatment.

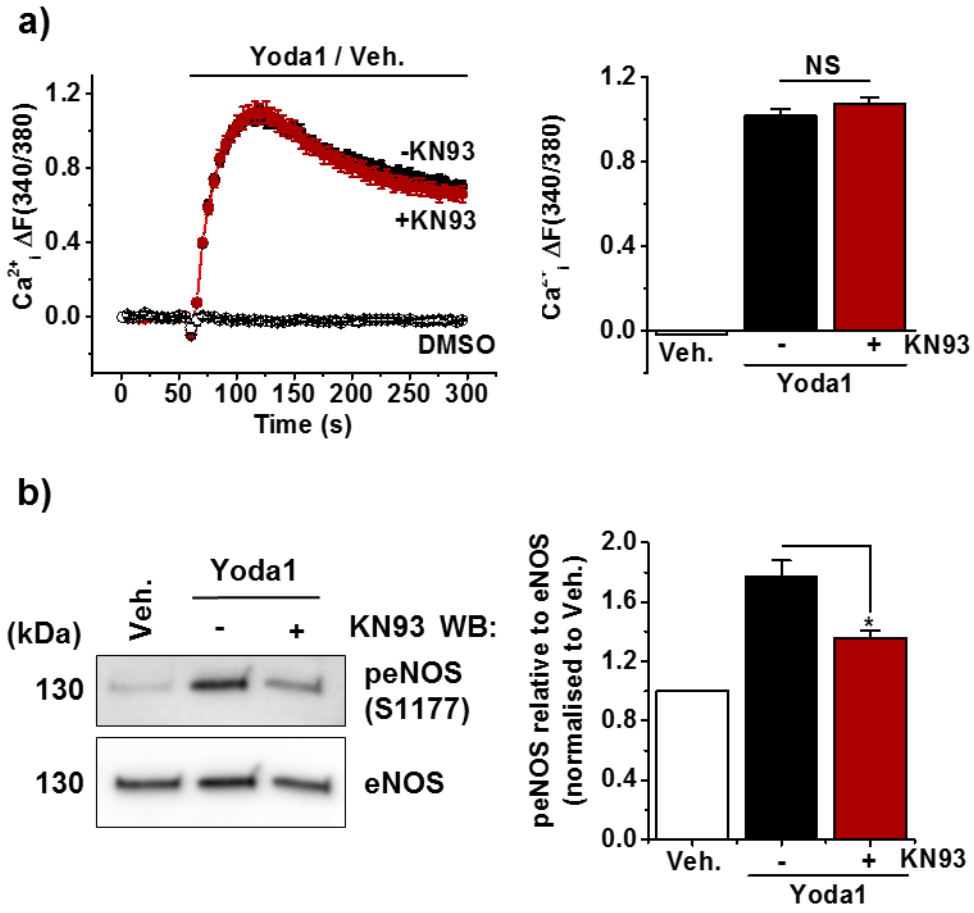

Figure 5.14 The CaMKII chemical inhibitor, KN93, inhibits Yoda1-evoked eNOS phosphorylation.

a) Left: example intracellular Ca^{2+} measurement trace in HUVECs during application of 2 μM Yoda1 or its vehicle (Veh.). Cells are pre-treated for 30-minutes with 10 μM KN93 (+ KN93) or its vehicle (- KN93). Right: Mean data for the type of experiment shown on the left (n/N=3/12-18). b) Left: Representative immunoblot for anti-S1177 phospho-eNOS and anti-total eNOS in HUVECs treated for 1-minute with 2 μM Yoda1 or its vehicle (Veh.). HUVECs were pre-treated as in (a). Right: mean data from n=3 experiments displayed as phospho-eNOS relative to total eNOS normalised to vehicle treatment.

5.5.3 CaMKIIδ is highly expressed in HUVECs

As it is clear from the literature that CK59 and KN93 are not selective for CaMKII and also act on various other targets including voltage gated ion channels (Karls and Mynlieff, 2013; Ledoux et al., 1999) it was important to examine the effects of CaMKII siRNA on Yoda1 evoked eNOS phosphorylation. CaMKII is a serine/threonine kinase and it has 28 different isoforms that are derived from the α, ß, δ and γ genes. Firstly experiments to investigate mRNA expression levels of CaMKIIα, ß, δ and γ were carried out. To test if the primers could amplify their target, *h*Brain mRNA was utilised. Indeed, primers for CaMKIIα, ß, δ and γ amplified products of the correct size (Figure 5.15a). mRNA expression of the CaMKII isoforms was examined in HUVECs and CaMKIIδ and γ were convincingly expressed (Figure 5.15b & c). The expression of CaMKIIδ was significantly higher than any other CaMKII isoform (Figure 5.15c). Thus, the role of CaMKIIδ was examined in further detail.

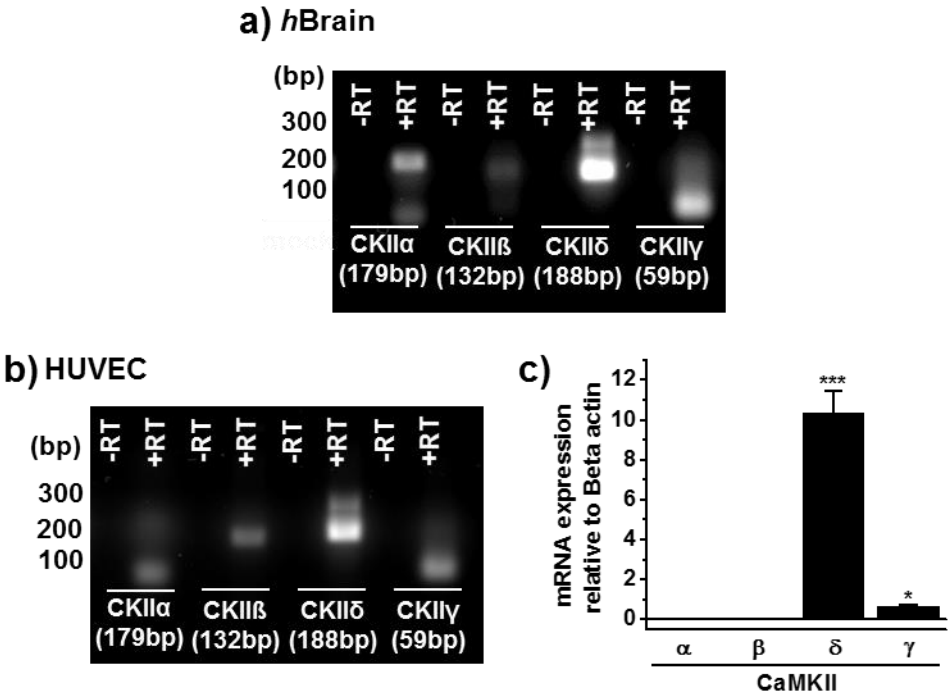

Figure 5.15 CaMKIIδ is highly expressed in HUVECs.

a) End-point PCR products obtained with CaMKIIα (CKIIα), CaMKIIß (CKIIß), CaMKIIδ (CKIIδ) and CaMKIIγ (CKIIγ) primers for human brain (*h*Brain) mRNA after reverse transcriptase reaction (+RT) or not (-RT) to generate cDNA. b) As in (a) but in HUVEC samples. c) Mean data and analysis from the type of experiment in (b) of CaMKIIα, CaMKIIß, CaMKIIδ and CaMKIIγ mRNA expression relative to beta actin (n=3). RT-qPCR performed by Fiona Bartoli.

5.5.4 siRNA targeting CaMKII does not affect Yoda1-mediated eNOS phosphorylation

As CaMKIIδ was the most highly expressed CaMKII isoform in HUVECs its role in Yoda1-mediated eNOS phosphorylation was examined. It is suggested to play an important role in bradykinin-driven eNOS activation (Murthy et al., 2017). siRNA was used targeting CaMKIIδ (si.CKIIδ) or a scrambled control sequence (si.Scr). RT-qPCR was used to examine the efficiency of the knockdown. CaMKIIδ expression was examined in HUVECs after treatment with CaMKIIδ (si.CKIIδ) siRNA, a scrambled control sequence (si.Scr) or a mock transfection (-siRNA). CaMKIIδ siRNA sufficiently knocked down CaMKIIδ mRNA expression by 89% compared to the scrambled control and importantly did not affect levels of Piezo1 and CaMKIIγ (Figure 5.16). In order to examine whether CaMKIIδ knockdown affected Piezo1 channel activation, intracellular Ca^{2+} measurements were carried out in HUVECs. CaMKIIδ mRNA knockdown had no effect on Yoda1 evoked Ca^{2+} entry (Figure 5.17a). Furthermore, CaMKIIδ mRNA knockdown also had no effect on Yoda1 evoked eNOS phosphorylation (Figure 5.17b). These data suggest that the CaMKIIδ isoform does not play a role in Yoda1-mediated eNOS phosphorylation, but a role for CaMKIIγ has not been ruled out.

As CaMKIIγ was also expressed in HUVECs its role in Yoda1-mediated eNOS phosphorylation was examined. HUVECs were treated with CaMKIIγ siRNA (si.CKIIγ) and RT-qPCR was used to examine the knockdown efficiency. End-point PCR reactions were run on a gel and primers were able to amplify the correct gene of interest (Figure 5.18). siRNA targeting CaMKIIγ was able to significantly knockdown CaMKIIγ mRNA expression by 53% compared to the cells treated with scrambled control siRNA (si.Scr) (Figure 5.18). Knockdown of CaMKIIγ had no effect on mRNA expression levels of Piezo1 or CaMKIIδ (Figure 5.18). Yoda1-mediated Piezo1 activity was examined in HUVECs with and without knockdown of CaMKIIγ. Knockdown of CaMKIIγ mRNA did not affect Yoda1-mediated Ca^{2+} entry or eNOS phosphorylation compared to cells treated with a scrambled control siRNA (Figure 5.19a & b). Taken together, even though chemical inhibitors of CaMKII suppressed Yoda1-mediated eNOS phosphorylation, RNAi data do not support a role for CaMKII in the Yoda-mediated eNOS phosphorylation signaling pathway.

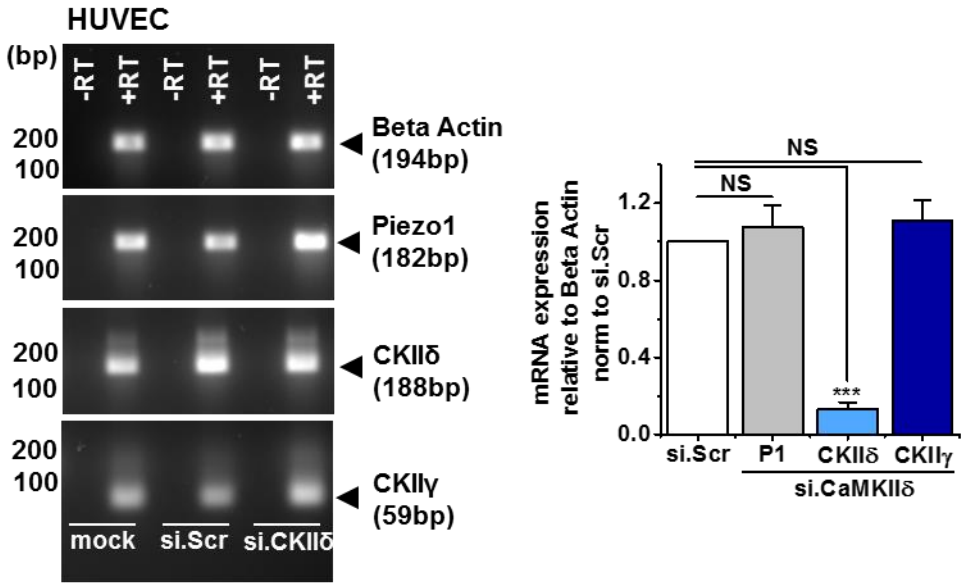

Figure 5.16 CaMKIIδ mRNA knockdown does not affect Piezo1 or CaMKIIγ mRNA expression.

Left: End-point PCR products obtained with primers for Beta actin, Piezo1, CaMKIIδ (CKIIδ) and CaMKIIγ (CKIIγ) for HUVEC mRNA after reverse transcriptase reaction (+RT) or not (-RT) to generate cDNA. HUVECs were treated with a mock transfection (-siRNA), scrambled siRNA (si.Scr) or CaMKIIδ siRNA (siCKIIδ). Right: Mean data and analysis of Piezo1, CaMKIIδ and CaMKIIγ mRNA relative to beta actin normalised to scrambled siRNA treated samples (n=4-5). RT-qPCR performed by Fiona Bartoli.

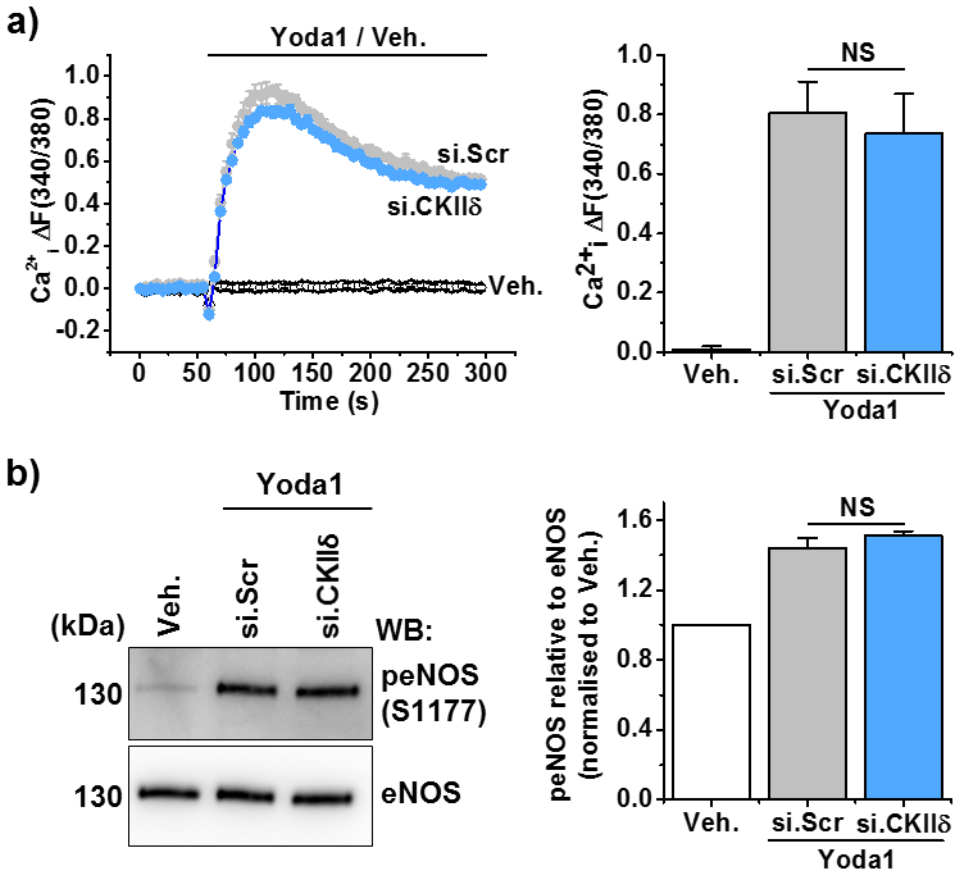

Figure 5.17 Genetic disruption of CaMKIIδ mRNA expression does not affect Yoda1-evoked eNOS phosphorylation.

a) Left: example intracellular Ca^{2+} measurement trace in HUVECs during application of 2 µM Yoda1 or its vehicle (Veh.). Cells are treated with siRNA targeting CaMKIIδ (si.CKIIδ) or a control scrambled sequence (si.Scr). Right: Mean data for the type of experiment shown on the left n/N=3/15-16 b) Left: Representative immunoblot for anti-S1177 phospho-eNOS and anti-eNOS in HUVECs with and without CaMKIIδ siRNA treated for 1-minute with 2 µM Yoda1 or its vehicle (Veh.). Right: mean data from n=3 experiments displayed as phosphorylated eNOS relative to total eNOS normalised to vehicle treatment.

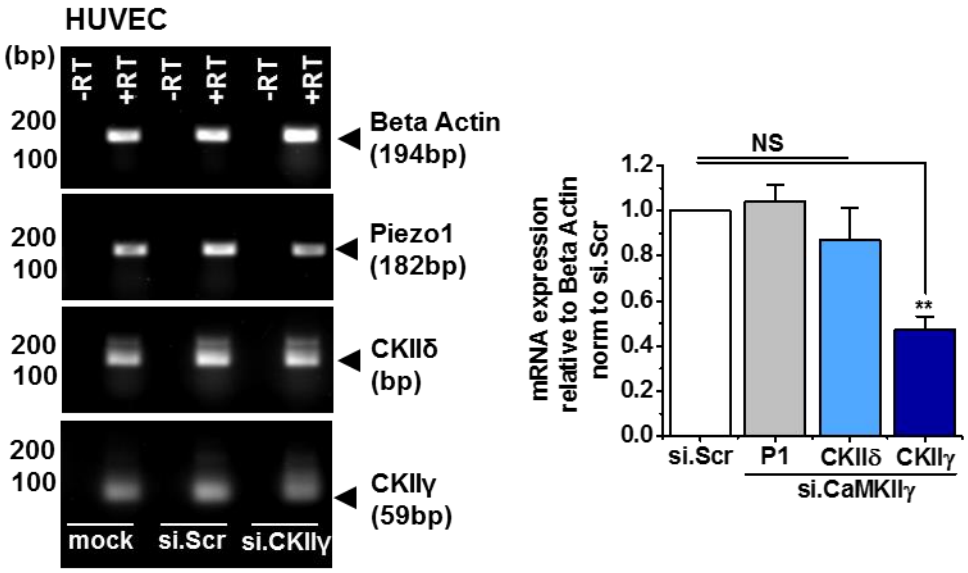

Figure 5.18 CaMKIIγ mRNA knockdown does not affect Piezo1 or CaMKIIδ mRNA expression.

Left: End-point PCR products obtained with primers for Beta actin, Piezo1, CaMKIIδ (CKIIδ) and CaMKIIγ (CKIIγ) for HUVEC mRNA after reverse transcriptase reaction (+RT) or not (-RT) to generate cDNA. HUVECs were treated with a mock transfection (-siRNA), scrambled siRNA (si.Scr) or CaMKIIγ siRNA (siCKIIγ). Right: Mean data and analysis of Piezo1, CaMKIIδ and CaMKIIγ mRNA relative to beta actin normalised to scrambled siRNA treated samples (n=4-5). RT-qPCR performed by Fiona Bartoli.

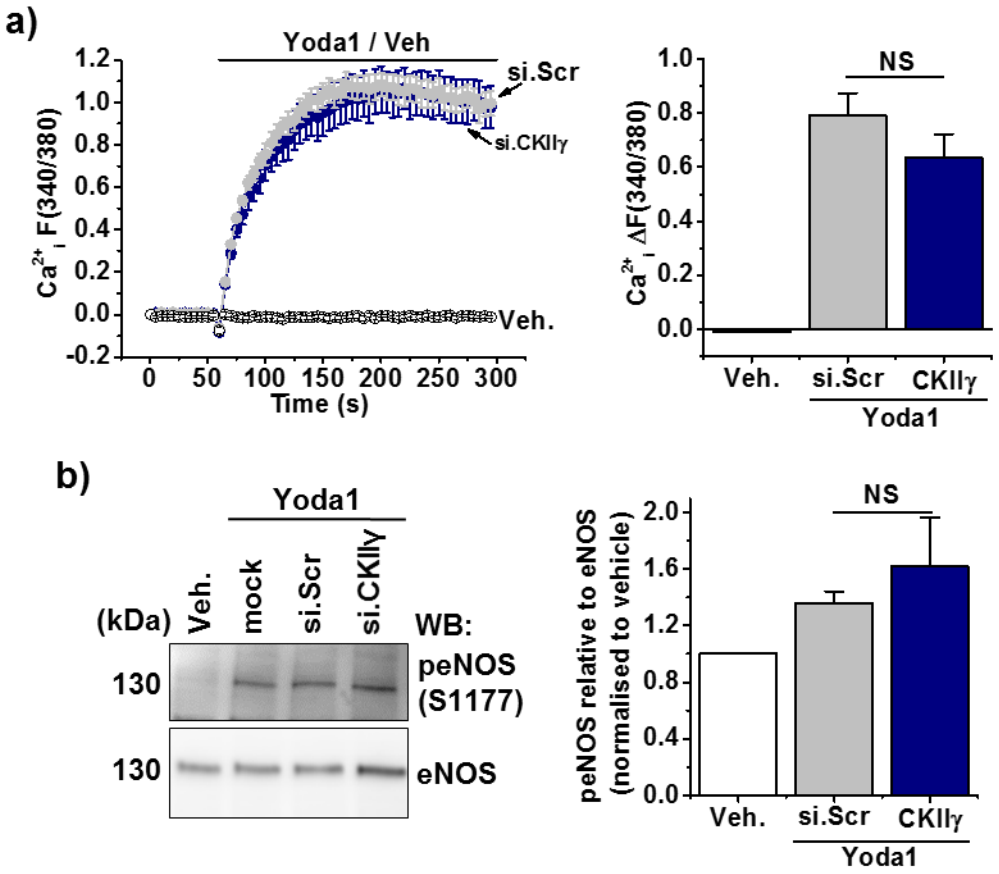

Figure 5.19 Genetic disruption of CaMKIIα, ß and γ mRNA expression does not affect Yoda1-evoked eNOS phosphorylation.

a) Left: example intracellular Ca^{2+} measurement trace in HUVECs during application of 2 µM Yoda1 or its vehicle (Veh.). Cells are treated with siRNA targeting CaMKIIα, ß and γ (si.CKIIα, ß and γ) or a control scrambled sequence (si.Scr). Right: Mean data for the type of experiment shown on the left n/N=3/15-16 b) Left: Representative immunoblot for anti-S1177 phospho-eNOS and anti-eNOS in HUVECs with and without CaMKIIα, ß and γ genetic disruption treated for 1-minute with 2 µM Yoda1 or its vehicle (Veh.). Right: mean data from n=5 experiments displayed as phosphorylated eNOS relative to total eNOS normalised to vehicle treatment.

5.5.5 The chemical calmodulin inhibitor, W7, does not affect Yoda1-mediated eNOS phosphorylation

Thus far, even though the data suggest that Ca^{2+} is mediating Yoda1-evoked eNOS phosphorylation a role for the Ca^{2+} sensitive kinase CaMKII has been ruled out. In order to further investigate CaM, the effect of inhibiting CaM directly was examined. W7 is a CaM inhibitor that is reported to inhibit insulin induced AKT and eNOS S1177 phosphorylation in HUVECs (Long et al., 2017). The effect of W7 pre-treatment on Yoda1-medaited Piezo1 channel activity was examined. To investigate Piezo1 channel activation FlexStation experiments were performed during application of Yoda1 after pre-treatment with 30 µM W7 for 30-minutes. Pre-treatment with W7 did not affect basal Ca^{2+} levels, suggesting that it is not altering Ca^{2+} handling (Figure 5.20a). However, W7 pre-treatment strongly potentiated Yoda1-induced Ca^{2+} entry (Figure 5.20a). W7 pre-treatment had no effect on Yoda1-mediated eNOS phosphorylation (Figure 5.20b). These data are in keeping with previous results in this chapter suggesting that CaMKII is not involved in this mechanism.

Taken together, these results suggest that even though Yoda-mediated eNOS phosphorylation is blocked by removing Ca^{2+}_{ex}, the mechanism is independent of classical Ca^{2+} regulated, CaM and CaMKII.

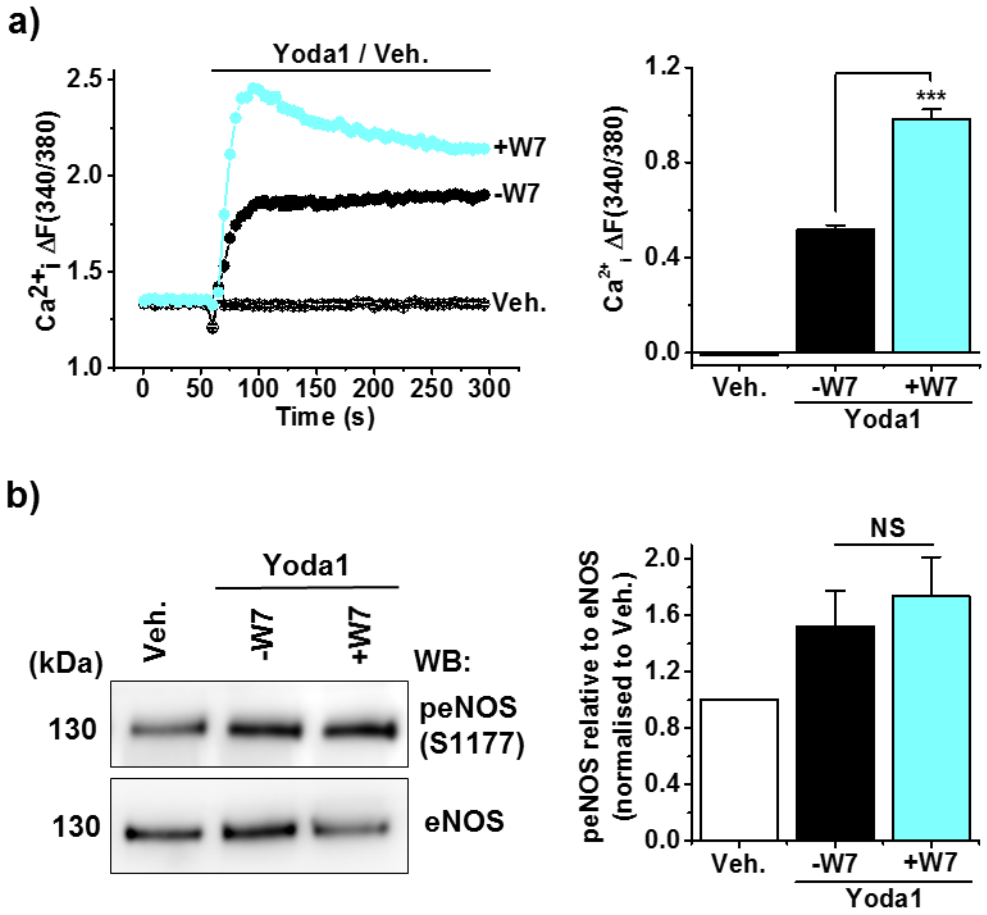

Figure 5.20 Pre-treatment with W7 does not affect Yoda1-mediated eNOS phosphorylation.

a) Left: example intracellular Ca^{2+} measurement trace in HUVECs during application of 2 µM Yoda1 or its vehicle (Veh.) after pre-treatment with 30 µM W7 (+W7) or its vehicle (-W7) for 30-minutes. Right: Mean data for the type of experiment shown on the left n/N=6/36 b) Left: Representative immunoblot for anti-S1177 phospho-eNOS and anti-eNOS in HUVECs with (+W7) and without (-W7) pre-treatment with 30 µM W7 for 30-minutes followed by 1-minute treatment with 2 µM Yoda1 or its vehicle (Veh.). Right: mean data from n=5 experiments displayed as phosphorylated eNOS relative to total eNOS (normalised to vehicle treatment).

5.6 CaMKI RNAi does not affect Yoda1-mediated eNOS phosphorylation

In order to further investigate the role of the CaMK family in Yoda1-medaited eNOS phosphorylation, CaMKI was examined. CaMKI has been linked to NOS and NO in the literature. It is reported that neuronal NOS is inhibited by CaMKI (Song et al., 2004). Moreover, CaMKI has also been linked to endothelial cell inflammation via a Ca^{2+}, CaMKI and AMPK dependent mechanism (Guo et al., 2013). Interestingly, CaMKI is also suggested to be inhibited by the CaMKII inhibitor KN93. Data in Figure 5.14 suggest that pre-treatment with KN93 strongly supresses Yoda1-mediated eNOS phosphorylation, but further experiments ruled out a role for CaMKII itself. Initially characterisation of KN93 suggested that it was selective for CaMKII when tested against PKA, PKC and MLCK (Tokumitsu et al., 1990; Sumi et al., 1991) but, later studies proposed that other reported targets now include Fyn, Haspin, Hck, Lck, MLCK, Tec, TrKa and CAMKI (Pellicena and Schulman, 2014). All of these kinases play very different roles in different cell types. As CaMKI is reported to be sensitive to KN93 and as it has been linked to eNOS in the literature it was important to investigate the involvement of CaMKI in Yoda1 evoked eNOS phosphorylation.

As a positive control CaMKI primers were tested in *h*Brain mRNA and primers designed to amplify CaMKI were able to amplify a single product of the correct size (Figure 5.21a). Next, CaMKI mRNA expression was examined in HUVEC samples after treatment with CaMKI siRNA (si.CKI) or a siRNA targeting a scrambled control sequence (si.Scr). CaMKI siRNA was able to efficiently knockdown CaMKI mRNA expression by 89% compared to scrambled siRNA treated cells without effecting Piezo1 expression (Figure 5.21b). Intracellular Ca^{2+} measurement assays were undertaken to examine Piezo1 function after CaMKI knockdown. CaMKI mRNA knockdown (si.CKI) had no effect on Yoda1 evoked Ca^{2+} entry compared to the scrambled treated control (si.Scr) (Figure 5.22a). Finally, Yoda1 evoked eNOS phosphorylation was examined and CaMKI mRNA knockdown had no effect on this response (Figure 5.22b). Taken together these data suggest that Yoda1 acts independently of CaMKI to evoke eNOS phosphorylation.

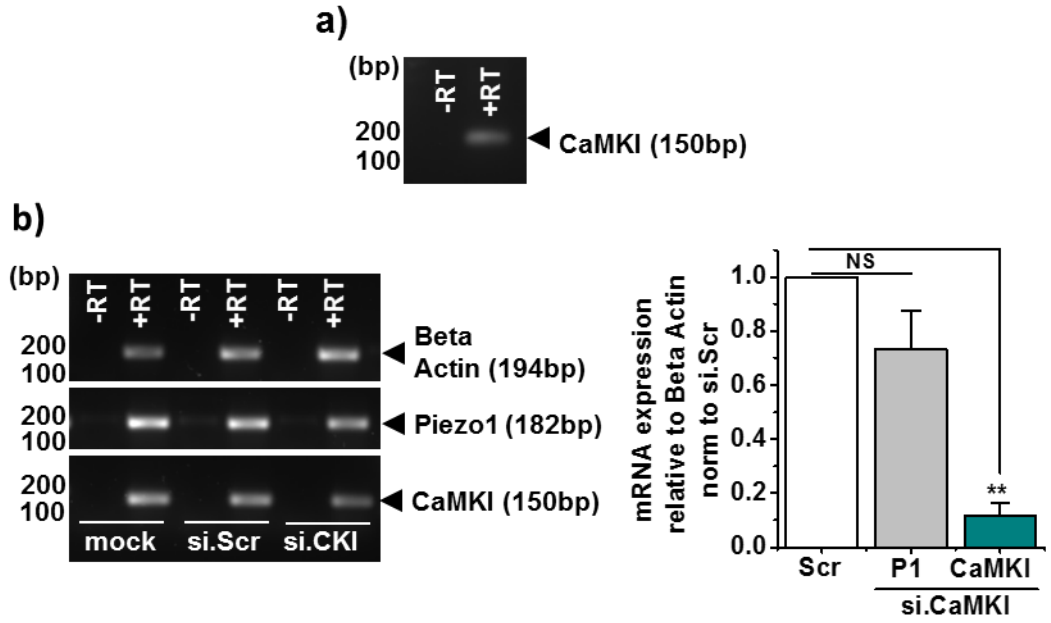

Figure 5.21 Knockdown of CaMKI mRNA does not affect Piezo1 expression.

a) End-point PCR products obtained with CaMKI primers for *h*Brain mRNA after reverse transcriptase reaction (+RT) or not (-RT) to generate cDNA. b) Left: as in (a) but with primers for Beta actin, Piezo1 and CaMKI for HUVECs treated with a mock (-siRNA), scrambled siRNA (si.Scr) or CaMKI siRNA (si.CKI). Right: Mean data and analysis of Piezo1 and CaMKI mRNA relative to beta actin (n=3).

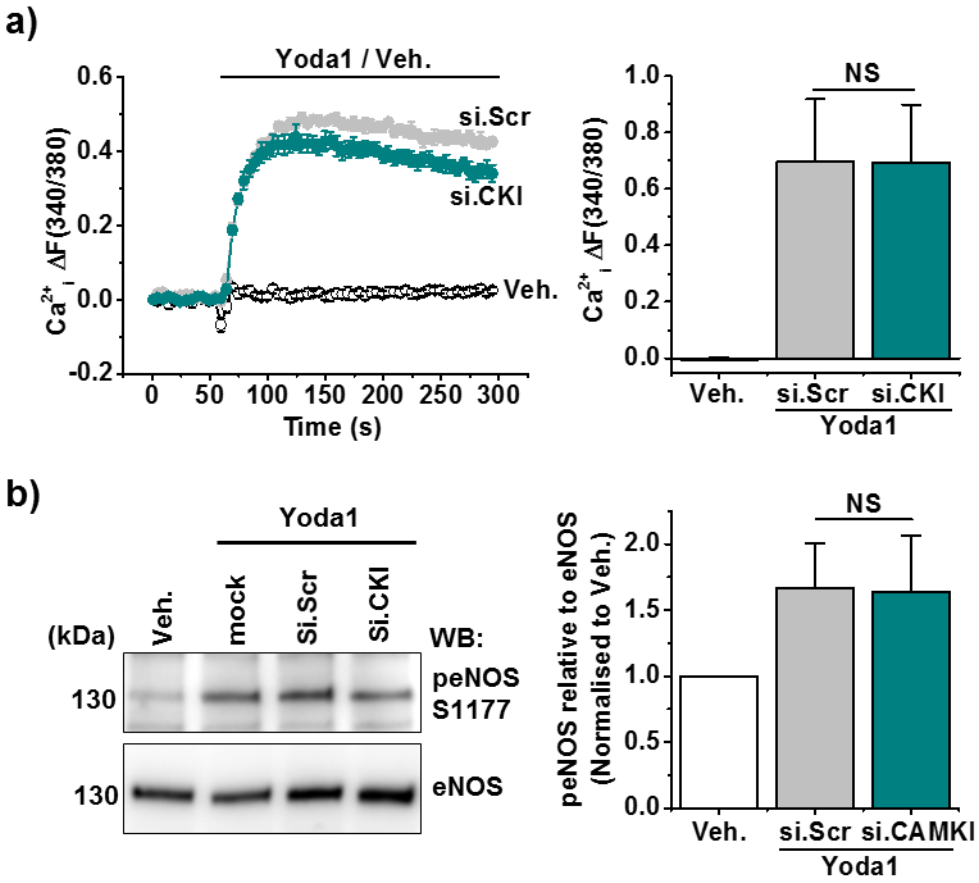

Figure 5.22 Genetic disruption of CaMKI mRNA expression does not affect Yoda1-evoked eNOS phosphorylation.

a) Left: example intracellular Ca^{2+} measurement trace in HUVECs during application of 2 μM Yoda1 or its vehicle (Veh.). Cells are treated with siRNA targeting CaMKI (si.CKI) or a scrambled sequence (si.Scr). Right: Mean data for the type of experiment shown on the left n/N=3/16 e) Left: Representative immunoblot for anti-S1177 phospho-eNOS and anti-eNOS in HUVECs with and without CaMKI genetic disruption treated for 1-minute with 2 μM Yoda1 or its vehicle (Veh.). Right: mean data from n=3 experiments displayed as phosphorylated eNOS relative to total eNOS (normalised to vehicle treatment).

5.7 Investigation into the involvement of PKC in Yoda1-evoked eNOS phosphorylation

As Yoda1-mediated eNOS phosphorylation was dependent on the presence of extracellular Ca^{2+} other Ca^{2+} dependent kinases were examined. PKC is reported to constitutively phosphorylate eNOS T495. PKC inhibitors attenuated the Ca^{2+} dependent phosphorylation of eNOS T495 evoked by bradykinin, suggesting a decrease in the binding of CaM to eNOS (Fleming et al., 2001; Matsubara et al., 2003). The role of PKC in S1177 phosphorylation is unclear. However, as it has been linked to Ca^{2+} evoked eNOS phosphorylation we chose to examine its role in Yoda1-mediated S1177 eNOS phosphorylation.

5.7.1 Chemical inhibition of PKC suppresses Yoda1-mediated S1177 eNOS phosphorylation

In order to examine the involvement of PKC, BIM, a chemical inhibitor of PKC activation was utilised. BIM is a published inhibitor of PKC suggested to inhibit all isoforms (Komander et al., 2004). HUVECs were pre-treated with 10 µM BIM for 30-minutes to inhibit PKC and Yoda1-mediated Piezo1 activity was examined. Intracellular Ca^{2+} measurements were taken during addition of Yoda1. Pre-treatment with BIM increased Yoda1-mediated Ca^{2+} entry and slightly increased basal Ca^{2+} levels compared to pre-treatment with its vehicle alone (Figure 5.23a). BIM is reported to negatively regulate Ca^{2+} release and Ca^{2+} entry which could explain the alterations to the Yoda1 response (Harper and Poole, 2011). Nevertheless, Yoda1-induced eNOS phosphorylation was examined after BIM pre-treatment. Interestingly, Yoda1-induced eNOS phosphorylation was attenuated after pre-treatment with BIM compared to its vehicle (Figure 5.23b). Even though BIM potentiated Yoda1-mediated Ca^{2+} entry it was able to suppress eNOS phosphorylation. The data suggest that a PKC is required for Yoda1-evoked eNOS phosphorylation.

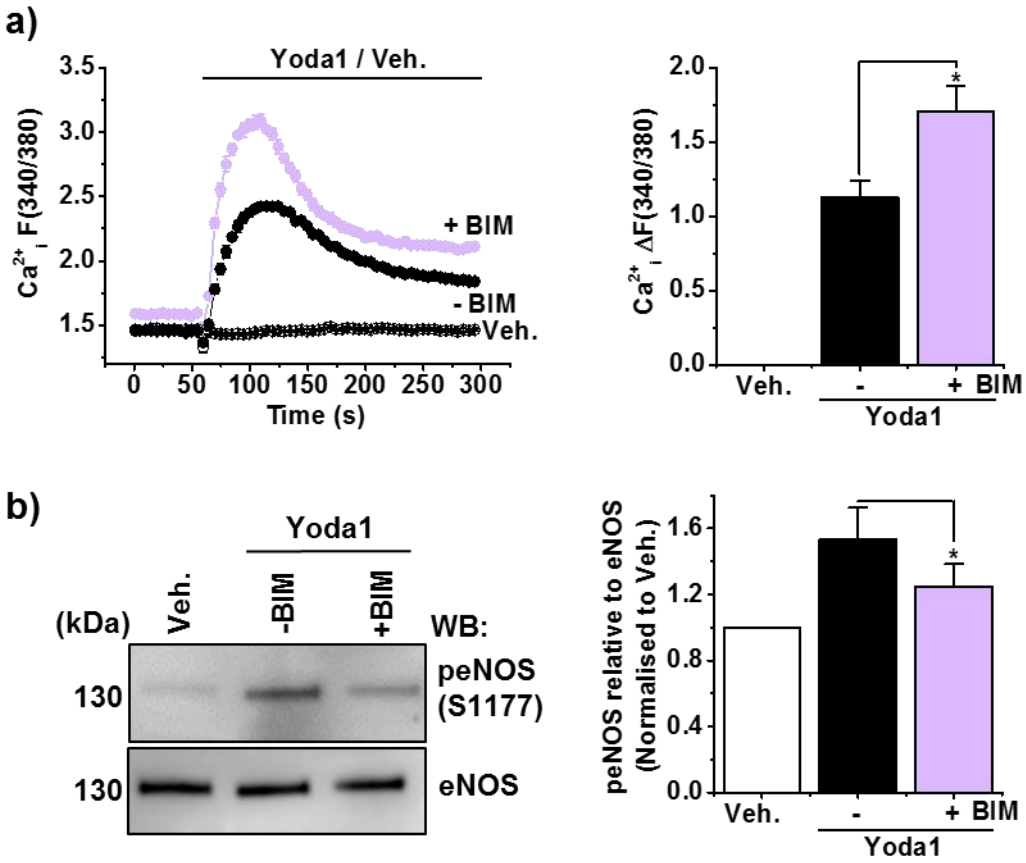

Figure 5.23 The general PKC inhibitor, BIM, inhibits Yoda1-evoked eNOS phosphorylation.

a) Left: example intracellular Ca^{2+} measurement trace in HUVECs during application of 2 µM Yoda1 or its vehicle (Veh.). Cells are pre-treated for 30-minutes with 10 µM BIM (+ BIM) or its vehicle (- BIM). Right: Mean data for the type of experiment shown on the left (n/N=3/14-15). b) Left: Representative immunoblot for anti-S1177 phospho-eNOS and anti-eNOS in HUVECs treated for 1-minute with 2 µM Yoda1 or its vehicle (Veh.). HUVECs were pre-treated as in a). Right: mean data from n=3 experiments displayed as phospho-eNOS relative to total eNOS normalised to vehicle treatment.

5.7.2 PKCα and PKCδ are highly expressed in HUVECs

As the generic PKC inhibitor, BIM, suppressed Yoda1-mediated eNOS phosphorylation the role of PKC was examined further. Firstly experiments to investigate mRNA expression levels of PKCα, ß, δ and γ isoforms were carried out. To test if the primers could amplify their target, *h*Brain mRNA was utilised. Indeed, primers for PKCα, ß, δ and γ amplified a product of the correct size (Figure 5.24a). mRNA expression of the PKC isoforms was examined in HUVECs. PKCα and δ were convincingly expressed in HUVECs (Figure 5.24b & c). The expression on PKCß and γ were very lowly expressed with the primers used (CT values 29 and 31 respectively), however they were detected explaining why there is a band on the gel (Figure 5.24b & c). Thus, the role of CaMKIIα and δ was examined in further detail.

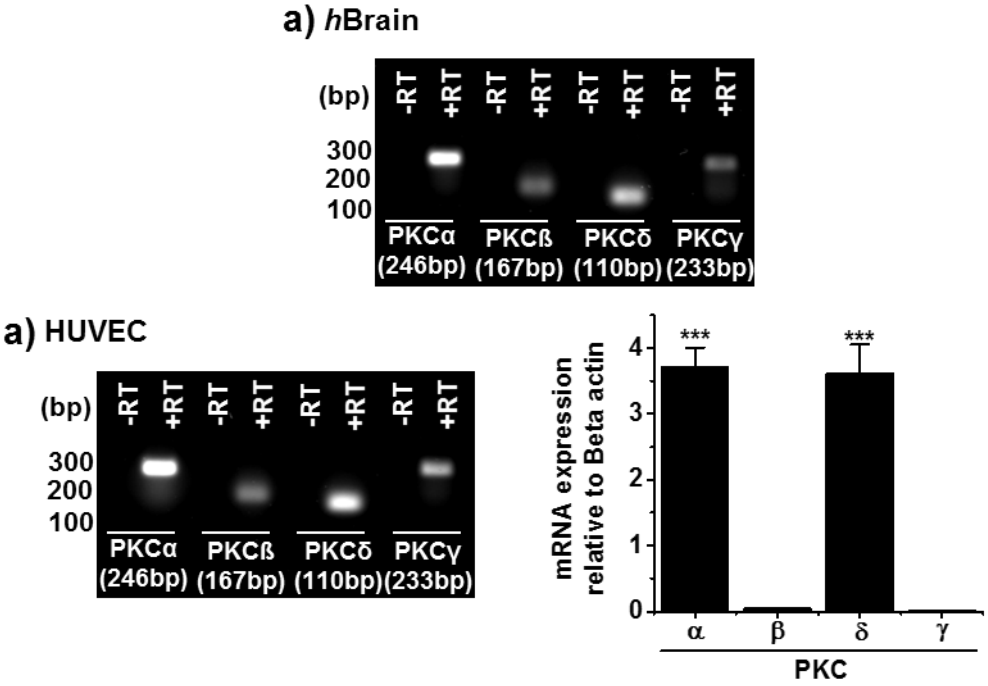

Figure 5.24 PKCα and PKCδ are highly expressed in HUVECs.

a) End-point PCR products obtained with PKCα, PKCß, PKCδ and PKCγ primers for human brain (*h*Brain) mRNA after reverse transcriptase reaction (+RT) or not (-RT) to generate cDNA. b) As in (a) but in HUVEC samples. c) Mean data and analysis from the type of experiment in (b) of PKCα, PKCß, PKCδ and PKCγ mRNA expression relative to beta actin (n=3). RT-qPCR performed by Fiona Bartoli.

5.7.3 Yoda1 phosphorylates eNOS independently of the Ca^{2+} sensitive PKC isoform, PKCα

In order to further examine the role of PKC in Yoda1-mediated eNOS phosphorylation siRNA genetic knockdown was utilised. As Yoda1 mediated Ca^{2+}-dependent eNOS phosphorylation the "classical" Ca^{2+}-dependent isoform of PKC that was convincingly expressed in HUVECs was examined, PKCα. siRNA targeting PKCα was used and RT-qPCR was performed to examine mRNA levels. End-point PCR reactions were run on a gel and this demonstrated that primers were able to specifically amplify mRNA of the correct size. Quantification confirms that treatment with PKCα siRNA knocked down PKCα mRNA expression by 87% compared to scrambled control (Figure 5.25). mRNA expression of Piezo1 was unchanged after PKCα knockdown however, PKCδ was also knocked down by 44% (Figure 5.25).

FlexStation experiments were performed to assess whether knocking down expression of PKCα mRNA affected the function of Piezo1. Unlike pre-treatment with the non-selective PKC inhibitor, BIM, knocking down PKCα mRNA had no effect on Yoda1-mediated Ca^{2+} entry in HUVECs compared to treatment with siRNA targeting a scrambled sequence (si.Scr) suggesting that this isoform is not involved in Piezo1 channel function (Figure 5.26a). Western blotting to examine Yoda1-mediated eNOS phosphorylation was performed. Yoda1-evoked eNOS phosphorylation was not affected by knocking down PKCα mRNA compared to HUVECs treated with a scrambled control siRNA (si.Scr) (Figure 5.26b-c). However, analysis of total eNOS expression (without Yoda1) revealed that knockdown of PKCα induced an increase in total eNOS expression (Figure 5.26d). Taken together, these data suggest that the classical Ca^{2+}-dependent PKC isoform, PKCα is not involved in Yoda-1 mediated eNOS phosphorylation. It is possible that PKCα negatively regulates eNOS expression but, nevertheless it does not mediate Yoda1-eNOS fast coupling. As BIM, the general PKC inhibitor, inhibited Yoda1-mediated Ca^{2+} entry, roles of other PKC isoforms have not yet been ruled out.

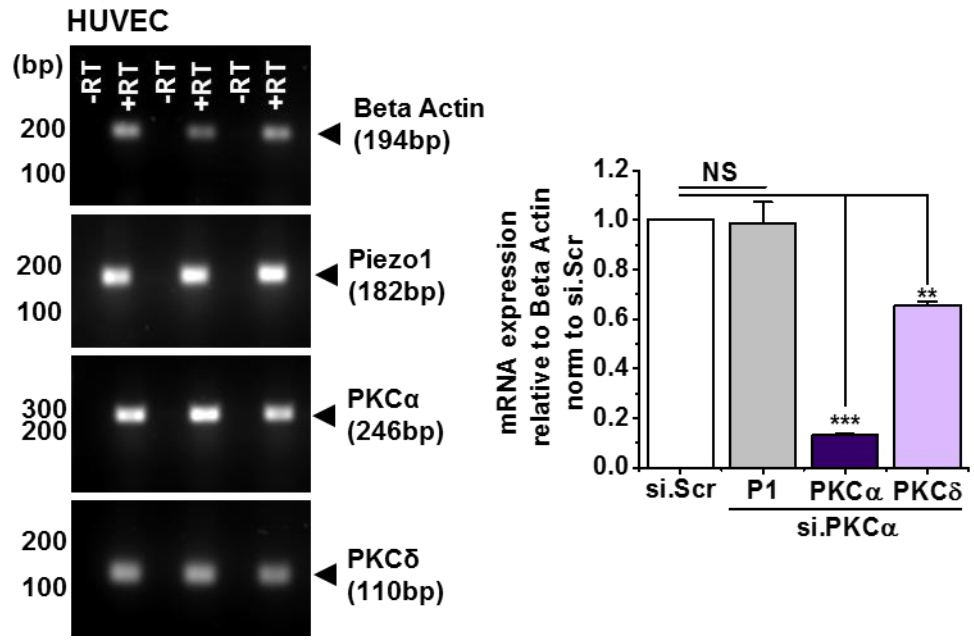

Figure 5.25 Genetic knockdown of PKCα mRNA does not affect Piezo1 expression.

Left: End-point PCR products obtained with primers for Beta actin, Piezo1, PKCα and PKCδ for HUVEC mRNA after reverse transcriptase reaction (+RT) or not (-RT) to generate cDNA. HUVECs were treated with a mock transfection (-siRNA), scrambled siRNA (si.Scr) or PKCα siRNA. Right: Mean data and analysis of Piezo1, PKCα and PKCδ mRNA relative to beta actin normalised to scrambled siRNA treated samples (n=3). RT-qPCR performed by Fiona Bartoli.

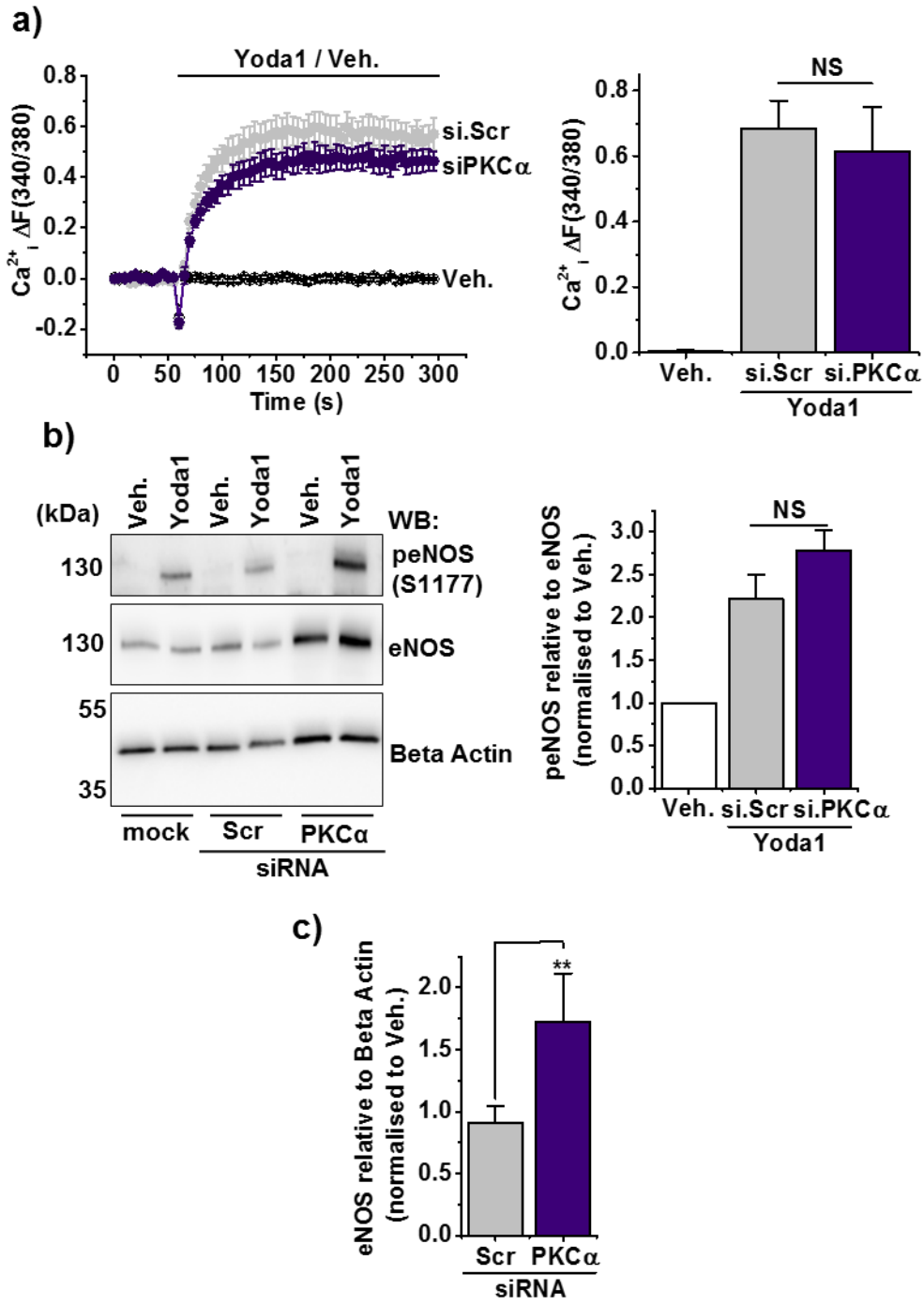

Figure 5.26 Yoda1-induced eNOS phosphorylation is independent of PKCα.

a) Left: example intracellular Ca^{2+} measurement trace in HUVECs during application of 2 μM Yoda1 or its vehicle (Veh.). Cells are treated with siRNA targeting PKCα or a control scrambled sequence (si.Scr). Right: Mean data for the type of experiment shown on the left n/N=3/18 b) Left: Representative immunoblot for anti-S1177 phospho-eNOS and anti-eNOS in HUVECs with and without PKCα genetic disruption treated for 1-minute with 2 μM Yoda1 or its vehicle (Veh.). Right: Mean data from n=6 experiments displayed as phosphorylated eNOS relative to total eNOS normalised to vehicle treatment. c) Mean data from n=6 experiments displayed as total eNOS relative to Beta Actin normalised to mock transfected cells.

5.7.4 Yoda1-mediated eNOS phosphorylation is dependent on the expression of PKCδ

PKCδ is a conventional/novel isoform of PKC that is reported to function independently of Ca^{2+}. PKCδ is highly expressed in HUVECs and is described to be important for Ca^{2+} independent VEGF induced von Willebrand factor release (Lorenzi et al., 2008). Interestingly, a functional interaction between PKCδ and Fyn is reported in human platelets and glioma cells (Crosby and Poole, 2003; Kronfeld et al., 2000). In glioma cells overexpression of dominant negative Fyn supressed PDGF tyrosine phosphorylation of PKCδ. Thus, PKCδ was an interesting kinase to investigate as data in (Figure 5.4 - Figure 5.6) suggest that Fyn is involved in the rapid coupling between Yoda1-activated Piezo1 and eNOS.

PKCδ was knocked down in HUVECs using siRNA and the effect of this on Yoda1-induced eNOS phosphorylation was examined. Firstly to assess whether siRNA targeting PKCδ was able to effectively knockdown its mRNA expression, RT-qPCR was used. To examine whether the primers designed to amplify PKCδ were able to specifically amplify a product of the correct size PCR end-products were run on a gel. Primers for PKCα, PKCδ, Piezo1 and Beta Actin were able to amplify products of the correct size in HUVECs (Figure 5.27). Quantification revealed that PKCδ siRNA was able to decrease the mRNA expression of PKCδ by 85% compared to cells treated with siRNA targeting a scrambled control sequence (si.Scr) (Figure 5.27). PKCδ mRNA knockdown did not affect the expression of Piezo1 but did however knock down PKCα by 32 % (Figure 5.27).

FlexStation experiments were performed on HUVECs with and without PKCδ genetic disruption to asses Yoda1-medaited Piezo1 channel function. Yoda1 evoked Ca^{2+} entry was not affected by PKCδ mRNA knockdown and this response was similar to cells treated with siRNA targeting a scrambled sequence (si.Scr) (Figure 5.28a). Examination of Yoda1-evoked eNOS phosphorylation established that the Yoda1-evoked eNOS phosphorylation was dramatically attenuated after PKCδ mRNA knockdown (si.PCKδ) compared to cells expressing PKCδ (si.Scr) (Figure 5.28b). Excitingly, for the first time we demonstrate that Yoda1-evoked eNOS phosphorylation is mediated via a PKCδ regulated signalling pathway.

In order to further test the involvement of PKCδ rottlerin, a specific PKCδ chemical inhibitor was examined. Rottlerin is able to differentiate between PKC isoforms and is at least 10-fold more potent at blocking PKCδ (EC_{50} 3-6 μM) compared to other isoforms (Gschwendt et al., 1994). 30-minute pre-treatment of HUVECs with 10 μM rottlerin suppressed Yoda1 mediated Ca^{2+} entry suggesting that it inhibits the function of Piezo1 itself (Figure 5.29a). As rottlerin inhibits Yoda1-mediated Piezo1 activation we did not use it in further experiments. It would be unclear if the effect of rottlerin was specific to PKCδ or due to a direct effect on Piezo1 channel function. The effect of two more siRNAs targeting two different sequences on PKCδ was examined and treatment of HUVECs with both siRNA sequences affected Piezo1 function. Knockdown of PKCδ using siRNA #2 blunted Yoda1 mediated Ca^{2+} entry whereas, treatment with siRNA #3 potentiated it (Figure 5.29b & c). PKCδ appears to be somewhat difficult to study due to the off target effect of the inhibitory tools. The data suggest that PKCδ mediates Yoda1-evoked eNOS phosphorylation. However, more work is needed to validate this finding.

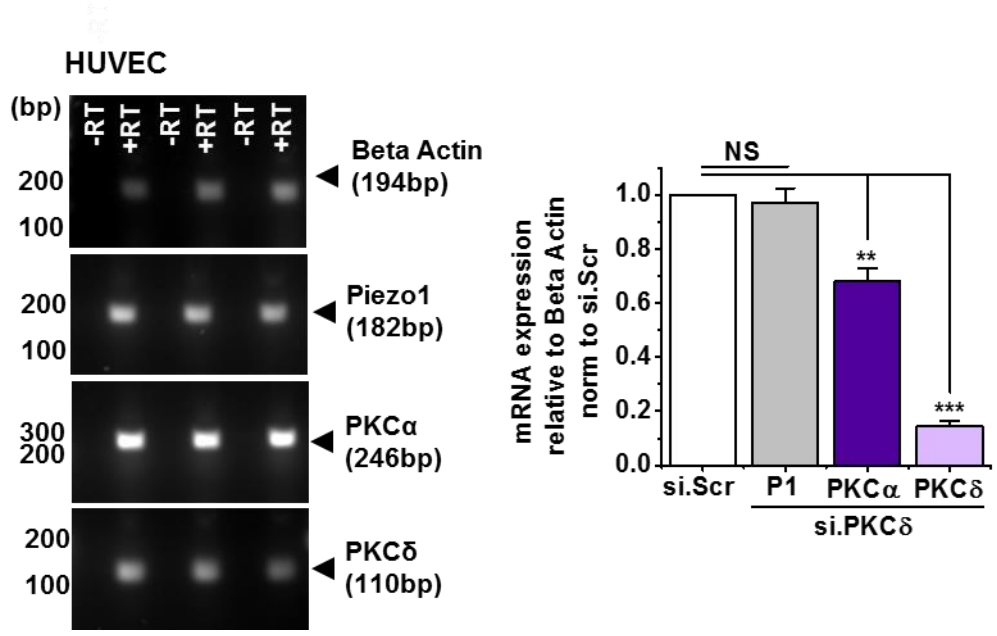

Figure 5.27 Genetic knockdown of PKCδ mRNA does not affect Piezo1 expression.

Left: End-point PCR products obtained with primers for Beta actin, Piezo1, PKCα and PKCδ for HUVEC mRNA after reverse transcriptase reaction (+RT) or not (-RT) to generate cDNA. HUVECs were treated with a mock transfection (-siRNA), scrambled siRNA (si.Scr) or PKCδ siRNA. Right: Mean data and analysis of Piezo1, PKCα and PKCδ mRNA relative to beta actin normalised to scrambled siRNA treated samples (n=3). RT-qPCR performed by Fiona Bartoli.

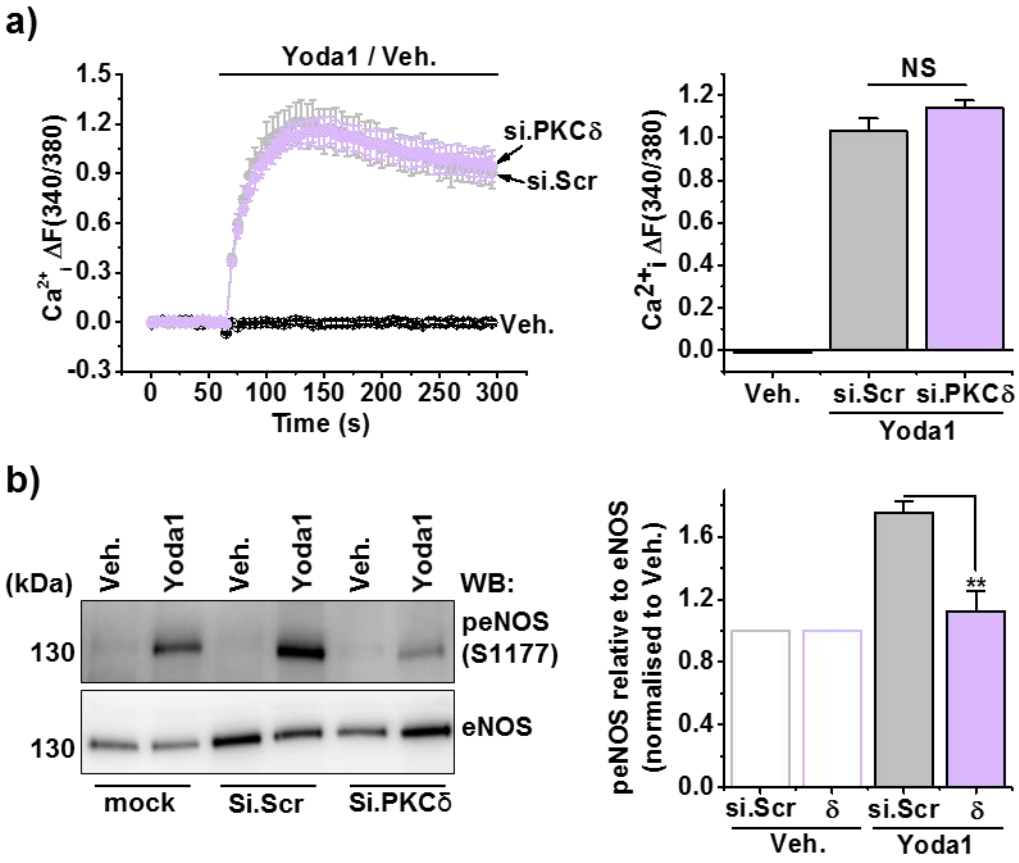

Figure 5.28 Genetic knockdown of PKCδ mRNA attenuates Yoda1-mediated eNOS phosphorylation.

a) Left: example intracellular Ca^{2+} measurement trace in HUVECs during application of 2 μM Yoda1 or its vehicle (Veh.). Cells are treated with siRNA targeting PKCδ (si.PKCδ) or a control scrambled sequence (si.Scr). Right: Mean data for the type of experiment shown on the left n/N=3/18 b) Left: Representative immunoblot for anti-S1177 phospho-eNOS and anti-eNOS in HUVECs with and without PKCδ genetic disruption treated for 1-minute with 2 μM Yoda1 or its vehicle (Veh.). Right: mean data from n=3 experiments displayed as phosphorylated eNOS relative to total eNOS (normalised to vehicle treatment).

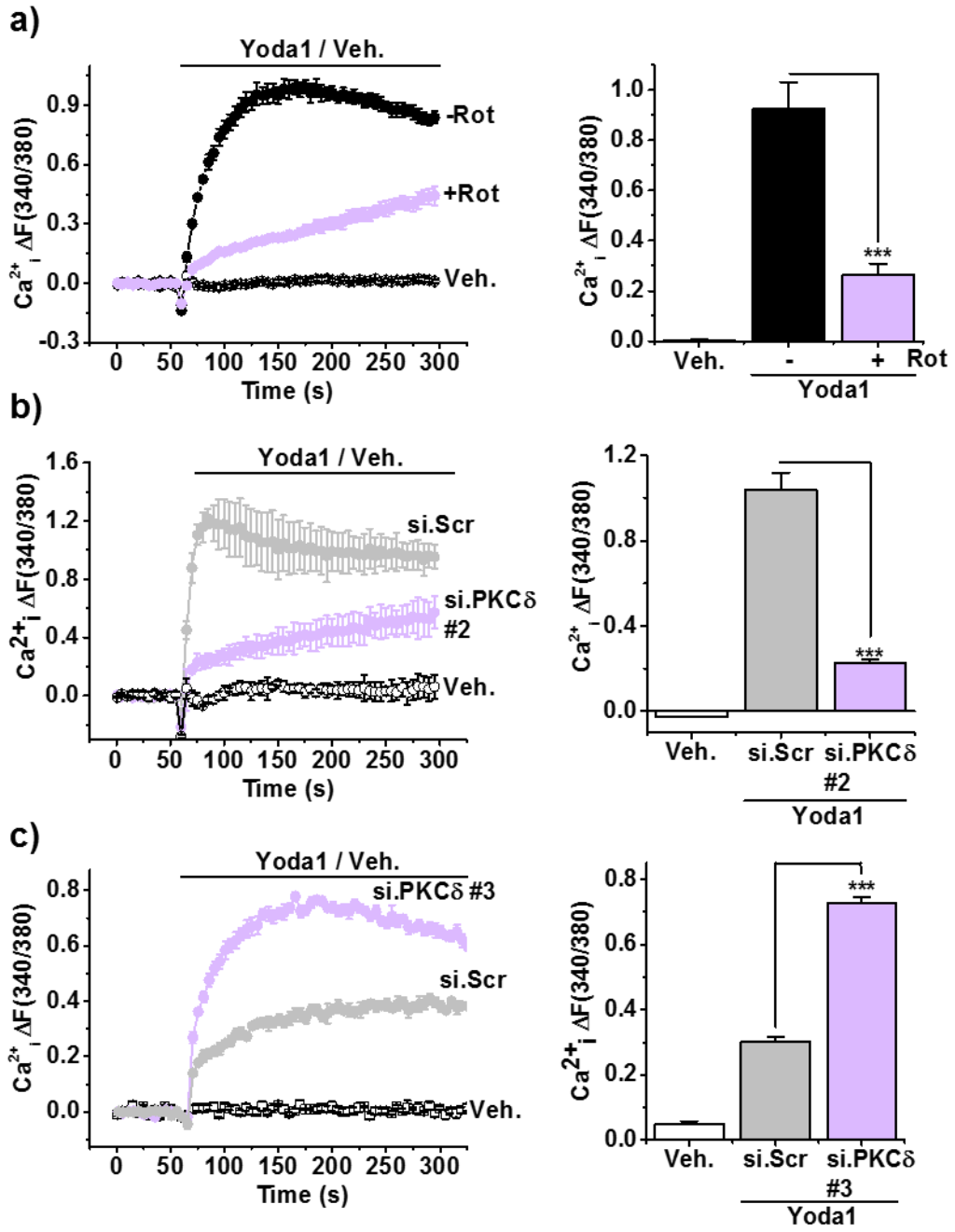

Figure 5.29 Chemical blockage or siRNA targeting PKCδ modulates Yoda1-mediated Piezo1 channel activity.

a) Left: example intracellular Ca^{2+} measurement trace in HUVECs during application of 2 μM Yoda1 or its vehicle (Veh.). Cells are pre-treated with 10 μM rottlerin or its vehicle (Veh.) for 30-minutes prior to Yoda1 addition. Right: Mean data for the type of experiment shown on the left n/N=3/20. b) as in a) but in HUVECs treated with siRNA targeting PKCδ (si.PKCδ #2) or a scrambled control sequence (si.Scr) (n/N=3/12-15). c) as in a) but in HUVECs treated with siRNA targeting a different PKCδ sequence (si.PKCδ #3) or a scrambled control sequence (si.Scr) (n/N=3/12) Experiment performed by Dr Marjolaine Debant (University of Leeds).

5.8 Yoda1 evokes eNOS phosphorylation independently of Ras proteins

Throughout this chapter candidate kinases were focused upon. Finally, investigation into the role of both HRas and RRas was sought. HRas has been reported to mediate VEGF-induced eNOS phosphorylation (Haeussler et al., 2013). Genetic disruption of HRas in human aortic endothelial cells blocked VEGF induced PI3K-dependent AKT and S1177 eNOS phosphorylation and NO dependent cell migration. Interestingly, Piezo1-eNOS studies demonstrated that VEGF-evoked eNOS phosphorylation was Piezo1 dependent (Li et al., 2014). Thus, HRas was an interesting candidate to examine. In order to investigate the role of HRas in Yoda1-mediated eNOS phosphorylation HRas siRNA was used to knockdown its expression. In HUVECs siRNA targeted to HRas effectively knocked down HRas protein expression by 77% compared to those treated with scrambled siRNA (si.Scr) (Figure 5.30a). HRas knockdown had no effect on Yoda1-mediated Ca^{2+} entry in HUVECs (Figure 5.30b). Similarly, HRas knockdown had no effect on Yoda1-mediated eNOS phosphorylation (Figure 5.30c). The data suggest that HRas is not involved in this mechanism.

The role of RRas in Yoda1-evoked eNOS phosphorylation was also examined. Even though RRas has not been linked to eNOS in the literature it is important to note that Fam38A (Piezo1) has been reported to mediate RRas recruitment to the ER leading to integrin activation (McHugh et al., 2010). In order to investigate whether RRas activation leads to Yoda1 evoked eNOS phosphorylation RRas was knocked down in HUVECs. Knockdown of RRas protein by 83% compared to the scrambled control (Figure 5.31a) had no effect on Yoda1 evoked Ca^{2+} entry (Figure 5.31b) or eNOS phosphorylation (Figure 5.31c). These data suggest that Yoda1 evokes eNOS phosphorylation independently of HRas and RRas.

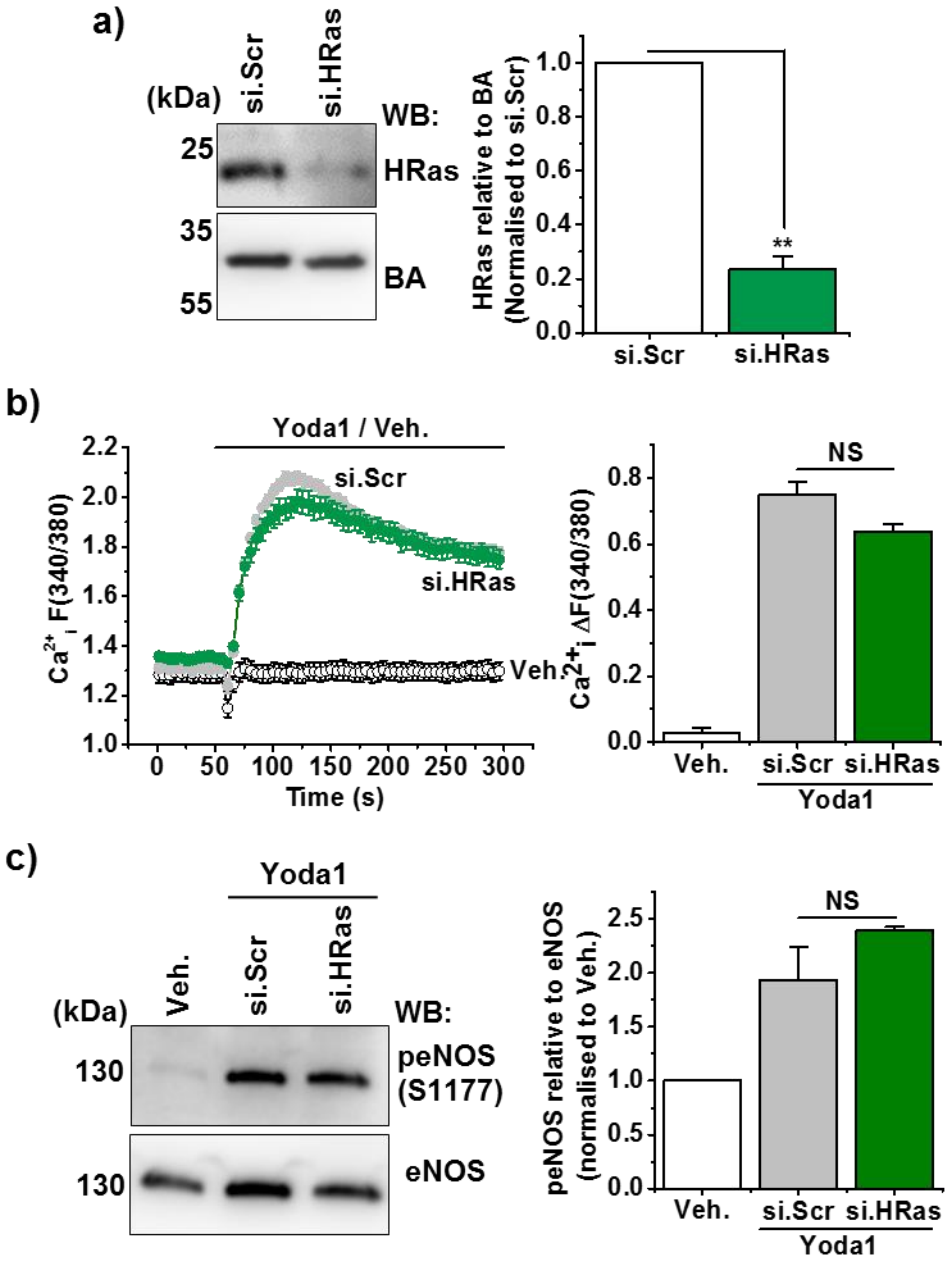

Figure 5.30 Knocking down HRas has no effect on Yoda1-evoked Piezo1 activation and eNOS phosphorylation.

a) Left: Representative immunoblot for anti-HRas and anti-beta actin in HUVECs treated with siRNA targeting HRas (si.HRas) or a scrambled control (si.Scr). Right: Mean data from n=3 experiments displayed as HRas relative to Beta actin (normalised to si.Scr). b) Left: example intracellular Ca^{2+} measurement trace in HUVECs during application of 2 µM Yoda1 or its vehicle (Veh.). Cells are treated with siRNA targeting HRas or a scrambled sequence. Right: Mean data for the type of experiment shown on the left n/N=3/17-18. c) Left: Representative immunoblot for anti-S1177 phospho-eNOS and anti-eNOS in HUVECs treated with siRNA targeting HRas or a scrambled control (si.Scr). Cells are treated for 1-minute with 2 µM Yoda1 or its vehicle (Veh.). Right: Mean data from n=3 experiments displayed as phospho-eNOS relative to eNOS (Normalised to vehicle treated cells).

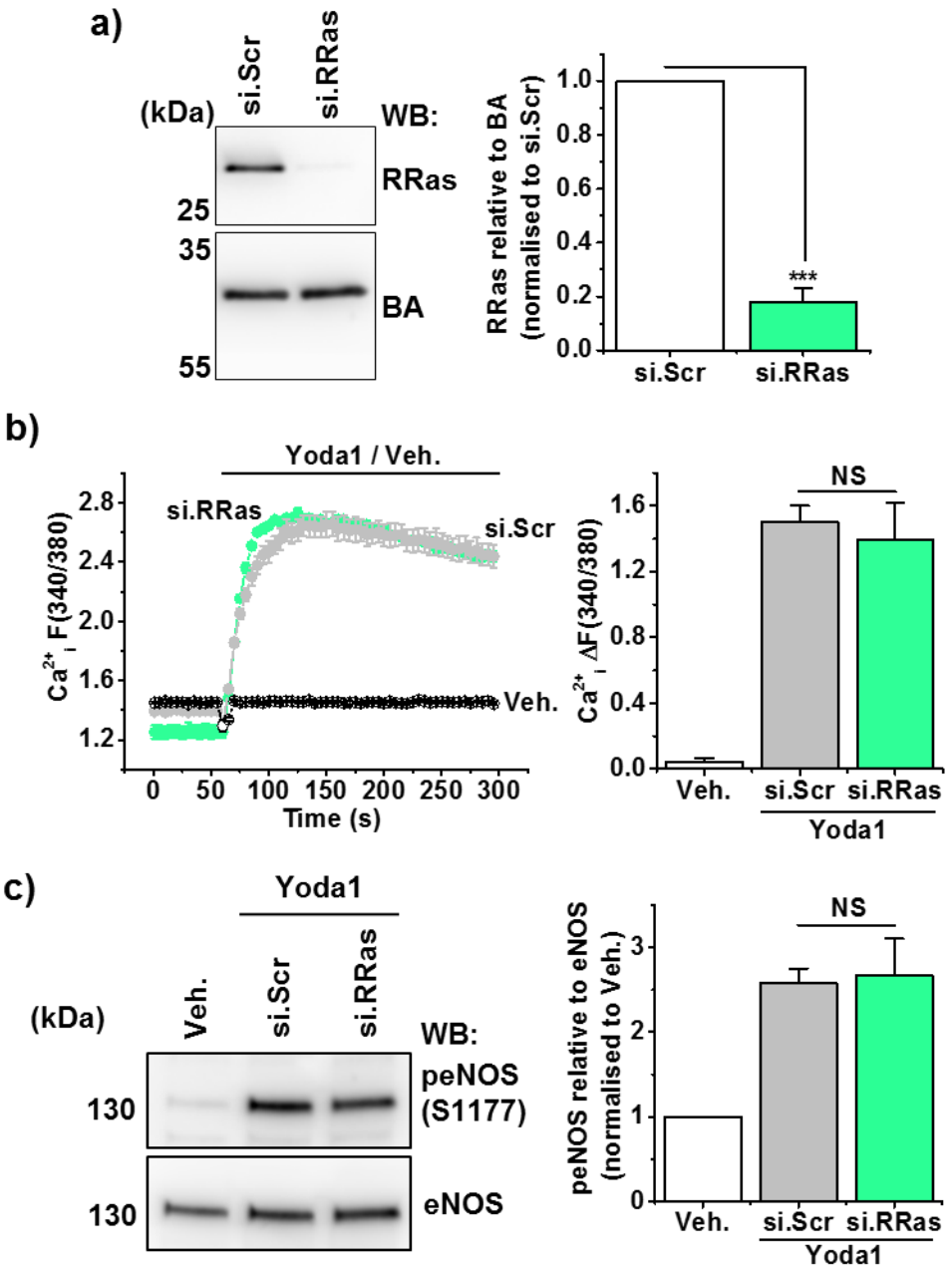

Figure 5.31 Knocking down RRas has no effect on Yoda1 evoked Piezo1 activation and eNOS phosphorylation.

a) Left: Representative immunoblot for anti-RRas and anti-beta actin in HUVECs treated with siRNA targeting RRas (si.RRas) or a scrambled control (si.Scr). Right: Mean data from n=3 experiments displayed as RRas relative to Beta actin (normalised to si.Scr). b) Left: example intracellular Ca^{2+} measurement trace in HUVECs during application of 2 µM Yoda1 or its vehicle (Veh.). Cells are treated with siRNA targeting RRas or a scrambled sequence. Right: Mean data for the type of experiment shown on the left n/N=3/17-18. c) Left: Representative immunoblot for anti-S1177 phospho-eNOS and anti-eNOS in HUVECs treated with siRNA targeting RRas or a scrambled control (si.Scr). Cells are treated for 1-minute with 2 µM Yoda1 or its vehicle (Veh.). Right: Mean data from n=3 experiments displayed as phospho-eNOS relative to eNOS (Normalised to vehicle treated cells).

5.9 Piezo1 activity is independent of Fyn kinase and PKCδ

Data so far suggest that among the candidate kinases and proteins screened, Fyn kinase and PKCδ are mediating Yoda1-evoked eNOS phosphorylation. It is clear that knocking down Fyn and PKCδ mRNA does not affect Yoda1-mediated Piezo1 channel activation as a measure of changes in intracellular Ca^{2+} levels. However, it is unknown whether their knockdown affects more physiological activation and functions of Piezo1. Next, hypotonicity-evoked Ca^{2+} signals were examined in HUVECs after mRNA knockdown of Fyn kinase and PKCδ as a more physiological method of measuring Piezo1 activation. Moreover, alignment assays were carried out to examine whether Fyn and PKCδ are involved in the mechanism behind Piezo1-mediated alignment or if their role is exclusive to eNOS phosphorylation.

5.9.1 Hypotonicity-evoked Ca^{2+} signals are independent of Fyn kinase and PKCδ

In the previous chapter an assay examining Piezo1-mediated hypotonicity-evoked Ca^{2+} signals was validated. Next, Ca^{2+} responses evoked by application of increasingly hypotonic solutions were examined with (si.Fyn) and without (si.Scr) Fyn mRNA knockdown. These experiments were carried out alongside the experiments in the previous chapter so the control scrambled siRNA response was common to all experiments but they are displayed separately for clarity. This was taken into account during the statistical analysis. Fyn mRNA knockdown had no effect on hypotonicity-evoked Ca^{2+} signals in HUVECs (Figure 5.32a). The EC_{50} of the response was unchanged with or without Fyn mRNA knockdown (93.27 mM and 86.67 mM mannitol respectively) and similarly the gradient of the slope of the hill curve was unchanged (Figure 5.32b - d).

Similar to data with Fyn knockdown, PKCδ mRNA knockdown (si.PKCδ) does not affect hypotonicity-induced Ca^{2+} signals in HUVECs. Amplitudes of the responses are comparable with and without PKCδ mRNA knockdown (Figure 5.33a). Moreover, EC_{50} values of the dose-response curve were unchanged with (88.20 mM) or without (86.67 mM) PKCδ mRNA knockdown and the gradient of the Hill slopes were comparable (Figure 5.33b-d). Taken together, these data suggest that even though Fyn and PKCδ are crucial for the integrity of Yoda1-mediated eNOS

phosphorylation they are not involved in Piezo1 channel activation evoked by hypotonicity.

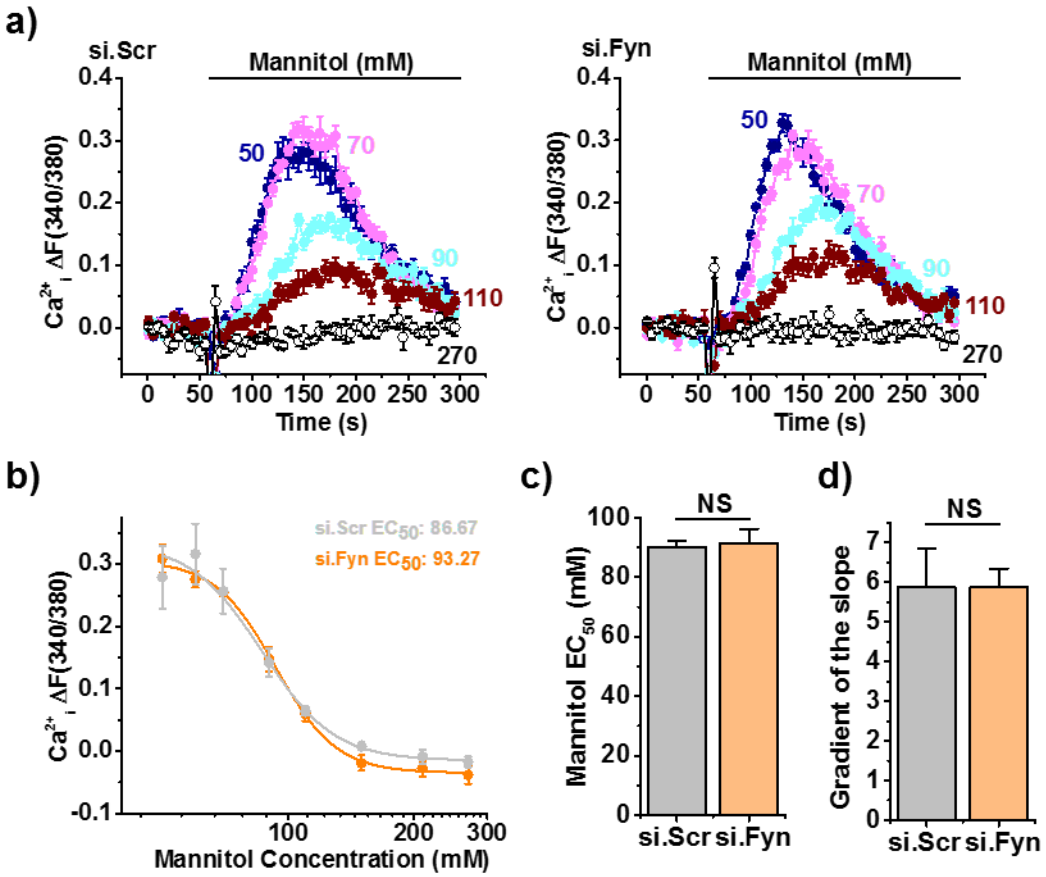

Figure 5.32 Fyn kinase RNAi does not affect hypotonicity-evoked cation channel activation.

a) Example intracellular Ca^{2+} measurement traces in HUVECs during application of varying mannitol concentrations (50-270 mM). Left: in cells treated with siRNA targeting a scrambled control sequence (si.Scr). Right: in cells treated with siRNA targeting Fyn (si.Fyn). (n/N=4/16). b) Concentration-response data for mannitol from the type of experiments in a) (n=4). The fitted curve is a hill equation indicating the 50% maximum effect (EC_{50}) at 86.67 mM and 93.27 mM mannitol with and without Fyn expression respectively. c) Mean data for the type of experiment shown in b) mean is an average of EC_{50}'s from individual repeats n=4. d) Mean data for the type of experiment shown in b) mean is an average of the gradient of the curves (n=4).

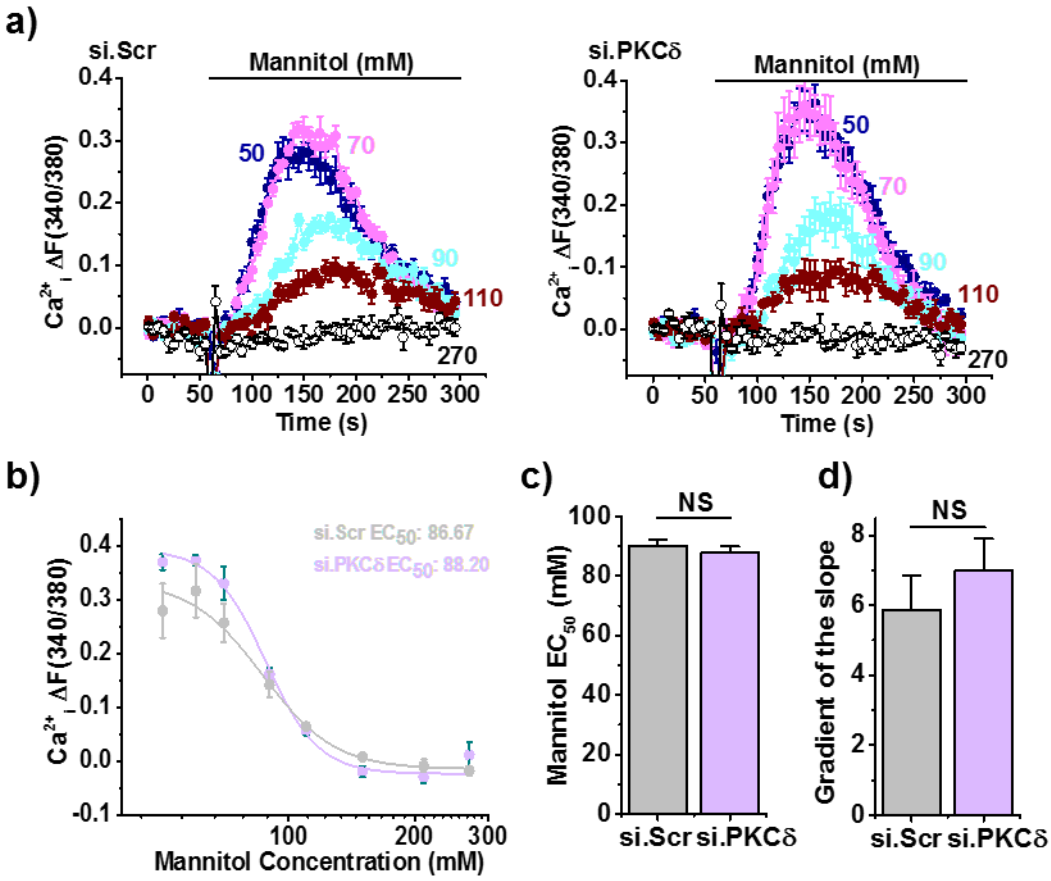

Figure 5.33 Figure 5.33 RNAi targeting PKCδ does not affect hypotonicity-evoked cation channel activation.

a) Example intracellular Ca^{2+} measurement traces in HUVECs during application of varying mannitol concentrations (50-270 mM). Left: in cells treated with siRNA targeting a scrambled control sequence (si.Scr). Right: in cells treated with siRNA targeting PKCδ (si. PKCδ). (n/N=4/16). b) Concentration-response data for mannitol from the type of experiments in (a) (n=4). The fitted curve is a hill equation indicating the 50% maximum effect (EC_{50}) at 86.67 mM and 88.20 mM mannitol with and without PKCδ expression respectively. c) Mean data for the type of experiment shown in (b) mean is an average of EC_{50}'s from individual repeats n=4. d) Mean data for the type of experiment shown in (b) mean is an average of the gradient of the curves (n=4).

5.9.2 Fyn kinase and PKCδ are not involved in alignment of endothelial cells

Endothelial cells align in the direction of laminar flow, and this is important for their function and maintenance of a healthy vasculature. It is widely reported that Piezo1 mediates endothelial alignment and work from our lab demonstrates that this is mediated by a pathway involving Piezo1-mediated Ca^{2+} entry and calpain activation (Li et al., 2014). Mice with systemic or heterozygote knockdown of Piezo1 present with disorganised endothelial structure. It is clear that Fyn and PKCδ are important for Piezo1-mediated phosphorylation of eNOS but it remains unknown if they mediate any other physiological Piezo1-mediated effects.

Alignment of HUVECs was examined after knockdown of Fyn kinase and PKCδ. 24 hours of 10 $dyn.cm^{-2}$ flow using the orbital shaker induced alignment of HUVECs in the direction of flow compared to static treated cells (Figure 5.34a-c). After treatment with siRNA to knockdown Fyn mRNA expression (si.Fyn) HUVECs were still able to align in the direction of flow compared to cells treated with a scrambled control siRNA (si.Scr) (Figure 5.34a-c). Similarly, knockdown of PKCδ mRNA expression (si.PKCδ) also had no effect on alignment of HUVECs compared to cells treated with a scrambled control (Figure 5.35). Taken together these data suggest that even though Fyn and PKCδ mediate Piezo1-evoked eNOS phosphorylation they are not involved in alignment. These data are in keeping with a previously published report from our group where eNOS siRNA had no effect on alignment of HUVECs (Li et al., 2014). In physiology Piezo1 channels are able to signal independently of both kinases to promote endothelial cell alignment.

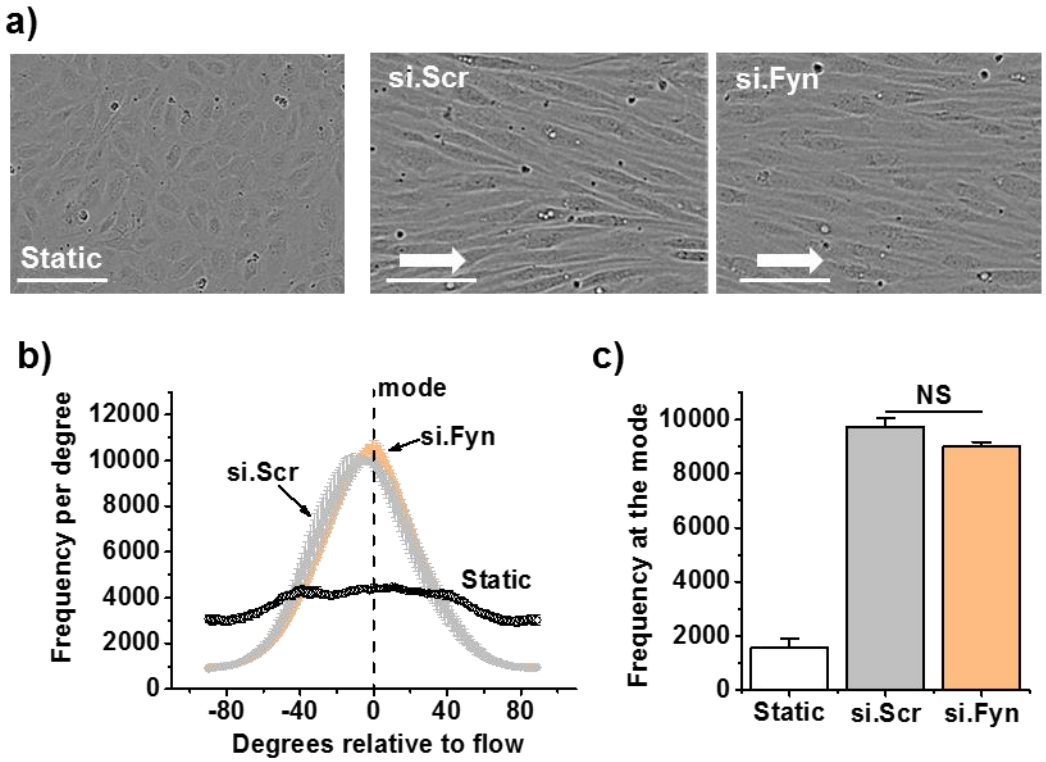

Figure 5.34 Fyn RNAi does not affect alignment of human endothelial cells.

a) Example phase contrast images of HUVECs subjected to 10 dyn.cm^{-2} shear stress for 24-hours or not (static). HUVECs are treated with siRNA targeting Fyn (si.Fyn) or a scrambled control sequence (si.Scr). Scale bar: 100 µm. b) Mean distribution from the type of data in (a) of alignment of HUVECs after exposure to 24-hours shear stress. Average alignment of HUVECs from the type of experiments in (a). Alignment was measured by the height of the peak at the mode of the Gaussian distribution curve. n=3 with N=3 images used for analysis per well. c) Average height of the Gaussian distribution from the type of experiments in (a) and (b) (n=3).

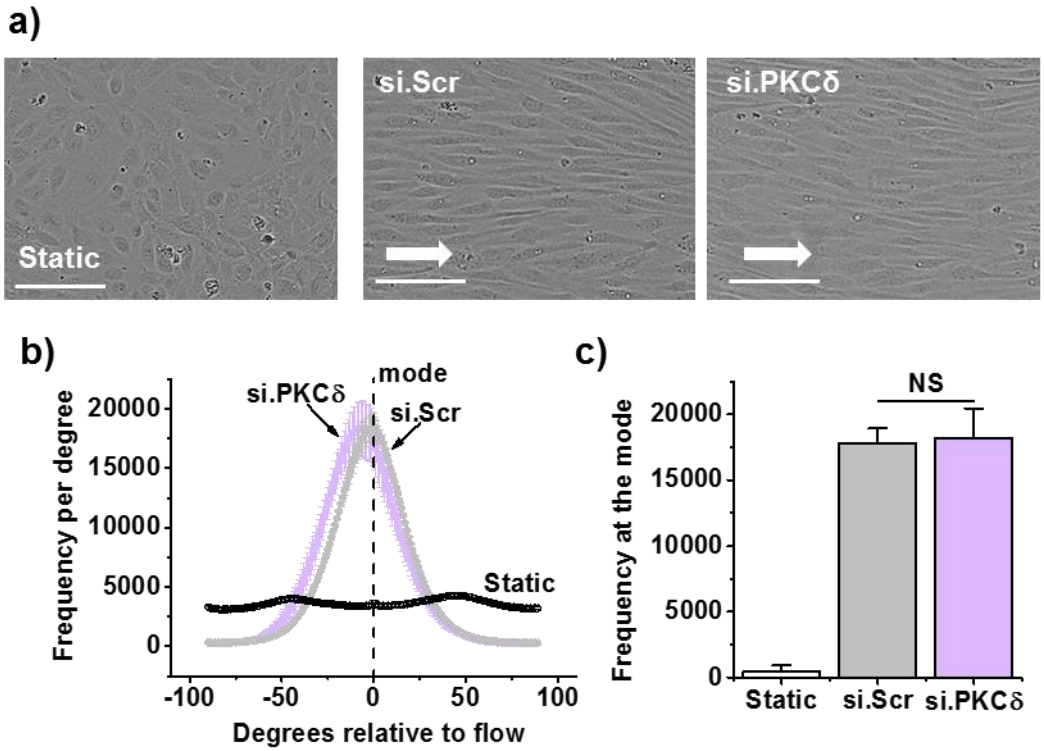

Figure 5.35 PKCδ RNAi does not affect alignment of human endothelial cells.

a) Example phase contrast images of HUVECs subjected to 10 dyn.cm^{-2} shear stress for 24-hours or not (static). HUVECs are treated with siRNA targeting PKCδ (si.PKCδ) or a scrambled control sequence (si.Scr). Scale bar: 100 μm. b) Mean distribution from the type of data in (a) of alignment of HUVECs after exposure to 24-hours shear stress. Average alignment of HUVECs from the type of experiments in (a). Alignment was measured by the height of the peak at the mode of the Gaussian distribution curve. n=3 with N=3 images used for analysis per well. c) Average height of the Gaussian distribution from the type of experiments in (a) and (b) (n=3).

5.10 Fyn kinase dissociates from Piezo1 upon application of Yoda1

In order to unravel the mechanism by which Fyn kinase mediates Yoda1-induced eNOS phosphorylation pull down experiments investigating the relationship between Piezo1 and Fyn were carried out. HEK 293 cells were co-transfected with Piezo1-mTurquoise2 (Piezo1mT) or its control (untagged Piezo1) and Fyn kinase. GFP Trap beads were used that bind to mTurquoise2 and expression of Piezo1 and Fyn were examined using western blotting. Input western blots demonstrate that Fyn and Piezo1 were both transfected (Figure 5.36a). GFP Trap beads were able to pull down Piezo1-mTurquoise2 but not the untagged version of Piezo1. There was slight non-specific binding of Fyn to the GFP trap beads as a faint band is present when Piezo1 is not pulled down (Figure 5.36a). However, this band was substantially stronger after pull down of Piezo1-mTurquoise2 suggesting that Fyn and Piezo1 interact when overexpressed in HEK 293 cells.

Src homology 3 (SH3) domains, an approximately 50 amino acid region present in various proteins, are reported to mediate protein-protein interactions involved in signal transduction (Mayer and Baltimore, 1993). Fyn contains an SH3 domain and alterations to this motif are reported to disrupt its binding to other proteins (Yamada and Bastie, 2014; Zamora-Leon et al., 2001). A plasmid expressing Fyn with a deleted SH3 domain was examined (Fyn∆). Piezo1 was still able to interact with Fyn∆ suggesting that its SH3 is not important for its interaction with Piezo1 (Figure 5.36a).

Next, cells were treated with Yoda1 to examine whether Piezo1 activation affects this interaction. Interestingly this treatment evoked a dissociation of Fyn and Fyn∆ from Piezo1. Piezo1-mTurquoise2 was still pulled down but Fyn was not present (Figure 5.36b). Taken together, these pilot data suggest that Fyn and Piezo1 interact and that treatment with Yoda1 provokes a dissociation of this interaction. More work is needed to examine this phenomenon.

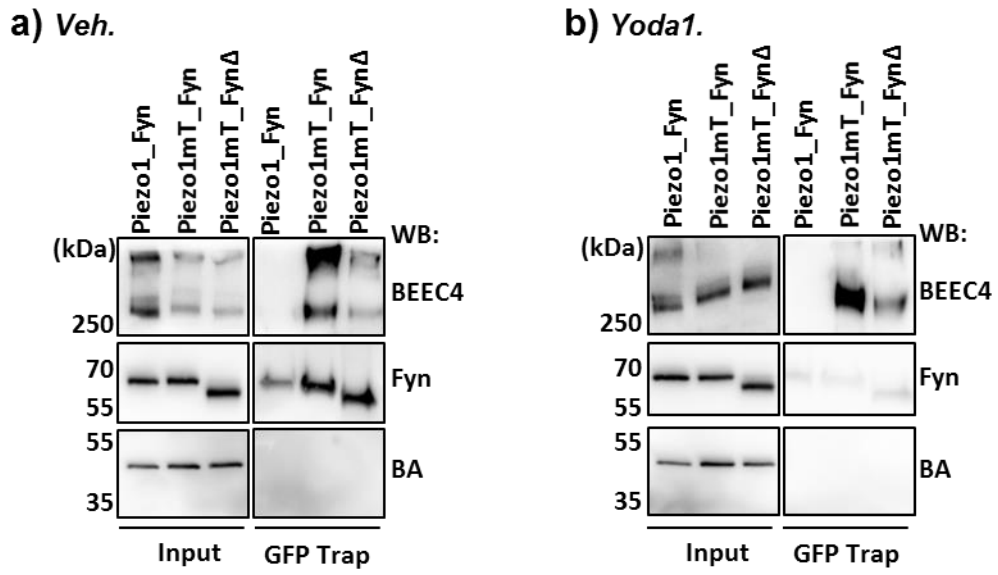

Figure 5.36 Fyn kinase interacts with Piezo1 and dissociates from Piezo1 upon application of Yoda1.

a) Representative immunoblot for anti-BEEC4 (Piezo1), anti-Fyn and anti-beta actin (BA). HEK cells were co-transfected with Fyn and Piezo1, Fyn and Piezo1-mTurquoise2 (mT) and Fyn with a deleted SH3 domain (FynΔ) and Piezo1mT. Input represents total lysate and a GFP trap was performed to pull down the mT tag on Piezo1. b) as in (a) but after treatment with 2 µM Yoda1 for 1-minute.

5.9 Discussion

This chapter focused on unravelling the kinase, or kinases, involved in the rapid tight coupling of Yoda1-activated Piezo1 to S1177 eNOS phosphorylation. A range of candidate kinases were screened and their role in Yoda1-mediated eNOS phosphorylation was examined. Even though it is widely reported that shear stress-mediated S1177 eNOS phosphorylation is dependent on AKT, PKA and AMPK, Yoda1 evoked phosphorylation of eNOS independently of these kinases, but dependently on PKCδ and Fyn. Over-expression studies demonstrated that Fyn interacts with Piezo1 and that treatment with Yoda1 evokes a dissociation of this interaction. Investigation into the role of extracellular Ca^{2+} suggested that Yoda1-mediated eNOS phosphorylation was Ca^{2+} dependent. CaMKII is classically reported to mediate Ca^{2+} dependent eNOS phosphorylation and when the CaMKII inhibitor, KN93, was used it attenuated Yoda1-mediated eNOS phosphorylation. However, experiments utilising siRNA targeting CaMKIIδ and γ did not support a role for them in this pathway. Furthermore, the classical Ca^{2+} regulated PKC isoforms (α, ß and γ) were also not involved. However, further investigation into PKC revealed that Yoda-mediated eNOS phosphorylation was dependent on PKCδ. RNAi targeting PKCδ and Fyn did not affect Yoda1 or hypotonicity induced Ca^{2+} signals or alignment of endothelial cells. The data suggest that Yoda1-mediated eNOS phosphorylation was dependent on both Fyn and PKCδ. However, it remains unclear how these kinases link to Ca^{2+}, the CD31/VE-Cadherin members of the triad and eNOS itself.

Fyn is a member of the Src family of kinases and is a member of the protein-tyrosine kinase oncogene family that typically codes for proteins that regulate cell growth. In this chapter we demonstrate that treatment with two different siRNAs targeting Fyn attenuated Yoda1-mediated eNOS phosphorylation without affecting Piezo1 expression or function. Fyn knockdown had no effect on hypotonicity induced Ca^{2+} signals or alignment of endothelial cells. Interestingly, shear stress is reported to mediate Src (Y416) phosphorylation that is dependent on the expression of Piezo1 (Wang et al., 2016). In the same study it was also reported that Piezo1 mediated shear stress evoked tyrosine phosphorylation of CD31. It would be surprising that Fyn could phosphorylate S1177 on eNOS directly. Data in Chapter 3 suggested that Yoda1 does not evoke tyrosine 657 phosphorylation on

eNOS (Figure 3.23). Thus, it seems reasonable to assume that Fyn phosphorylates a protein upstream of eNOS.

An interesting study suggested that stretch- and flow-induced tyrosine phosphorylation of CD31 was dependent on Fyn expression (Chiu et al., 2008). Knockdown of Fyn, but not Src or Yes, suppressed stretch- and flow- elicited CD31 phosphorylation in BAECs. Thus, suggesting that Fyn and CD31 are essential components of a CD31-based mechanosensory complex in endothelial cells. Interestingly, data in chapter 4 demonstrated that CD31 and VE-Cadherin proteins of the mechanosensory triad play a critical role in Yoda1-mediated eNOS phosphorylation. In our study it could be possible for Yoda1- activated Piezo1 to evoke Fyn to tyrosine phosphorylate CD31 to mediate further downstream signalling resulting in eNOS phosphorylation. It is puzzling that the data support a role of CD31 and VE-Cadherin proteins of the triad in Yoda1-mediated eNOS phosphorylation but rule out a role for AKT. It is widely reported that the triad is linked to PI3K/AKT dependent eNOS phosphorylation, activation and vasodilation (Fleming et al., 2005; Jin et al., 2003; Feliers et al., 2005). However, data in the previous chapter rule out a role for AKT. So far a link between Piezo1 and the triad has been made (Fyn) but it remains unclear how the triad evokes eNOS phosphorylation. More work is needed to examine this further. Perhaps a different kinase is involved in this process. It would be interesting to examine whether Yoda1 can evoke tyrosine phosphorylation of CD31 at both 1-minute and at longer time points and to investigate whether this is dependent on Fyn expression.

The data of Figure 5.12 suggest that Yoda1-mediated eNOS phosphorylation is dependent on the presence of extracellular Ca^{2+}. Pre-treatment with 0 mM Ca^{2+}_{ex} abolished Yoda1-mediated eNOS phosphorylation. It is important to note that a major criticism of this experiment is that treatment of HUVECs with 0 mM Ca^{2+}_{ex} may drastically alter Ca^{2+} handling in the cell and may not allow meaningful interpretation. Complete removal of Ca^{2+}_{ex} may disrupt extracellular Ca^{2+} interactions and cause downregulation of all intracellular Ca^{2+} mechanisms. Maybe lowering Ca^{2+}_{ex} levels without abolishing them would be a beneficial assay to perform and may add clarification to this result. Investigation into “classical” Ca^{2+} dependent kinases, such as CaMKII suggest that they are not involved in Yoda-mediated eNOS phosphorylation. Even though inhibitors of CaMKII suppress Yoda1-mediated eNOS phosphorylation further investigation with siRNA targeting 2 different isoforms of CaMKII, that are expressed in HUVECs, argued against their

involvement. Similarly, even though chemically blocking PKC using BIM suppressed Yoda1-mediated eNOS phosphorylation, further investigation using siRNA targeting Ca^{2+} sensitive isoforms of PKC (α, β and γ) ruled out their involvement. Further investigation into the PKC family led to the discovery of PKCδ mediated Yoda1-induced eNOS phosphorylation. siRNA targeting PKCδ to knockdown its expression supressed Yoda1-mediated eNOS phosphorylation without affecting Piezo1 expression or function. There is limited literature linking PKCδ to eNOS phosphorylation. However, interestingly a few papers have suggested a functional interaction between PKCδ and Fyn. In human platelets alboaggregin A treatment led to phosphorylation of PKCδ (Crosby and Poole, 2003). Pull down experiments suggest that Fyn (but not syk, src or btk) specifically interacts with PKCδ (but not PKCε or PKCλ). Furthermore, tyrosine phosphorylation and translocation of PKCδ in platelets to the plasma membrane induced by alboaggregin A is blocked by chemical inhibition of Fyn, suggesting a functional interaction between PKCδ and Fyn. Similarly, a separate study investigating glioma cell functions also suggests a functional partnership between of PKCδ and Fyn (Kronfeld et al., 2000). Tyrosine phosphorylation of PKCδ induced by PDGF was abolished after pre-treatment with src kinase family inhibitors. Furthermore, overexpression of a dominant negative mutant of Fyn suppressed the PDGF tyrosine phosphorylation of PKCδ. Taken together these data suggest that Fyn and PKCδ interact and are able to function in partnership together. In our pathway it could be possible that Fyn is able to tyrosine phosphorylate PKCδ. It would be interesting to examine whether PKCδ and Fyn are able to function in partnership in endothelial cells to evoke eNOS phosphorylation. However, more work is needed to examine this hypothesis and investigate the relationship to CD31.

The exact role of PKCδ appears difficult to examine. Even though one siRNA is able to knockdown PKCδ mRNA expression without affecting Piezo1 function, two other siRNAs and two inhibitors modulate the function of Piezo1. This could either be revealing additional roles for PKCδ in modulating Piezo1 channel activity or the blockers and siRNAs could be non-specific. This renders PKCδ difficult to study.

The role of PKCδ in the vasculature has been examined. A study examining embryonic stem cells suggests that PKCδ is involved in vasculogenesis and is downstream of AKT (Bekhite et al., 2011). Interestingly, *in-vivo* global double knockout of PKCδ and PKCε is embryonic lethal at E9.5 (Carracedo et al., 2014).

Embryos displayed growth retardation, swollen pericardium and impaired vessel formation and structure. The phenotype of these mice is very similar to that of the Piezo1 knockout mouse model (Li et al., 2014). Global Piezo1 knockout is embryonic lethal in mice around E9.9-11.5 and mice present with impaired vascular development and growth retardation at E10.5. It is interesting that the phenotype of both knockout mouse models is similar and it suggests that *in-vivo* they could have similar functions or that Piezo1 is signalling via PKCδ and PKCε to promote vasculogenesis. In the absence of shear stress Piezo1 channel activity is reported to drive endothelial cell migration through eNOS (Li et al., 2014). Endothelial cell migration was similarly suppressed by Piezo1 depletion, eNOS depletion, and NOS inhibition. PKCδ and PKCε could be signalling downstream of Piezo1 in endothelial cells to contribute to endothelial cell migration and embryonic vascular development. The role of PKCε wasn't examined in this thesis but it would be interesting to investigate this kinase.

One limitation of work in this chapter is the lack of data to confirm knockdown of protein levels of the various candidate kinases. Ideally western blotting should have been carried out to confirm knockdown at the protein level and positive control experiments should have been undertaken to confirm that the level of knockdown achieved was sufficient to block known responses. These experiments have been completed post submission of this thesis.

5.10 Summary

In brief, throughout this chapter evidence has been generated to suggest a novel rapid tight coupling mechanism for Yoda1-activated Piezo1 and eNOS phosphorylation. The data suggest that Yoda1-mediated eNOS phosphorylation is dependent on Fyn kinase and PKCδ. Investigation into the role of extracellular Ca^{2+} revealed that Yoda1-mediated eNOS phosphorylation was Ca^{2+} dependent but appeared independent of classical Ca^{2+} regulated kinases including; CaMKII, CaMKI and PKCα, ß and γ. As discussed, due to the nature of the experiment the role of Ca^{2+}_{ex} needs to be further examined to validate this. The response was also independent of kinases that are well known to phosphorylate eNOS on its S1177 site; AKT, PKA and AMPK. We propose a pathway whereby Yoda1 activates Ca^{2+} entry that somehow mediates Fyn to dissociate from Piezo1 to activate PKCδ to

phosphorylate eNOS (Figure 5.37). In the previous chapter we describe a role for both CD31 and VE-Cadherin proteins of the triad in this process. However, it remains unclear how all of the pathway fits together. More work is needed to unravel this. The discovery of a novel mechanism by which Piezo1 evokes eNOS phosphorylation is exciting and important for the development of novel therapeutic targets for high blood pressure and endothelial dysfunction.

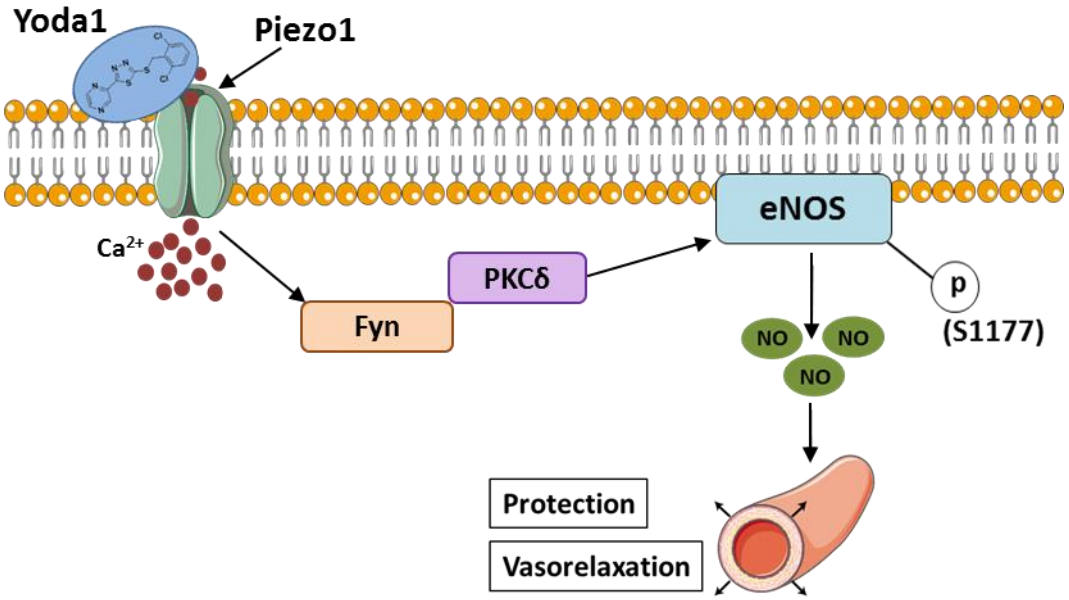

Figure 5.37 Schematic of the proposed mechanism linking Yoda1-mediated Piezo1 activation to S1177 eNOS phosphorylation.

Yoda1 activates Piezo1 channels to evoke eNOS phosphorylation that is dependent of Fyn and PKCδ.

Chapter 6 Conclusion and Future Directions

6.1 Summary of results

- Yoda1, the chemical activator of Piezo1, rapidly and potently activates Ca^{2+} signals in HUVECs and these responses are predominantly due to Ca^{2+} entry.
- siRNA to knockdown Piezo1 mRNA expression revealed that Yoda1-mediated Ca^{2+} entry is via activation of endogenous human Piezo1. Furthermore, acute inhibition of Piezo1 using the inhibitors ruthenium red and gadolinium suppresses this response.
- Yoda1 mimics shear stress to phosphorylate p44/42 ERK (T202/Y204) at 2-minutes and AKT (S473) at the longer time point of 10-minutes.
- Yoda1 evokes rapid dose-dependent phosphorylation of S1177 eNOS. 1-minute treatment with Yoda1 is sufficient to evoke this response and this treatment time was used throughout experiments.
- Yoda1 evokes ~1.5-2 fold increase in S1177 eNOS phosphorylation and eNOS activation which is similar to that of physiological activators of eNOS including VEGF and shear stress.
- Yoda1 evoked S1177 eNOS phosphorylation is suppressed by RNAi targeting Piezo1 and acute blockade of Piezo1 using gadolinium in HUVECs. Furthermore, liver endothelial cells isolated from an inducible Piezo1 endothelial knockout mouse model present with a blunted Yoda1-evoked eNOS phosphorylation response.
- An inactivate analogue of Yoda1, KC69, does not evoke eNOS phosphorylation. However, the KC159 analogue with better ADME properties evokes similar eNOS phosphorylation compared to Yoda1.
- Pre-treatment with dooku1, the inhibitor of Yoda1 activated Piezo1, suppresses Yoda1 mediated eNOS phosphorylation.
- Consistent with Yoda1 evoking activation of eNOS Yoda1 also acts on the S615 activating residue on eNOS but does not phosphorylate the inhibitory residues, Y657 and T495.
- At a short treatment time of 1-minute Yoda1 evokes eNOS phosphorylation independently of ATP, P2Y2 and AKT.

- CD31 and VE-Cadherin proteins of the mechanosensory triad are required for the integrity of Yoda1-mediated eNOS phosphorylation without affecting Yoda1- or hypotonicity- evoked Ca^{2+} signals.
- A high throughput 96 well assay was developed to activate mechanical hypotonicity-induced activation of Piezo1. Suramin, a blocker of P2 receptors, inhibits this response consist with previous reports.
- Consistent with reports suggesting that Yoda1 potentiates mechanical activation of Piezo1, Yoda1 potentiates hypotonicity-induced Ca^{2+} signals.
- Piezo1 knockdown does not affect CD31 activation of ß1-integrin.
- Pull down experiments using GFP-Trap beads suggests that when overexpressed in HEK 293 cells Piezo1 interacts with CD31, VE-Cadherin and VEGFR2.
- Set up of a FLIM/FRET system revealed that Piezo1 and CD31 directly interact when overexpressed in HEK 293 cells.
- Yoda1 evokes eNOS phosphorylation independently of classical kinases that are involved in shear stress mediated S1177 eNOS phosphorylation including: AKT, AMPK and PKA.
- Yoda1-evoked eNOS phosphorylation is dependent on extracellular Ca^{2+} but independent of classical Ca^{2+} regulated kinases including: CaMKIIδ, CaMKIIγ and PKCα.
- Yoda1-induced eNOS phosphorylation is independent of RRas and HRas proteins.
- Comparison of the src family of kinases revealed that Fyn kinase is highly expressed in HUVECs and knockdown of Fyn tyrosine kinase using two different siRNA sequences suppresses Yoda1-mediated eNOS phosphorylation.
- Knockdown of Fyn kinase does not affect Yoda1-mediated or hypotonicity-mediated Ca^{2+} signals.
- Expression of PKCδ is required for Yoda1-mediated eNOS phosphorylation but not Yoda1- or hypotonicity- evoked Ca^{2+} signals suggesting that it acts downstream of Piezo1.
- Fyn kinase and PKCδ are not required for alignment of HUVECs suggesting that they are not important for all Piezo1 signalling and functions but specifically for eNOS phosphorylation.
- Overexpression studies revealed that Fyn interacts with Piezo1 and that Yoda1 treatment evokes a dissociation of Fyn from Piezo1.

6.2 Final discussion and future directions

The overall aim of this study was to gain an understanding of Piezo1-mediated downstream signalling pathways and to examine Piezo1 partner proteins in endothelial cells. This work was aided by the novel selective small molecule Piezo1 activator, Yoda1. Investigation into the mechanism by which Yoda1 mediates S1177 eNOS phosphorylation was sought. Experiments revealed an important partnership between Piezo1 and CD31 and VE-Cadherin proteins of the mechanosensory triad and Fyn kinase and PKCδ. These novel partnerships may have multiple beneficial effects influencing Piezo1 function in physiological and pathophysiological states. However, further work is required to understand how the proteins and kinases act in partnership to evoke eNOS phosphorylation.

6.2.1 Final hypotheses

Work throughout this thesis begins to reveal the mechanism linking Piezo1 to eNOS signalling. We describe a novel mechanism coupling Piezo1 to Fyn kinase and PKCδ. Even though it is incompletely understood how these kinases link Piezo1 to eNOS phosphorylation, taken together with the literature we propose various hypotheses.

Basal conditions

Overexpression studies in a reconstituted HEK 293 system using GFP Trap beads to pull out proteins with a mTurquoise2 tag revealed that Fyn kinase and CD31, VE-Cadherin and VEGFR2 members of the mechanosensitive triad are interacting with Piezo1 (Figure 6.1a). We hypothesise that PKCδ is cytosolic. Reports suggest that in endothelial cells, upon stimulation with PMA, PKCδ is translocated to the membrane compared to the diffuse cytosolic location without treatment (Hendey et al., 2002). Under these conditions S1177 eNOS is not phosphorylated.

Hypothesis #1

Upon stimulation with Yoda1 Ca^{2+} enters endothelial cells via activated Piezo1. Overexpression studies demonstrate that Yoda1 treatment evokes a dissociation of the Piezo1-Fyn interaction. Literature report that upon agonist stimulation, Fyn is involved in translocation and tyrosine phosphorylation of PKCδ (Kronfeld et al.,

2000). Furthermore, reports suggest an interaction between Fyn and PKCδ (Crosby and Poole, 2003). Perhaps Yoda1 is able to evoke translocation of PKCδ to the endothelial cell membrane where it is able to interact and be phosphorylated by Fyn kinase to serine phosphorylate eNOS at residue 1177 (Figure 6.1b). CD31 and VE-Cadherin members of the triad might be important for the cellular organisation of the fast-coupling pathway in this instance.

Hypothesis #2

The second hypothesis is that stimulation with Yoda1 evokes Ca^{2+} to enter endothelial cells via activated Piezo1 to evoke a dissociation of the Piezo1-Fyn complex. Reports suggest that Fyn is required for tyrosine phosphorylation of CD31 upon application of stretch and flow stimulation (Chiu et al., 2008). Data in this thesis suggest that Yoda1 mimics shear stress stimulated downstream pathways. Thus, Yoda1 activation of Piezo1 might evoke Fyn kinase-mediated CD31 tyrosine phosphorylation which is coupled to VE-Cadherin to evoke PKCδ mediated S1177 eNOS phosphorylation (Figure 6.1c). However, more work is needed to validate this mechanism. It remains unclear how VE-Cadherin would link to PKCδ and eNOS signalling as VEGFR2 is usually required for triad mechanosignalling.

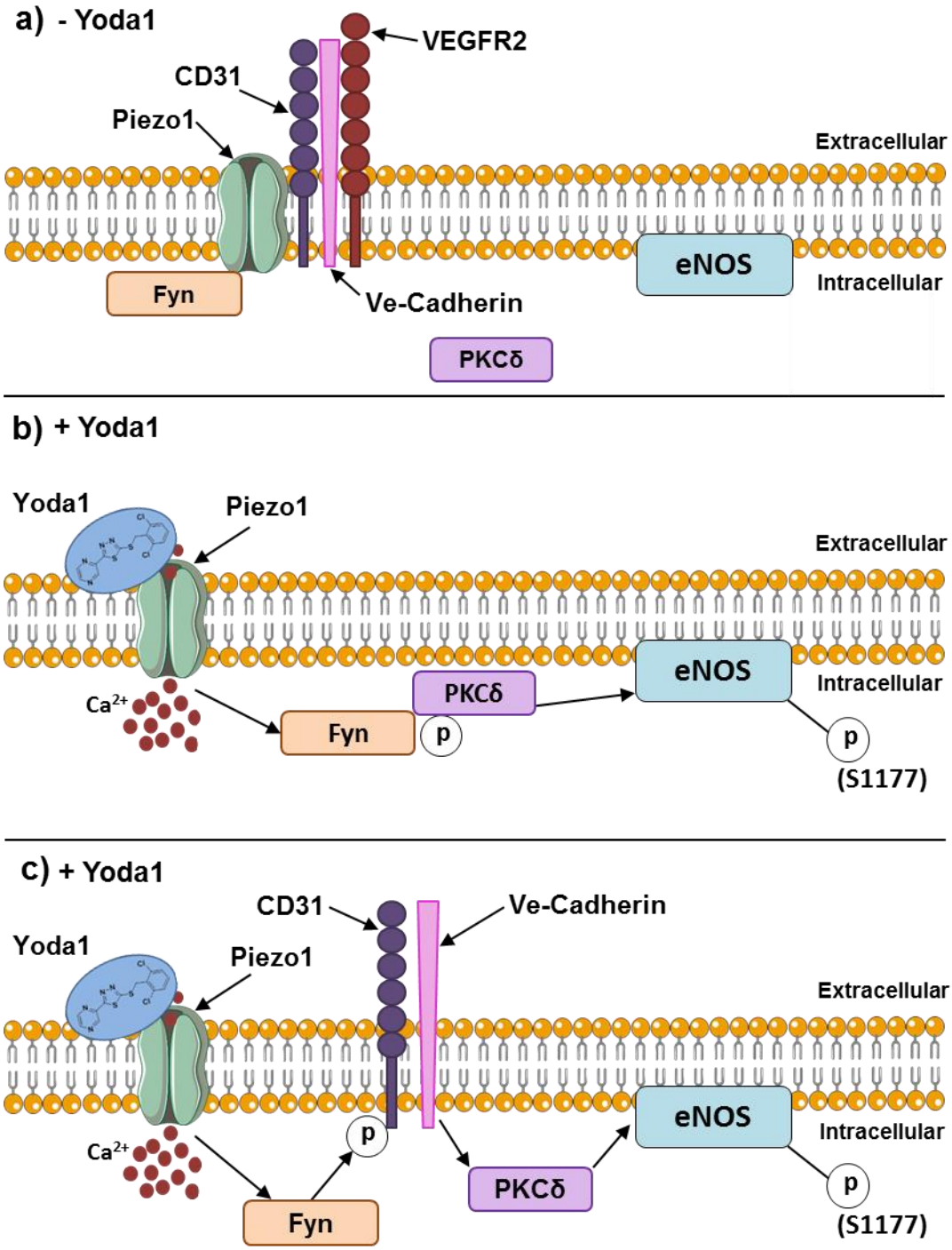

Figure 6.1 Schematic depiction of the opposed mechanisms mediating Yoda1-evoked eNOS phosphorylation.

a) Under basal conditions Piezo1 channels are inactive but bound to Fyn kinase, CD31, Ve-Cadherin and VEGFR2. eNOS is tethered to the membrane and CD31 and Ve-Cadherin proteins are maintaining endothelial cell-cell junctions. b-c) Application of Yoda1 evokes Piezo1 activation and Ca^{2+} entry into endothelial cells which induces a dissociation of Fyn kinase from Piezo1. b) Fyn may directly interact and tyrosine phosphorylate PKCδ to evoke serine eNOS phosphorylation or c) Fyn might tyrosine phosphorylate CD31 which works with Ve-Cadherin to activate PKCδ mediated eNOS phosphorylation.

6.2.2 Future work

More work is needed to reveal the exact pathway coupling Piezo1, Fyn, PKCδ and the mechanosensory triad proteins (CD31 and Ve-Cadherin) to eNOS. There are many limitations to this study and future work is important to propose a definitive mechanism.

6.2.2.1 HA-Piezo1 mice

One major limitation to this study is the lack of an antibody that is able to detect endogenous Piezo1. BEEC4 was developed for the lab by Cambridge Bioscience and is able to detect over-expressed human Piezo1 by western blotting. However, no endogenous Piezo1 band can be detected. Dr Melanie Ludlow has set up the CRISPR technique in our lab. In collaboration with Antony Adamson and Neil Humphries (Manchester University), Piezo1-HA CRISPR mice have been developed. Piezo1-HA is functional when overexpressed in HEK 293 cells and the mice are viable. Work needs to be carried out to characterise these mice to prove that a Piezo1-HA band can be detected via western blotting and immunostaining. Furthermore, endothelial cells need to be isolated from these mice to confirm that the endogenous Piezo1-HA channels are functional. The development of these mice could be a considerable turning point and will facilitate experiments to further understand Piezo1 biology in endothelial cells.

In this study these mice would be useful to allow us to detect endogenous Piezo1 via the use of anti-HA antibodies. Liver endothelial cells could be isolated from these mice and Piezo-HA pull down experiments could be performed. HA pull down experiments have already been optimised in the lab. These experiments would allow further investigation into endogenous Piezo1 interactions with and without Yoda1 stimulation. It is important to examine whether the complexes that have been determined with the overexpression system are physiological or whether they are an artefact of protein overexpression. Furthermore, immunocytochemistry could be carried out to examine localisation of endogenous Piezo1 channels in endothelial cells and whether they are trafficked with the CD31/Ve-Cadherin proteins of the triad.

6.2.2.2 Tyrosine phosphorylation pull-down experiments

Apart from the phosphorylation of eNOS itself, a key phosphorylation event in our proposed signalling pathway is the tyrosine phosphorylation evoked by Fyn kinase activation. Reports suggest that Fyn is capable of phosphorylating both CD31 and PKCδ (Chiu et al., 2008; Kronfeld et al., 2000). However, in our pathway it is unclear how Fyn couples Piezo1 to eNOS phosphorylation. A key experiment to further understand this is phospho-tyrosine pull down experiments.

Considerable effort has been made to optimise this protocol however, further work is needed. Pull down experiments using a pan phospho-tyrosine antibody would allow investigation into which proteins (if any) are tyrosine phosphorylated upon Yoda1 stimulation. This experiment could be performed with and without Fyn kinase knockdown to decipher which proteins are phosphorylated by Fyn. These data would allow us to make a definitive conclusion as to whether CD31/Ve-Cadherin are involved in the pathway or whether they are involved in the cellular organisation.

6.2.2.3 Immunocytochemistry

It would be interesting to investigate the localisation of Fyn kinase and PKCδ and examine whether they translocate upon stimulation with Yoda1. Immunocytochemistry experiments using antibodies to detect Fyn and PKCδ could be useful. If Yoda1 evokes a translocation then HUVECs could be treated with RNAi targeting Piezo1 or *m*LECs isolated from Piezo1$^{\Delta EC}$ mice to examine the Piezo1 dependence of the response. Furthermore, Piezo1-HA endothelial cells could be isolated from mice and staining performed to examine trafficking of HA (Piezo1) and Fyn/PKCδ upon treatment with Yoda1.

To examine whether CD31 and Ve-Cadherin are involved in the cellular organisation in endothelial cells CD31 and Ve-Cadherin knockdown could be an important aspect to study here to investigate whether they are involved in kinase translocation.

6.2.2.4 Cryo-EM CD31

One interesting finding in our study is the direct interaction between Piezo1 and CD31. Even though this is yet to be examined endogenously the interaction using two biochemical techniques is striking. These data could revolutionise the field of endothelial mechanosensing confirming that indeed mechanosensors work together to promote certain physiological responses. Currently work is being undertaken using Cryo-EM to examine the structural interaction between Piezo1 and CD31. Determining the interaction site between Piezo1 and CD31 could be useful to further understand the mechanism in which they sense and respond to shear stress but also to be able to inhibit the interaction to test its importance in physiology.

6.2.2.5 Knockout mice models

During this project CD31 global knockout mice were obtained from a group at Yale University. The mice were viable however, there were problems with their breeding. CD31 knockout liver endothelial cells would be useful to further examine the role of CD31 in Yoda1-mediated eNOS phosphorylation. They would also be useful to examine whether CD31 is important for the intracellular localisation of Fyn kinase and PKCδ. Experiments using these endothelial cells could allow us to conclude whether CD31 is imported for the pathway linking Piezo1 to eNOS or if it is important for cellular organisation.

It would also be interesting to purchasing a global Fyn knockout mouse. Experiments could be undertaken to further examine the role of Fyn kinase in this pathway. Furthermore, wire myograph experiments could be undertaken on the vessels from the mice to examine if regulation of vascular tone is altered. Additionally, it would be interesting to give the mice access to a running wheel to examine whether Fyn knockout mice present with the same phenotype as the inducible Piezo1 knockout.

6.2.2.6 Ca^{2+} involvement

As Piezo1 is a Ca^{2+} channel and as eNOS was first reported to be Ca^{2+} sensitive it was logical to examine the role of Ca^{2+} in Yoda1-mediated eNOS phosphorylation. Interestingly, removal of extracellular Ca^{2+} abolished Yoda1-mediated eNOS

phosphorylation. However, complete removal of extracellular Ca^{2+} could affect a variety of Ca^{2+} signalling in endothelial cells so it is hard to conclude that this mechanism is Ca^{2+} dependent. This work has been confirmed by Dr Marjolaine Debant (University of Leeds) where a dose-dependent decrease in extracellular Ca^{2+} dose-dependently decreased eNOS phosphorylation. However, the 'classical' Ca^{2+} regulated kinase CaMKII was not involved. During a visit to Yale University, Professor William Sessa, an expert in the eNOS signalling field suggested examining the role of Ca^{2+} dependent isoforms of PKC isoforms. mRNA expression of PKCß and γ is low in HUVECs and knockdown of PKCα had no effect on the eNOS response. Instead, the Ca^{2+} independent, PKCδ, was involved.

Work is ongoing to examine the involvement of protein tyrosine kinase 2 beta (PYK2) in Yoda1-mediated eNOS phosphorylation. PYK2 is a Ca^{2+} dependent tyrosine kinase that is reported to be involved in the phosphorylation of eNOS, NO production and blood flow recovery after hind limb ischemia (Matsui et al., 2007). Preliminary data from Dr Marjolaine Debant (University of Leeds) using PYK2 inhibitors suggests that PYK2 is involved in Yoda1-mediated eNOS phosphorylation. However, more work is needed to examine how PYK2 fits in with our proposed pathway.

6.3 Clinical Relevance

Heart disease and stroke are among the top 5 causes of premature death in England (www.nhs.uk). Thus, developing novel therapies targeting these diseases are critical. Current therapies include the cardio-selective ß blockers and angiotensin-converting-enzyme (ACE) inhibitors.

ACE inhibitors inhibit the angiotensin converting enzyme that is a key component of the renin-angiotensin system to lower arteriolar resistance and increase venous capacity. ß blockers act on receptor sites for adrenaline and noradrenaline on ß adrenergic receptors. ß adrenergic receptors are coupled to G proteins and inhibit smooth muscle cell contraction via inhibition of PLC activated, IP3, and DAG rise in Ca^{2+}. It is therefore conceivable that modulating Piezo1 ion channels could lead to the development of a novel class of anti-hypertensives, via NO production and subsequent vessel dilation. This would be dependent upon better understanding of

Piezo1 function in different vascular beds, and the development of Yoda1 analogues with improved ADME properties.

Peripheral vascular disease (PVD) is a common complication in patients with diabetes. This blood circulation disorder is characterised by a build-up of fatty plaques leading to narrowed vessels. Patients can present with lower limb ischaemia and retinal vascular problems. Patients with high blood pressure have increased incidence of developing PVD. Thus, treating high blood pressure is one way to combat this disease. Again, targeting Piezo1 channels as a treatment for high blood pressure and control of vasomotor tone could be important in PVD therapy.

Recently Piezo1 expression in placental endothelial cells was reported (Morley et al., 2018). In these cells Piezo1 channels are functional and are able to respond to Yoda1 via an increase in Ca^{2+} entry. In pregnancy, placental vascular dysfunction can cause fetal growth restriction and pre-eclampsia- which increase the risk of morbidity and mortality for both mother and baby. As such, a Piezo1 activator could be a novel treatment for improving placental blood flow.

Overall, treatment with agonists of Piezo1, i.e. Yoda1 or more translational analogues with better ADME properties could allow better control of vasomotor tone to widen blood vessels and promote blood flow in various vascular beds. However, as the role of Piezo1 channels is suggested to vary depending on the vascular beds more work is need to examine Yoda1-medaited eNOS phosphorylation in endothelial cells from different vascular origins (Rode et al., 2017).

6.4 Conclusions

Modulation of Piezo1 channel activity is implicated in a growing number of human diseases including cardiovascular disease and is critical for murine vascular development and sensing whole body physical activity. Piezo1 has been reported to be involved in eNOS phosphorylation subsequently evoking NO production and vessel relaxation. Thus, Piezo1 is an attractive therapeutic target in vascular disease. We have identified that a chemical activator of Piezo1, Yoda1, that mimics

shear stress is able to evoke eNOS phosphorylation and that Fyn kinase and PKCδ are required for the integrity of this response. Furthermore, for the first time, we suggest a partnership between Piezo1 and CD31 and Ve-Cadherin proteins of the mechanosensory triad. Specific targeting of Piezo1 with Yoda1 or drug-like analogues could assist better understanding of Piezo1 in vascular disease and importantly could be novel therapeutics to aid better control of vasomotor tone and vascular protection.

List of References

Armbruster, B.N. et al. 2007. Evolving the lock to fit the key to create a family of G protein-coupled receptors potently activated by an inert ligand. *Proc Natl Acad Sci U S A.* **104**(12), pp.5163-8.

Ayajiki, K. et al. 1996. Intracellular pH and tyrosine phosphorylation but not calcium determine shear stress-induced nitric oxide production in native endothelial cells. *Circ Res.* **78**(5), pp.750-8.

Bae, C. et al. 2013. Xerocytosis is caused by mutations that alter the kinetics of the mechanosensitive channel PIEZO1. *Proc Natl Acad Sci U S A.* **110**(12), pp.E1162-8.

Bagi, Z. et al. 2005. PECAM-1 mediates NO-dependent dilation of arterioles to high temporal gradients of shear stress. *Arterioscler Thromb Vasc Biol.* **25**(8), pp.1590-5.

Beech, D.J. 2012. Orai1 calcium channels in the vasculature. *Pflugers Arch.* **463**(5), pp.635-47.

Beech, D.J. 2013. Characteristics of transient receptor potential canonical calcium-permeable channels and their relevance to vascular physiology and disease. *Circ J.* **77**(3), pp.570-9.

Bekhite, M.M. et al. 2011. VEGF-mediated PI3K class IA and PKC signaling in cardiomyogenesis and vasculogenesis of mouse embryonic stem cells. *J Cell Sci.* **124**(Pt 11), pp.1819-30.

Berridge, M.J. et al. 2003. Calcium signalling: dynamics, homeostasis and remodelling. *Nat Rev Mol Cell Biol.* **4**(7), pp.517-29.

Berridge, M.J. et al. 2000. The versatility and universality of calcium signalling. *Nat Rev Mol Cell Biol.* **1**(1), pp.11-21.

Bleakley, C. et al. 2015. Endothelial Function in Hypertension: Victim or Culprit? *J Clin Hypertens (Greenwich).* **17**(8), pp.651-4.

Boo, Y.C. et al. 2002a. Shear stress stimulates phosphorylation of eNOS at Ser(635) by a protein kinase A-dependent mechanism. *Am J Physiol Heart Circ Physiol.* **283**(5), pp.H1819-28.

Boo, Y.C. et al. 2002b. Shear stress stimulates phosphorylation of endothelial nitric-oxide synthase at Ser1179 by Akt-independent mechanisms: role of protein kinase A. *J Biol Chem.* **277**(5), pp.3388-96.

Bredt, D.S. et al. 1990. Localization of nitric oxide synthase indicating a neural role for nitric oxide. *Nature.* **347**(6295), pp.768-70.

Brough, G.H. et al. 2001. Contribution of endogenously expressed Trp1 to a Ca2+-selective, store-operated Ca2+ entry pathway. *Faseb j.* **15**(10), pp.1727-38.

Busse, R. et al. 2002. EDHF: bringing the concepts together. *Trends Pharmacol Sci.* **23**(8), pp.374-80.

Busse, R. and Mulsch, A. 1990. Calcium-dependent nitric oxide synthesis in endothelial cytosol is mediated by calmodulin. *FEBS Lett.* **265**(1-2), pp.133-6.

Cahalan, M.D. 2009. STIMulating store-operated Ca(2+) entry. *Nat Cell Biol.* **11**(6), pp.669-77.

Cahalan, S.M. et al. 2015. Piezo1 links mechanical forces to red blood cell volume. *Elife.* **4**.

Cao, M.Y. et al. 1998. Regulation of mouse PECAM-1 tyrosine phosphorylation by the Src and Csk families of protein-tyrosine kinases. *J Biol Chem.* **273**(25), pp.15765-72.

Carmeliet, P. 2005. Angiogenesis in life, disease and medicine. *Nature.* **438**(7070), pp.932-6.

Carmeliet, P. et al. 1999. Targeted deficiency or cytosolic truncation of the VE-cadherin gene in mice impairs VEGF-mediated endothelial survival and angiogenesis. *Cell.* **98**(2), pp.147-57.

Carracedo, S. et al. 2014. Redundant Role of Protein Kinase C Delta and Epsilon during Mouse Embryonic Development. *PLoS One.* **9**(8).

Caterina, M.J. et al. 1997. The capsaicin receptor: a heat-activated ion channel in the pain pathway. *Nature.* **389**(6653), pp.816-24.

Catterall, W.A. 2011. Voltage-Gated Calcium Channels. *Cold Spring Harb Perspect Biol.* **3**(8).

Chachisvilis, M. et al. 2006. G protein-coupled receptors sense fluid shear stress in endothelial cells. *Proc Natl Acad Sci U S A.* **103**(42), pp.15463-8.

Chen, J. et al. 2014. Transient receptor potential (TRP) channels, promising potential diagnostic and therapeutic tools for cancer. *Biosci Trends.* **8**(1), pp.1-10.

Chen, K.D. et al. 1999. Mechanotransduction in response to shear stress. Roles of receptor tyrosine kinases, integrins, and Shc. *J Biol Chem.* **274**(26), pp.18393-400.

Chen, Z. and Tzima, E. 2009. PECAM-1 is necessary for flow-induced vascular remodeling. *Arterioscler Thromb Vasc Biol.* **29**(7), pp.1067-73.

Chistiakov, D.A. et al. 2017. Effects of shear stress on endothelial cells: go with the flow. *Acta Physiol (Oxf).* **219**(2), pp.382-408.

Chiu, Y.J. et al. 2008. Mechanotransduction in an extracted cell model: Fyn drives stretch- and flow-elicited PECAM-1 phosphorylation. *J Cell Biol.* **182**(4), pp.753-63.

Clapham, D.E. 1995. Calcium signaling. *Cell.* **80**(2), pp.259-68.

Clapham, D.E. 2007. Calcium signaling. *Cell.* **131**(6), pp.1047-58.

Collins, H.E. et al. 2013. STIM1/Orai1-mediated SOCE: current perspectives and potential roles in cardiac function and pathology. *Am J Physiol Heart Circ Physiol.* **305**(4), pp.H446-58.

Conway, D.E. and Schwartz, M.A. 2013. Flow-dependent cellular mechanotransduction in atherosclerosis. *J Cell Sci.* **126**(Pt 22), pp.5101-9.

Cooke, J.P. 2000. The endothelium: a new target for therapy. *Vasc Med.* **5**(1), pp.49-53.

Cooke, J.P. and Losordo, D.W. 2002. Nitric oxide and angiogenesis. *Circulation.* **105**(18), pp.2133-5.

Coste, B. et al. 2013. Gain-of-function mutations in the mechanically activated ion channel PIEZO2 cause a subtype of Distal Arthrogryposis. *Proc Natl Acad Sci U S A.* **110**(12), pp.4667-72.

Coste, B. et al. 2010. Piezo1 and Piezo2 are essential components of distinct mechanically activated cation channels. *Science.* **330**(6000), pp.55-60.

Coste, B. et al. 2015. Piezo1 ion channel pore properties are dictated by C-terminal region. *Nature Communications.* **6**, p7223.

Coste, B. et al. 2012. Piezo proteins are pore-forming subunits of mechanically activated channels. *Nature.* **483**(7388), pp.176-81.
Cox, C.D. et al. 2016. Removal of the mechanoprotective influence of the cytoskeleton reveals PIEZO1 is gated by bilayer tension. *Nature Communications.* **7**, p10366.
Crosby, D. and Poole, A.W. 2003. Physical and functional interaction between protein kinase C delta and Fyn tyrosine kinase in human platelets. *J Biol Chem.* **278**(27), pp.24533-41.
Cybulsky, M.I. et al. 2001. A major role for VCAM-1, but not ICAM-1, in early atherosclerosis. *J Clin Invest.* **107**(10), pp.1255-62.
Damann, N. et al. 2008. TRPs in our senses. *Curr Biol.* **18**(18), pp.R880-9.
Dardik, A. et al. 2005. Differential effects of orbital and laminar shear stress on endothelial cells. *J Vasc Surg.* **41**(5), pp.869-80.
Davda, R.K. et al. 1994. Protein kinase C modulates receptor-independent activation of endothelial nitric oxide synthase. *Eur J Pharmacol.* **266**(3), pp.237-44.
dela Paz, N.G. et al. 2017. Shear stress induces Gα(q/11) activation independently of G protein-coupled receptor activation in endothelial cells. *Am J Physiol Cell Physiol.* **312**(4), pp.C428-37.
Delmas, P. et al. 2002. Constitutive activation of G-proteins by polycystin-1 is antagonized by polycystin-2. *J Biol Chem.* **277**(13), pp.11276-83.
Devika, N.T. and Jaffar Ali, B.M. 2013. Analysing calcium dependent and independent regulation of eNOS in endothelium triggered by extracellular signalling events. *Mol Biosyst.* **9**(11), pp.2653-64.
Dimmeler, S. et al. 2000. Phosphorylation of the endothelial nitric oxide synthase at ser-1177 is required for VEGF-induced endothelial cell migration. *FEBS Lett.* **477**(3), pp.258-62.
Dimmeler, S. et al. 1999. Activation of nitric oxide synthase in endothelial cells by Akt-dependent phosphorylation. *Nature.* **399**(6736), pp.601-5.
Dolmetsch, R.E. et al. 1998. Calcium oscillations increase the efficiency and specificity of gene expression. *Nature.* **392**(6679), pp.933-6.
Dorn, G.W., 2nd. 2007. The fuzzy logic of physiological cardiac hypertrophy. *Hypertension.* **49**(5), pp.962-70.
Dubin, A.E. et al. 2017. Endogenous Piezo1 Can Confound Mechanically Activated Channel Identification and Characterization. *Neuron.* **94**(2), pp.266-270.e3.
Dusting, G.J. et al. 1978. Vascular actions of arachidonic acid and its metabolites in perfused mesenteric and femoral beds of the dog. *Eur J Pharmacol.* **49**(1), pp.65-72.
Edwards, G. et al. 1998. K+ is an endothelium-derived hyperpolarizing factor in rat arteries. *Nature.* **396**(6708), pp.269-72.
Edwards, J.M. et al. 2010. Exercise training decreases store-operated Ca2+entry associated with metabolic syndrome and coronary atherosclerosis. *Cardiovasc Res.* **85**(3), pp.631-40.
Evans, E.L. et al. 2018. Yoda1 analogue (Dooku1) which antagonizes Yoda1-evoked activation of Piezo1 and aortic relaxation. *Br J Pharmacol.* **175**(10), pp.1744-1759.
Feliers, D. et al. 2005. VEGF regulation of endothelial nitric oxide synthase in glomerular endothelial cells. *Kidney Int.* **68**(4), pp.1648-59.
Feske, S. et al. 2006. A mutation in Orai1 causes immune deficiency by abrogating CRAC channel function. *Nature.* **441**(7090), pp.179-85.

Fisslthaler, B. et al. 2000. Phosphorylation and activation of the endothelial nitric oxide synthase by fluid shear stress. *Acta Physiol Scand.* **168**(1), pp.81-8.

Fisslthaler, B. et al. 2008. Inhibition of endothelial nitric oxide synthase activity by proline-rich tyrosine kinase 2 in response to fluid shear stress and insulin. *Circ Res.* **102**(12), pp.1520-8.

Flammer, A.J. and Luscher, T.F. 2010. Human endothelial dysfunction: EDRFs. *Pflugers Arch.* **459**(6), pp.1005-13.

Fleming, I. 2010. Molecular mechanisms underlying the activation of eNOS. *Pflugers Arch.* **459**(6), pp.793-806.

Fleming, I. et al. 2001. Phosphorylation of Thr(495) regulates Ca(2+)/calmodulin-dependent endothelial nitric oxide synthase activity. *Circ Res.* **88**(11), pp.E68-75.

Fleming, I. et al. 2005. Role of PECAM-1 in the shear-stress-induced activation of Akt and the endothelial nitric oxide synthase (eNOS) in endothelial cells. *J Cell Sci.* **118**(Pt 18), pp.4103-11.

Fleming, I. et al. 2003. AMP-activated protein kinase (AMPK) regulates the insulin-induced activation of the nitric oxide synthase in human platelets. *Thromb Haemost.* **90**(5), pp.863-71.

Forstermann, U. et al. 1994. Nitric oxide synthase isozymes. Characterization, purification, molecular cloning, and functions. *Hypertension.* **23**(6 Pt 2), pp.1121-31.

Fotiou, E. et al. 2015. Novel mutations in PIEZO1 cause an autosomal recessive generalized lymphatic dysplasia with non-immune hydrops fetalis. **6**, p8085.

Fu, S. et al. 2011. Aberrant lipid metabolism disrupts calcium homeostasis causing liver endoplasmic reticulum stress in obesity. *Nature.* **473**, p528.

Fulton, D. et al. 1999. Regulation of endothelium-derived nitric oxide production by the protein kinase Akt. *Nature.* **399**(6736), pp.597-601.

Furchgott, R.F. and Zawadzki, J.V. 1980. The obligatory role of endothelial cells in the relaxation of arterial smooth muscle by acetylcholine. *Nature.* **288**(5789), pp.373-6.

Galie, P.A. et al. 2014. Fluid shear stress threshold regulates angiogenic sprouting. *Proc Natl Acad Sci U S A.* **111**(22), pp.7968-73.

Gallis, B. et al. 1999. Identification of flow-dependent endothelial nitric-oxide synthase phosphorylation sites by mass spectrometry and regulation of phosphorylation and nitric oxide production by the phosphatidylinositol 3-kinase inhibitor LY294002. *J Biol Chem.* **274**(42), pp.30101-8.

Garland, C.J. et al. 1995. Endothelium-dependent hyperpolarization: a role in the control of vascular tone. *Trends Pharmacol Sci.* **16**(1), pp.23-30.

Ge, J. et al. 2015. Architecture of the mammalian mechanosensitive Piezo1 channel. *Nature.* **527**(7576), pp.64-9.

Givens, C. and Tzima, E. 2016. Endothelial Mechanosignaling: Does One Sensor Fit All? *Antioxid Redox Signal.* **25**(7), pp.373-88.

Gnanasambandam, R. et al. 2015. Ionic Selectivity and Permeation Properties of Human PIEZO1 Channels. *PLoS One.* **10**(5).

Goedhart, J. et al. 2012. Structure-guided evolution of cyan fluorescent proteins towards a quantum yield of 93%. *Nat Commun.* **3**, pp.751-.

Gonzales, E.B. et al. 2009. Pore architecture and ion sites in acid sensing ion channels and P2X receptors. *Nature.* **460**(7255), pp.599-604.
Grynkiewicz, G. et al. 1985. A new generation of Ca2+ indicators with greatly improved fluorescence properties. *J Biol Chem.* **260**(6), pp.3440-50.
Gschwendt, M. et al. 1994. Rottlerin, a novel protein kinase inhibitor. *Biochem Biophys Res Commun.* **199**(1), pp.93-8.
Gu, L. et al. 1998. Absence of monocyte chemoattractant protein-1 reduces atherosclerosis in low density lipoprotein receptor-deficient mice. *Mol Cell.* **2**(2), pp.275-81.
Gu, Y. and Gu, C. 2014. Physiological and Pathological Functions of Mechanosensitive Ion Channels. *Mol Neurobiol.* **50**(2), pp.339-47.
Gudi, S. et al. 2003. Rapid activation of Ras by fluid flow is mediated by Galpha(q) and Gbetagamma subunits of heterotrimeric G proteins in human endothelial cells. *Arterioscler Thromb Vasc Biol.* **23**(6), pp.994-1000.
Gudi, S.R. et al. 1996. Fluid flow rapidly activates G proteins in human endothelial cells. Involvement of G proteins in mechanochemical signal transduction. *Circ Res.* **79**(4), pp.834-9.
Guo, L. et al. 2013. CaMKIα regulates AMPK-dependent, TORC-1 independent autophagy during LPS-induced acute lung neutrophilic inflammation(,). *J Immunol.* **190**(7), pp.3620-8.
Guo, Y.R. and MacKinnon, R. 2017. Structure-based membrane dome mechanism for Piezo mechanosensitivity. **6**.
Haeussler, D.J. et al. 2013. Endomembrane H-Ras Controls Vascular Endothelial Growth Factor-induced Nitric-oxide Synthase-mediated Endothelial Cell Migration. *J Biol Chem.* **288**(21), pp.15380-9.
Hahn, C. and Schwartz, M.A. 2009. Mechanotransduction in vascular physiology and atherogenesis. *Nat Rev Mol Cell Biol.* **10**(1), pp.53-62.
Harper, M.T. and Poole, A.W. 2011. PKC inhibition markedly enhances Ca2+ signaling and phosphatidylserine exposure downstream of protease-activated receptor-1 but not protease-activated receptor-4 in human platelets. *J Thromb Haemost.* **9**(8), pp.1599-607.
Hartmannsgruber, V. et al. 2007. Arterial response to shear stress critically depends on endothelial TRPV4 expression. *PLoS One.* **2**(9), pe827.
Hattori, K. et al. 2002. Placental growth factor reconstitutes hematopoiesis by recruiting VEGFR1(+) stem cells from bone-marrow microenvironment. *Nat Med.* **8**(8), pp.841-9.
Haynes, M.P. et al. 2003. Src kinase mediates phosphatidylinositol 3-kinase/Akt-dependent rapid endothelial nitric-oxide synthase activation by estrogen. *J Biol Chem.* **278**(4), pp.2118-23.
Hendey, B. et al. 2002. Fas activation opposes PMA-stimulated changes in the localization of PKCdelta: a mechanism for reducing neutrophil adhesion to endothelial cells. *J Leukoc Biol.* **71**(5), pp.863-70.
Herchuelz, A. et al. 2007. Role of Na/Ca exchange and the plasma membrane Ca2+-ATPase in beta cell function and death. *Ann N Y Acad Sci.* **1099**, pp.456-67.
Herrmann, J. and Lerman, A. 2001. The endothelium: dysfunction and beyond. *J Nucl Cardiol.* **8**(2), pp.197-206.
Hirakawa, M. et al. 2004. Sequential activation of RhoA and FAK/paxillin leads to ATP release and actin reorganization in human endothelium. *J Physiol.* **558**(Pt 2), pp.479-88.

Hoeben, A. et al. 2004. Vascular endothelial growth factor and angiogenesis. *Pharmacol Rev.* **56**(4), pp.549-80.

Hotamisligil, G.S. 2010. Endoplasmic reticulum stress and the inflammatory basis of metabolic disease. *Cell.* **140**(6), pp.900-17.

Hurt, K.J. et al. 2002. Akt-dependent phosphorylation of endothelial nitric-oxide synthase mediates penile erection. *Proc Natl Acad Sci U S A.* **99**(6), pp.4061-6.

Ilkan, Z. et al. 2017. Evidence for shear-mediated Ca(2+) entry through mechanosensitive cation channels in human platelets and a megakaryocytic cell line. *J Biol Chem.* **292**(22), pp.9204-9217.

Irie, S. and Tavassoli, M. 1991. Transendothelial transport of macromolecules: the concept of tissue-blood barriers. *Cell Biol Rev.* **25**(4), pp.317-33, 340-1.

Jalali, S. et al. 2001. Integrin-mediated mechanotransduction requires its dynamic interaction with specific extracellular matrix (ECM) ligands. *Proc Natl Acad Sci U S A.* **98**(3), pp.1042-6.

Jardin, I. et al. 2008. Phosphatidylinositol 4,5-bisphosphate enhances store-operated calcium entry through hTRPC6 channel in human platelets. *Biochim Biophys Acta.* **1783**(1), pp.84-97.

Jeremy, J.Y. et al. 1999. Nitric oxide and the proliferation of vascular smooth muscle cells. *Cardiovasc Res.* **43**(3), pp.580-94.

Ji, G. et al. 2002. PECAM-1 (CD31) regulates a hydrogen peroxide-activated nonselective cation channel in endothelial cells. *J Cell Biol.* **157**(1), pp.173-84.

Jin, Z.G. et al. 2003. Ligand-independent activation of vascular endothelial growth factor receptor 2 by fluid shear stress regulates activation of endothelial nitric oxide synthase. *Circ Res.* **93**(4), pp.354-63.

Jordt, S.E. et al. 2004. Mustard oils and cannabinoids excite sensory nerve fibres through the TRP channel ANKTM1. *Nature.* **427**(6971), pp.260-5.

Jordt, S.E. et al. 2003. Lessons from peppers and peppermint: the molecular logic of thermosensation. *Curr Opin Neurobiol.* **13**(4), pp.487-92.

Karkkainen, M.J. et al. 2004. Vascular endothelial growth factor C is required for sprouting of the first lymphatic vessels from embryonic veins. *Nat Immunol.* **5**(1), pp.74-80.

Karls, A. and Mynlieff, M. 2013. Nonspecific, reversible inhibition of voltage gated calcium channels by CaMKII inhibitor CK59. *Cell Mol Neurobiol.* **33**(5), pp.723-9.

Katoh, O. et al. 1995. Expression of the vascular endothelial growth factor (VEGF) receptor gene, KDR, in hematopoietic cells and inhibitory effect of VEGF on apoptotic cell death caused by ionizing radiation. *Cancer Res.* **55**(23), pp.5687-92.

Kawasaki, K. et al. 2003. Activation of the phosphatidylinositol 3-kinase/protein kinase Akt pathway mediates nitric oxide-induced endothelial cell migration and angiogenesis. *Mol Cell Biol.* **23**(16), pp.5726-37.

Kawate, T. et al. 2009. Crystal structure of the ATP-gated P2X4 ion channel in the closed state. *Nature.* **460**, p592.

Keck, P.J. et al. 1989. Vascular permeability factor, an endothelial cell mitogen related to PDGF. *Science.* **246**(4935), pp.1309-12.

Khazaei, M. et al. 2008. Vascular endothelial function in health and diseases. *Pathophysiology.* **15**(1), pp.49-67.
Kim, S.E. et al. 2012. The role of Drosophila Piezo in mechanical nociception. *Nature.* **483**(7388), pp.209-12.
Kirichok, Y. et al. 2004. The mitochondrial calcium uniporter is a highly selective ion channel. *Nature.* **427**(6972), pp.360-4.
Kohler, R. et al. 2006. Evidence for a functional role of endothelial transient receptor potential V4 in shear stress-induced vasodilatation. *Arterioscler Thromb Vasc Biol.* **26**(7), pp.1495-502.
Komander, D. et al. 2004. Interactions of LY333531 and other bisindolyl maleimide inhibitors with PDK1. *Structure.* **12**(2), pp.215-26.
Kronfeld, I. et al. 2000. Phosphorylation of protein kinase Cdelta on distinct tyrosine residues regulates specific cellular functions. *J Biol Chem.* **275**(45), pp.35491-8.
Kuchan, M.J. et al. 1994. Role of G proteins in shear stress-mediated nitric oxide production by endothelial cells. *Am J Physiol.* **267**(3 Pt 1), pp.C753-8.
Lahoz, C. and Mostaza, J.M. 2007. [Atherosclerosis as a systemic disease]. *Rev Esp Cardiol.* **60**(2), pp.184-95.
Landmesser, U. et al. 2004. Endothelial function: a critical determinant in atherosclerosis? *Circulation.* **109**(21 Suppl 1), pp.Ii27-33.
Lebart, M.C. and Benyamin, Y. 2006. Calpain involvement in the remodeling of cytoskeletal anchorage complexes. *Febs j.* **273**(15), pp.3415-26.
Leung, D.W. et al. 1989. Vascular endothelial growth factor is a secreted angiogenic mitogen. *Science.* **246**(4935), pp.1306-9.
Leung, D.Y. et al. 1976. Cyclic stretching stimulates synthesis of matrix components by arterial smooth muscle cells in vitro. *Science.* **191**(4226), pp.475-7.
Li, C. 2015. Piezo1 forms mechanosensitive ion channels in the human MCF-7 breast cancer cell. **5**.
Li, J. et al. 2011a. Orai1 and CRAC channel dependence of VEGF-activated Ca2+ entry and endothelial tube formation. *Circ Res.* **108**(10), pp.1190-8.
Li, J. et al. 2014. Piezo1 integration of vascular architecture with physiological force. *Nature.* **515**(7526), pp.279-282.
Li, J. et al. 2011b. Nanomolar potency and selectivity of a Ca(2)(+) release-activated Ca(2)(+) channel inhibitor against store-operated Ca(2)(+) entry and migration of vascular smooth muscle cells. *Br J Pharmacol.* **164**(2), pp.382-93.
Li, Y.S. et al. 1996. The Ras-JNK pathway is involved in shear-induced gene expression. *Mol Cell Biol.* **16**(11), pp.5947-54.
Libby, P. 2002. Inflammation in atherosclerosis. *Nature.* **420**(6917), pp.868-74.
Libby, P. et al. 2011. Progress and challenges in translating the biology of atherosclerosis. *Nature.* **473**(7347), pp.317-25.
Liu, X. et al. 2000. Trp1, a candidate protein for the store-operated Ca(2+) influx mechanism in salivary gland cells. *J Biol Chem.* **275**(5), pp.3403-11.
Long, Y. et al. 2017. ATP2B1 gene Silencing Increases Insulin Sensitivity through Facilitating Akt Activation via the Ca(2+)/calmodulin Signaling

Pathway and Ca(2+)-associated eNOS Activation in Endothelial Cells. *Int J Biol Sci.* **13**(9), pp.1203-12.

Lorenzi, O. et al. 2008. Protein kinase C-delta mediates von Willebrand factor secretion from endothelial cells in response to vascular endothelial growth factor (VEGF) but not histamine. *J Thromb Haemost.* **6**(11), pp.1962-9.

Lukacs, V. et al. 2015. Impaired PIEZO1 function in patients with a novel autosomal recessive congenital lymphatic dysplasia. *Nature Communications.* **6**, p8329.

Ma, S. et al. 2018. Common PIEZO1 Allele in African Populations Causes RBC Dehydration and Attenuates Plasmodium Infection. *Cell.* **173**(2), pp.443-455.e12.

Malek, A.M. et al. 1999. Hemodynamic shear stress and its role in atherosclerosis. *Jama.* **282**(21), pp.2035-42.

Matsubara, M. et al. 2003. Regulation of endothelial nitric oxide synthase by protein kinase C. *J Biochem.* **133**(6), pp.773-81.

Matsui, A. et al. 2007. Central role of calcium-dependent tyrosine kinase PYK2 in endothelial nitric oxide synthase-mediated angiogenic response and vascular function. *Circulation.* **116**(9), pp.1041-51.

Matthys, K.E. and Bult, H. 1997. Nitric oxide function in atherosclerosis. *Mediators Inflamm.* **6**(1), pp.3-21.

Mayer, B.J. and Baltimore, D. 1993. Signalling through SH2 and SH3 domains. *Trends Cell Biol.* **3**(1), pp.8-13.

McHugh, B.J. et al. 2010. Integrin activation by Fam38A uses a novel mechanism of R-Ras targeting to the endoplasmic reticulum. *J Cell Sci.* **123**(Pt 1), pp.51-61.

McHugh, B.J. et al. 2012. Loss of the integrin-activating transmembrane protein Fam38A (Piezo1) promotes a switch to a reduced integrin-dependent mode of cell migration. *PLoS One.* **7**(7), pe40346.

McKemy, D.D. 2005. How cold is it? TRPM8 and TRPA1 in the molecular logic of cold sensation. *Mol Pain.* **1**, p16.

McKemy, D.D. et al. 2002. Identification of a cold receptor reveals a general role for TRP channels in thermosensation. *Nature.* **416**(6876), pp.52-8.

Mendoza, S.A. et al. 2010. TRPV4-mediated endothelial Ca2+ influx and vasodilation in response to shear stress. *Am J Physiol Heart Circ Physiol.* **298**(2), pp.H466-76.

Michel, J.B. et al. 1997. Reciprocal regulation of endothelial nitric-oxide synthase by Ca2+-calmodulin and caveolin. *J Biol Chem.* **272**(25), pp.15583-6.

Michell, B.J. et al. 2001. Coordinated control of endothelial nitric-oxide synthase phosphorylation by protein kinase C and the cAMP-dependent protein kinase. *J Biol Chem.* **276**(21), pp.17625-8.

Michell, B.J. et al. 1999. The Akt kinase signals directly to endothelial nitric oxide synthase. *Curr Biol.* **9**(15), pp.845-8.

Michell, B.J. et al. 2002. Identification of regulatory sites of phosphorylation of the bovine endothelial nitric-oxide synthase at serine 617 and serine 635. *J Biol Chem.* **277**(44), pp.42344-51.

Minke, B. et al. 1975. Induction of photoreceptor voltage noise in the dark in Drosophila mutant. *Nature.* **258**(5530), pp.84-7.

Miyamoto, T. et al. 2014. Functional role for Piezo1 in stretch-evoked Ca(2)(+) influx and ATP release in urothelial cell cultures. *J Biol Chem.* **289**(23), pp.16565-75.

Moncada, S. and Vane, J.R. 1979. The role of prostacyclin in vascular tissue. *Fed Proc.* **38**(1), pp.66-71.

Monteith, G.R. et al. 2012. Calcium Channels and Pumps in Cancer: Changes and Consequences. *Journal of Biological Chemistry.* **287**(38), pp.31666-31673.

Morley, L.C. et al. 2018. PIEZO1 CHANNELS ARE MECHANOSENSORS IN HUMAN FETOPLACENTAL ENDOTHELIAL CELLS. *Mol Hum Reprod.*

Muller, J.M. et al. 1997. Integrin signaling transduces shear stress--dependent vasodilation of coronary arterioles. *Circ Res.* **80**(3), pp.320-6.

Murthy, S. et al. 2017. Endothelial CaMKII as a regulator of eNOS activity and NO-mediated vasoreactivity. *PLoS One.* **12**(10), pe0186311.

Noria, S. et al. 1999. Transient and steady-state effects of shear stress on endothelial cell adherens junctions. *Circ Res.* **85**(6), pp.504-14.

O'Brien, C.D. et al. 2001. PECAM-1 (CD31) engagement activates a phosphoinositide-independent, nonspecific cation channel in endothelial cells. *Faseb j.* **15**(7), pp.1257-60.

Orrenius, S. et al. 2003. Regulation of cell death: the calcium-apoptosis link. *Nat Rev Mol Cell Biol.* **4**(7), pp.552-65.

Osawa, M. 2002. Evidence for a role of platelet endothelial cell adhesion molecule-1 in endothelial cell mechanosignal transduction: is it a mechanoresponsive molecule? **158**(4), pp.773-85.

Otte, L.A. et al. 2009. Rapid changes in shear stress induce dissociation of a G alpha(q/11)-platelet endothelial cell adhesion molecule-1 complex. *J Physiol.* **587**(Pt 10), pp.2365-73.

Palmer, R.M. et al. 1988. Vascular endothelial cells synthesize nitric oxide from L-arginine. *Nature.* **333**(6174), pp.664-6.

Palmer, R.M. et al. 1987. Nitric oxide release accounts for the biological activity of endothelium-derived relaxing factor. *Nature.* **327**(6122), pp.524-6.

Panza, J.A. et al. 1993. Role of endothelium-derived nitric oxide in the abnormal endothelium-dependent vascular relaxation of patients with essential hypertension. *Circulation.* **87**(5), pp.1468-74.

Papapetropoulos, A. et al. 1997. Nitric oxide production contributes to the angiogenic properties of vascular endothelial growth factor in human endothelial cells. *J Clin Invest.* **100**(12), pp.3131-9.

Parmar, K.M. et al. 2006. Integration of flow-dependent endothelial phenotypes by Kruppel-like factor 2. *J Clin Invest.* **116**(1), pp.49-58.

Pathak, M.M. et al. 2014. Stretch-activated ion channel Piezo1 directs lineage choice in human neural stem cells. *Proc Natl Acad Sci U S A.* **111**(45), pp.16148-53.

Pellicena, P. and Schulman, H. 2014. CaMKII inhibitors: from research tools to therapeutic agents. *Front Pharmacol.* **5**, p21.

Piali, L. et al. 1995. CD31/PECAM-1 is a ligand for alpha v beta 3 integrin involved in adhesion of leukocytes to endothelium. *J Cell Biol.* **130**(2), pp.451-60.

Pierre, L.N. and Davenport, A.P. 1999. Blockade and reversal of endothelin-induced constriction in pial arteries from human brain. *Stroke.* **30**(3), pp.638-43.

Pizzo, P. and Pozzan, T. 2007. Mitochondria-endoplasmic reticulum choreography: structure and signaling dynamics. *Trends Cell Biol.* **17**(10), pp.511-7.

Prakriya, M. et al. 2006. Orai1 is an essential pore subunit of the CRAC channel. *Nature.* **443**, p230.

Prevarskaya, N. et al. 2014. Remodelling of Ca(2+) transport in cancer: how it contributes to cancer hallmarks? *Philos Trans R Soc Lond B Biol Sci.* **369**(1638).

Prevarskaya, N. et al. 2011. Calcium in tumour metastasis: new roles for known actors. *Nat Rev Cancer.* **11**(8), pp.609-18.

Ranade, S.S. et al. 2014. Piezo1, a mechanically activated ion channel, is required for vascular development in mice. *Proc Natl Acad Sci U S A.* **111**(28), pp.10347-52.

Randriamboavonjy, V. 2004. Insulin Induces the Release of Vasodilator Compounds From Platelets by a Nitric Oxide–G Kinase–VAMP-3–dependent Pathway. **199**(3), pp.347-56.

Rezakhaniha, R. et al. 2012. Experimental investigation of collagen waviness and orientation in the arterial adventitia using confocal laser scanning microscopy. *Biomech Model Mechanobiol.* **11**(3-4), pp.461-73.

Rizzo, V. et al. 1998. Rapid mechanotransduction in situ at the luminal cell surface of vascular endothelium and its caveolae. *J Biol Chem.* **273**(41), pp.26323-9.

Rode, B. et al. 2017. Piezo1 channels sense whole body physical activity to reset cardiovascular homeostasis and enhance performance. *Nature Communications.* **8**(1), p350.

Rodriguez-Feo, J.A. et al. 2005. Modulation of collagen turnover in cardiovascular disease. *Curr Pharm Des.* **11**(19), pp.2501-14.

Romac, J.M.J. et al. 2018. Piezo1 is a mechanically activated ion channel and mediates pressure induced pancreatitis. *Nat Commun.* **9**.

Roos, J. et al. 2005. STIM1, an essential and conserved component of store-operated Ca2+ channel function. *J Cell Biol.* **169**(3), pp.435-45.

Salido, G.M. et al. 2009. TRPC channels and store-operated Ca(2+) entry. *Biochim Biophys Acta.* **1793**(2), pp.223-30.

Saotome, K. et al. 2018. Structure of the mechanically activated ion channel Piezo1. *Nature.* **554**(7693), pp.481-486.

Sawano, A. et al. 2001. Flt-1, vascular endothelial growth factor receptor 1, is a novel cell surface marker for the lineage of monocyte-macrophages in humans. *Blood.* **97**(3), pp.785-91.

Schneider, J.C. et al. 2003. Involvement of Ca2+/calmodulin-dependent protein kinase II in endothelial NO production and endothelium-dependent relaxation. *Am J Physiol Heart Circ Physiol.* **284**(6), pp.H2311-9.

Schwarz, G. et al. 1992. Shear stress-induced calcium transients in endothelial cells from human umbilical cord veins. *J Physiol.* **458**, pp.527-38.

Sessa, W.C. 2004. eNOS at a glance. *J Cell Sci.* **117**(Pt 12), pp.2427-9.

Sheikh, A.Q. et al. 2012. Diabetes alters intracellular calcium transients in cardiac endothelial cells. *PLoS One.* **7**(5), pe36840.
Simons, M. 2005. Angiogenesis: where do we stand now? *Circulation.* **111**(12), pp.1556-66.
Sinha, B. et al. 2011. Cells respond to mechanical stress by rapid disassembly of caveolae. *Cell.* **144**(3), pp.402-13.
Song, J.W. and Munn, L.L. 2011. Fluid forces control endothelial sprouting. *Proc Natl Acad Sci U S A.* **108**(37), pp.15342-7.
Song, T. et al. 2004. Calcium/calmodulin-dependent protein kinase I inhibits neuronal nitric-oxide synthase activity through serine 741 phosphorylation. *FEBS Lett.* **570**(1-3), pp.133-7.
Suchyna, T.M. et al. 2000. Identification of a peptide toxin from Grammostola spatulata spider venom that blocks cation-selective stretch-activated channels. *J Gen Physiol.* **115**(5), pp.583-98.
Suchyna, T.M. et al. 2004. Bilayer-dependent inhibition of mechanosensitive channels by neuroactive peptide enantiomers. *Nature.* **430**(6996), pp.235-40.
Sugimoto, A. et al. 2017. Piezo type mechanosensitive ion channel component 1 functions as a regulator of the cell fate determination of mesenchymal stem cells. *Sci Rep.* **7**.
Sumi, M. et al. 1991. The newly synthesized selective Ca2+/calmodulin dependent protein kinase II inhibitor KN-93 reduces dopamine contents in PC12h cells. *Biochem Biophys Res Commun.* **181**(3), pp.968-75.
Sun, R.J. et al. 2002. Shear stress induces caveolin-1 translocation in cultured endothelial cells. *Eur Biophys J.* **30**(8), pp.605-11.
Syeda, R. et al. 2015. Chemical activation of the mechanotransduction channel Piezo1. *Elife.* **4**.
Tai, L.K. et al. 2002. Fluid shear stress activates proline-rich tyrosine kinase via reactive oxygen species-dependent pathway. *Arterioscler Thromb Vasc Biol.* **22**(11), pp.1790-6.
Takahashi, H. and Shibuya, M. 2005. The vascular endothelial growth factor (VEGF)/VEGF receptor system and its role under physiological and pathological conditions. *Clin Sci (Lond).* **109**(3), pp.227-41.
Taylor, S.G. and Weston, A.H. 1988. Endothelium-derived hyperpolarizing factor: a new endogenous inhibitor from the vascular endothelium. *Trends Pharmacol Sci.* **9**(8), pp.272-4.
Tokumitsu, H. et al. 1990. KN-62, 1-[N,O-bis(5-isoquinolinesulfonyl)-N-methyl-L-tyrosyl]-4-phenylpiperazi ne, a specific inhibitor of Ca2+/calmodulin-dependent protein kinase II. *J Biol Chem.* **265**(8), pp.4315-20.
Topper, J.N. et al. 1996. Identification of vascular endothelial genes differentially responsive to fluid mechanical stimuli: cyclooxygenase-2, manganese superoxide dismutase, and endothelial cell nitric oxide synthase are selectively up-regulated by steady laminar shear stress. *Proc Natl Acad Sci U S A.* **93**(19), pp.10417-22.
Tran, Q.K. et al. 2000. Calcium signalling in endothelial cells. *Cardiovasc Res.* **48**(1), pp.13-22.
Tseng, H. et al. 1995. Fluid shear stress stimulates mitogen-activated protein kinase in endothelial cells. *Circ Res.* **77**(5), pp.869-78.

Tzima, E. et al. 2001. Activation of integrins in endothelial cells by fluid shear stress mediates Rho-dependent cytoskeletal alignment. **20**(17), pp.4639-47.

Tzima, E. et al. 2005. A mechanosensory complex that mediates the endothelial cell response to fluid shear stress. *Nature.* **437**(7057), pp.426-31.

Wang, S. et al. 2016. Endothelial cation channel PIEZO1 controls blood pressure by mediating flow-induced ATP release. *J Clin Invest.* **126**(12), pp.4527-4536.

Wang, S. et al. 2015. P2Y(2) and Gq/G(1)(1) control blood pressure by mediating endothelial mechanotransduction. *J Clin Invest.* **125**(8), pp.3077-86.

Wang, Y. et al. 2018. A lever-like transduction pathway for long-distance chemical- and mechano-gating of the mechanosensitive Piezo1 channel. *Nature Communications.* **9**(1), p1300.

Warboys, C.M. et al. 2014. Disturbed flow promotes endothelial senescence via a p53-dependent pathway. *Arterioscler Thromb Vasc Biol.* **34**(5), pp.985-95.

Watanabe, H. et al. 2002. Heat-evoked activation of TRPV4 channels in a HEK293 cell expression system and in native mouse aorta endothelial cells. *J Biol Chem.* **277**(49), pp.47044-51.

Webster, P.J. et al. 2017. Upregulated WEE1 protects endothelial cells of colorectal cancer liver metastases. *Oncotarget.* **8**(26), pp.42288-42299.

Wei, S.C. and Yang, J. 2016. Forcing through Tumor Metastasis: The Interplay between Tissue Rigidity and Epithelial-Mesenchymal Transition. *Trends Cell Biol.* **26**(2), pp.111-120.

Wes, P.D. et al. 1995. TRPC1, a human homolog of a Drosophila store-operated channel. *Proc Natl Acad Sci U S A.* **92**(21), pp.9652-6.

Woo, S.H. et al. 2015. Piezo2 is the principal mechanotransduction channel for proprioception. **18**(12), pp.1756-62.

Woo, S.H. et al. 2014. Piezo2 is required for Merkel-cell mechanotransduction. *Nature.* **509**(7502), pp.622-6.

Yamada, E. and Bastie, C.C. 2014. Disruption of Fyn SH3 domain interaction with a proline-rich motif in liver kinase B1 results in activation of AMP-activated protein kinase. *PLoS One.* **9**(2), pe89604.

Yamamoto, K. et al. 2000. Fluid shear stress activates Ca(2+) influx into human endothelial cells via P2X4 purinoceptors. *Circ Res.* **87**(5), pp.385-91.

Yamamoto, K. et al. 2006. Impaired flow-dependent control of vascular tone and remodeling in P2X4-deficient mice. *Nat Med.* **12**(1), pp.133-7.

Yang, X.N. et al. 2014. Piezo1 is as a novel trefoil factor family 1 binding protein that promotes gastric cancer cell mobility in vitro. *Dig Dis Sci.* **59**(7), pp.1428-35.

Ye, R. et al. 2011. Inositol 1,4,5-trisphosphate receptor 1 mutation perturbs glucose homeostasis and enhances susceptibility to diet-induced diabetes. *J Endocrinol.* **210**(2), pp.209-17.

Yi, M. et al. 2004. Control of mitochondrial motility and distribution by the calcium signal: a homeostatic circuit. *J Cell Biol.* **167**(4), pp.661-72.

Yin, G. et al. 2003. Angiotensin II signaling pathways mediated by tyrosine kinases. *Int J Biochem Cell Biol.* **35**(6), pp.780-3.

Yu, J. et al. 2006. Direct evidence for the role of caveolin-1 and caveolae in mechanotransduction and remodeling of blood vessels. *J Clin Invest.* **116**(5), pp.1284-91.

Zamora-Leon, S.P. et al. 2001. Binding of Fyn to MAP-2c through an SH3 binding domain. Regulation of the interaction by ERK2. *J Biol Chem.* **276**(43), pp.39950-8.

Zarychanski, R. et al. 2012. Mutations in the mechanotransduction protein PIEZO1 are associated with hereditary xerocytosis. *Blood.* **120**(9), pp.1908-15.

Zhang, Q.J. et al. 2009. Endothelial nitric oxide synthase phosphorylation in treadmill-running mice: role of vascular signalling kinases. *J Physiol.* **587**(Pt 15), pp.3911-20.

Zhang, S.L. et al. 2005. STIM1 is a Ca2+ sensor that activates CRAC channels and migrates from the Ca2+ store to the plasma membrane. *Nature.* **437**(7060), pp.902-5.

Zhang, Y. et al. 2006. AMP-activated protein kinase is involved in endothelial NO synthase activation in response to shear stress. *Arterioscler Thromb Vasc Biol.* **26**(6), pp.1281-7.

Zhao, Q. et al. 2016. Ion Permeation and Mechanotransduction Mechanisms of Mechanosensitive Piezo Channels. *Neuron.* **89**(6), pp.1248-1263.

Zhao, Q. et al. 2018. Structure and mechanogating mechanism of the Piezo1 channel. *Nature.* **554**, p487.

Zhao, T. and Newman, P.J. 2001. Integrin activation by regulated dimerization and oligomerization of platelet endothelial cell adhesion molecule (PECAM)-1 from within the cell. *J Cell Biol.* **152**(1), pp.65-73.